

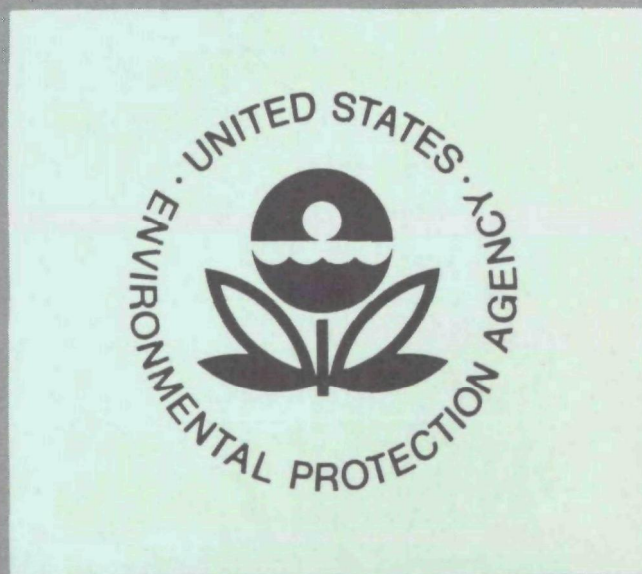
EPA-600/3-77-014a

February 1977

Ecological Research Series

MECHANISMS OF PHOTOCHEMICAL REACTIONS IN URBAN AIR

Volume I. Chemistry Studies



Environmental Sciences Research Laboratory
Office of Research and Development
U.S. Environmental Protection Agency
Research Triangle Park, North Carolina 27711

RESEARCH REPORTING SERIES

Research reports of the Office of Research and Development, U.S. Environmental Protection Agency, have been grouped into five series. These five broad categories were established to facilitate further development and application of environmental technology. Elimination of traditional grouping was consciously planned to foster technology transfer and a maximum interface in related fields. The five series are:

1. Environmental Health Effects Research
2. Environmental Protection Technology
3. Ecological Research
4. Environmental Monitoring
5. Socioeconomic Environmental Studies

This report has been assigned to the ECOLOGICAL RESEARCH series. This series describes research on the effects of pollution on humans, plant and animal species, and materials. Problems are assessed for their long- and short-term influences. Investigations include formation, transport, and pathway studies to determine the fate of pollutants and their effects. This work provides the technical basis for setting standards to minimize undesirable changes in living organisms in the aquatic, terrestrial, and atmospheric environments.

This document is available to the public through the National Technical Information Service, Springfield, Virginia 22161.

MECHANISMS OF PHOTOCHEMICAL REACTIONS IN URBAN AIR

Volume I. Chemistry Studies

by

James N. Pitts, Jr.
Statewide Air Pollution Research Center
and
Department of Chemistry
University of California
Riverside, CA 92521

Grant No. 800649 - 13, 14, 15

Project Officer

Marcia C. Dodge
Atmospheric Chemistry and Physics Division
Environmental Sciences Research Laboratory
Research Triangle Park, North Carolina 27711

ENVIRONMENTAL SCIENCES RESEARCH LABORATORY
OFFICE OF RESEARCH AND DEVELOPMENT
U.S. ENVIRONMENTAL PROTECTION AGENCY
RESEARCH TRIANGLE PARK, NORTH CAROLINA 27711

DISCLAIMER

This report has been reviewed by the Environmental Sciences Research Laboratory, U.S. Environmental Protection Agency, and approved for publication. Approval does not signify that the contents necessarily reflect the views and policies of the U.S. Environmental Protection Agency, nor does mention of trade names or commercial products constitute endorsement or recommendation for use.

ABSTRACT

Results are presented of a research program concerned with selected aspects of the kinetics, mechanisms and products of reactions involved in photochemical air pollution.

Rate constants were determined, using competitive and modulation-phase shift techniques, for the gas phase reaction of $O(^3P)$, atoms with a variety of organic and inorganic species over the temperature range 296-423°K. Products for the gas phase reaction of $O(^3P)$ atoms with toluene and 1-methylcyclohexene were also studied.

The products and mechanisms of the reaction of nitric oxide with methyl peroxy radicals were investigated at 296°K using long path infrared spectroscopic and gas chromatographic techniques.

The reactions of peroxyacetyl nitrate were investigated in the gas phase with selected constituents of polluted atmospheres, and in the liquid phase with a variety of organics. Chemiluminescence from the reaction of peroxyacetyl nitrate with a series of amines was studied in the liquid phase. The mechanism and products of gas phase reactions of ozone with a variety of organics was investigated in low pressure flow systems using chemiluminescent and photoionization mass spectrometric techniques.

The NO_2 -catalyzed geometric isomerization of 2-butenes and 2-pentenenes was studied over the temperature range 298-400°K while an investigation of the NO_x -propylene photooxidation system was carried out at room temperature.

CONTENTS

Abstract	iii
List of Figures	vi
List of Tables	ix
Acknowledgments	xi
I. Introduction	1
II. Conclusions	4
III. Recommendations	8
IV. Experimental Methods, Results and Discussion	9
1. Determination of absolute rate constants for the reaction of O(³ P) atoms with organics over the temperature range 299-392°K	10
2. Rate constants for the reaction of O(³ P) atoms with selected olefins, monoterpenes and unsaturated aldehydes	23
3. The reaction of O(³ P) atoms with toluene and 1-methyl- cyclohexene	36
4. A long-path infrared spectroscopic study of the reaction of methylperoxy free radicals with nitric oxide	49
5. Rate constants for the gas-phase reaction of peroxy- acetyl nitrate with selected atmospheric constituents	62
6. Chemiluminescence detection of PAN and PBzN	74
7. Solution phase reactions of PAN with molecules of biological significance	82
8. Thermal and photochemical processes of NO and NO ₂ and the application of the results to the chemistry of polluted atmospheres	86
9. 40-meter long-path infrared studies of the propylene/ NO _x /hν system	97
10. The ozone-induced chemiluminescent oxidation of acetaldehyde	109
11. Low-pressure gas-phase ozone-olefin reactions. Chemi- luminescence, kinetics, and mechanisms	114
12. Photooxidation mass spectrometer studies of gas-phase ozone-olefin reactions	150

LIST OF FIGURES

<u>Number</u>		<u>Page</u>
1.1	Plots of $2\pi\nu/\tan \phi$ against xylene concentration for o-, m-, and p-xylenes at room temperature	13
1.2	Arrhenius plots for the aromatic hydrocarbons	15
1.3	Arrhenius plots of $\log k$ against $1000/T$	16
2.1	Plots of ethylene yield versus N_2 yield for cyclopentene alone and for four runs with differing limonene/cyclopentene ratios	26
2.2	Arrhenius plots of $\log k_2^A/k_2^{CP}$ against $1000/T$	27
2.3	Arrhenius plots of $\log k_2^A/k_2^{CP}$ against $1000/T$	28
3.1	Plot of selected product yields ($N_2 = 1$) against total N_2O pressure for the reaction of $O(^3P)$ atoms with 1-methylcyclohexene at $296 \pm 2^\circ K$	44
4.1	Infrared spectra of CH_3ONO , NO , NO_2 ; Infrared spectra of azomethane, NO , and O_2 before and after photolysis	53
4.2	Typical time dependence of CH_3ONO , CH_3ONO_2 , NO_2 and NO in the photooxidation of azomethane in the presence of NO	55
5.1	Plots of $d \ln[PAN]/dt$ against reactant concentration for O_3 and H_2O	65
5.2	Plots of $\ln[PAN]$ against time for the reaction of PAN with NO in air diluent	67
6.1	Chemiluminescent detection unit	75
6.2	Emission spectra of chemiluminescence reactions of triethylamine with PAN and ozone	78
6.3	Decay curves of chemiluminescence generated in reaction of triethylamine with PAN and ozone	79
8.1	Plot of the mole fraction of <u>trans</u> -2-butene <u>vs</u> time for the <u>cis</u> - to <u>trans</u> - NO_2 catalyzed geometric isomerization of <u>cis</u> -2-butene	88

LIST OF FIGURES (cont.)

<u>Number</u>		<u>Page</u>
8.2	Arrhenius parameters for the NO ₂ catalyzed geometric isomerization of <u>cis</u> - or <u>trans</u> -2-butene	90
8.3	Arrhenius parameters for the NO ₂ catalyzed geometric isomerization of <u>cis</u> - or <u>trans</u> -2-pentene	91
9.1	Typical concentration-time profile for the NO ₂ photooxidation of C ₃ H ₆	100
9.2	Typical concentration-time profile for the NO ₂ photooxidation of C ₃ H ₆	101
9.3	A typical GC-MS total ion chromatogram of an irradiated NO ₂ -C ₃ H ₆ -air mixture	104
9.4	GC-MS computer spectrum of CH ₃ CHO as obtained from the total ion chromatogram of an irradiated NO ₂ -C ₃ H ₆ -air mixture	105
9.5	GC-MS computer spectrum of (CH ₃) ₂ CO as obtained from the total ion chromatogram of an irradiated NO ₂ -C ₃ H ₆ -air mixture	106
9.6	GC-MS computer spectrum of CH ₃ OH as obtained from the total ion chromatogram of an irradiated NO ₂ -C ₃ H ₆ -air mixture	107
10.1	Emission spectra from 500 to 800 nm in the chemiluminescent reactions of ozone with acetaldehyde and H atoms	110
10.2	Emission spectra from 700 to 1100 nm from the chemiluminescent reactions of ozone with acetaldehyde and H atoms	111
11.1	Schematic of apparatus used in chemiluminescence and kinetic studies	116
11.2	Chemiluminescent emission spectra in the visible region from the reaction of 2% O ₃ /O ₂ with ethylene, <u>trans</u> -2-butene, and isobutene	120
11.3	Comparison of the chemiluminescent emission (700-1100 nm) from the ozone- <u>cis</u> -2-butene reaction to the OH Meinel bands from the H + O ₃ reaction	122
11.4	Chemiluminescent emission spectra (300-550 nm) from the reactions of 2% O ₃ in O ₂ or N ₂ with ethylene, <u>cis</u> -2-butene, and isobutene	123

LIST OF FIGURES (cont.)

<u>Number</u>		<u>Page</u>
11.5	Chemiluminescent emission spectra (300-600 nm) from the reactions of 2% O ₃ in N ₂ or O ₂ with 2-butene-d ₈ , and isobutene-d ₈	125
11.6	Semilogarithmic plots of relative emission intensities and ozone absorbance vs reaction distance for the reaction of <u>cis</u> -2-butene with 2% O ₃ /O ₂ or 2% O ₃ /N ₂	128
12.1	Resonance lamp energies and ionization potentials of relevant species	152
12.2	Kinetic behavior of HCO + C ₂ H ₅ , CH ₂ CO, and CH ₃ CHO observed in the <u>cis</u> -2-butene-ozone reaction	156
12.3	Kinetic behavior of HCHO, CH ₃ OH, HCOOH, C ₂ H ₅ , and H ₂ O ₂ observed in the <u>cis</u> -2-butene-ozone reaction	157
12.4	Dependence of signal at m/e 104 on olefin concentration and on time in the <u>cis</u> -2-butene-ozone reaction	158
12.5	Kinetic behavior of HCHO and CH ₃ CO in the ethylene-ozone reaction	160
12.6	Kinetic behavior of HCHO and CH ₃ COCH ₃ in the isobutene-ozone reaction	161

LIST OF TABLES

<u>Number</u>		<u>Page</u>
1.1	Rate constants k_2 for the reaction of $O(^3P)$ atoms with organics	17
1.2	Arrhenius parameters for $O(^3P)$ atom reactions	18
1.3	Comparison of the room temperature rate constants, k_2 , and the activation energies, E , for n-butane and the aromatics from the present work with selected literature values	19
2.1	Relative rate constants k_2^A/k_2^{CP} for the reaction of $O(^3P)$ atoms	29
2.2	Arrhenius parameters for the reaction of $O(^3P)$ atoms	31
2.3	Comparison of the room temperature rate constants, k_2 , and activation energies, E , for ketene, acrolein and croton-aldehyde from the present work with literature values	33
3.1	Product yields observed from the reaction of $O(^3P)$ atoms with toluene	40
3.2	Product yields from the reaction of $O(^3P)$ atoms with 1-methylcyclohexene ($N_2 = 1$)	43
4.1	Columns used in gas chromatographic analysis of the products of the photooxidation of azomethane in the presence of NO at room temperature	51
4.2	Infrared extinction coefficients and limits of detection of some reactants and products in the photooxidation of azomethane in the presence of NO at room temperature	52
4.3	Reactant concentrations, rates of product formation and quantum yields in the photooxidation of azomethane in the presence of NO at room temperature	56
5.1	Experimental conditions used and the rate constants k_2 obtained for the reaction of PAN with SO_2 , CO_2 , NO_2 , NH_3 , H_2O , O_3 , isobutene and acetaldehyde	66
5.2	Initial conditions and observed first order constants, k_{obs} , for the reaction of PAN with NO	68

LIST OF TABLES (cont.)

<u>Number</u>		<u>Page</u>
5.3	Chemical lifetimes of PAN in a typical Los Angeles polluted atmosphere	72
6.1	Chemiluminescence efficiency of amines reacting with PAN (1000 ppm) in the gas phase and in solution	76
7.1	PAN products, % of total, from reaction of isobutyraldehyde .	83
8.1	Thermodynamic and Arrhenius parameters for the NO ₂ catalyzed geometric isomerization of the 2-butenes and 2-pentenenes	92
8.2	Calculated and experimental data for the reactions of nitrogen dioxide with selected olefins	94
9.1	Analytical methods	99
9.2	Reaction products from the photooxidation of C ₃ H ₆ by NO ₂	103
11.1	Summary of the chemiluminescing species (200 < λ < 1100 nm) identified in ozone-olefin reactions in the presence and absence of oxygen	126
11.2	Reaction orders of emitting species in ozone and olefin in the presence and absence of oxygen	127
11.3	Rate constants for the <u>cis</u> -2-butene and isobutene reactions with ozone under varying conditions of total pressure and oxygen concentrations	130
11.4	Comparison of the rate constants obtained in this work with literature room-temperature absolute values	132
11.5	Absolute rates of light emission for each emitting species in the reactions of 2% O ₃ /O ₂ with ethylene and <u>cis</u> -2-butene .	131
12.1	Observed peak mass numbers and their assignments	153
12.2	Stable products observed in the reaction of ozone with ethylene, isobutene, and <u>cis</u> -2-butene	162

ACKNOWLEDGEMENTS

The following personnel performed the experimental work or otherwise contributed directly to the research described in this report:

Roger Atkinson
Karen R. Darnall
Barbara J. Finlayson
Dennis R. Fitz
Hartmut Fuhr
Jeffrey S. Gaffney
D. Alan Hansen
Dennis M. Hebert
Alan C. Lloyd
Christopher T. Pate
John W. Peters
Jeremy L. Sprung
Peter H. Wendschuh

SECTION I

INTRODUCTION

The research work described in this report was carried out in the Department of Chemistry, University of California, Riverside, under EPA Grant 800649 (formerly AP-109) during December 1, 1971 - November 30, 1974. The work described deals with various aspects of the kinetics, mechanisms, and products of reactions involved in photochemical air pollution and possible implications for the chemical reaction mechanism employed in urban airshed models.

The principal components of an ab initio urban airshed model of the formation of photochemical smog are an emission inventory, a meteorological program, and a chemical reaction mechanism. The emission inventory specifies where, when, which, and in what concentrations pollutants are emitted into an air parcel; the meteorological program specifies the size and trajectory of an air parcel; and the reaction mechanism specifies the chemical and, if possible, physical (gas-to-particle conversion) transformations which the pollutants undergo within the air parcel. Together, these three components of the airshed model specify the rate of formation of secondary pollutants--such as ozone, nitrogen dioxide, oxygenates, nitrogenous compounds, and aerosol--as a function of both place and time.

Before it can be applied to an assessment of air pollution problems, an airshed model must be validated against ambient air data characteristic of the air basin for which it is a model. Successful validation of an ab initio airshed model for the formation of photochemical smog would complement and extend existing, largely empirical airshed models and would clearly be of great utility for the cost-effective formulation of air pollution control strategies, land-use plans, environmental impact statements, and air pollution episode health warning systems.^{1,2}

Because the chemistry of photochemical smog is exceedingly complex³⁻⁷ even homogeneous reaction mechanisms for smog formation are unusually lengthy, and validation of such mechanisms requires the development of a very broad and detailed data base. Homogeneous reaction mechanisms constructed from

the current data base simulate the rates of disappearance of aliphatic hydrocarbons and the rate conversion of NO to NO₂ with encouraging fidelity. However, the behavior of many photooxidation products and aromatic compounds, such as toluene, is still modeled with considerable uncertainty, and no existing models treat such heterogeneous processes as aerosol formation in detail.

The types of data most urgently needed to permit further refinement and ultimate validation of smog reaction mechanisms have been authoritatively reviewed^{5,8-10} and discussed.¹¹ Such data include:

- Precise concentration/time profiles for all major and significant trace smog species formed during nitrogen-oxide-promoted photooxidations of characteristic hydrocarbon pollutants and their major atmospheric oxidation products.
- The effects of added SO₂ and particulate upon the course of hydrocarbon/nitrogen oxide photooxidations, particularly the formation of sulfate and aerosol.
- Rates of formation and properties of aerosols formed during hydrocarbon/nitrogen oxide photooxidations.
- Photolytic behavior of photoactive secondary pollutants, especially aldehydes and nitrous acid.
- Temperature-dependent homogeneous and heterogeneous rate and equilibrium data for the reactions between oxides of nitrogen and water and their oxyacid products.
- Mechanistic data defining the effects of molecular oxygen upon atmospheric hydrocarbon oxidation pathways.
- Data on reaction rates and products, both stable and transient, formed by the reactions of O(³P) atoms, and particularly OH and HO₂ radicals, with important atmospheric pollutants and their major oxidation products--e.g., reactions of OH with olefins and aromatic compounds yield products of uncertain identity and quantity.

The studies of the University of California have focused on selected aspects of these requirements, including reactions of O(³P) with olefins and aromatic compounds and selected reactions of CH₃O₂ and O₃.

REFERENCES

1. J. N. Pitts, Jr., A. C. Lloyd and J. L. Sprung, "Chemical Reactions in Urban Atmospheres and Their Application to Air Pollution Control Strategies," Proceedings of the International Symposium on Environmental Measurements, Beckman Instruments Process S.A., Geneva, October 2-4, p. 27 (1974).
2. J. N. Pitts, Jr., A. C. Lloyd and J. L. Sprung, Chem. Brit., 11, 247 (1975).
3. P. A. Leighton, "Photochemistry of Air Pollution," Academic Press, New York, New York (1961).
4. A. P. Altshuller and J. J. Bufalini, Environ. Sci. Technol., 5, 39 (1971).
5. K. L. Demerjian, J. A. Kerr and J. G. Calvert, Adv. Environ. Sci. Technol., 4, 1 (1974).
6. J. N. Pitts, Jr. and B. J. Finlayson, "The Mechanisms of Photochemical Air Pollution and the Chemist: Past Perspectives and Future Challenges," Angewandte Chem. Int. Ed., 14, 1 (1975).
7. B. J. Finalyson and J. N. Pitts, Jr., Science 192, 111 (1976).
8. M. C. Dodge, "Workshop on Mathematical Modeling of Photochemical Smog: Summary of the Proceedings," EPA-R4-73-010, U. S. Environmental Protection Agency, Research Triangle Park, North Carolina, January, 1973.
9. J. H. Seinfeld, T. A. Hecht and P. M. Roth, "Existing Needs in the Experimental and Observational Study of Atmospheric Chemical Reactions," EPA-R4-73-031, U. S. Environmental Protection Agency, Washington, D.C., June, 1973.
10. M. C. Dodge and T. A. Hecht, Abstracts of Papers to be presented at the "Symposium on Chemical Kinetics Data for the Lower and Upper Atmosphere," Warrenton, Virginia, September, 1974, U. S. Environmental Protection Agency, Research Triangle Park, North Carolina, August, 1974.
11. Triangle Universities Consortium on Air Pollution, "Symposium on Chemical Aspects of Air Quality Modeling," University of North Carolina, Chapel Hill, North Carolina, April, 1974.

SECTION II

CONCLUSIONS

- Absolute rate constants have been determined for the reaction of ground state oxygen $O(^3P)$ atoms with a series of organics (ethylene, propylene, benzene, toluene, o-, m-, p-xylene, 1,2,3-, 1,2,4-, and 1,3,5-trimethylbenzene) and the inorganics $NO(M = N_2O)$ and $SO_2(M = N_2O)$ over the temperature range 299–392°K, using a modulation-phase shift technique. In addition, absolute rate constants were determined for the reaction of $O(^3P)$ atoms with n-butane, methoxybenzene, and o-cresol at room temperature. The rate constants at room temperature were observed to range from $(1.44 \pm 0.2) \times 10^7$ liter mole⁻¹ sec⁻¹ for benzene to $(2.01 \pm 0.22) \times 10^9$ liter mole⁻¹ sec⁻¹ for propylene.

- Rate constants for the reaction of $O(^3P)$ atoms with selected olefins (propylene, 1-methylcyclohexene, and 1,3-cyclohexadiene), monoterpenes (α -pinene, β -pinene, and d-limonene), and unsaturated aldehydes (acrolein and crotonaldehyde) were determined over the temperature range 296–423°K, relative to that for the reaction of $O(^3P)$ atoms with cyclopentene. In addition, relative rate constants for the reaction of $O(^3P)$ atoms with ketene and toluene were determined at 296°K and 423°K, respectively. These relative rate constants were placed on an absolute basis, using a rate constant for the reaction of $O(^3P)$ atoms with propylene derived from the literature. The absolute room temperature rate constants obtained ranged from 2.3×10^8 liter mole⁻¹ sec⁻¹ for acrolein to 6.5×10^{10} liter mole⁻¹ sec⁻¹ for d-limonene.

- Products from the gas phase reaction of $O(^3P)$ atoms with toluene and 1-methylcyclohexene have been studied in order to determine the effect of aromaticity on the reaction mechanism. $O(^3P)$ atoms were generated by the mercury photosensitization of N_2O in a static system and products were analyzed by gas chromatography. For toluene, the major volatile products observed were the cresols (mainly o-cresol), CO, and phenol, together with a large amount of tar formation. In the case of 1-methylcyclohexene, the products were the $C_7H_{12}O$ isomers expected from the general reaction mechanism of Cvetanovic.¹ The differences in the products between the cyclic olefin

and the aromatic hydrocarbon were explained by the differences in the rate constants for reaction of $O(^3P)$ atoms with the reactant and with the reaction products. Thus, the reaction of $O(^3P)$ atoms with the aromatic hydrocarbons is slow and produces mainly highly reactive unsaturated products, while for the simple olefins the initial reaction is very fast and forms largely saturated, and hence unreactive, products. Therefore, the extent of secondary reactions is much smaller in the latter case.

- The reaction of NO with CH_3O_2 radicals generated in the photooxidation of azomethane ($\lambda > 320$ nm) was investigated at $296 \pm 2^\circ K$ using long-path infrared and gas chromatographic techniques. At short photolysis times, CH_3ONO and NO_2 were identified as products with quantum yields of 1.7 ± 0.2 and 1.9 ± 0.3 , respectively. The data show that the reaction $CH_3O_2 + NO_2 \rightarrow CH_3O + NO_2$ is the only reaction path for the reaction of CH_3O_2 radicals with NO.

- Rate constants for the removal of peroxyacetyl nitrate (PAN) in the presence of SO_2 , isobutene, CO, CH_3CHO , NO_2 , H_2O , O_3 , NH_3 , and NO were determined at $296 \pm 1^\circ K$ by monitoring the decay of PAN in excess reactant as a function of time by long-path infrared spectroscopy and/or gas chromatography. The reactions with all the reactants, except O_3 and NO, were sufficiently slow that heterogeneous removal processes for PAN in their presence could not be excluded. For the reaction of PAN with NO, the initial rates of removal of PAN were observed to be first order in PAN and independent of NO concentration, with a first-order rate constant of $(2.8 \pm 0.8) \times 10^{-4} \text{ sec}^{-1}$. A possible reaction mechanism for the thermal reactions of PAN is proposed.

- Chemiluminescence from the reactions of PAN with a series of amines has been investigated. In addition, spectra have been obtained for the gas-phase reactions of PAN ($\lambda_{\text{max}} \sim 650$ nm) and ozone ($\lambda_{\text{max}} \sim 520$ nm) with triethylamine at atmospheric pressure. The two chemiluminescent reactions can be distinguished optically, and PAN concentrations as low as 6 ppb were detected by this technique.

- A study of the solution-phase reactions of PAN with a variety of organic molecules (aldehydes, alcohols, amines, mercaptans, and sulfides) containing functionality found in common biological systems has been carried out.

- The NO_2 -catalyzed geometric isomerization of 2-butene and 2-pentene has been studied over the temperature range $298\text{--}400^\circ K$. Both kinetic and equilibrium data have been obtained. The combination of these results with

thermodynamic calculations permits the estimation of rate constants for the addition of NO_2 to the double bond of simple olefins. Comparison of these rate constants to those for reaction of olefins with O_3 suggests that atmospheric consumption of olefins by processes initiated by NO_2 addition cannot be significant.

- A study of the NO_x -propylene photooxidation system has been carried out using long-path infrared, gas chromatographic, and combined gas chromatographic-mass spectrometric techniques.

- The vibration-rotation Meinel bands of $\text{OH}(X^2\pi_1)$ have been observed in the chemiluminescent gas-phase reaction of ozone with acetaldehyde at ~3 torr total pressure and room temperature. A weaker emission in the visible region was tentatively identified as formaldehyde emission.

- Chemiluminescence from $\text{HCHO}(^1A'' \rightarrow ^1A_1)$, $\text{OH}(X^2\pi_1)_{v' \leq 9}$, and $\text{OH}(A^2\Sigma^+)$ has been observed in the gas-phase reactions of 2% O_3 in O_2 , N_2 , or He with a series of simple olefins in a flow system at room temperature and at total pressures of 2-10 torr. The vibration-rotation emission from $\text{OH}(X^2\pi_1)_{v' \leq 9}$ was virtually identical with OH Meinel band emission from the reaction, $\text{H} + \text{O}_3 \rightarrow \text{OH}(X^2\pi_1)_{v' \leq 9} + \text{O}_2$, confirming that H atoms are formed in O_3 -olefin reactions under these experimental conditions. In the presence of O_2 , glyoxal phosphorescence was identified in the 2-butene (cis or trans) reaction, and methylglyoxal phosphorescence was tentatively identified from the reactions of isobutene, 2-methyl-2-butene, and 2,3-dimethyl-2-butene with ozone. The number of quanta emitted per molecule of reactant consumed at 4.6 torr total pressure in the ethylene and cis-2-butene reactions were estimated to be 10^{-7} for $\text{HCHO}(^1A'' \rightarrow ^1A_1)$ and 10^{-5} quanta for $(\text{CHO})_2(^3A_u \rightarrow ^1A_g)$ in the cis-2-butene reaction. Approximately 10^{-7} quanta were emitted in the (9,3) transition of vibrationally excited OH per molecule of reactant consumed, indicating that the formation of vibrationally excited OH is a surprisingly efficient process under these conditions. In the ethylene, cis-2-butene, and isobutene reactions, the time decay of light emission from each excited species was exponential in O_2 but nonexponential in N_2 or He, with increased emission intensities occurring at reaction times ≤ 0.1 sec in the latter case. Rate constants, determined from the loss of O_3 in both O_2 and N_2 as diluents, assuming 1:1 stoichiometry, were a factor of 2-5 times greater in N_2 . In 10 torr of O_2 , the measured rate constants for the ethylene, cis-2-butene, and isobutene reactions, respectively, were

$(1 \pm 1) \times 10^3$, $(6.3 \pm 1.9) \times 10^4$, and $(5.4 \pm 2.3) \times 10^3$ liter mole⁻¹ sec⁻¹.

Major products of the reaction of cis-2-butene with ozone in either O₂ or N₂ as the carrier gas were, in addition to acetaldehyde, 2-butanone (possibly from the OH-cis-2-butene reaction) and methyl vinyl ketone, which was observed only in oxygen. The results are discussed in terms of the O'Neal-Blumstein theory of gas-phase ozone-olefin reactions, and the possible role of these reactions in photochemical smog formation is considered.

- The room-temperature gas-phase reactions of O₃ with ethylene, propylene, and cis-2-butene have been investigated at total pressures of ~2 torr, using photoionization mass spectrometry. Both radical species and stable products were identified and monitored as a function of time.

REFERENCE

1. R. J. Cvetanovic, Adv. Photochem., 1, 115 (1963).

SECTION III

RECOMMENDATIONS

From the results described in the report and literature data, it is apparent that the following data need to be obtained in order to more fully understand the chemistry of photochemical air pollution.

- a) To determine the products and mechanism of the reaction of ozone with a series of olefins at atmospheric pressure in the presence of O_2 . A full product study as a function of O_3 /olefin ratio, total pressure, O_2 concentration would be preferable.
- b) The products of the reaction of $O(^3P)$ atoms with aromatics should be determined, using as wide a variety of techniques as possible (such as photoionization mass spectroscopy, gas chromatography, etc.). In addition, the effect of O_2 on the products and mechanism should be investigated.
- c) Rate constants, products, and mechanisms of the reaction of OH radicals with olefins and aromatic hydrocarbons should be determined. Products of such reactions should be determined, if possible, under conditions applicable to polluted urban atmospheres.
- d) The rate constants and products of the reactions of HO_2 , alkoxy, and alkylperoxy radicals with NO, NO_2 , O_2 , and selected organics should be determined.

This research work will require major efforts involving difficult experimental systems, but such knowledge is a necessary input into detailed chemical kinetic computer models of photochemical air pollution.

SECTION IV

EXPERIMENTAL METHODS, RESULTS AND DISCUSSION

1. DETERMINATION OF ABSOLUTE RATE CONSTANTS FOR THE REACTION OF $O(^3P)$ ATOMS WITH ORGANICS OVER THE TEMPERATURE RANGE 299-392°K

Experimental. Ground state oxygen atoms were generated by the mercury photosensitization of N_2O in a flow system.^{1,2} 253.7 nm resonance radiation was emitted by a modulated radio-frequency-powered low pressure mercury arc driven by a six-turn coil connected to a 14.0 MHz radio frequency generator operating at ~125 watts.

The 253.7 nm resonance line was isolated by passage through a Corning 7-54 filter plus an aqueous solution of 210 gm $NiSO_4$ /60 gm $CoSO_4$ liter⁻¹. The 253.7 radiation was collimated into the reaction cell and was monitored by a Bausch and Lomb UV monochromator-RCA 1P28 photomultiplier combination. The Pyrex reaction cell, 12 cm in length and 2.5 cm in diameter, had Supracil end windows and a short sidearm fitted with a Pyrex window. Oxygen atoms were monitored by observation of the NO_2 afterglow produced by the addition of known flows of NO to the reactant stream. The afterglow emission was detected through the Pyrex side window by a cooled EMI 9659A photomultiplier tube fitted with a cut-off filter transmitting $\lambda \geq 450$ nm. The phase shift, ϕ , between the incident 253.7 radiation and the NO_2 air afterglow was determined using a PAR HR8 lock-in amplifier with a Type C preamplifier.¹⁻² The reaction cell was enclosed in a furnace whose temperature was measured by a thermocouple probe. The reactant gas stream was observed to be within $\pm 0.5^\circ K$ of the furnace temperature under all conditions used.

Absorbed light intensities in the reaction cell were determined by GC analysis of propylene oxide from the $O(^3P) +$ propylene reaction³ at ~50 torr total pressure to be typically 1×10^{16} quanta sec⁻¹, corresponding to an $O(^3P)$ atom production rate of 5×10^{-7} mole liter⁻¹. With these absorbed light intensities, residence times in the reaction cell of 0.26-0.46 sec, and the flows used (total flow rate $(2.8-5.1) \times 10^{-4}$ mole sec⁻¹), reactant conversions ranged from $\leq 2\%$ for propylene or 1,3,5-trimethylbenzene to $\leq 0.03\%$ for n-butane or benzene.

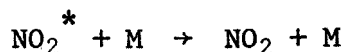
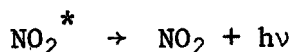
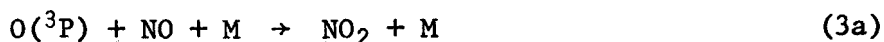
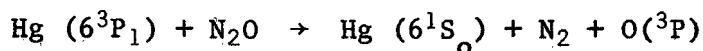
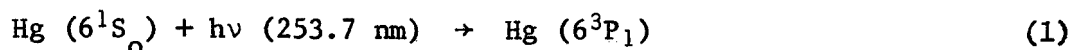
The gases used had the following purity levels, according to the manufacturer: $N_2O \geq 98.0\%$; $NO \geq 99.0\%$; Ar $\geq 99.998\%$; ethylene $\geq 99.5\%$; propylene $\geq 99.0\%$; n-butane $\geq 99.9\%$; $SO_2 \geq 99.8\%$; o-cresol $\geq 99.0\%$; methoxybenzene $\geq 99.0\%$. Analysis by GC showed the following impurities in the less reactive hydrocarbons: n-butane, ~0.01% butenes, mainly trans-2-butene; benzene, 0.5%

toluene and $\leq 0.5\%$ xylene; toluene, 0.1% benzene and 0.05% m-xylene; o-xylene, $\leq 0.2\%$ impurity; m-xylene, 1.0% p-xylene and 0.4% ethylbenzene; p-xylene, 0.3% m-xylene; 1,2,3-trimethylbenzene, 0.2% of the 1,3,5-isomer and 2.2% of the 1,2,4-isomer; 1,2,4-trimethylbenzene, 1.0% of the 1,3,5-isomer; 1,3,5-trimethylbenzene, 0.2% of the 1,2,4-isomer and 0.1% ethyltoluene. $\sim 10\%$ NO in argon was passed through Linde Molecular Sieve 13X to remove any H_2O and NO_2 present, while N_2O , SO_2 , ethylene, propylene and n-butane were dried by passage through traps containing Drierite.

For the rate constant determinations for the aromatics, a known fraction of the N_2O flow was saturated with the aromatic vapor at 22°C (11°C in the case of benzene). Aromatic concentrations in the gas stream were determined before entering the reaction cell by their UV absorption using a 10.0 cm path length cell and a Cary 15 spectrophotometer. The absorption cell was calibrated using known pressures of the aromatic as measured by a MKS Baratron gauge. NO, SO_2 , ethylene, propylene and n-butane concentrations were calculated, with an estimated accuracy of $\pm 3\text{--}4\%$, from the observed partial flow rates and total pressure in the reaction cell. The gas stream was saturated with mercury vapor at room temperature before entering the reaction cell. All flows were monitored by calibrated rotameters and controlled by needle valves.

Results. The reactions of $\text{O}(^3\text{P})$ atoms with NO, SO_2 , ethylene, propylene, n-butane, and a series of aromatics were studied at room temperature.² No chemiluminescent emission was observed in the absence of NO, except in the case of $\text{O}(^3\text{P}) + \text{ethylbenzene}$ which precluded any rate constant determination for this hydrocarbon.

For sinusoidally modulated 253.7 nm radiation and the following reaction scheme:^{1,2}



The phase shift, ϕ , between the NO_2 afterglow emissions and the incident 253.7 nm radiation under the conditions used is given by^{1,2}

$$\tan \phi = 2\pi\nu/k_2[\text{reactant}] + k_3[\text{NO}][\text{M}]$$

where $k_3 = k_{3a} + k_{3b}$ and ν is the modulation frequency. In this study, the modulation frequency was in all cases 1200 ± 1 Hz and total pressure varied over the range 48-135 torr.

The rate constant k_3 for the reaction $\text{O} + \text{NO} + \text{M}$ was determined directly using the equation

$$2\pi\nu/\tan \phi = k_3[\text{NO}][\text{M}] \quad (\text{II})$$

The fact that argon is a less efficient third body than N_2O in reaction (3) was corrected for using literature rate constant data⁴ for reaction (3).

For determinations of the rate constants k_2 , $[\text{NO}][\text{M}]$ was held constant and $[\text{reactant}]$ varied. Figure 1.1 shows an example of plots of $2\pi\nu/\tan \phi$ against $[\text{reactant}]$ for the xylenes at room temperature. It is seen from equation I that such plots have intercepts of $k_3[\text{NO}][\text{M}]$ and slopes of k_2 . The intercepts of such plots were determined from the experimental $[\text{NO}][\text{M}]$ and the rate constant k_3 . Runs to check these intercepts agreed with the calculated values within the expected experimental error of a single run (5-10%). Table 1.1 gives the values of k_2 obtained.

The Arrhenius parameters ($k = A e^{-E/RT}$) obtained from this data are

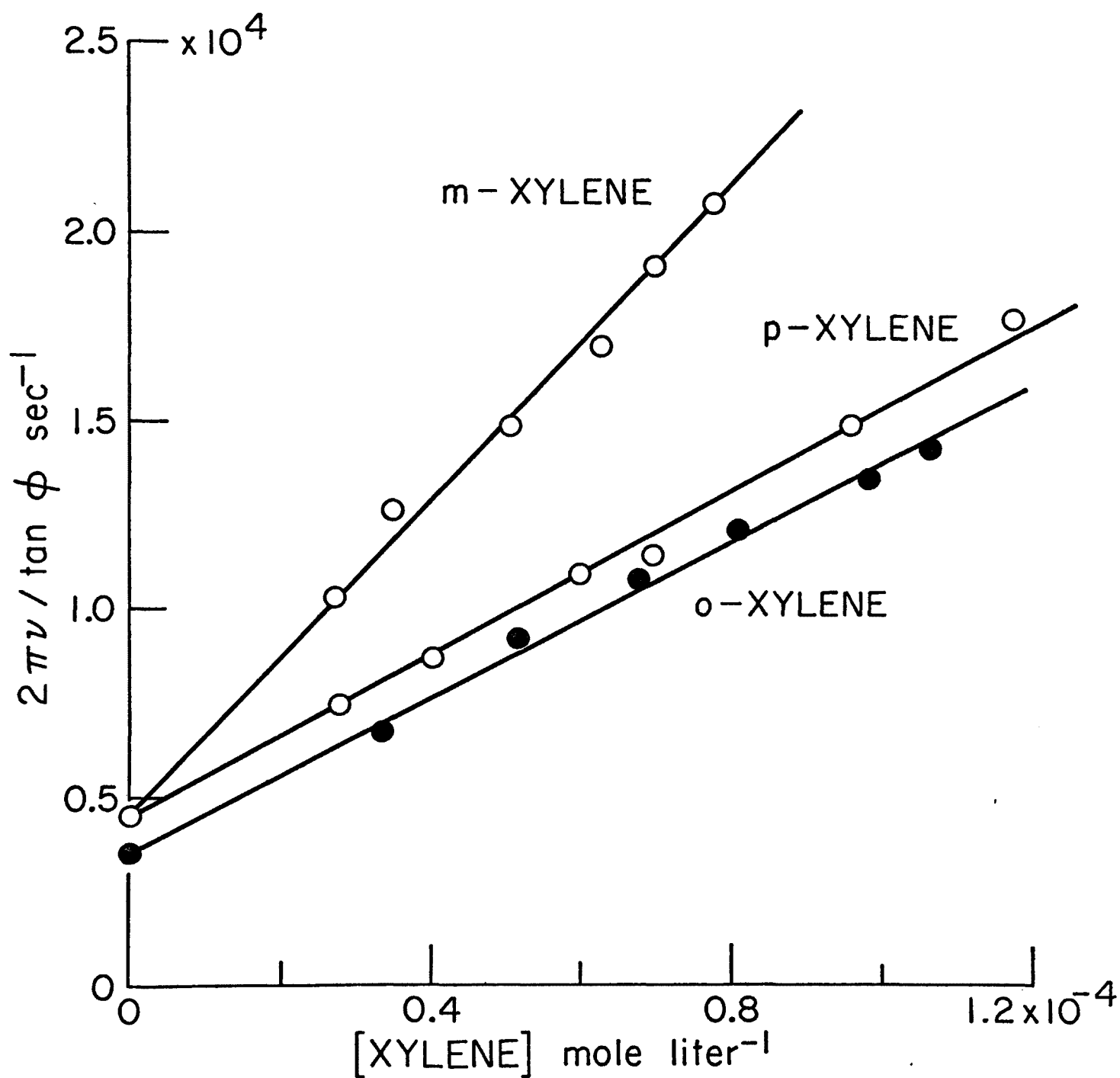


Figure 1.1 Plots of $2\pi\nu / \tan \phi$ against xylene concentration for o-, m-, and p-xylenes at room temperature.

given in Table 1.2 while Figure 1.2 shows Arrhenius plots for $O(^3P) +$ aromatic hydrocarbons.

Discussion. As shown in Figure 1.3, for propylene there is very good agreement with the data of Kurylo⁵ ($E = 0.076 \pm 0.044$ kcal mole⁻¹), Huie et al.,⁶ Stuhl and Niki⁷ and Cvetanovic and co-workers.⁸ For ethylene, the present room temperature value is in good agreement with those of Stuhl and Niki,^{7,9} and Cvetanovic and co-workers.⁸ While the temperature dependence determined in this work agrees well with that of Davis et al.¹⁰ ($E = 1.13 \pm 0.032$ kcal mole⁻¹), their absolute values (and that of Kurylo and Huie¹¹) lie some 15-20% higher. Earlier literature data for C_2H_4 obtained by discharge flow techniques range from $(2.2-7.2) \times 10^8$ liter mole⁻¹ sec⁻¹ at room temperature,¹²⁻¹⁷ with reported activation energies of 1.6 kcal mole⁻¹,^{12,13} and 1.1-2.8 kcal mole⁻¹.¹⁴

For the reaction $O + NO + M$ ($M = N_2O$) the present room temperature value of k_3 agrees with those obtained by Kaufman and Kelso⁴ ($k_3 = 4.7 \times 10^{10}$ liter² mole⁻² sec⁻¹) and Atkinson and Cvetanovic¹⁸ ($k_3 = (3.9 \pm 0.3) \times 10^{10}$ liter² mole⁻² sec⁻¹), although the activation energy obtained in this work ($E = 0.90 \pm 0.2$ kcal mole⁻¹) is lower than previously reported: -1.93 ± 0.1 ($M = N_2$);¹⁹ -1.8 ± 0.4 ($M = O_2$);²⁰ -2.0 ($M = Ar$)²¹ and -1.6 ± 0.3 kcal mole⁻¹ ($M = N_2O$).¹⁸ No immediate reason for this discrepancy is obvious.

There is no previously reported value of k_2 for the reaction $O + SO_2 + M$ ($M = N_2O$), but the temperature dependence obtained in this work ($E = 2.00 \pm 0.4$ kcal mole⁻¹) is in good agreement with the value of $E = 2.24$ kcal mole⁻¹ for $M = N_2$ obtained by Davis²² using a flash photolysis-resonance fluorescence technique.

Table 1.3 compares the present room temperature rate constants, k_2 , and activation energies, E , for n-butane and the aromatic hydrocarbons with the literature data. It can be seen that there is generally good agreement with the relative rate data of Cvetanovic and co-workers,²³⁻²⁶ placed on an absolute basis using k_2 (ethylene) = $3.37 \times 10^9 e^{-(1270 \pm 300)/RT}$ liter mole⁻¹ sec⁻¹ determined in this work. The present value for n-butane falls in between those of Herron and Huie²⁷ and of Elias and Schiff.¹²

It can be seen from Table 1.3 that the room temperature rate constants obtained by Mani and Sauer²⁹ using a pulsed radiolysis technique are a factor of 3-6 higher than the present work, possibly because of the complexity of their experimental technique. Similarly, the room temperature rate constant

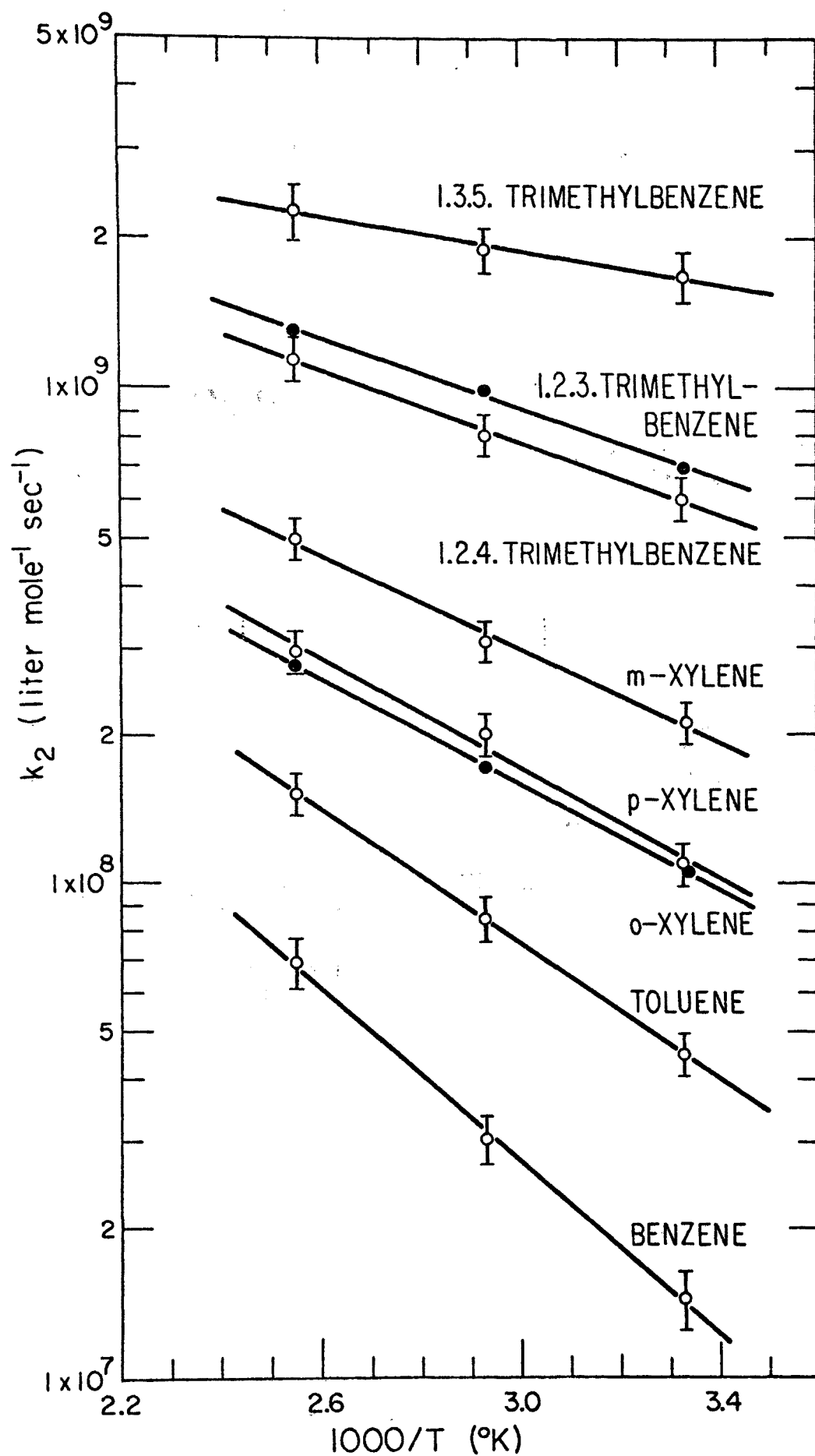


Figure 1.2 Arrhenius plots for the aromatic hydrocarbons

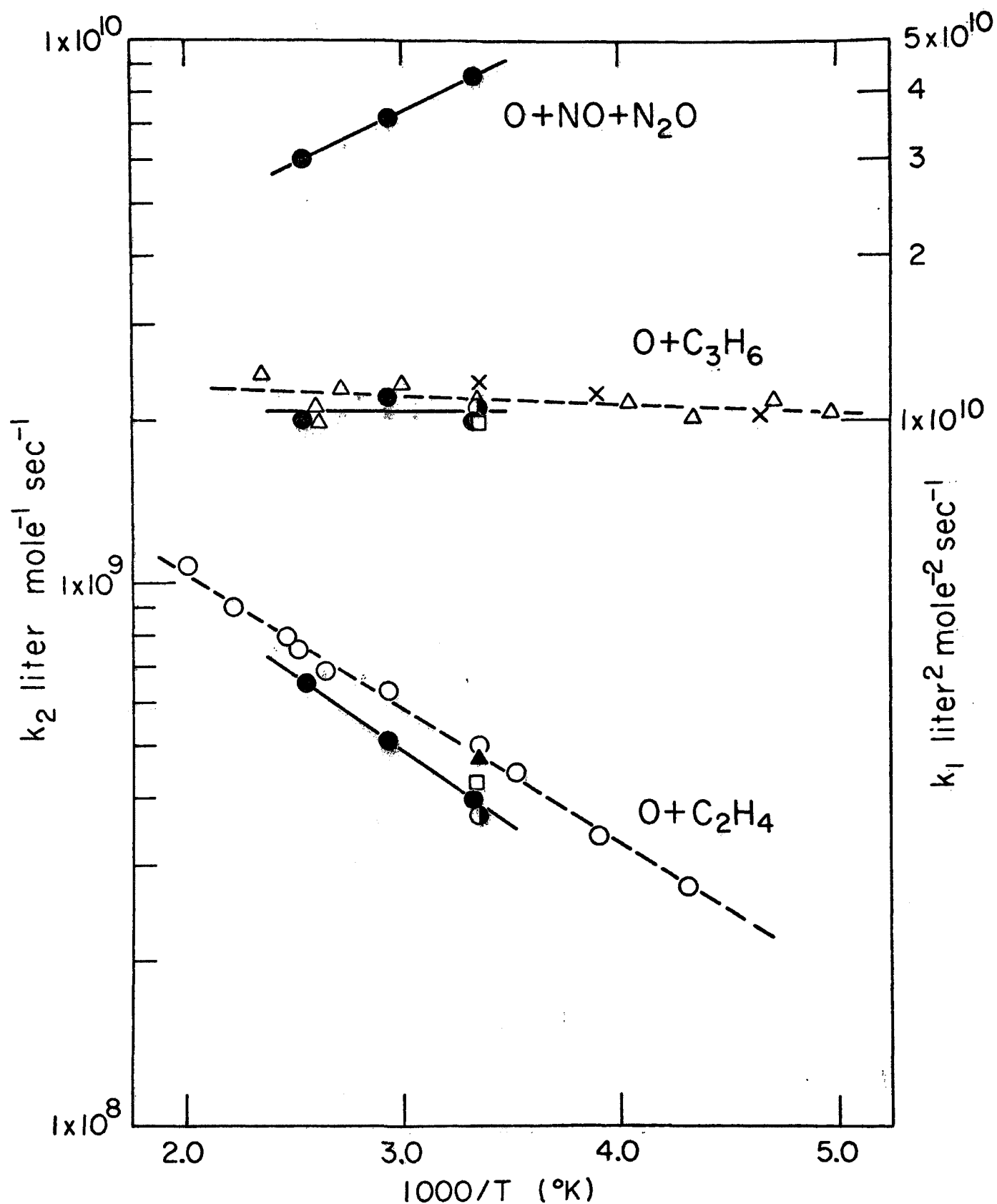


Figure 1.3 Arrhenius plots of $\log k$ against $1000/T$:

—●— This work; —○— Davis et al;¹⁰ —△— Kurylo;⁵
 X Huie et al;⁶ ▲ Kurylo and Huie;¹¹ □ Furuyama et al;⁸
 ● Stuhl and Niki^{7,9}

Table 1.1

Rate constants k_2 for the reaction of $O(^3P)$ atoms with organics. The errors include precision limits derived from least squares standard deviations and estimated accuracy of other parameters such as pressure and composition of mixtures.

Reactant	Temperature °K	$10^{-8} \times k_2$ liter mole ⁻¹ sec ⁻¹
Ethylene	300.7 ± 0.3	4.00 ± 0.40
	341.2 ± 0.5	5.15 ± 0.50
	392.2 ± 0.5	6.58 ± 0.65
Propylene	300.0 ± 0.2	20.1 ± 2.2
	341.2 ± 0.5	22.2 ± 2.3
	392.2 ± 0.5	20.1 ± 2.0
n-Butane	301.4 ± 0.2	0.188 ± 0.02
Benzene	300.3 ± 0.3	0.144 ± 0.02
	341.2 ± 0.5	0.303 ± 0.035
	392.2 ± 0.5	0.69 ± 0.08
Toluene	300.4 ± 0.2	0.450 ± 0.045
	341.2 ± 0.5	0.85 ± 0.09
	392.2 ± 0.5	1.52 ± 0.15
o-Xylene	299.1 ± 0.3	1.05 ± 0.11
	341.2 ± 0.5	1.72 ± 0.18
	392.2 ± 0.5	2.77 ± 0.3
m-Xylene	299.5 ± 0.5	2.12 ± 0.21
	341.2 ± 0.5	3.09 ± 0.3
	392.2 ± 0.5	5.0 ± 0.5
p-Xylene	300.4 ± 0.5	1.09 ± 0.11
	341.2 ± 0.5	2.01 ± 0.2
	392.2 ± 0.5	2.94 ± 0.3
1,2,3-Trimethylbenzene	299.7 ± 0.4	6.9 ± 0.7
	341.2 ± 0.5	9.9 ± 1.0
	392.2 ± 0.5	13.0 ± 1.5
1,2,4-Trimethylbenzene	300.2 ± 0.3	6.0 ± 0.6
	341.2 ± 0.5	8.1 ± 0.8
	392.2 ± 0.5	11.5 ± 1.2
1,3,5-Trimethylbenzene	299.9 ± 0.5	16.8 ± 2.0
	341.2 ± 0.5	18.9 ± 2.0
	392.2 ± 0.5	22.8 ± 3.0
Methoxybenzene	302.4 ± 0.2	0.66 ± 0.7
o-Cresol	301.5 ± 0.2	3.5 ± 0.8

Table 1.1 (cont.)

<u>Reactant</u>	<u>Temperature °K</u>	<u>$10^{-10} \times k_2$ or k_3 (liter² mole⁻² sec⁻¹)</u>
NO(M = N ₂ O)	300.5 ± 0.4	4.29 ± 0.43
	341.2 ± 0.5	3.62 ± 0.33
	392.2 ± 0.5	3.02 ± 0.31
SO ₂ (M = N ₂ O)	299.2 ± 0.5	0.115 ± 0.015
	341.2 ± 0.5	0.175 ± 0.02
	399.2 ± 0.5	0.255 ± 0.03

Table 1.2

Arrhenius parameters for O(³P) atom reactions

<u>Reactant</u>	<u>$A \times 10^{-9}$ (liter mole⁻¹ sec⁻¹)</u>	<u>E (kcal mole⁻¹)</u>
Ethylene	3.37	1.27 ± 0.2
Propylene	2.08	0.00 ± 0.3
Benzene	11.1	3.98 ± 0.4
Toluene	8.2	3.10 ± 0.3
o-Xylene	6.25	2.43 ± 0.3
m-Xylene	7.7	2.15 ± 0.3
p-Xylene	7.9	2.54 ± 0.3
1,2,3-Trimethylbenzene	10.3	1.60 ± 0.3
1,2,4-Trimethylbenzene	9.35	1.65 ± 0.3
1,3,5-Trimethylbenzene	6.05	0.77 ± 0.3
	<u>$A \times 10^{-9}$ (liter² mole⁻² sec⁻¹)</u>	<u>E (kcal mole⁻¹)</u>
NO(M = N ₂ O)	9.6	-0.90 ± 0.2
SO ₂ (M = N ₂ O)	33.2	2.00 ± 0.4

Table 1,3

Comparison of the room temperature rate constants, k_2 , and the activation energies, E, for n-butane and the aromatics from the present work with selected literature values.

Reactant	$10^{-8} \times k_2$ liter mole ⁻¹ sec ⁻¹			E kcal mole ⁻¹		
	Present work	Literature	Derived from relative rates ^{a)}	Present work	Literature	Derived from relative rates ^{a)}
n-Butane	0.188 ± 0.02	0.25 ¹² 0.13 ²⁷	0.18			
Benzene	0.144 ± 0.02	0.28 ± 0.07 ²⁸ 0.36 ± 0.07 ²⁹	0.16	3.98 ± 0.4	4.4 ± 0.5 ²⁸	3.27 ± 0.7
Toluene	0.45 ± 0.045	1.4 ± 0.3 ²⁹		3.10 ± 0.3		2.47 ± 0.4
o-Xylene	1.05 ± 0.11	6.7 ± 1.6 ²⁹		2.43 ± 0.3		
m-Xylene	2.12 ± 0.21	7.7 ± 2.0 ²⁹		2.15 ± 0.3		
p-Xylene	1.09 ± 0.11	4.5 ± 1.4 ²⁹		2.54 ± 0.3		

^{a)} Ref. 23-26. Placed on an absolute basis using $k_2 = (\text{ethylene}) = 3.37 \times 10^9 e^{-(1270 \pm 300)/RT}$ liter mole⁻¹ sec⁻¹.

for benzene of Bonanno et al.²⁸ obtained by discharge flow-mass spectrometry is a factor of 2 higher than the present value, although their activation energy of 4.6 ± 0.5 kcal mole⁻¹, obtained over the range 255-305°K, is in good agreement with that determined in this work.

REFERENCES

1. R. Atkinson and R. J. Cvetanovic, J. Chem. Phys., 55, 659 (1971).
2. R. Atkinson and J. N. Pitts, Jr., J. Phys. Chem., 78, 1780 (1974); 79, 295 (1975); 79, 541 (1975).
3. R. J. Cvetanovic, Can. J. Chem., 36, 623 (1958).
4. F. Kaufman and J. R. Kelso, Symp. Chemiluminescence, Duke University, Durham, USA, (1965).
5. M. J. Kurylo, Chem. Phys. Letters, 14, 117 (1972).
6. R. E. Huie, J. T. Herron and D. D. Davis, J. Phys. Chem., 76, 3311 (1972).
7. F. Stuhl and H. Niki, J. Chem. Phys., 55, 3954 (1971).
8. S. Furuyama, R. Atkinson, A. J. Colussi and R. J. Cvetanovic, Int. J. Chem. Kinet., 6, 741 (1974).
9. F. Stuhl and H. Niki, J. Chem. Phys., 57, 5403 (1972).
10. D. D. Davis, R. E. Huie, J. T. Herron, M. J. Kurylo and W. Braun, J. Chem. Phys., 56, 4868 (1972).
11. M. J. Kurylo and R. E. Huie, J. Chem. Phys., 58, 1258 (1973).
12. L. Elias and H. I. Schiff, Can. J. Chem., 38, 1657 (1960).
13. L. Elias, J. Chem. Phys., 38, 989 (1963).
14. A. A. Westenberg and N. deHaas, Symp. Combust., 12th, Univ. Poitiers, France, 1968, 289 (1969).
15. J. M. Brown and B. A. Thrush, Trans. Faraday Soc., 63, 630 (1967).
16. C. Tanaka, S. Tsuchiya and T. Hikita, J. Fac. Eng. Univ. Tokyo Ser. A, 5, 62 (1967).
17. H. Niki, E. E. Daby and B. Weinstock, Symp. Combust., 12th Univ. Poitiers, France, 1968, 277 (1969).
18. R. Atkinson and R. J. Cvetanovic, J. Chem. Phys., 56, 432 (1972).
19. F. S. Klein and J. T. Herron, J. Chem. Phys., 41, 1285 (1964).
20. M. A. A. Clyne and B. A. Thrush, Proc. Roy. Soc., A269, 404 (1962).
21. T. G. Slanger, B. J. Wood and G. Black, Int. J. Chem. Kinet., 5, 615 (1973).
22. D. D. Davis, Can. J. Chem., 52, 1405 (1974).

REFERENCES (cont.)

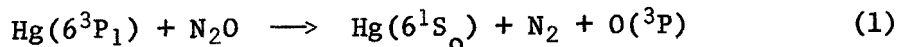
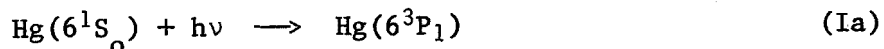
23. R. J. Cvetanovic, J. Chem. Phys., 33, 1063 (1960).
24. R. J. Cvetanovic, Adv. Photochem., 1, 115 (1963).
25. G. Boocock and R. J. Cvetanovic, Can. J. Chem., 39, 2436 (1961).
26. G. R. H. Jones and R. J. Cvetanovic, Can. J. Chem., 39, 2444 (1961).
27. J. T. Herron and R. E. Huie, J. Phys., Chem., 73, 3327 (1969).
28. R. A. Bonanno, P. Kim, J. H. Lee and R. B. Timmons, J. Chem. Phys., 57, 1377 (1972).
29. I. Mani and M. C. Sauer, Jr., Adv. Chem. Ser., 82, 142 (1968).

2. RATE CONSTANTS FOR THE REACTION OF O(³P) ATOMS WITH SELECTED OLEFINS, MONOTERPENES AND UNSATURATED ALDEHYDES

As part of an investigation into the rates and products of the reactions of O(³P) atoms with unsaturated organic compounds involved in the formation of photochemical air pollution, rate constants for the reactions of O(³P) atoms with ketene, acrolein, crotonaldehyde, α-pinene, β-pinene, d-limonene, 1-methylcyclohexene, and 1,3-cyclohexadiene have been determined relative to that for the reaction of O(³P) atoms with cyclopentene over the temperature range 296-423°K. The reaction of O(³P) atoms with cyclopentene has been thoroughly investigated¹ and has been extensively used to determine relative O(³P) atoms reaction rate constants by Cvetanovic and co-workers.^{2,3}

In order to test the experimental system and to place the relative rate constants on an absolute basis, propylene was included in the compounds studied as its absolute rate constant is known to a good degree of accuracy⁴⁻⁸ over the temperature range used in this work.

Experimental. Ground state O(³P) oxygen atoms were generated by the mercury photosensitization of nitrous oxide at 253.7 nm:

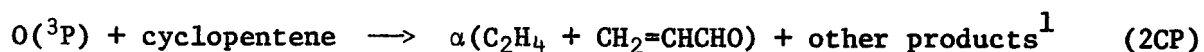


In order to minimize short wavelength photolysis of the reactants and products, the 253.7 nm resonance radiation from a low pressure mercury arc was passed through a Corning 7-54 filter to remove wavelengths ≤235 nm. A conventional static high vacuum system was used, fitted with greaseless stopcocks to minimize absorption of reagents and products. The cylindrical quartz reaction cell, diameter 5.0 cm, length 20.0 cm, had a volume of 393 cm³ and, in order to ensure homogeneity, the gas mixture was circulated in a total volume of 1043 cm³ by means of a magnetically driven all-glass circulating fan. The reaction cell and circulating system were enclosed by a furnace where temperature could be held constant to better than ±1°K over the temperature range 296-423°K. Reactant pressures were measured using either a 0-20 torr Wallace and Tiernan FA160 absolute pressure gauge or a 0-800 torr mercury manometer.

Reactant purities and purification procedures were as follows: ketene was prepared by the pyrolysis of acetone⁹ and degassed and vacuum distilled at 196°K. The resulting ketene purity level was ≥98% with acetone being the major impurity. All other reagents were ≥98% stated purity and were further purified by thorough degassing at 196°K or 77°K and bulb-to-bulb distillation in vacuum. As a further check on the reactant purities, the reagents used were gas chromatographed on a 10 ft × 1/8" β,β'-oxydipropionitrile (9.7% on 80/100 mesh Firebrick) column using a flame ionization detector, and mass spectra were obtained on a Finnigan 3100D quadrupole mass spectrometer. In all cases purity levels consistent with the above were observed.

Photolysis times were typically 5-15 minutes during which 5 cm³ samples were periodically removed for analysis by a Carle gas sampling valve. The sample was split into two streams and N₂ from the N₂O and C₂H₄ from cyclopentene were analyzed by gas chromatography. N₂ was measured on a 5 ft × 1/4" Linde Molecular Sieve 13X column at room temperature by a thermal conductivity detector, while C₂H₄ was analyzed on a 6 ft × 1/8" Poropak Q column at room temperature by a flame ionization detector. (18.9 ± 0.4)% C₂H₄ in N₂ was used to periodically check retention times and relative responses in the detectors.

Results. Relative rate constants were determined using the same technique developed by Cvetanovic and co-workers.^{2,3} From the reaction scheme:



with rate constants k_2^{CP} and k_2^{A} respectively, it can be shown that

$$\frac{(\text{C}_2\text{H}_4/\text{N}_2)^{\text{A}=0}}{(\text{C}_2\text{H}_4/\text{N}_2)^{\text{A}}} = 1 + \frac{k_2^{\text{A}}[\text{A}]}{k_2^{\text{CP}}[\text{CP}]} \quad (\text{I})$$

where $(\text{C}_2\text{H}_4/\text{N}_2)^{\text{A}=0}$ and $(\text{C}_2\text{H}_4/\text{N}_2)^{\text{A}}$ are the C₂H₄/N₂ yield ratios in the absence and presence of reactant A, respectively. In all cases runs were carried out in the absence of cyclopentene to check that ethylene was not produced from the reaction of O(³P) atoms with reactant A. Only for ketene and acrolein was any ethylene production observed. However, in both cases the C₂H₄ pro-

duction from the reactant was calculated to cause less than 2% error in the determination of the relative rate constants.

The C_2H_4/N_2 ratio for the reaction of $O(^3P)$ atoms with cyclopentene was determined before and after every rate determination and was observed to be constant to better than $\pm 5\%$ at any given temperature providing that the reaction cell was heated to $\geq 373^\circ K$ under vacuum between rate constant determinations for the pinenes, limonene, acrolein and crotonaldehyde. The C_2H_4/N_2 ratio from the reaction of $O(^3P)$ atoms with cyclopentene alone was determined to be 0.23 ± 0.02 over the pressure range 200–500 torr at temperatures from 296–623°K in good agreement with the work of Cvetanovic, Ring and Doyle.¹

For each run, at a given reactant/cyclopentene ratio, several determinations of the ethylene and nitrogen yields were carried out as a function of time. Typical results are shown in Figure 2.1, which shows the C_2H_4 yield versus N_2 yield for cyclopentene alone and for four runs with differing limonene/cyclopentene ratios.

Relative rate constants k_2^A/k_2^B determined from the slopes of the plots of C_2H_4 yield versus N_2 yield are plotted in Arrhenius form in Figures 2.2 and 2.3, and given in Table 2.1. The relative Arrhenius parameters,

$$\frac{k_2^A}{k_2^{CP}} = \frac{A^A}{A^{CP}} e^{-(E^A - E^{CP})/RT}, \text{ obtained by least squares analysis, are given in}$$

Table 2.2, along with the absolute Arrhenius parameters obtained by using $k_2(\text{propylene}) = 2.4 \times 10^9 e^{-76/RT}$ liter mole⁻¹ sec⁻¹, ($k_2(\text{propylene}) = 2.10 \times 10^9$ liter mole⁻¹ sec⁻¹ at 298°K), derived from the recent literature rate constant data.⁴⁻⁸

Discussion. In all cases, experiments were carried out under conditions of low conversion where secondary reactions of $O(^3P)$ atoms with the products should have been negligible. Similarly, the reaction of $O(^3P)$ atoms with impurities was estimated to cause errors in the measured rate constants of $\leq 5\%$.

The value of $k_2(\text{propylene})/k_2(\text{cyclopentene})$ of 0.181 ± 0.010 at $296 \pm 2^\circ K$ determined here is in good agreement with the ratio of 0.192 obtained by Cvetanovic.² Similarly, the present ratio of $k_2(\text{toluene})/k_2(\text{cyclopentene}) = 0.026 \pm 0.003$ at $423 \pm 1^\circ K$ agrees well with that of 0.023 interpolated from the data of Jones and Cvetanovic.¹⁰ When placed on an absolute basis using the derived rate expression for $O(^3P) + \text{cyclopentene}$, the value of $k_2(\text{toluene}) = (2.4 \pm 0.3) \times 10^8$ liter mole⁻¹ sec⁻¹ at $423 \pm 1^\circ K$ agrees within experimental error with the absolute value of 2.05×10^8 liter mole⁻¹ sec⁻¹ calculated from

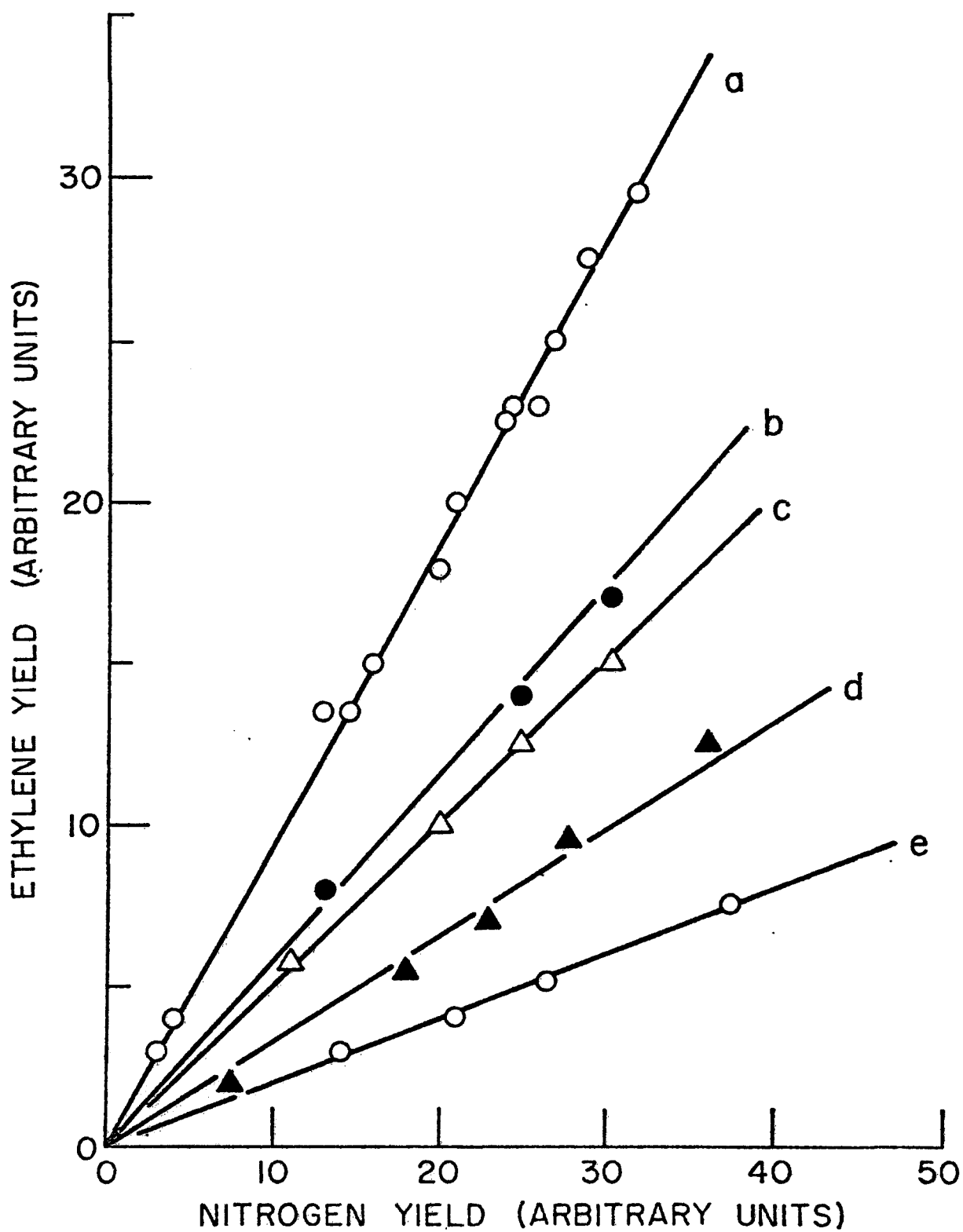


Figure 2.1 Plots of ethylene yield versus N_2 yield for: a) cyclopentene alone, b-e) cyclopentene/limonene = 8.64(b); 6.54(c); 3.24(d); 1.91(e)

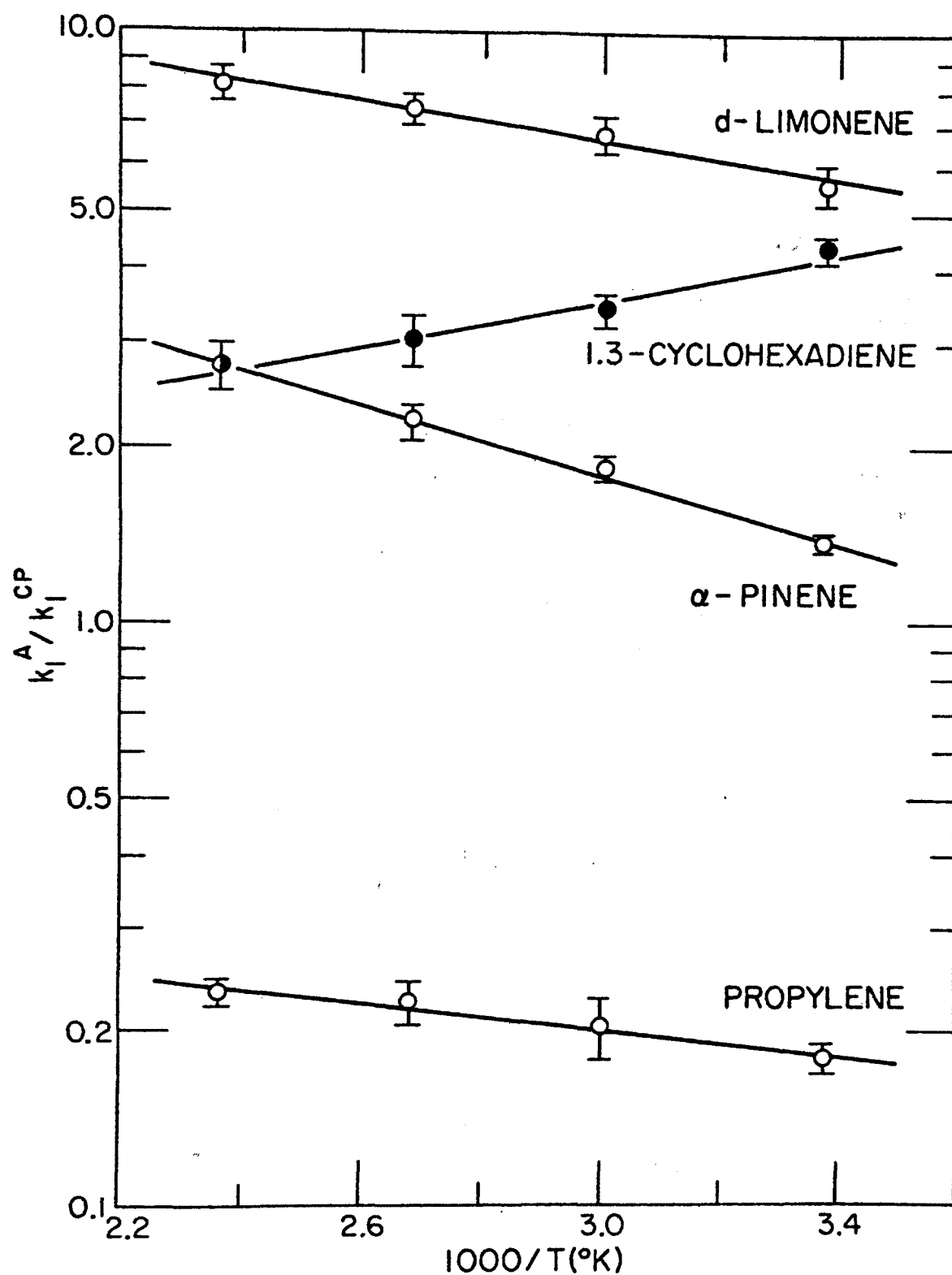


Figure 2.2 Arrhenius plots of $\log k_2^A/k_2^{CP}$ against $1000/T$

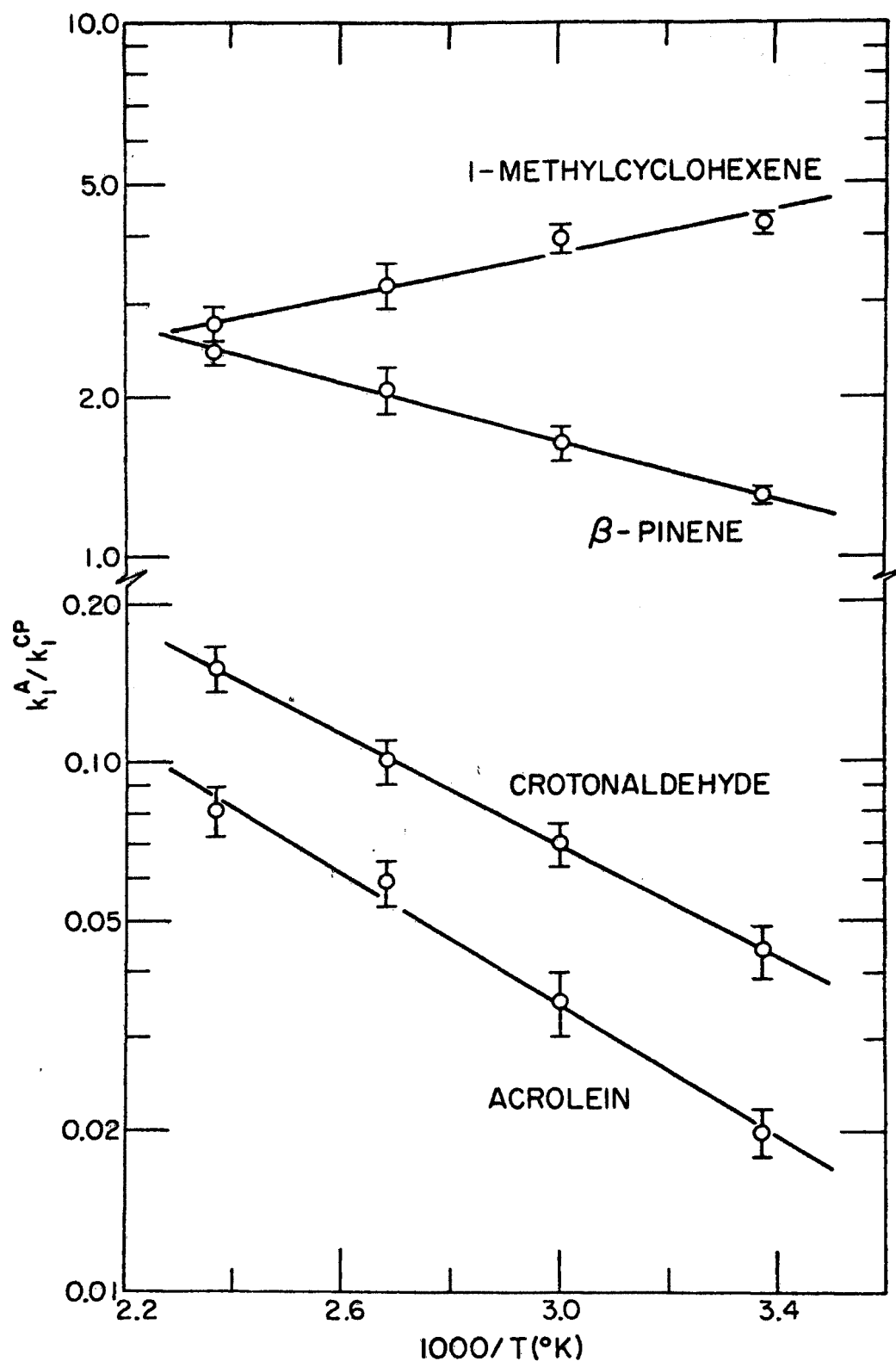


Figure 2.3 Arrhenius plots of $\log k_2^A/k_2^{CP}$ against $1000/T$

Table 2,1

Relative rate constants k_2^A/k_2^{CP} for the reaction of $O(^3P)$ atoms. The error limits are the least square standard deviations.

<u>Reactant A</u>	<u>Temperature °K</u>	<u>k_2^A/k_2^{CP}</u>
Propylene	296 ± 2	0.181 ± 0.010
	333 ± 1	0.203 ± 0.026
	373 ± 1	0.225 ± 0.019
	423 ± 1	0.231 ± 0.012
α -Pinene	296 ± 2	1.38 ± 0.05
	333 ± 1	1.84 ± 0.09
	373 ± 1	2.22 ± 0.15
	423 ± 1	2.73 ± 0.27
β -Pinene	296 ± 2	1.30 ± 0.05
	333 ± 1	1.64 ± 0.11
	373 ± 1	2.07 ± 0.20
	423 ± 1	2.41 ± 0.12
d-Limonene	296 ± 2	5.61 ± 0.45
	333 ± 1	6.74 ± 0.50
	373 ± 1	7.45 ± 0.45
	423 ± 1	8.16 ± 0.57
1-Methylcyclohexene	296 ± 2	4.21 ± 0.17
	333 ± 1	3.93 ± 0.25
	373 ± 1	3.22 ± 0.32
	423 ± 1	2.71 ± 0.27
1,3-Cyclohexadiene	296 ± 2	4.33 ± 0.20
	333 ± 1	3.43 ± 0.24
	373 ± 1	3.05 ± 0.31
	423 ± 1	2.74 ± 0.27

Table 2.1 (cont.)

<u>Reactant A</u>	<u>Temperature °K</u>	<u>k_2^A/k_2^{CP}</u>
Ketene	296 ± 2	0.024 ± 0.003
Acrolein	296 ± 2	0.020 ± 0.002
	333 ± 1	0.035 ± 0.005
	373 ± 1	0.059 ± 0.006
	423 ± 1	0.081 ± 0.009
Crotonaldehyde	296 ± 2	0.044 ± 0.005
	333 ± 1	0.070 ± 0.007
	373 ± 1	0.100 ± 0.010
	423 ± 1	0.150 ± 0.015
Toluene	423 ± 1	0.026 ± 0.003

Table 2.2

Arrhenius parameters for the reaction of $O(^3P)$ atoms. The indicated errors in the activation energies are the least square standard deviations.

Reactant A	A^A/A^{CP}	$(E^A - E^{CP}) \text{ kcal mole}^{-1}$	$A^A \text{ liter mole}^{-1} \text{ sec}^{-1 a)}$	$E^A \text{ kcal mole}^{-1 a)}$
Propylene	0.43	0.50 ± 0.08	2.4×10^9	0.076
Cyclopentene	1.00	0.00	5.6×10^9	-0.43 ± 0.08
α -Pinene	13.46	1.34 ± 0.06	7.5×10^{10}	0.91 ± 0.14
β -Pinene	10.77	1.24 ± 0.06	6.0×10^{10}	0.82 ± 0.14
d-Limonene	19.63	0.72 ± 0.07	1.1×10^{11}	0.30 ± 0.15
1-Methylcyclohexene	0.95	-0.90 ± 0.14	5.3×10^9	-1.33 ± 0.22
1,3-Cyclohexadiene	0.92	-0.89 ± 0.11	5.1×10^9	-1.32 ± 0.18
Acrolein	2.46	2.82 ± 0.19	1.4×10^{10}	2.40 ± 0.27
Crotonaldehyde	2.62	2.41 ± 0.05	1.5×10^{10}	1.98 ± 0.13

a) Placed on an absolute basis using $k_2(\text{propylene}) = 2.4 \times 10^9 e^{-76/RT} \text{ liter mole}^{-1} \text{ sec}^{-1}$. ⁴⁻⁸

the Arrhenius parameters obtained recently in these laboratories¹¹ using a modulation technique. Furthermore, from the activation energy for cyclopentene ($E = -0.43 \pm 0.08$ kcal mole⁻¹) an activation energy for $O(^3P)$ + toluene of $E = 2.8$ kcal mole⁻¹ can be obtained from the data of Jones and Cvetanovic¹⁰ in good agreement with $E = 3.10 \pm 0.3$ kcal mole⁻¹ determined recently.¹¹

Table 2.3 compares the room temperature rate constants and the activation energies determined in the present work for the reaction of $O(^3P)$ atoms with ketene, acrolein and crotonaldehyde with the literature values determined using discharge flow techniques.¹²⁻¹⁷ There is seen to be general agreement within the likely experimental errors for acrolein and crotonaldehyde,¹²⁻¹⁴ and for ketene, the present rate constant is in good agreement with that determined recently by Mack and Thrush,¹⁵ but lies between those of Jones and Bayes¹⁶ and of glass et al.¹⁷

It can be seen from Table 2.2 that cyclopentene, 1,3-cyclohexadiene and 1-methylcyclohexene have similar preexponential factors and negative activation energies. This behavior is similar to that observed for other simple olefins such as cis-2-butene and tetramethylethylene.¹⁸ Negative activation energies have also been reported for the other group VIa atoms with olefins¹⁹ and seem to be a general phenomena for the reaction of group VIa atoms with olefins of low ionization potential. Possible reasons for the observation of negative Arrhenius activation energies have been discussed by previous workers.¹⁸⁻²¹ Two recently postulated reasons for the observation of negative Arrhenius activation energies are that either the preexponential factor is temperature dependent^{18,19,21} or that there is a temperature dependent potential energy curve crossing probability.²⁰

However, α -pinene, β -pinene and d-limonene have preexponential factors which are a factor of ~ 10 -20 higher than those for cyclopentene, 1-methylcyclohexene and 1,3-cyclohexadiene and have low but positive activation energies. It may be that for these more complex molecules abstraction reactions are occurring together with addition of $O(^3P)$ atoms to the double bond. Thus the preexponential factors for $O(^3P)$ atom abstraction from cyclopentane and cyclohexane are 1.3×10^{11} liter mole⁻¹ sec⁻¹ and 2.2×10^{11} liter mole⁻¹ sec⁻¹ respectively,^{22,23} while the preexponential factors for $O(^3P)$ atoms addition to simple olefins are in the region of 5×10^9 liter mole⁻¹ sec⁻¹.^{22,24-27} Similar behavior is postulated to occur in the case of the

Table 2.3

Comparison of the room temperature rate constants, k_2 , and activation energies, E , for ketene, acrolein and crotonaldehyde from the present work with literature values.

<u>Reactant</u>	<u>$k_2 \times 10^{-8}$ liter mole⁻¹ sec⁻¹</u>		<u>E kcal mole⁻¹</u>	
	<u>Present work</u>	<u>Literature</u>	<u>Present work</u>	<u>Literature</u>
Ketene	2.78 ± 0.35	3.4 ± 0.3^{15} 1.7 ± 0.4^{16} 5.3^{17}		
Acrolein	2.32 ± 0.23	$1.6^{12,13}$	2.40 ± 0.27	$2.0^{12,13}$
Crotonaldehyde	5.10 ± 0.58	5^{14}	1.98 ± 0.13	2.3^{14}

reaction of $O(^3P)$ atoms with 1-butene where the abstraction reaction may become important above $\sim 260^\circ K$.

REFERENCES

1. R. J. Cvetanovic, D. F. Ring and L. C. Doyle, J. Phys. Chem., 75, 3056 (1971).
2. R. J. Cvetanovic, Adv. Photochem., 1, 115 (1963).
3. R. J. Cvetanovic, J. Chem. Phys., 30, 19 (1959); 33, 1063 (1960).
4. R. Atkinson and J. N. Pitts, Jr., J. Phys. Chem., 78, 1780 (1974).
5. F. Stuhl and H. Niki, J. Chem. Phys., 55, 3954 (1971).
6. M. J. Kurylo, Chem. Phys. Letters, 14, 117 (1972).
7. R. Atkinson and J. N. Pitts, Jr., Chem. Phys. Letters, 27, 467 (1974).
8. S. Furuyama, R. Atkinson, A. J. Colussi and R. J. Cvetanovic, Int. J. Chem. Kinetics, 6, 741 (1974).
9. J. W. Williams and C. D. Hurd, J. Org. Chem., 5, 122 (1940).
10. G. R. H. Jones and R. J. Cvetanovic, Can. J. Chem., 39, 2444 (1961).
11. R. Atkinson and J. N. Pitts, Jr., J. Phys. Chem., 79, 295 (1975).
12. R. D. Cadle and E. R. Allen, "Chemical Reactions in Urban Atmospheres," C. S. Tuesday, Ed., Elsevier, p. 63 (1971).
13. R. D. Cadle, S. S. Lin and R. F. Hausman, Jr., Chemosphere, 1, 15 (1972).
14. R. D. Cadle, H. H. Wickman, C. B. Hall and K. M. Eberle, paper presented at 167th American Chemical Society Meeting, Los Angeles, California (1974).
15. G. P. R. Mack and B. A. Thrush, J. Chem. Soc., Faraday Trans. I., 70, 187 (1974).
16. I. T. N. Jones and K. D. Bayes, Proc. Roy. Soc., A335, 567 (1973).
17. R. W. Carr, Jr., I. D. Gay, G. P. Glass and H. Niki, J. Chem. Phys., 49, 846 (1968).
18. D. D. Davis, R. E. Huie and J. T. Herron, J. Chem. Phys., 59, 628 (1973).
19. D. D. Davis and R. B. Klemm, Int. J. Chem. Kinet., 5, 841 (1973).
20. J. Connor, A. Van Roodselaar, R. W. Fair and O. P. Strausz, J. Amer. Chem. Soc., 93, 560 (1971).
21. R. Atkinson and R. J. Cvetanovic, J. Chem. Phys., 56, 432 (1972).
22. J. T. Herron and R. E. Huie, J. Phys. Chem., Ref. Data, 2, 467 (1963), and references therein.

REFERENCES (cont.)

23. J. T. Herron and R. E. Huie, J. Phys. Chem., 73, 3327 (1969).
24. M. J. Kurylo, Chem. Phys. Letters, 14, 117 (1972).
25. R. Atkinson and J. N. Pitts, Jr., Chem. Phys. Letters, 27, 467 (1974).
26. D. D. Davis, R. E. Huie, J. T. Herron, M. J. Kurylo and W. Braun, J. Chem. Phys., 56, 4868 (1972).
27. R. E. Huie, J. T. Herron and D. D. Davis, J. Phys. Chem., 76, 3311 (1972).

3. THE REACTION OF $O(^3P)$ ATOMS WITH TOLUENE AND 1-METHYLCYCLOHEXENE

As part of an investigation into the rates and products of the reactions of $O(^3P)$ atoms with a variety of unsaturated organic compounds, the products obtained from the reaction of $O(^3P)$ atoms with toluene and 1-methylcyclohexene have been studied in order to determine the effect of aromaticity on the reaction mechanism.

Experimental. The experimental system has been described in detail in Section 2 of this report, and only the essential details will be given here. Ground state oxygen atoms were produced by the mercury photosensitization of N_2O in a closed circulating reaction system. The volumes of the reaction and circulating systems were 4000 cm^3 and 1043 cm^3 for the studies on toluene and 1-methylcyclohexene, respectively. The reaction system was enclosed by a furance whose temperature could be held constant to better than $\pm 1^\circ\text{K}$ over the temperature range $295\text{--}425^\circ\text{K}$.

5 cm^3 samples were periodically removed for analysis using a Carle gas sampling valve. In all cases, the N_2 yield from the N_2O photosensitization was used as an internal actinometer to monitor the number of $O(^3P)$ atoms produced during the irradiations.

The experimental details for the two reaction systems studied are as follows:

$O(^3P)$ + toluene

Reactions were carried out at $373 \pm 2^\circ\text{K}$ in order to avoid problems associated with adsorption of reaction products on the glass and/or stainless steel components of the gas sampling system. The product samples were split into two fractions: CO and N_2 were analyzed by gas chromatography on a $5\text{ ft} \times \frac{1}{4}"$ Linde Molecular Sieve 13X column at $296 \pm 2^\circ\text{K}$ using a thermal conductivity detector, while the organic products were detected by gas chromatography using a flame ionization detector. Thus, CH_4 and C_2H_6 were analyzed on a $6\text{ ft} \times \frac{1}{8}"$ Porapak Q column at $296 \pm 2^\circ\text{K}$ while the volatile phenolic products were analyzed on a $10\text{ ft} \times \frac{1}{8}"$ 3% polyphenyl ether on DCMS Chromasorb W column at $388 \pm 2^\circ\text{K}$. In all cases gas chromatographic peaks were identified by comparison of their retention times with those of authentic samples and were quantified by calibration using known pressures of the reagents in the reaction system.

A few subsidiary experiments were carried out at $296 \pm 2^\circ\text{K}$ in a 9.4 cm

pathlength cylindrical quartz cell fitted with NaCl end windows. The reactions were monitored by in-situ infrared absorption spectroscopy using a Perkin-Elmer 221 spectrophotometer.

All chemicals used were of $\geq 98\%$ purity.

O(3P) + 1-methylcyclohexene

CO and N₂ were analyzed as described above while the volatile organic products were analyzed by gas chromatography on a 10 ft \times 1/8" 9.7% β,β -oxydipropionitrile on 80/100 mesh Firebrick column at $363 \pm 2^\circ\text{K}$ using a flame ionization detector.

Identification of the gas chromatographic peaks was made by comparison of their retention times with those of authentic samples, wherever possible, and for the organic products, by elucidation of their structures from nmr, infrared and mass spectrometric data.

In order to have sufficient reaction product to obtain pure samples for spectral identification, a flow system similar to that described by Grovenstein and Mosher¹ was used and samples of the reaction products separated and collected by preparative gas chromatography. A flow of $3.5 \text{ cm}^3 \text{ sec}^{-1}$ of N₂O was bubbled through mercury, then through 1-methylcyclohexene and the resulting flow stream irradiated in a quartz photolysis tube by a spiral low pressure mercury resonance lamp. Condensable products and unreacted 1-methylcyclohexene were trapped out at $196 \pm 2^\circ\text{K}$, with a typical reactant conversion of $\sim 11\%$. This flow system was operated at $296 \pm 2^\circ\text{K}$ and 735 ± 10 torr total pressure (mainly N₂O). Identical gas chromatographic peaks were observed with this system as with experiments carried out at lower conversions and at lower total pressures in the closed circulating system. With the β,β -oxydipropionitrile column operated at $296 \pm 2^\circ\text{K}$, six of the seven product peaks were collected in quantities sufficient to obtain nuclear magnetic resonance (NMR) (Varian A60 and A60D instruments), infrared (Perkin-Elmer 221 spectrophotometer) and mass spectra (Finnigan 3100D and 3200E quadrupole mass spectrometers).

1-Methyl-1,2-epoxycyclohexane was synthesized by an adaption of Hibbert and Burt's procedure.² 3.0 cm^3 of 1-methylcyclohexene (0.025 moles) was added to a solution of 5.2 gm of m-chloroperbenzoic acid (85% purity, 0.025 moles) in 100 cm^3 of methylene chloride. The solution was stirred for 3-4 hours at 273°K . The precipitated m-chlorobenzoic acid was removed by filtration and the resulting solution was washed with a) excess 10% sodium sulfite

solution to remove any remaining peracid, b) 10% sodium carbonate to remove any remaining benzoic acid and c) water to remove carbonate and any traces of benzoic acid. The solution was then dried over anhydrous sodium sulfate, filtered and the methylene chloride removed under vacuum. Gas chromatographic analysis of the product showed the 1-methyl-1,2-epoxycyclohexane to be $\geq 98\%$ purity, with the remainder being mainly unreacted 1-methylcyclohexene. Commercially available 1-methylcyclohexene and 2-methylcyclohexanone had purity levels $\geq 98\%$ as confirmed by combined gas chromatography-mass spectrometric analyses.

Calibration of the gas chromatograph for CO and N₂ was carried out by gas sampling known pressures of these compounds.

Calibration using liquid samples of 1-methyl-1,2-epoxycyclohexane and 2-methylcyclohexanone showed them to produce equal responses, in terms of peak areas, and it was assumed that this response was valid for liquid injection of all the other C₇H₁₂O isomers observed in this work.³ Gas phase sampling via the Carle valve from the reaction system of identical pressures of 1-methyl-1,2-epoxyhexane and 2-methylcyclohexanone yielded a relative response for these two compounds of 2.43:1 at $296 \pm 2^\circ\text{K}$ and 1.17:1 at $423 \pm 1^\circ\text{K}$. This deviation from unity of the relative responses for gas sampling probably results from absorption of the more polar compounds on the stainless steel components of the gas sampling system. When the relative amounts of 1-methyl-1,2-epoxycyclohexane and 2-methylcyclohexanone produced at 400 torr total pressure and $296 \pm 2^\circ\text{K}$ were corrected for the relative response factor of the gas sampling system, they were within 2% of that obtained by direct liquid injection of the product mixture collected from the flow system at 735 ± 10 torr total pressure and $296 \pm 2^\circ\text{K}$. Responses for gas sampling of the other products at 296°K were then derived by comparison of the direct liquid injection of the flow study products with the gas phase sampling of the reaction carried out at 400 torr total pressure, assuming the product distribution to be identical.

Gas chromatographic calibration factors for samples from the gas phase system at $423 \pm 1^\circ\text{K}$ were based on the fact that only a 17% difference in response between 1-methyl-1,2-epoxycyclohexane and 2-methylcyclohexanone was observed. Responses for the other products were derived by interpolation based on their relative retention times. A maximum error of $\pm 10\%$ in the product yields was expected in this case.

Results and Discussion

O(³P) + Toluene. This reaction was studied extensively at $373 \pm 2^\circ\text{K}$ over the pressure range of 80-400 torr of N_2O , with toluene pressures ranging from 2-10 torr. The reaction products observed were CO, o-cresol, p-cresol, phenol, an unknown and a reddish-yellow tar. The product yields, relative to the N_2 yield, are given in Table 3.1 along with the yields of the volatile addition products expressed as a percentage of the total volatile addition products. No benzaldehyde, benzyl alcohol or biphenyl were detected. In addition, small amounts of CH_4 and C_2H_6 were observed in experiments carried out at $296 \pm 2^\circ\text{K}$ and $423 \pm 1^\circ\text{K}$, with the CH_4/N_2 ratio being determined as 0.01 at $296 \pm 2^\circ\text{K}$.

Room temperature experiments, monitoring the reaction by infrared absorption spectroscopy, showed the production of CO and CH_4 and small amounts of a very broad carbonyl band at $\sim 1725\text{ cm}^{-1}$. The latter band remained after evacuation of the cell suggesting that it was associated with the tar. An NMR spectrum of the reddish-yellow tar material in acetone- d_6/CDCl_3 showed no evidence of aromatic protons. Instead a very broad signal from methine protons and from protons in methyl groups were observed, suggesting a mixture of materials.

Table 3.1 also gives the product data obtained at room temperature by Jones and Cvetanovic⁴ and by Grovenstein and Mosher.¹ It can be seen that there is general agreement on the products obtained from this reaction, and that the volatile addition products account for only a small fraction (15-25%) of the O(³P) atoms consumed. However, there are differences in the relative amounts of the individual phenolic compounds observed, with Grovenstein and Mosher¹ finding more m-cresol than either Jones and Cvetanovic⁴ or the present work. Also, the present observation of phenol is in agreement with Grovenstein and Mosher,¹ while Jones and Cvetanovic⁴ did not detect this product. In all cases extensive tar formation was observed, and the present finding of the lack of aromaticity in the tar is in agreement with the work of Boocock and Cvetanovic⁵ on the reaction of O(³P) atoms with benzene. The detection of CH_4 and C_2H_6 in the present work suggests the presence of CH_3 radicals which can abstract an H atom to form CH_4 or recombine to form C_2H_6 .

The available evidence suggests that the initial reaction step is that of addition of an oxygen atom to the aromatic ring, predominately in the ortho position, followed by isomerization to phenolic compounds or ring

Table 3.1

Product yields observed from the reaction of $O(^3P)$ atoms with toluene

Product A	This work ^{a)}		Ref 4 ^{b)}		Ref 1 ^{c)}
	A/N ₂	% Yield ^{d)}	A/N ₂	% Yield ^{d)}	% Yield ^{d)}
Phenol	0.02	8.7 ± 1.9	--	--	8.0
o-Cresol	0.20	80.5 ± 1.7	0.12	78	58.8
m-Cresol	{ 0.01 ^{e)}	{ 4.7 ± 0.7 ^{e)}	{ 0.034 ^{f)}	{ 22 ^{f)}	15.3
p-Cresol					17.9
CO	0.140 ± 0.018		0.093(100 torr) -0.059(680 torr)		
H ₂ O			0.07		
CH ₄	0.01 ^{g)}				
C ₂ H ₆	0.005 ^{g)}				

a) $P_{\text{total}} = 80\text{--}400$ torr N₂O; T = 373 ± 2°K. Includes 6.1% of an unknown.

b) $P_{\text{total}} = 385 \pm 5$ torr N₂O; T = 298°K. No pressure dependence of the cresol yields noted on pressure from 100–680 torr N₂O.

c) $P_{\text{total}} = 740 \pm 4$ torr N₂O; T = 303 ± 1°K. Volatile addition products analyzed only.

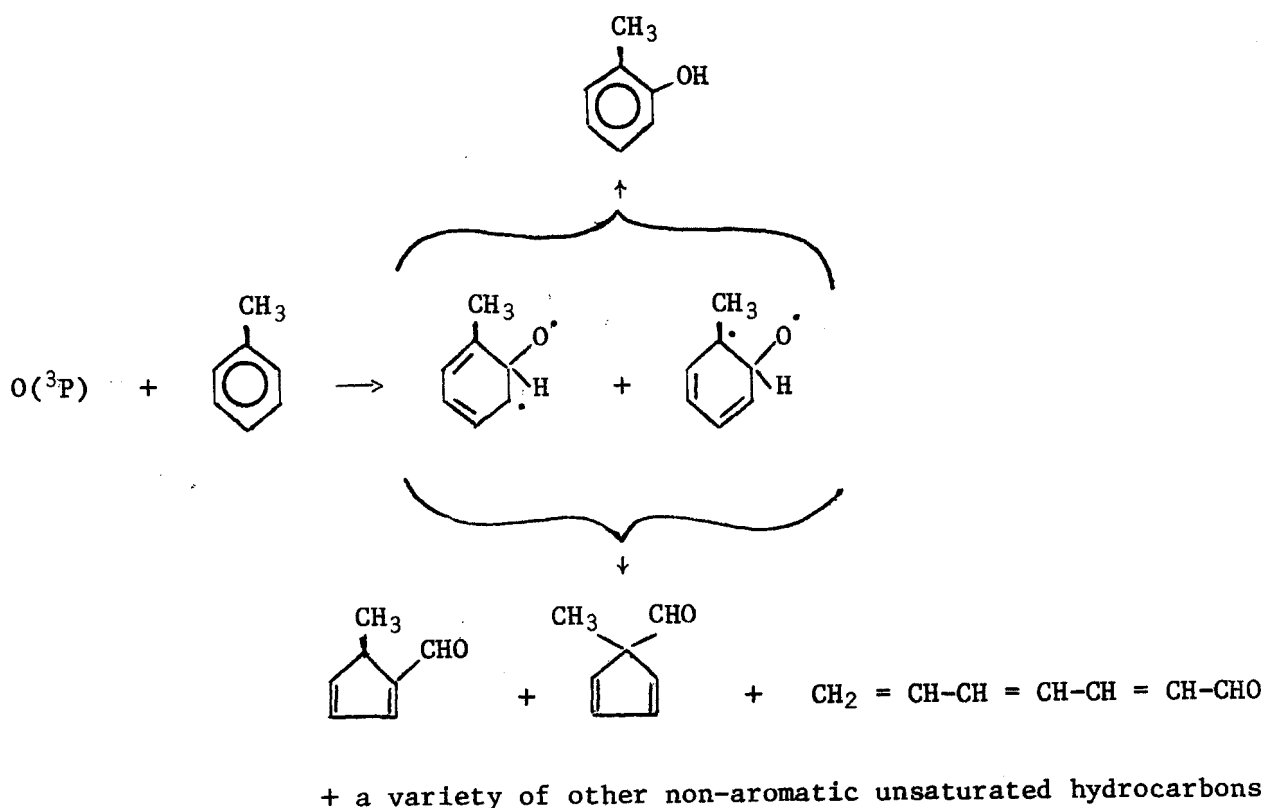
d) Yield of the observed volatile addition products = 100%.

e) m-, p-cresol not separated; mass spectra shown m-cresol ≤10% of the p-cresol.

f) m-, p-cresol not separated; infrared spectra show m-cresol ≤4–5% of total cresol yield.

g) At 296 ± 2°K.

cleavage contraction to form a variety of highly reactive olefinic species which will consume $O(^3P)$ atoms in secondary reactions, ultimately producing a tar or polymer containing few or no aromatic protons. Thus at 373°K, the rate constant for the reaction of $O(^3P)$ atoms with toluene is 1.25×10^8 liter mole⁻¹ sec⁻¹ while it is expected that the rate constants for the reaction of $O(^3P)$ atoms with the olefinic product species will be $\sim 1 \times 10^{10}$ liter mole⁻¹ sec⁻¹.⁷⁻¹⁰ Also, it is likely that the reaction will undergo fewer secondary reactions at higher temperatures where the rate constant for $O(^3P)$ atoms with toluene will approach those for $O(^3P)$ atoms with the olefinic products, as may be indicated by the data in Table 3.1. A possible reaction sequence is shown below for attack at the ortho position:



The formation of phenol presumably proceeds by addition of an $O(^3P)$ atom at the 1-position followed by an intermolecular methyl migration and subsequent H atom abstraction by the phenoxy radical to form phenol and by the methyl radical to form CH_4 .

$O(^3P)$ + Methylcyclohexene. The products from this reaction were studied at $296 \pm 2^\circ\text{K}$ over the range 55–400 torr total pressure of N_2O and at $423 \pm 1^\circ\text{K}$

at 170 torr total pressure of N_2O with typically 1-3 torr of 1-methylcyclohexene. As noted above, the product peaks observed on the β,β -oxydipropionitrile column under these conditions were identical with those obtained from the flow system at $296 \pm 2^\circ\text{K}$ and 735 ± 10 torr total pressure of N_2O . The six products collected by preparatory gas chromatography from the flow system study were all shown by combined gas chromatography-mass spectrometry to be isomers of molecular formula $\text{C}_7\text{H}_{12}\text{O}$. NMR and infrared spectra were obtained for all of these products and two of the major ones were found to have NMR, infrared and mass spectra and gas chromatographic retention times identical to those of 2-methylcyclohexanone and 1-methyl-1,2-epoxycyclohexane. The NMR, infrared and mass spectra of the other collected unknowns allowed them to be identified as 1-methylcyclopentenecarbaldehyde, methylcyclopentylketone, 2-methyl-5-hexenal and a product peak which was identified as a mixture of 1-hepten-6-one and 2-methyl-2-hexenal, the latter probably a mixture of cis and trans-, all of which are in accord with the mechanism shown below. The mass spectrum of the seventh product peak was obtained using combined gas chromatographic-mass spectrometric analysis, and its possible identity is discussed below. CO was also detected as a reaction product.

Table 3.2 shows the product/ N_2 ratios obtained at $296 \pm 2^\circ\text{K}$ and $423 \pm 1^\circ\text{K}$, while Figure 3.1 shows some of the product/ N_2 ratios at $296 \pm 2^\circ\text{K}$ plotted against the N_2O pressure. It can be seen that all of the addition products show a slight increase in yield with increasing total pressure as expected if they arise from a highly energetic intermediate which can be quenched to yield stable addition products. On the other hand, the CO yield decreases with increasing pressure, as expected for a fragmentation product formed from an energetic intermediate. The data at $423 \pm 1^\circ\text{K}$ are very similar to those obtained at $296 \pm 2^\circ\text{K}$ showing that the effect of temperature on the system to be very slight.

By analogy with the very extensive work of Cvetanovic and co-workers^{7,11-16} on the reaction mechanism for the reactions of $\text{O}(^3\text{P})$ atoms with a variety of olefinic systems, the following simplified reaction scheme can account for all the addition products observed:

Table 3.2

Product yields from the reaction of $O(^3P)$ atoms with 1-methylcyclohexene ($N_2 = 1$)

$T^\circ K$	P_{total} torr	MCXO	MCXN	MCPA	MCPN	MHA	X_1	X_2	CO	$\Sigma O(^3P)$
296 ± 2	55	0.315	0.070	0.050	0.030	0.036	0.040	0.004	0.020	0.565
		\pm	\pm	\pm	\pm	\pm	\pm	\pm	\pm	\pm
		0.063	0.021	0.010	0.009	0.006	0.010	0.0005	0.005	0.125
296 ± 2	115	0.306	0.066	0.036	0.029	0.037	0.042	0.003	0.014	0.533
		\pm	\pm	\pm	\pm	\pm	\pm	\pm	\pm	\pm
		0.017	0.002	0.002	0.004	0.002	0.004	0.0002	0.004	0.035
296 ± 2	210	0.355	0.090	0.044	0.036	0.051	0.056	0.006	0.010	0.648
		\pm	\pm	\pm	\pm	\pm	\pm	\pm	\pm	\pm
		0.028	0.005	0.005	0.001	0.007	0.003	0.0007	0.002	0.052
296 ± 2	400	0.369	0.122	0.062	0.042	0.053	0.070	0.007	0.007	0.732
		\pm	\pm	\pm	\pm	\pm	\pm	\pm	\pm	\pm
		0.015	0.009	0.003	0.004	0.004	0.004	0.0003	0.002	0.014
423 ± 1	170	0.340	0.070	0.038	0.032	0.042	0.053	0.005	---	0.580
		\pm	\pm	\pm	\pm	\pm	\pm	\pm		\pm
		0.015	0.004	0.003	0.001	0.004	0.003	0.0003		0.030

MCXO = 1-methyl-1,2-epoxycyclohexane

MCXN = 2-methylcyclohexanone

MCPA = 1-methylcyclopentenecarbaldehyde

MCPN = methylcyclopentylketone

MHA = 2-methyl-5-hexenal

X_1 = ~60% 1-hepten-6-one + ~40% 2-methyl-2-hexenal

X_2 = unknown, tentatively identified as 3-methyl-2-oxepene (see text)

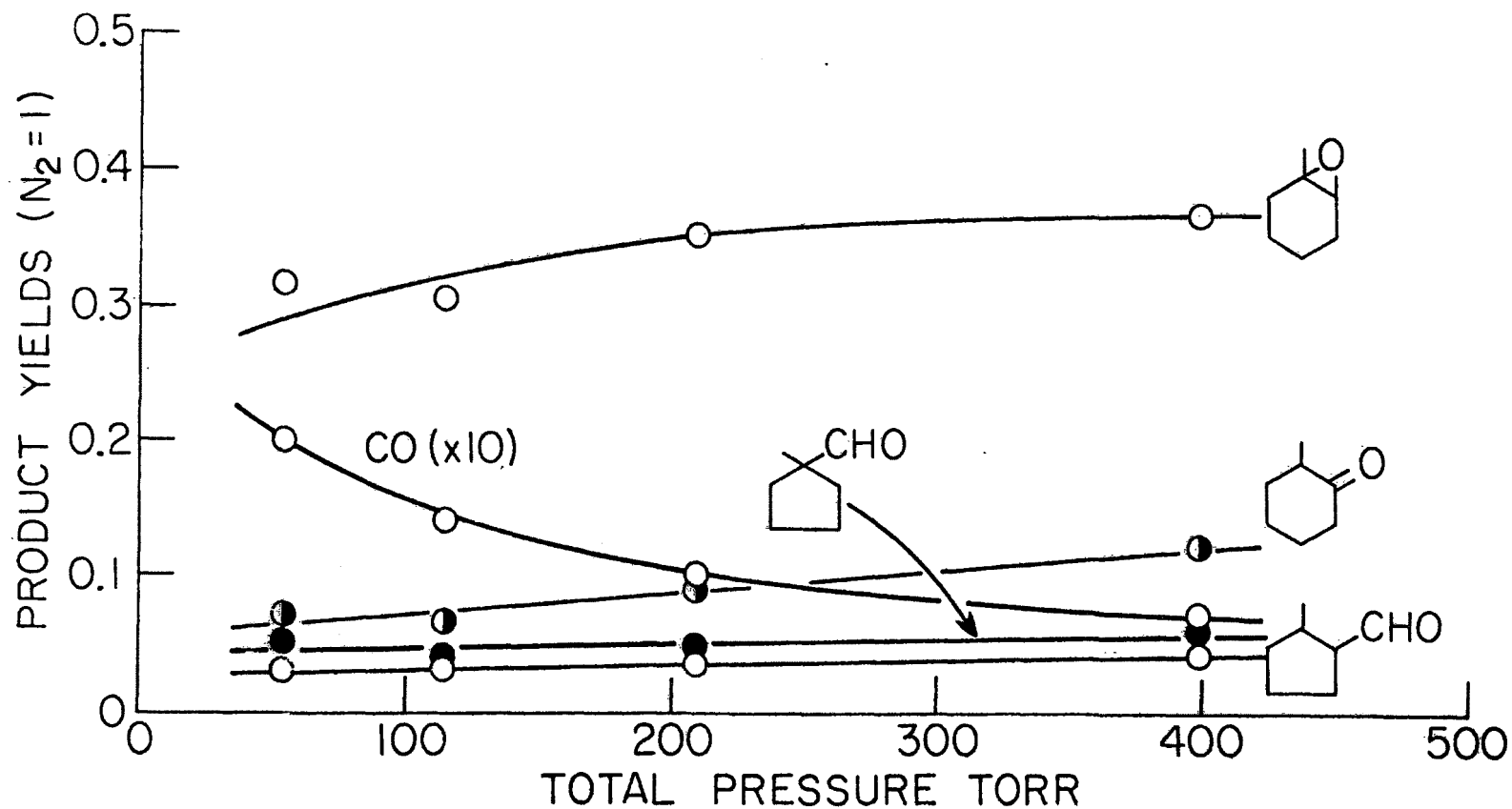
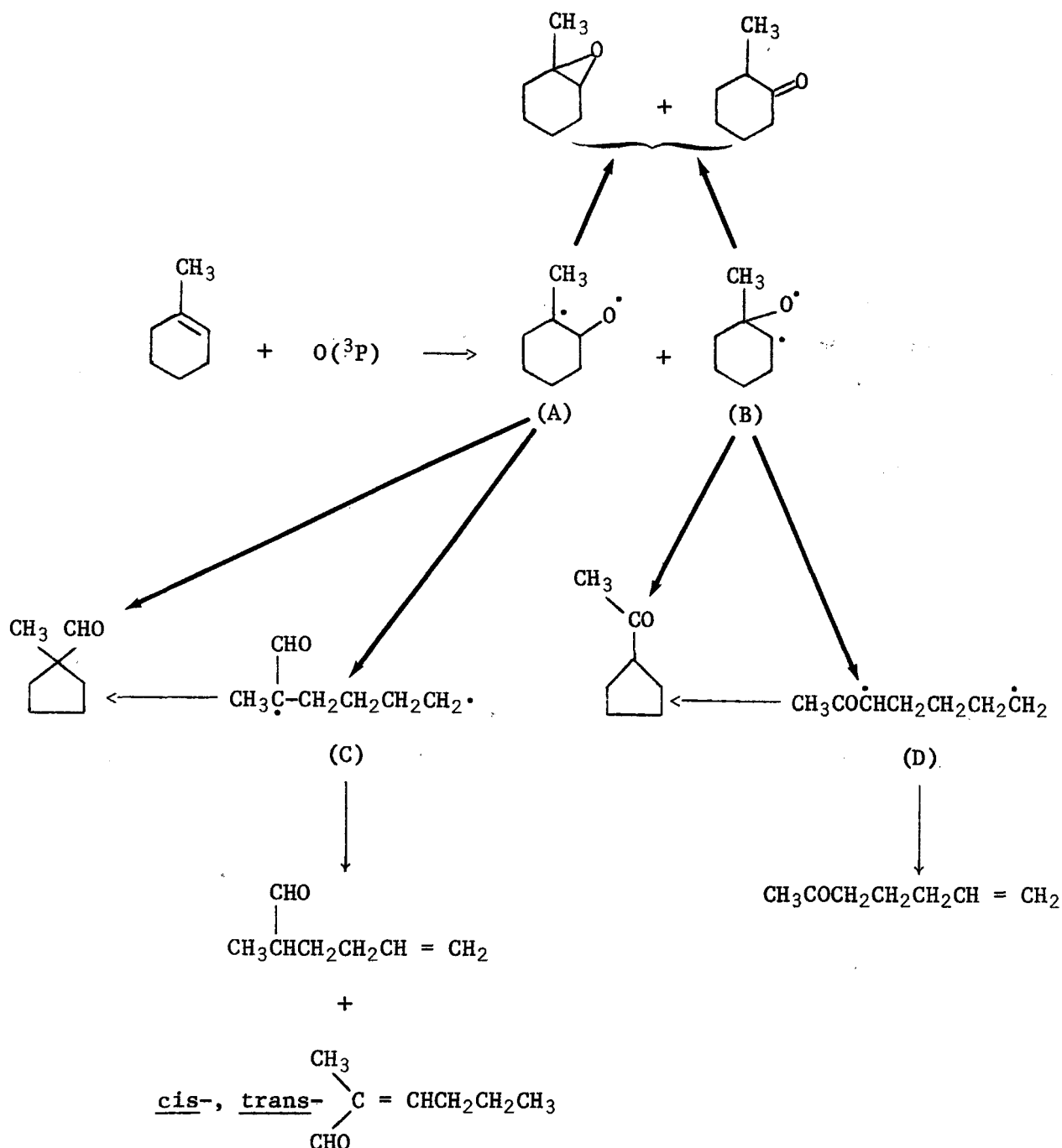


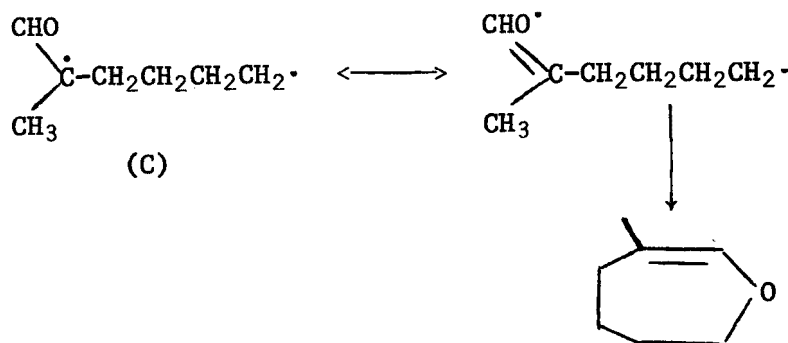
Figure 3.1 Plot of selected product yields ($N_2 = 1$) against total N_2O pressure for the reaction of $O(^3P)$ atoms with 1-methylcyclohexene at $296 \pm 2^\circ K$. (Data for 2-methyl-5-hexenal and products X_1 and X_2 are omitted for clarity).



1-Methyl-1,2-epoxycyclohexane may be formed from either of the initially formed biradicals (A) or (B) by ring closure, while 2-methylcyclohexanone may be formed from (A) by a 1,2-H atom shift or from (B) by 1,2-methyl migration. 1,2-ring contraction leads to 1-methylcyclopentenecarbaldehyde and methyl cyclopentyl ketone from (A) and (B) respectively, probably via either a concerted reaction, previously shown to occur for the reaction of

$O(^3P)$ atoms with cyclopentene at 77°K,^{15,17} or via ring opening α to the oxygen atom position to give the biradicals (C) and (D) which can then either recyclize to 1-methylcyclopentenecarbaldehyde and to methyl cyclopentyl ketone respectively, or can isomerize to form the open chain unsaturated aldehydes and ketones observed. Fragmentation, such as to CO, of the vibrationally or electronically excited products formed will be more important at low pressures in the absence of stabilizing collisions and hence the addition product yields will increase with pressure while the fragmentation product yields will decrease, as observed.

In this system an estimate of the relative amounts of the biradicals (A) and (B) formed can be obtained from the yields of 1-methylcyclopentenecarbaldehyde and methyl cyclopentyl ketone and also from the yields of the open chain unsaturated ketones and aldehydes. It can be seen from Table 3.2 that the biradical (A) is formed ~60-65% of the time, in agreement with the work Cvetanovic and co-workers^{7,15,16} which shows that the $O(^3P)$ atom adds predominately to the less substituted of the two doubly bonded carbon atoms. Analogous to the observation of dihydropyran from the reaction of $O(^3P)$ atoms with cyclopentene,¹⁶ it is possible that the unknown product, X_2 , observed in the present work is the unsaturated ether, 3-methyl-2-oxepene, formed from the cyclization of an isomeric form of the biradical (C):



This is not inconsistent with the mass spectrum observed for this product, which shows predominant mass peaks at $m/e = 112, 97, 71$ and 69 . In addition, the short retention time observed on the β, β' -oxydipropionitrile column is consistent with the low polarity expected for this compound.

The present reaction system shows great similarity with the reactions of $O(^3P)$ atoms with cyclohexene (major products 1,2-epoxycyclohexane, cyclo-

hexanone and cyclopentenecarbaldehyde) and cyclopentene, the latter being extensively studied by Cvetanovic, Ring and Doyle.¹⁶ There the major products observed were the analogous 1,2-epoxycyclopentane, cyclopentanone and cyclobutenecarbaldehyde, together with equal amounts of ethylene and acrolein. Smaller amounts of ring-opened products identified as 4-pentenal, dihydropyran and possibly 2-pentenal were also observed.¹⁶

Conclusion. From this and previous work^{7,12,16} the reactions of $O(^3P)$ atoms with simple cyclic olefins and with the aromatic hydrocarbons can be satisfactorily explained in terms of a general mechanism such as shown above. The difference in products between the cyclic olefins and aromatic hydrocarbons arises because of the difference in the rate constants for reaction of $O(^3P)$ atoms with the reactant and with the reaction products. Thus the reaction of $O(^3P)$ atoms with the aromatic hydrocarbons is slow⁶ and produces largely highly reactive unsaturated products (the rate constants for reaction of $O(^3P)$ atoms with o-cresol have, however, been shown to be only ~8 times faster than with toluene at temperature).¹⁸ However, for the simple olefins the initial reaction is very fast and forms largely saturated, and hence unreactive, products. Thus the extent of secondary reactions are much smaller in these cases, as observed.

REFERENCES

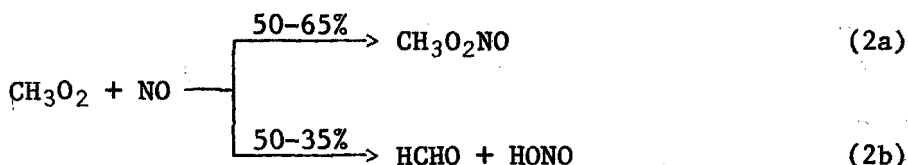
1. E. Grovenstein, Jr. and A. J. Mosher, J. Amer. Chem. Soc., 92, 3810 (1970).
2. H. Hibbert and P. Burt, Org. Sym. Coll., 1, 494 (1944).
3. J. H. Purnell, "Gas Chromatography," Wiley and Sons, New York, (1962).
4. G. R. H. Jones and R. J. Cvetanovic, Can. J. Chem., 39, 2444 (1961).
5. G. Boocock and R. J. Cvetanovic, Can. J. Chem., 39, 2436 (1961).
6. R. Atkinson and J. N. Pitts, Jr., J. Phys. Chem., 79, 295 (1975).
7. R. J. Cvetanovic, Adv. Photochem., 1, 115 (1963).
8. J. S. Gaffney, R. Atkinson and J. N. Pitts, Jr., J. Amer. Chem. Soc., 97, 5049 (1975).
9. J. S. Gaffney, R. Atkinson and J. N. Pitts, Jr., J. Amer. Chem. Soc., 97, 6481 (1975).
10. J. T. Herron and R. E. Huie, J. Phys. Chem. Ref. Data, 2, 467 (1973).
11. R. J. Cvetanovic, J. Chem. Phys., 23, 1375 (1955); 25, 376 (1956).
12. R. J. Cvetanovic, Can. J. Chem., 36, 623 (1958).
13. S. Sato and R. J. Cvetanovic, Can. J. Chem., 36, 279, 970, 1668 (1958); 37, 953 (1959).
14. R. J. Cvetanovic and L. C. Doyle, Can. J. Chem., 38, 2187 (1960).
15. R. J. Cvetanovic, J. Phys. Chem., 74, 2730 (1970).
16. R. J. Cvetanovic, D. F. Ring and L. C. Doyle, J. Phys. Chem., 75, 3056 (1971).
17. M. D. Scheer and R. Klein, J. Phys. Chem., 74, 2732 (1970).
18. R. Atkinson and J. N. Pitts, Jr., J. Phys. Chem., 79, 541 (1975).

4. A LONG-PATH INFRARED SPECTROSCOPIC STUDY OF THE REACTION OF METHYLPEROXY FREE RADICALS WITH NITRIC OXIDE

The reaction of alkylperoxy radicals with nitric oxide is generally assumed¹⁻³ to proceed by the oxidation of nitric oxide to nitrogen dioxide with formation of an alkoxy radical:



Reaction (1) is believed to be an important route for oxidizing NO to NO₂ in photochemical smog. In addition, the alkoxy radical, RO, may react further in the atmosphere to produce HO₂⁴ which also converts NO to NO₂. However, a mass spectrometric study⁵ indicated that reaction (1) with R = CH₃ does not occur as written but rather proceeds as follows:



Secondary reactions of the HCHO and of the CH₃O₂NO adduct with O₂ were postulated to form methyl nitrate and formic acid, the observed products.⁵ More recent studies⁶ suggest that the reaction of NO with CH₃O₂ occurs via reaction (1) approximately 79 ± 8% of the time.

In this work a reinvestigation of this important reaction has been carried out by long-path infrared (LPIR) spectroscopy and gas chromatography (GC), using millitorr reactant concentrations. The results of this study confirm that methylperoxy radicals do react with nitric oxide as shown in reaction (1); no evidence for the existence of alternate reaction paths was found.

Experimental. Azomethane (Merck, Sharp and Dohme) was degassed at liquid nitrogen temperature and then passed through Ascarite (Arthur H. Thomas, Co.) to remove traces of carbon dioxide. Nitric oxide (Matheson, ≥99.0%) was passed through Linde molecular sieve 13X to remove any NO₂ and water present. NO₂ (Matheson, ≥99.0%) was distilled over oxygen. The O₂ (Liquid Carbonic, ≥99.95%), N₂ (Matheson, ≥99.995%), and He (Liquid Carbonic, ≥99.995%) were used as received.

Authentic samples of methyl nitrite⁷ and methyl nitrate⁸ were prepared by standard procedures. The methyl nitrite was purified by passage through sodium bicarbonate and Ascarite. The methyl nitrate was purified by GC.

Irradiations were carried out in an FEP Teflon-coated cylindrical vessel (25 cm diameter, 95 cm length) which housed the White cell optics of the 40 m path length Perkin-Elmer Model 621 infrared spectrometer. The cell was evacuated to 6.0×10^{-4} torr between runs. Unfiltered light from a medium pressure 1200 watt mercury arc (Hanovia Model 3A-44V) entered the sample tank through six 7.5×7.5 cm ports of 6 mm thick window plate which transmitted light of $\lambda > 320$ nm. Hence the 366 nm mercury line was the primary photolytic wavelength.⁹ For several runs the light intensity was reduced with wire screens in order to determine its effects on the reaction.

Reaction mixtures were prepared by expansion from a calibrated volume of known pressures (MKS Baratron Type 90, 0-10 torr pressure gauge) of the reactants into the reaction chamber of the LPIR followed by pressurizing to 760 torr with He or N₂. Initial concentrations were: CH₃N₂CH₃, 33-369 mtorr, NO, 25-76 mtorr; O₂, 2200-5320 mtorr. These reactant concentrations were chosen to minimize the thermal oxidation of NO to NO₂^{10,11} and the reaction of CH₃ with NO.^{12,13} Dark runs confirmed that the thermal conversion of NO to NO₂ was negligible during the short duration of these experiments (~15 min).

The extinction coefficients for CH₃N₂CH₃, CH₃ONO, CH₃ONO₂, and NO₂ were determined from Beer's Law studies of measured millitorr concentrations of each of these compounds in 760 torr of He or N₂. During an experiment, methyl nitrite (CH₃ONO) was determined from its absorbance at 800 cm^{-1} . Nitrogen dioxide (NO₂) was determined from the total absorbance at 1600 cm^{-1} by subtracting out that due to CH₃ONO. Methyl nitrate (CH₃ONO₂) was measured from its absorbance at 1300 cm^{-1} .

In some runs, methyl nitrite, methyl nitrate and other products were also monitored by GC or combined gas chromatography-mass spectrometry (GC-MS). Table 4.1 lists the columns, detector and operating conditions used.

A search for HCHO was also carried out by flushing the contents of the cell through two traps in series containing distilled water and subsequently identifying HCHO by the chromotropic acid test.¹⁴

Actinometry was done by photolyzing measured concentrations of azomethane in 760 torr He and following the rate of nitrogen formation using Column E of Table 4.1. Since the quantum yield for N₂ formation from azomethane is

Table 4.1

Columns used in gas chromatographic analysis of the products of the photooxidation of azomethane in the presence of NO at room temperature

Column designation	Column description	Carrier gas flow rate (ml/min)	Column temperature (°C)	Compounds identified	Model & detector
A	3 m × 3 mm 10% Carbowax 600 on 100/120 acid washed firebrick	25	23	CH ₃ ONO, CH ₃ ONO ₂	Varian Aerograph Hy-Fy 600, electron capture detector
B	3 m × 3 mm 10% Carbowax 600 on 100/120 acid washed firebrick	50	50	CH ₃ ONO, CH ₃ ONO ₂ CH ₃ NO ₂	Varian Aerograph 1400 with flame ionization detector
C	3 m × 3 mm 10% Carbowax 600 on 100/120 acid washed firebrick	50	23	CH ₃ ONO, CH ₃ ONO ₂	Finnigan Model 3100 combined gas chromatograph mass spectrometer
D	3 m × 3 mm 20% XF 1150 cyanosilicone on 80/100 HMDS treated chromosorb	23	23	CH ₃ ONO	Varian Aerograph 1400 with flame ionization detector
E	6 m × 6 mm Linde molecular seive, 13X	30	0	N ₂ , O ₂	Perkin-Elmer 900, thermal conductivity detector

1.0,¹⁵ the rate of its formation is also the rate of light absorption by azomethane, I_a . As a check, N_2 was also monitored during one experiment with NO and O_2 present and its rate of formation was shown to agree with that determined in actinometry runs.

Results. Figure 4.1 shows typical infrared spectra of the individual reactants and products. These spectra agree well with those reported in the literature.¹⁶⁻¹⁸ The limits of detection of the products and the relevant extinction coefficients are given in Table 4.2.

Table 4.2

Infrared extinction coefficients^a and limits of detection of some reactants and products in the photooxidation of azomethane in the presence of NO at room temperature.

Compound	Wave number, cm ⁻¹	Extinction coefficient, mtorr ⁻¹ m ⁻¹	Detection limit, mtorr
CH ₃ N ₂ CH ₃	1000	1.46×10^{-5}	-
CH ₃ ONO	800	5.63×10^{-4}	0.5
	1600	3.03×10^{-4}	-
NO ₂	1600	9.15×10^{-4}	0.6
CH ₃ ONO ₂	1300	9.58×10^{-4}	0.5

^a To base 10

Figure 4.1c gives the infrared spectrum of a typical reactant mixture before and after photolysis to 1% conversion of azomethane. It is seen that the only detectable products are NO₂, CH₃ONO, and small amounts of CH₃ONO₂. Extensive analysis by GC (Table 4.1) confirmed the presence of CH₃ONO and CH₃ONO₂ and revealed traces of CH₃NO₂ and one other unidentified product. Small amounts of HCHO were also detected by the chromotropic acid test.¹⁴ The observation of these products is in agreement with an earlier LPIR study¹⁹ of this system, as well as with the more recent GC studies⁶ of this reaction.

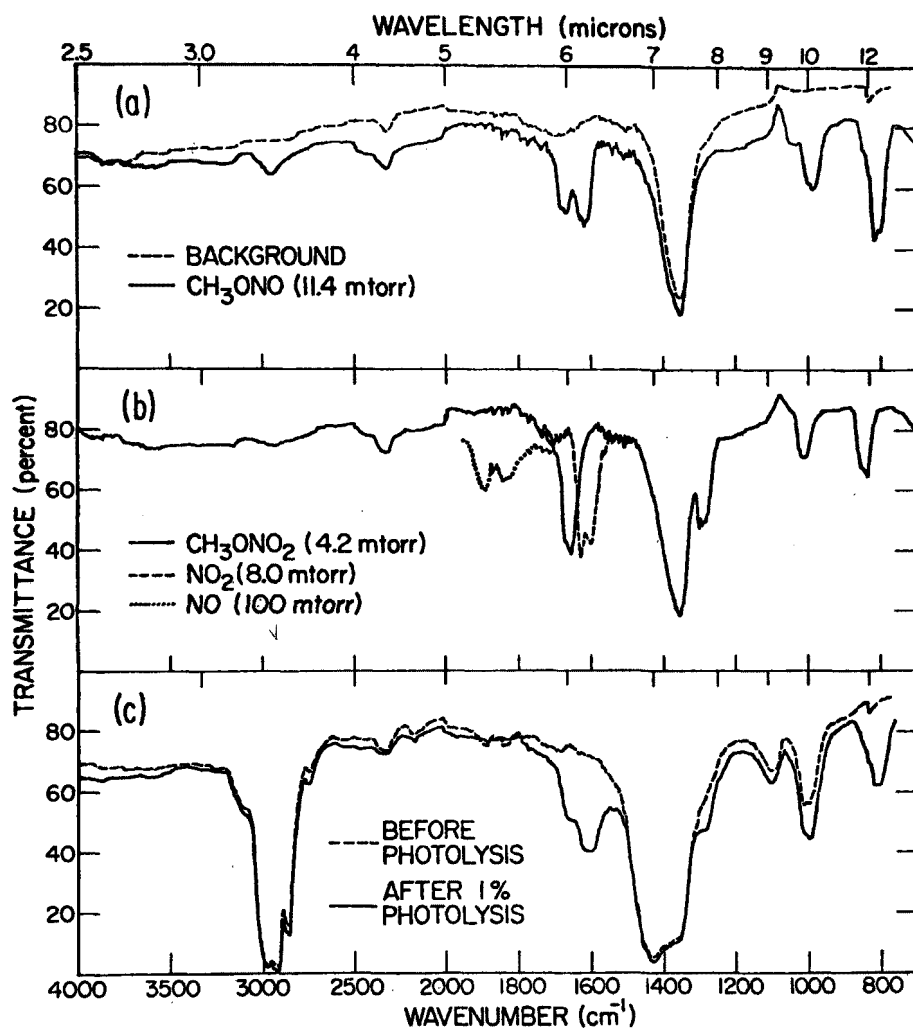


Figure 4.1 (a) Infrared spectrum of the empty cell and of 11.4 mtorr CH₃ONO; (b) Infrared spectrum of: 100 mtorr NO; 8.0 mtorr NO₂; (c) Infrared spectrum before and after 1% photolysis of 340 mtorr azomethane, 39 mtorr NO, and 3130 mtorr O₂.

Figure 4.2 shows a typical plot of product formation and NO loss with time. Both CH_3ONO and NO_2 grow linearly during the initial stages of the reaction when CH_3ONO_2 formation is negligible. At longer reaction times the NO_2 concentration levels off and the CH_3ONO_2 begins to increase non-linearly. Finally, at low NO concentrations, the rate of CH_3ONO formation falls, while that of CH_3ONO_2 increases substantially.

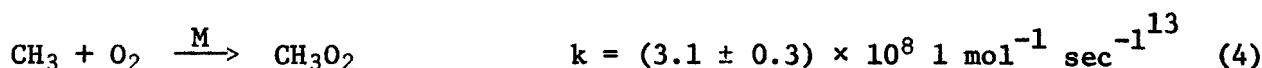
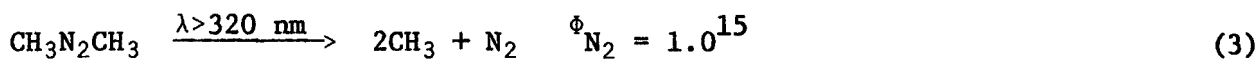
The low extinction coefficient for NO at 1900 cm^{-1} ($4 \times 10^{-5}\text{ mtorr}^{-1}\text{ m}^{-1}$) precludes its accurate measurement by infrared at the low concentrations used in these experiments. For example, the point at 65 minutes in Figure 4.2 corresponds to the limit of detection of NO in this system. Hence the NO data even at short reaction times are only accurate to about $\pm 15\%$.

The quantum yields of CH_3ONO and NO_2 were calculated as the ratio of their initial rates of formation to the rate of azomethane loss. Because both NO_2 and CH_3ONO absorb light of $\lambda > 320\text{ nm}$,^{9,20,21} their quantum yields were calculated under conditions such that their loss by photolysis was small. Since the extinction coefficients for NO_2 and CH_3ONO at 366 nm are 1.5×10^2 and $48\text{ l mol}^{-1}\text{ cm}^{-1}$ respectively, compared to $3\text{ l mol}^{-1}\text{ cm}^{-1}$ for $\text{CH}_3\text{N}_2\text{CH}_3$,⁹ all quantum yields were determined under conditions such that

$$\frac{[\text{CH}_3\text{N}_2\text{CH}_3]}{[\text{NO}_2]} > 50 \text{ and } \frac{[\text{CH}_3\text{N}_2\text{CH}_3]}{[\text{CH}_3\text{ONO}]} > 15.$$

Table 4.3 gives, for a series of runs of varying initial reactant concentrations and light intensity, (1) the initial rates of product formation as a ratio to the azomethane concentration and (2) the corresponding quantum yields. The NO_2 quantum yield is 1.9 ± 0.3 while that for CH_3ONO is 1.7 ± 0.2 where the specified errors represent one standard deviation. An upper limit for the quantum yield of CH_3ONO_2 is 0.01 from its initial rate of formation. Typically, CH_3ONO_2 was not detected by GC (detection limit $4 \times 10^{-3}\text{ mtorr}$) in the first 3 minutes of photolysis.

Discussion. The following reactions describe the photooxidation of azomethane in the presence of the nitric oxide under these conditions:



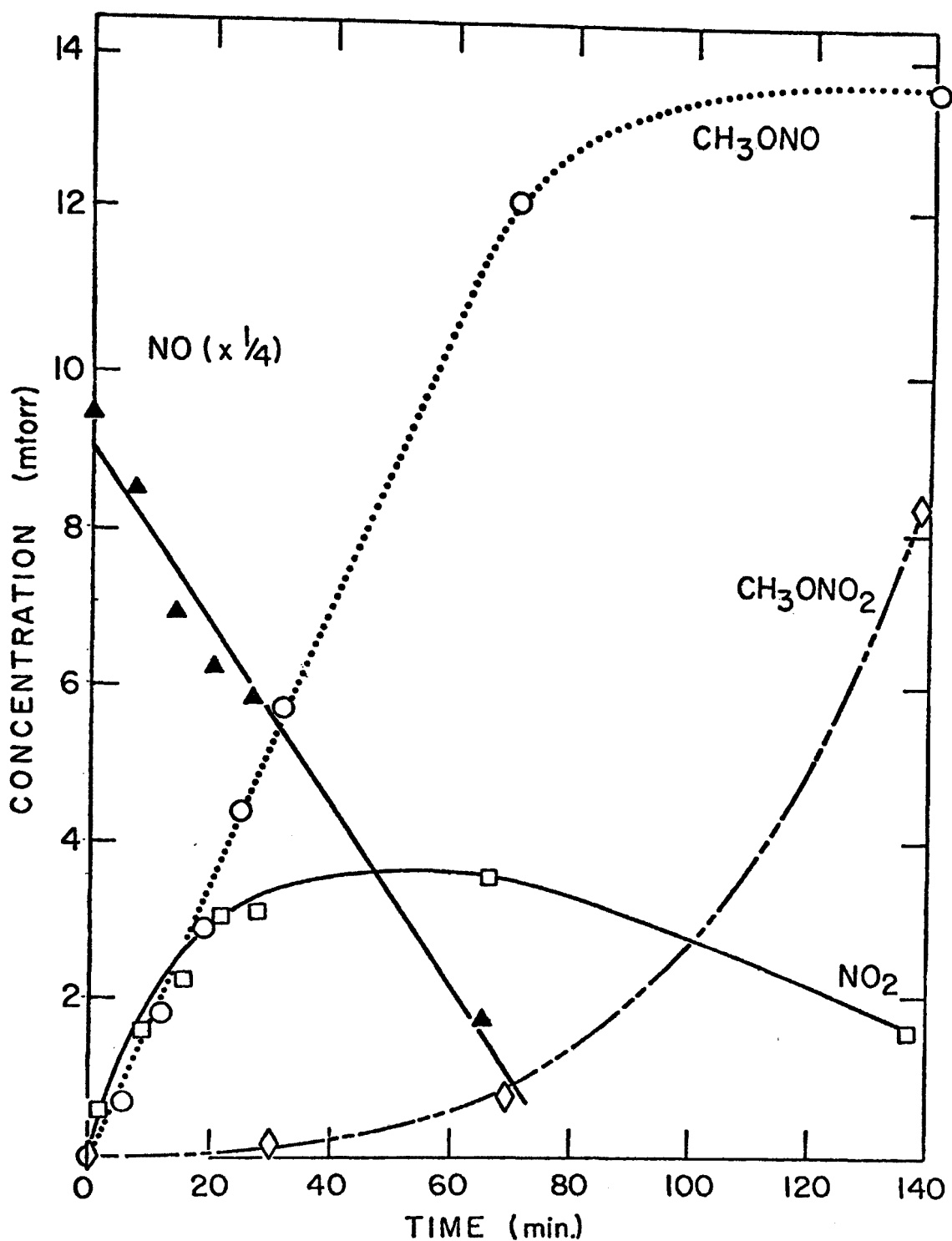


Figure 4.2 Typical time dependence of CH_3ONO , CH_3ONO_2 , NO_2 and NO in the photooxidation of azomethane in the presence of NO . Initial conditions, azomethane 132 mtorr; O_2 2830 mtorr; NO 38 mtorr.

Table 4.3

Reactant concentrations, rates of product formation and quantum yields in the photooxidation of azomethane in the presence of NO at room temperature.

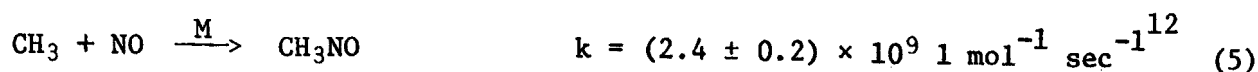
Initial reactant concentrations ^a			$R_{\text{CH}_3\text{ONO}} \times 10^3$ ^b	$\phi_{\text{CH}_3\text{ONO}}$	$R_{\text{NO}_2} \times 10^3$ ^b	ϕ_{NO_2}
$[\text{CH}_3\text{N}_2\text{CH}_3]$	$[\text{NO}]_0$	$[\text{O}_2]_0$	$\frac{R_{\text{CH}_3\text{ONO}} \times 10^3}{[\text{CH}_3\text{N}_2\text{CH}_3]_0}$		$\frac{R_{\text{NO}_2} \times 10^3}{[\text{CH}_3\text{N}_2\text{CH}_3]_0}$	
mtorr	mtorr	mtorr	min ⁻¹		min ⁻¹	
$I_a = (7.0 \pm 0.7) \times 10^{-4} \text{ min}^{-1}\text{c}$						
369	37	3040	0.99	1.4	1.4	2.0
340	39	3130	1.1	1.5	1.2	1.7
322	40	3340	1.2	1.7	1.1	1.5
289	39	3040	1.1	1.6	1.3	1.8
253	36	3040	1.2	1.8	1.6	2.3
217	30	3040	1.1	1.6	1.4	1.9
204	37	3040	1.2	1.7	1.6	2.3
149	36	3040	1.2	1.7	1.3	1.8
132	38	2830	1.3	1.9	1.4	2.0
97	36	3040	1.3	1.9	1.3	1.9
33	25	3040	1.5	2.2	1.8	2.6
241	67	3040	1.3	1.8	1.2	1.7
268	52	3040	1.2	1.7	1.1	1.6
239	44	3040	1.2	1.7	1.5	2.1
270	30	3040	1.1	1.6	1.3	1.9
336	37	5320	1.1	1.6	1.3	1.9
250	37	3800	1.1	1.6	NA ^d	NA ^d
295	39	2280	0.91	1.3	1.1	1.6
275	38	2200	1.1	1.5	1.2	1.7
163	57	3040	1.1	1.6	1.2	1.7
153	76	3040	1.3	1.8	1.5	2.1
172	56	3040	1.3	1.9	1.3	1.9
			1.2 ± 0.1		1.3 ± 0.2	
$I_a = (1.3 \pm 0.1) \times 10^{-4} \text{ min}^{-1}\text{c}$						
349	41	3040	0.19	1.5	0.28	2.2
314	41	3040	0.19	1.5	0.22	1.7
$I_a = (0.88 \pm 0.09) \times 10^{-4} \text{ min}^{-1}\text{c}$						
239	40	3040	0.19	2.2	0.18	2.1
				1.7 ± 0.2		1.9 ± 0.3

^a 1 mtorr = 1.3 parts per million (ppm)

^b $R_{\text{CH}_3\text{ONO}}$ and R_{NO_2} are rates of formation of methyl nitrite and nitrogen dioxide, respectively

^c I_a is the rate of light absorption by $\text{CH}_3\text{N}_2\text{CH}_3$

^d NA = not available



Under these experimental conditions, removal of CH_3 by reaction with NO ^{12,13} will occur $\leq 10\%$ of the time, particularly since the NO concentration is decreasing during the reaction. At low azomethane conversions ($\sim 1\%$) the contribution of reaction (6) to the removal of CH_3 radicals is also small, although it does account for the trace quantities of CH_3NO_2 observed by GC.

The reaction (8) of methoxy radicals with NO can occur either by combination (step a) or by abstraction (step b) with $k_{8b}/k_8 = 0.143$.²²⁻²⁵ Similarly, reaction (9), which is minimal at short reaction times, can also occur by combination or abstraction with $k_{9b}/k_9 = 0.08$.²³ Estimates of the rate constant ratio $\frac{k_8}{k_9}$ range from 1.2²³ to 2.9.^{26,27} Hence reaction (9) will become competitive with reaction (8) at longer reaction times when the NO concentration approaches that of NO_2 . Reaction (10) is too slow^{23,25,28} ($k_{10} = 1.6 \times 10^3 \text{ l mol}^{-1} \text{ sec}^{-1}$) to be significant.

The experimental results are consistent with the above scheme in that (1) the major products at short photolysis times are CH_3ONO and NO_2 , (2) NO_2 accumulates linearly with time until its removal by both reaction (9) and photolysis becomes competitive with its rate of formation, and (3) small amounts of HCHO and CH_3NO_2 are observed. At longer reaction times, reaction (9) becomes competitive with reaction (8) and hence the CH_3ONO_2 concentration increases and NO_2 decreases. Simultaneously, the rate of CH_3ONO formation

falls. HCHO was not detected by IR since its detection limit in this system is ~3 mtorr and the maximum yield of HCHO from reaction (8b) in any of these runs was 2.3 mtorr. Under these conditions, loss of HCHO by photolysis is negligible.⁹

Estimates of the rates of reaction of HNO with itself and with O₂^{23,29} indicate that these rates are sufficiently slow that HNO should accumulate in this system. While the IR extinction coefficient for HNO is unknown, it is not surprising that the low yield is below the present detection limit. The same is true of the small yields of CH₃NO anticipated from reaction (5). At these low conversions, HONO is also expected to be undetected.³⁰

Both our experimental results and the kinetic data available in the literature suggest that for the purposes of kinetic analysis, at short photolysis times where the loss of NO₂ is negligible, reactions (5), (6), (9) and (10) may be neglected. Using a simplified scheme consisting of the remaining reactions (3), (4), (7) and (8), the following relations can be derived:

$$R_{\text{NO}_2} = \frac{d[\text{NO}_2]}{dt} = 2.0 I_a [\text{CH}_3\text{N}_2\text{CH}_3]_0 \quad (\text{I})$$

$$R_{\text{CH}_3\text{ONO}} = \frac{d[\text{CH}_3\text{ONO}]}{dt} = 1.71 I_a [\text{CH}_3\text{N}_2\text{CH}_3]_0 \quad (\text{II})$$

where I_a is the rate of light absorption by azomethane in min^{-1} and $[\text{CH}_3\text{N}_2\text{CH}_3]_0$ is the initial azomethane concentration. Hence $R_{\text{NO}_2}/[\text{CH}_3\text{N}_2\text{CH}_3]_0$ and $R_{\text{CH}_3\text{ONO}}/[\text{CH}_3\text{N}_2\text{CH}_3]_0$ should be independent of initial reactant concentrations, as found (Table 4.3). From the average values of these ratios, $I_a = (6.5 \pm 1.0) \times 10^{-4} \text{ min}^{-1}$ from NO₂ formation and $I_a = (7.0 \pm 0.7) \times 10^{-4} \text{ min}^{-1}$ from CH₃ONO formation, within 7% of the value $(7.0 \pm 0.7) \times 10^{-4} \text{ min}^{-1}$ determined in separate actinometry experiments. This scheme also predicts quantum yields of 2.0 and 1.7 for NO₂ and CH₃ONO respectively, in excellent agreement with the results given in Table 4.3.

The carbon and nitrogen mass balances in the initial stages of the reaction are reasonably good. For example, in Figure 4.2, 1.9 ± 0.20 mtorr NO₂ and 1.8 ± 0.09 mtorr CH₃ONO have been produced at 10 minutes while 4.7 ± 0.7 mtorr of NO and 0.92 ± 0.1 mtorr of CH₃N₂CH₃ have reacted. According to the above mechanism, 3.7 ± 0.6 mtorr of NO is predicted to react during this

time interval. Since $k_{8a}/k_8 = 0.86$, the carbon and nitrogen balances are $110 \pm 20\%$ and $85 \pm 30\%$, respectively. The particularly large uncertainty in the nitrogen balance is due to the inaccuracies in measuring NO by infrared spectroscopy as discussed above, which precludes accurate mass balance computations in the present system. At long reaction times, however, it appears that the nitrogen balance may be somewhat poorer. For example, at 140 minutes the percentages of carbon and nitrogen accounted for in the observed products are $103 \pm 20\%$ and $71 \pm 30\%$, respectively. This is likely due to secondary reactions producing nitrogen compounds which are not easily detected by LPIR and GC or which may be adsorbed on the walls. Since this study was concerned only with the mechanism at short reaction times where all the carbon and nitrogen could be accounted for, no further investigation of the poor nitrogen balance at longer photolysis times were done.

Our observations of the time dependence of methyl nitrate formation are in agreement with those of earlier investigators in that it is formed with an "induction period" which depends on the rate of light absorption. This is understandable since according to the above mechanism,

$$\frac{d[\text{NO}]}{dt} = -4 I_a [\text{CH}_3\text{N}_2\text{CH}_3]_0 \quad (\text{III})$$

Higher rates of light absorption correspond to higher rates of NO loss, hence reaction (9) forming CH_3ONO_2 , will become competitive with reaction (8) at shorter reaction times. In addition, it appears that with the rate of loss of NO given in equation (III), little NO would remain after the induction periods found by these investigators⁵ and hence secondary reactions might well then produce HCOOH . It is puzzling, however, that CH_3ONO was not detected in their studies in the early stages of the reaction, either by mass spectrometry or gas chromatography.⁵

In conclusion, our results confirm that under these experimental conditions, methylperoxy radicals oxidize NO to NO_2 . We find no evidence of alternate modes of reaction occurring between these two species.

REFERENCES

1. H. Niki, E. E. Daby and B. Weinstock, Adv. Chem. Ser. No. 113, 16 (1971).
2. A. P. Altshuller and J. J. Bufalini, Photochem. Photobiol., 4, 97 (1965).
3. T. A. Hecht and J. A. Seinfeld, Environ. Sci. Technol., 6, 47 (1972).
4. J. Heicklen, K. Westberg and N. Cohen, Center for Air Environmental Studies Report No. 115-69, The Pennsylvania State University (1969).
5. C. W. Spicer, A. Villa, H. A. Wiebe and J. Heicklen, J. Amer. Chem. Soc., 95, 13 (1973).
6. R. Simonaitis and J. Heicklen, J. Phys. Chem., 78, 2417 (1974).
7. W. H. Hartung and F. Crossley, Org. Syn. Coll., 2, 363 (1943).
8. A. P. Black and F. H. Babers, Org. Syn. Coll., 2, 412 (1943).
9. J. G. Calvert and J. N. Pitts, Jr., "Photochemistry," John Wiley and Sons, Inc., New York, N. Y., 1966, and references therein.
10. J. Heicklen and N. Cohen, Advan. Photochem., 5, 157 (1968).
11. D. H. Stedman and H. Niki, Environ. Sci. Technol., 7, 735 (1973).
12. N. Basco, D. G. L. James and R. D. Stuart, Int. J. Chem. Kinet., 2, 215 (1970).
13. N. Basco, D. G. L. James and F. C. James, Int. J. Chem. Kinet., 4, 129 (1972).
14. P. W. West and B. Sen, Z. Analyt. Chem., 153, 12 (1956) and references therein.
15. M. H. Jones and E. W. R. Steacie, J. Chem. Phys., 21, 1018 (1953).
16. R. H. Pierson, A. N. Fletcher and E. Gantz, Analyt. Chem., 28, 1218 (1956).
17. P. Klaboe, D. Jones and E. R. Lippincott, Spectrochimica Acta, 23A, 2957 (1967).
18. E. R. Stephens and M. A. Price, IR spectrum of CH_3ONO_2 , personal communication, 1974.
19. P. L. Hanst and J. G. Calvert, J. Phys. Chem., 63, 2071 (1959).
20. G. R. McMillan, J. Kumari and D. L. Snyder, "Chemical Reactions in Urban Atmospheres," Ed. C. S. Tuesday, Elsevier Publishing Co., pp. 35-44 (1969).

REFERENCES (cont.)

21. I. T. N. Jones and K. D. Bayes, J. Chem. Phys., 59, 4836 (1973) and references therein.
22. H. A. Wiebe and J. Heicklen, J. Amer. Chem. Soc., 95, 1 (1973).
23. H. A. Wiebe, A. Villa, T. M. Hellman and J. Heicklen, J. Amer. Chem. Soc., 95, 7 (1973).
24. G. E. McGraw and H. S. Johnston, Int. J. Chem. Kinet., 1, 89 (1969).
25. W. Glasson, Abstracts, 167th National Meeting of the American Chemical Society, Los Angeles, CA, March 31 - April 5, 1974, Phys. No. 41.
26. G. Baker and R. Shaw, J. Chem. Soc., 6965 (1965).
27. P. Gray, R. Shaw and J. C. J. Thynne, Progress in Reaction Kinetics, 4, 63 (1967).
28. J. Heicklen, Adv. Chem. Ser., No. 76, 23 (1968).
29. K. L. Demerjian, J. A. Kerr and J. G. Calvert, Advan. Environ. Sci. & Technol., 4, 1 (1973).
30. L. H. Jones, R. M. Badger and G. E. Moore, J. Chem. Phys., 19, 1599 (1951).

5. RATE CONSTANTS FOR THE GAS PHASE REACTION OF PEROXYACETYL NITRATE WITH SELECTED ATMOSPHERIC CONSTITUENTS

The gas phase reactions of PAN with several compounds typically present in photochemically polluted urban atmospheres have been studied with a view to determining the rate constants for these reactions in order to assess the importance of these processes for the removal of PAN in polluted urban atmospheres. In addition, a product analysis was carried out for the reaction of PAN with NO.

Experimental. Most reactions were carried out in a 65 liter FEP Teflon-lined aluminum tank which enclosed the 40 meter pathlength multiple reflection white cell optics of a Perkin-Elmer 621 spectrophotometer. The reaction tank could be routinely evacuated by an oil diffusion pump to $\leq 7 \times 10^{-4}$ torr. Reactants and products were monitored in situ by long-path infrared (LPIR) spectroscopy using experimentally determined or literature extinction coefficients. Thus PAN was monitored by its infrared absorption bands at 5.76 and 12.61 μ using the extinction coefficients determined by Stephens.¹ The reaction of PAN with SO₂ was studied in a 23 liter cylindrical Pyrex cell connected via a Carle gas sampling valve to a gas chromatograph fitted with an electron capture detector. In this case PAN was quantitatively analyzed²⁻⁴ on a 22" \times 1/8" Teflon column packed with Carbowax 600 on 60/80 firebrick with an N₂ flow rate of 30 cm³ min⁻¹ at 296 \pm 1°K.

Reactant mixtures were introduced into either reaction vessel from a conventional mercury-free high vacuum gas handling system. Reactant pressures in calibrated volumes of this gas handling rack were measured by either an MKS Baratron gauge (0-10 torr) or by a 0-800 torr Wallace and Tiernan FA 160 absolute pressure gauge.

A product analysis was undertaken for the reaction of PAN with NO using a Finnigan 3100D combined gas chromatograph-mass spectrometer with a 10 ft \times 1/8" stainless steel column packed with Carbowax 600 on firebrick, and also by conventional gas chromatography using an electron capture detector equipped with a 20 ft \times 1/8" stainless steel column of Carbowax 400 on 60/80 firebrick.

Peroxyacetyl nitrate (1000 ppm in tanks pressurized by N₂)⁵ was used as received. CO (\geq 99.5% purity) was passed over glass beads at 77°K in order to remove any traces of iron carbonyl present, while NO (\geq 99.0% purity) was passed through activated Linde Molecular Sieve 13X to remove any NO₂ and H₂O present.

Isobutene ($\geq 99.8\%$), SO_2 ($\geq 99.98\%$), NH_3 ($\geq 99.99\%$), CH_3CHO ($\geq 99.3\%$) and NO_2 ($\geq 99.5\%$) were subjected to several freeze-thaw vacuum distillations prior to their use. Approximately 2% ozone in oxygen was produced by passing oxygen ($\geq 99.99\%$ purity) through a Welsbach Model T-408 ozonizer and its concentration was monitored in situ by LPIR spectroscopy using the $9.5\ \mu$ adsorption band and the published absorptivity.⁶ In the reactions involving water vapor, portions of room air at ~50% relative humidity were admitted to the reaction vessel which were subsequently diluted with a synthetic air mixture to atmospheric pressure and the resulting H_2O concentration was measured by LPIR spectroscopy at $5.02\ \mu$. LPIR spectroscopic analysis showed that the only other significant contaminant in the H_2O air mixture was CO_2 .

In all cases the pressurizing gas was a synthetic mixture of N_2 ($\geq 99.995\%$) plus O_2 (99.99%) or N_2 ($\geq 99.995\%$). All rate constant determinations were carried out at $296 \pm 1^\circ\text{K}$ with the added reactant in large excess of the initial PAN concentration, so that the reactant concentration remained essentially constant throughout the run. PAN concentrations were monitored by LPIR spectroscopy and/or electron capture gas chromatography as a function of time after the reagents were admitted to the reaction vessel.

Results. PAN decays were routinely determined in the absence of any added reactant. The decays were observed to be first order in PAN and PAN half-lives were typically of the order of 35-40 hours. Thus, for example, 0.045 ppm of PAN in the 23 liter Pyrex cell had a decay rate of $k_1 = (3.0 \pm 0.3) \times 10^{-4}\ \text{min}^{-1}$ while 8.0 ppm of PAN in the 65 liter Teflon-coated aluminum tank had a decay rate of $k_1 = (2.45 \pm 0.3) \times 10^{-4}\ \text{min}^{-1}$.

SO_2 , CH_3CHO , H_2O , iso- C_4H_8 , CO , NO_2 , NH_3 , O_3

With these reactants in large excess (except for NH_3 -- see below) pseudo-first order plots of $\ln [\text{PAN}]$ against time were observed to be linear with slopes which increased linearly with the reactant concentration. Hence

$$\ln \frac{[\text{PAN}]_0}{[\text{PAN}]_t} = (k_1 + k_2[\text{reactant}]) (t - t_0) \quad (\text{I})$$

where $[\text{PAN}]_0$, $[\text{PAN}]_t$ are the PAN concentrations at time t_0 and t respectively, k_2 is the rate constant for the reaction



and k_1 is the first order rate constant for the loss of PAN in the absence of other reactants. Plots of the PAN decay rate, defined as $(t-t_0)^{-1} \ln [\text{PAN}]_0 / [\text{PAN}]_t$, against the reactant concentration are shown in Figure 5.1 for the reactants H_2O and O_3 . Linear plots were obtained for the reactants H_2O , NO_2 and CH_3CHO , although a large degree of scatter was observed for NO_2 as the reactant and the rate constants k_2 derived from the slopes of these plots are given in Table 5.1 along with the initial concentrations of PAN and reactant. For CO , SO_2 and isobutene only upper limits for k_2 could be obtained from the experimental data. For O_3 a plot of PAN decay rate against O_3 concentration was observed to be curved (Figure 5.1) and the value of k_2 given in Table 5.1 is that obtained from the initial slope as the O_3 concentration approaches zero. In the case of NH_3 , the ammonia concentration was observed to decay rapidly either in the presence or absence of PAN presumably due to wall absorption. Hence the PAN and NH_3 concentrations were simultaneously monitored and k_2 was obtained directly from the expression

$$-d[\text{PAN}]/dt = k_2 [\text{PAN}][\text{NH}_3] \quad (\text{II})$$

NO

With NO in excess of PAN in air diluent, pseudo-first order plots of $\ln [\text{PAN}]$ against time showed curvature for reaction times typically exceeding one half-life of PAN, as shown in Figure 5.2. However, PAN decay rates, defined as $(t-t_0)^{-1} \ln [\text{PAN}]_0 / [\text{PAN}]$, derived from the initial linear portions of such plots were observed to be independent of the initial NO and PAN concentrations as shown in Table 5.2 and Figure 5.2 and were approximately a factor of 60 higher than the PAN decay rates in the absence of NO. Hence the reaction initially obeys the rate expression

$$-d[\text{PAN}]/dt = k_{\text{obs}} [\text{PAN}] \quad (\text{III})$$

with the PAN decay rate being identified with k_{obs} .

Changing the diluent from air to N_2 or the addition of ~12000 ppm H_2O (~50% relative humidity) caused no change in k_{obs} within the likely experimental errors, although a much larger degree of scatter in the data was

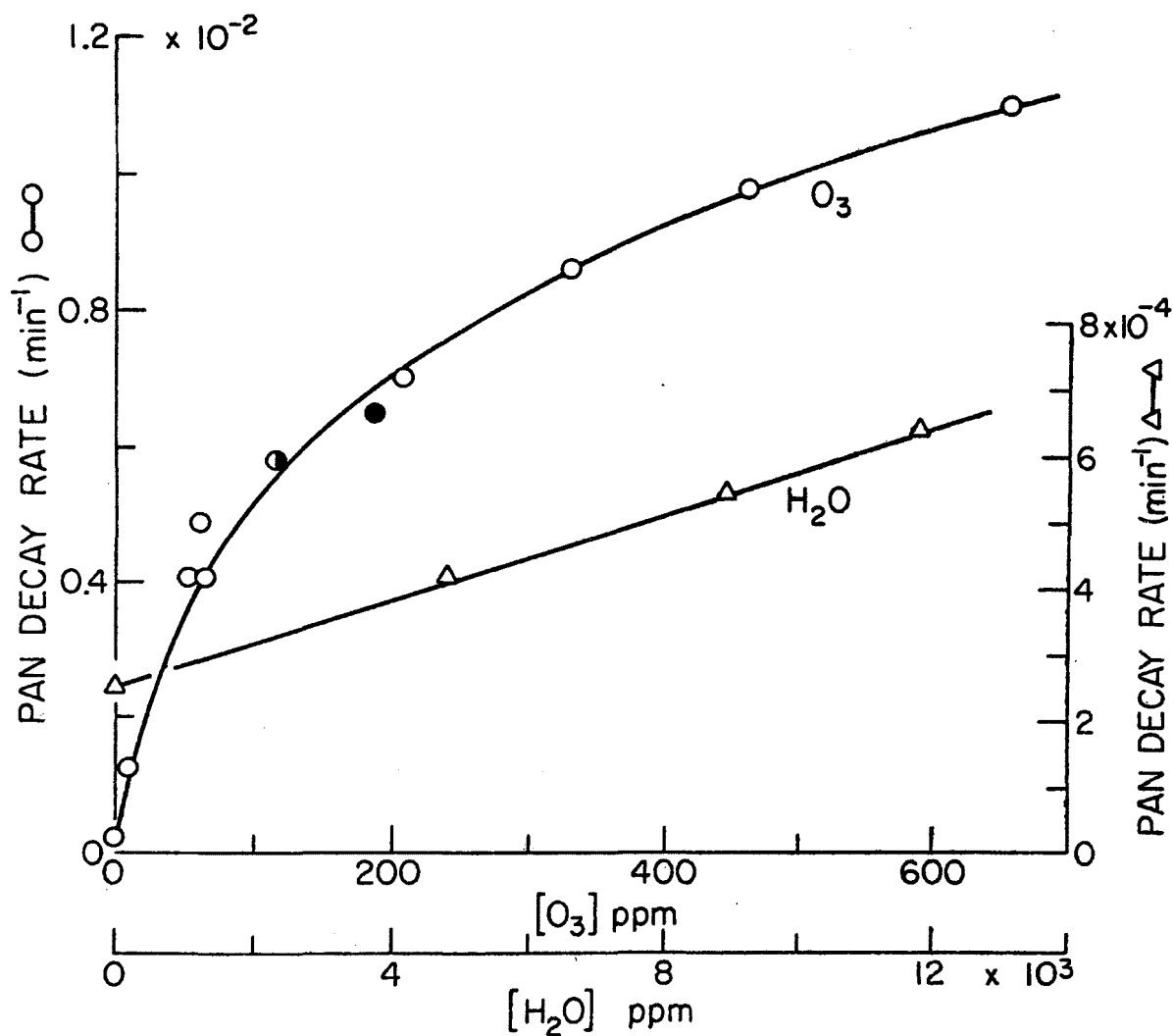


Figure 5.1 Plots of $d \ln[\text{PAN}]/dt$ against reactant concentration for O_3 (initial PAN concentrations 5.1–6.4 ppm (○), 3.0 ppm (◐), 9.7 ppm (●)) and H_2O (Δ, initial PAN concentration 7.6–8.3 ppm).

Table 5.1

Experimental conditions used and the rate constants k_2 obtained for the reaction of PAN with SO_2 , CO , NO_2 , NH_3 , H_2O , O_3 , isobutene and acetaldehyde.

Reactant	Reactant concentration ppm	Initial PAN Concentration ppm	k_2 ppm ⁻¹ min ⁻¹ ^{a)}
SO_2	1260 - 3540	0.042	$<2 \times 10^{-8}$
iso- C_4H_8	51	5.8	$<1 \times 10^{-6}$
CO	232	11.0	$<2 \times 10^{-7}$
CH_3CHO	83 - 312	3.9 - 5.1	$(1.1 \pm 0.2) \times 10^{-6}$
NO_2	26 - 52	3.0 - 9.3	$(2.6 \pm 1.2) \times 10^{-6}$
H_2O	5900 - 12,000	7.6 - 8.3	$(3.3 \pm 0.5) \times 10^{-8}$
O_3	13 - 660	2.9 - 9.6	$\sim 8 \times 10^{-5}$ ^{a)}
NH_3	28 - 50	4.3 - 8.4	$(2.6 \pm 1.0) \times 10^{-5}$

a) Indicated error limits are the estimated overall errors which include least square standard deviations of plots of equation I and the estimated accuracy limits of other parameters such as PAN and reactant concentrations.

b) Derived from the initial slope ($[\text{O}_3] \rightarrow 0$) of Figure 1.

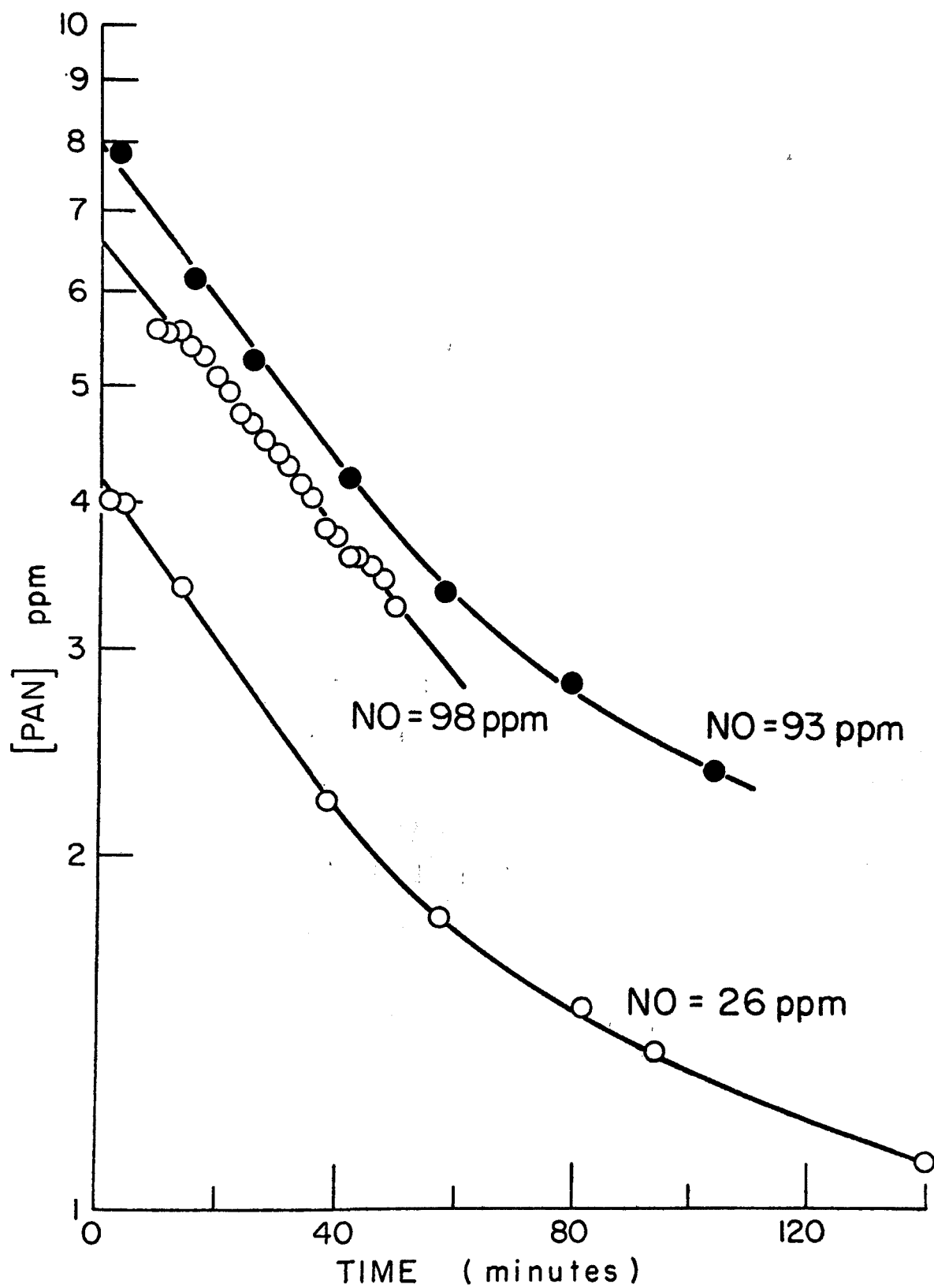


Figure 5.2 Plots of $\ln[PAN]$ against time for the reaction of PAN with NO in air diluent.

Table 5.2

Initial conditions and observed first order rate constants, k_{obs} , for the reaction of PAN with NO.

Diluent	[PAN] ppm	[NO] ppm	$10^2 \times k_{obs} \text{ min}^{-1}$ ^{a)}
Air	4.1	52	1.9 ± 0.2
	4.2	26	1.6 ± 0.1
	4.3	109	1.8 ± 0.1
	5.1	50	1.8 ± 0.1
	6.6	98	1.4 ± 0.1
	7.6	50	1.6 ± 0.1
	7.9	93	1.5 ± 0.1
	17.6	211	1.3 ± 0.1
		<u>Mean</u>	1.6 ± 0.2
Air + 12000 ppm H ₂ O	3.2-8.2	46-202	<u>Mean</u> 1.5 ± 0.6 (5 runs)
N ₂	2.8	50	1.9 ± 0.2
	3.6	50	1.9 ± 0.1
	3.8	50	1.8 ± 0.1
	4.0	25	2.0 ± 0.1
	4.1	75	2.0 ± 0.2
	4.2	101	2.3 ± 0.1
	4.3	101	2.3 ± 0.1
		<u>Mean</u>	2.0 ± 0.2

a) Error limits are least square standard deviations.

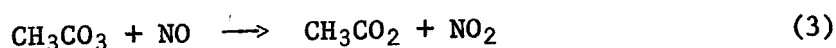
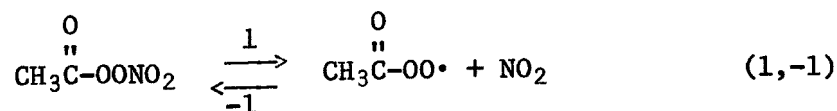
observed for air with 12000 ppm H₂O diluent. The overall value of k_{obs} determined from the data in Table 5.2 is $k_{\text{obs}} = (1.7 \pm 0.5) \times 10^{-2} \text{ min}^{-1}$, where the indicated error is the estimated overall error limit. This value is in good agreement with $k_{\text{obs}} = 2.06 \times 10^{-2} \text{ min}^{-1}$ determined by Schuck et al.⁹ in a 20-liter stirred flow reactor.

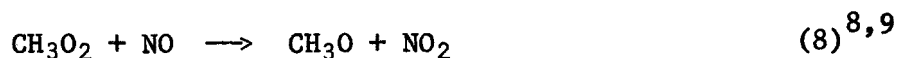
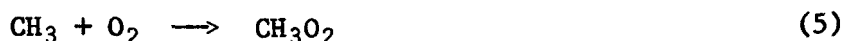
A product analysis of the reaction of PAN with NO was carried out with N₂ as diluent, using a combined gas chromatograph-mass spectrometer and infrared techniques. The observed products were NO₂, CO₂, CH₃ONO, CH₃ONO₂, CH₃NO and CH₃NO₂. The yields of NO₂, CO₂, CH₃ONO and CH₃ONO₂ relative to the loss in the PAN concentration were determined to be 1.7 ± 0.3 , 0.54 ± 0.05 , 0.02 ± 0.01 and 0.08 ± 0.02 , respectively. CH₃NO and CH₃NO₂ were observed to be present in small amounts (<0.05 of the PAN consumed).

Because of the NO-NO₂ thermal conversion in air diluent, no quantitative product analysis study was carried out in this case. However, the same major products (NO₂, CO₂, CHONO and CH₃ONO₂) were observed with the CO₂ yield being similar ($\Delta\text{CO}_2/\Delta\text{PAN} = 0.5 \pm 0.1$) to that observed for PAN + NO in N₂ diluent.

Discussion. The decay of PAN in the absence of added reactant, although first order in PAN, could be either a homogeneous unimolecular loss process or heterogeneous involving wall reactions. Although the decay rates k_1 were observed to be similar in either the 23-liter Pyrex cell or the 66-liter Teflon-coated vessel, no firm conclusions as to the mode of PAN decomposition can be drawn from this data alone.

For the reaction of PAN with NO, the rate law of $-d[\text{PAN}]/dt = k_{\text{obs}}[\text{PAN}]$, determined in N₂ or air diluents, and the value of k_{obs} obtained are in agreement with the work of Schuck et al.,⁷ as is the observation of curvature in the $\ln[\text{PAN}]$ versus time plots. A mechanism which can account for the kinetics of this reaction as well as the products observed is as follows:





Reactions (5-10) account for the observed products in both air and N_2 diluent, with reactions (6),(7) occurring in N_2 but reaction (5) predominately in air. Using the steady-state approximation for the CH_3CO_3 radical,

$$\frac{-d[\text{PAN}]}{dt} = \frac{k_1 k_3 [\text{PAN}] [\text{NO}]}{k_{-1} [\text{NO}_2] + k_3 [\text{NO}]} \quad (\text{IV})$$

When $k_3 [\text{NO}] \gg k_{-1} [\text{NO}_2]$, then $-d[\text{PAN}]/dt = k_1 [\text{PAN}]$ in agreement with the initial stages of the reaction, with $k_1 = k_{\text{obs}}$. However, when this inequality no longer holds, then the PAN decay rate decreases as the ratio $[\text{NO}_2]/[\text{NO}]$ increases, as occurs in the late stages of the reaction, and finally, when $k_{-1} [\text{NO}_2] \gg k_3 [\text{NO}]$, the reaction should obey the rate law

$$\frac{-d[\text{PAN}]}{dt} = \frac{k_1 k_3}{k_{-1}} \frac{[\text{PAN}] [\text{NO}]}{[\text{NO}_2]}$$

It is likely that for the other reactants a similar scheme applies, with reaction (3) being replaced by



If $k_{-1} [\text{NO}_2] \gg k_{11} [\text{reactant}]$ or $k_{12} [\text{reactant}]$, the observed first order dependence on PAN and reactant concentrations will be observed. However, because of the slowness of the removal of PAN in the presence of NO_2 , H_2O , CH_3CHO and NH_3 , the involvement of heterogeneous processes cannot be excluded. In the

case of O_3 as reactant, the observed dependence of the PAN decay rate on the O_3 concentration (Figure 1) may fit an equation similar to equation (IV):

$$\frac{-d[PAN]}{dt} = \frac{k_1 k_a [PAN] [O_3]}{k_{-1} [NO_2] + k_a [O_3]} \quad (VI)$$

where $k_a = k_{11}$ or k_{12} . This would account for the first order dependence on O_3 concentration at low O_3 concentrations, tending to a zero order dependence at high O_3 concentrations.

For atmospheric purposes the half-life, $\tau_{1/2}$, of PAN is of interest. Table 5.3 gives the calculated PAN half-lives using the rate constants obtained in this work, assuming them to be those for the homogeneous gas phase reactions, and typical ambient atmosphere concentrations of the reactants studied. For NO, the minimum PAN half-life of ~0.7 hrs. occurs with NO in excess of NO_2 . In typically polluted atmospheres the presence of NO_2 will increase the half-life of PAN substantially. It can thus be seen that the important atmospheric loss processes of PAN are by reaction with NO and possibly H_2O , although the latter may be heterogeneous in character.

Table 5.3

Chemical lifetimes of PAN in a typical Los Angeles polluted atmosphere

Reactant	Reactant concentration ppm	PAN lifetime ^{a)} $\tau_{1/2}$, hours
CO ^{b)}	10	$>5 \times 10^3$
iso-C ₄ H ₈ ^{b)}	0.004	$>3 \times 10^6$
CH ₃ CHO ^{c)}	0.05	2×10^5
NO ₂ ^{d)}	0.1	4.4×10^4
SO ₂ ^{e)}	0.03	$>2 \times 10^7$
NH ₃ ^{e)}	0.09	5×10^3
O ₃ ^{d)}	0.2	$\sim 7 \times 10^2$
H ₂ O ^{d)}	12,000	29
NO ^{f)}		≥ 0.7

a) $\tau_{1/2} = 0.693/k[\text{reactant}]$

b) W. A. Lonneman, S. L. Kopczynski, P. E. Darley and F. O. Sutterfield, Environ. Sci. and Technol., 8, 229 (1974).

c) Estimate

d) Los Angeles County APCD, Annual Report, 1973.

e) Characterization of Aerosols in California by Science Center, Rockwell International (ARB Contract No. 358) Dec. 15, 1973.

f) See text

REFERENCES

1. E. R. Stephens, Anal. Chem., 36, 928 (1964).
2. E. F. Darley, K. A. Kettner and E. R. Stephens, Anal. Chem., 35, 589 (1961).
3. E. R. Stephens and M. A. Price, J. Chem. Ed., 50, 351 (1973).
4. R. G. Smith, R. J. Bryan, M. Feldstein, B. Levachi, F. A. Miller and E. R. Stephens, Health Laboratory Science, 8, 48 (1971).
5. E. R. Stephens, F. R. Burleson and E. A. Cardiff, J. Air Poll. Contr. Assoc., 15, 87 (1965).
6. P. L. Hanst, E. R. Stephens, W. E. Scott and R. C. Doerr, Anal. Chem., 33, 1113 (1961).
7. E. A. Schuck, E. R. Stephens, M. A. Price and K. R. Darnall, 163rd American Chemical Society Meeting, Boston, MA, U.S.A. (1972).
8. C. T. Pate, B. J. Finlayson and J. N. Pitts, Jr., J. Amer. Chem. Soc., 96, 6554 (1974).
9. R. Simonaitis and J. Heicklen, J. Phys. Chem., 78, 2417 (1974).

6. CHEMILUMINESCENCE DETECTION OF PAN AND PBzN

Our investigations of the chemical reactivity of peroxyacetyl nitrate (PAN) have led to the discovery of chemiluminescent reactions of PAN with tertiary amines which potentially possess the capability of providing a more versatile and sensitive means of monitoring PAN in the atmosphere than the present gas chromatographic technique. The usefulness of such reactions as the basis for monitoring instrumentation has already been realized in the now standard ethylene-ozone chemiluminescent reaction for measuring ambient ozone levels.^{1,2}

Experimental. The reaction vessel consisted of a silvered 1-liter chemiluminescence cuvette provided with two gas inlets centered above the optical window which formed the bottom of the cuvette. Light generated in the reaction cuvette was chopped mechanically at 330 Hz and the output of the photomultiplier (E.M.I. 9659 QB) was fed into a lock-in amplifier (Princeton Applied Research, Model HR8). Cutoff filters were mounted in a wheel arrangement between the optical window and mechanical chopper (Figure 6.1). Low-resolution spectra were obtained with a Bausch and Lomb monochromator (Model 33-86-03) located between the chopper and multiplier phototube. The amplified signals were displayed on a 100 mV potentiometric Sargent recorder (Model SRG). The monochromator-multiplier phototube unit was calibrated by use of a standard lamp (G.E. quartz iodine lamp EPI-1452, 1000 W) and the spectra were corrected for spectral sensitivity.

Identical spectra were obtained whether the amine was added to the reaction cuvette in a stream of nitrogen or whether an excess of amine (liquid-vapor equilibrium) was present in the cuvette. Variable concentrations of both PAN and ozone were prepared and passed into the cuvette at a constant flow rate (~10 cc/sec). All experiments were performed at room temperature.

Peroxyacetyl nitrate (1000 ppm, pressurized tanks) was kindly provided by the University of California Statewide Air Pollution Research Center at Riverside. Ozone (~2% V/V) was produced by passing oxygen (Matheson, ultra-high-purity grade) through a Welsbach Model T-408 ozonizer. Triethylamine (Matheson, Coleman & Bell or Mallinckrodt gave identical results) was checked for purity by glc (>99.95%) and used without further purification.

Results and Discussion. Various amines (in the gas and solution phase) were tested for their chemiluminescence efficiency when reacted with PAN (see

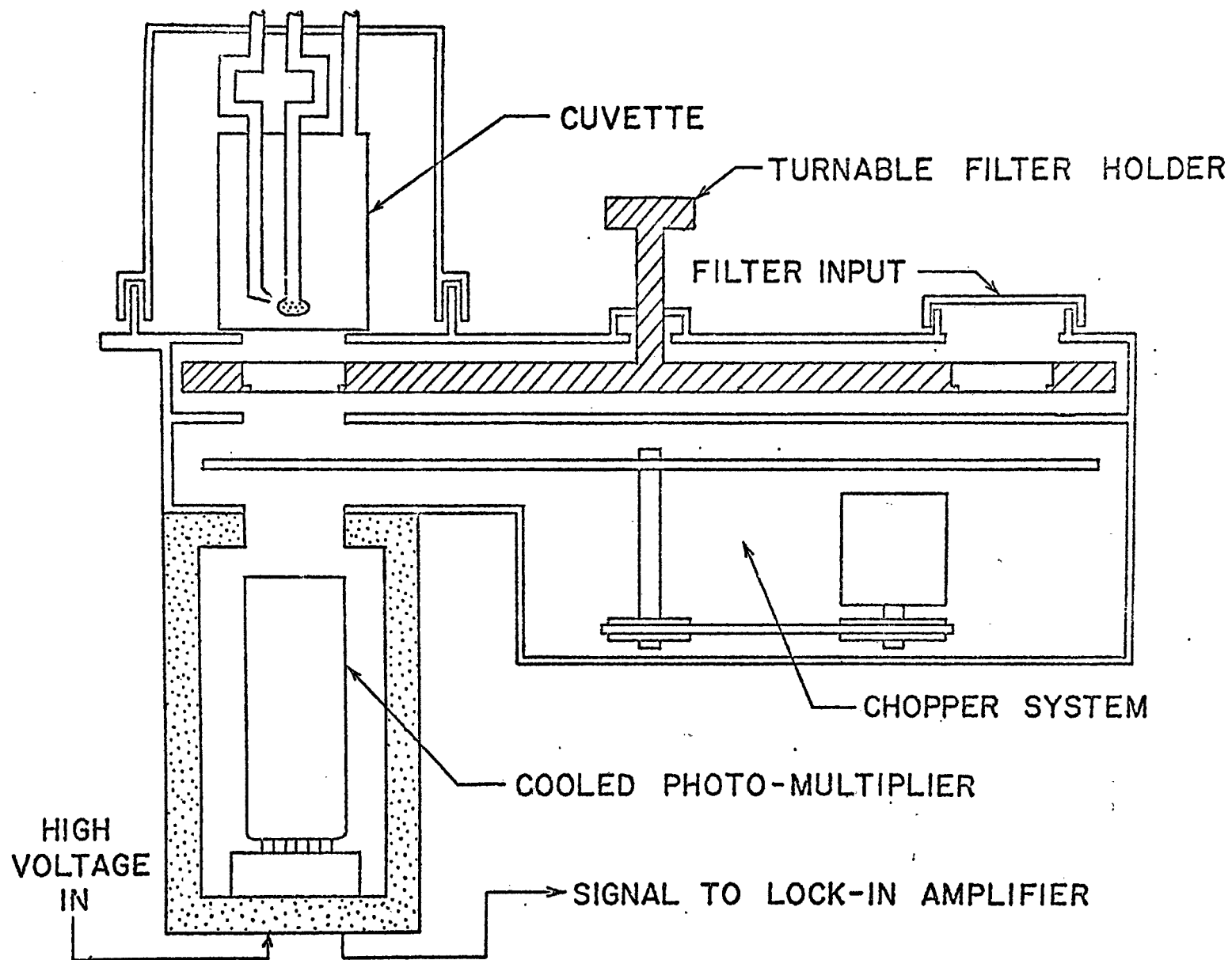


Figure 6.1 Chemiluminescent detection unit

Table 6.1). For both the gas and solution phase, triethylamine was found to yield the highest light output when reacted with PAN. The emission from the liquid-phase reaction of 1% triethylamine in acetone with PAN gives constant

Table 6.1

Chemiluminescence efficiency of amines reacting with PAN (1000 ppm) in the gas phase and in solution.

Compound	Vapor pressure (torr) 25°C	I_{Rel} (Et ₃ N in acetone = 100)
Ammonia	gas	0
Methylamine	gas	0
Ethylamine	(in water) saturated gas stream	3
Propylamine	300.8	1.0
Butylamine	53.7	0.7
Dimethylamine	112 (in water)	0
Diethylamine	57.5	11.5
Dipropylamine	saturated	4.7
Diisopropylamine	saturated	2.4
Dibutylamine	saturated	10
Diisobutylamine	18.00	4
Trimethylamine	128 (in water)	16
Triethylamine	saturated	40
Aniline	liquid phase, 1% in acetone	0.8
N,N-Dimethylaniline	" "	52.5
Diphenylamine	" "	1.3
Tribenzylamine	" "	18.6
Triethylamine	" "	100

reproducible chemiluminescence for a given PAN concentration with the intensity immediately dropping to the dark-current level as the flow of PAN is terminated.

This is in contrast to the gas phase reaction which produces a long lasting afterglow. Concentrations of PAN as low as 6 ppb were detected with a signal-to-noise ratio of about 3. This is nearly as sensitive as present gas chromatographic techniques.³ Improvement of the light detection system may permit measurement of PAN concentrations as low as 1 ppb or less.

We have recently found that the gas phase reaction of peroxybenzoyl nitrate (PBzN) with triethylamine is also chemiluminescent. The emission spectrum using cutoff filters shows a sharp maximum from 590 to 610 nm. Concentrations of PBzN at least as low as 5 ppb could be detected by this method.

Corrected low-resolution spectra of the light emissions produced in the reactions of PAN (1000 ppm) and ozone (20,000 ppm) with triethylamine vapor were obtained independently and are shown in Figure 6.2 for comparison. The relative intensity maximum was arbitrarily set at unity. The maxima were separated by approximately 130 nm.

In control experiments, methylnitrate, ethylnitrate, ethylnitrite, and NO₂, all of which are possible contaminants of PAN, were mixed with triethylamine vapor in the reaction cuvette and showed no evidence of luminescence. In a similar control experiment, the reaction of nitric oxide (1000 ppm) with triethylamine resulted in a weak luminescence which was enhanced in the presence of air. However, the emission observed from 10 ppm nitric oxide was insignificant compared to that produced from 0.4 ppm PAN.

The reaction of PAN with triethylamine produced a slowly decaying afterglow which lasted for several minutes even at the lowest PAN concentrations employed. This behavior is contrasted to that of the corresponding ozone reaction in which the emission rapidly decayed after the ozone flow ceased. The respective decay curves are illustrated in Figure 6.3.

To distinguish the chemiluminescence induced by the reaction of triethylamine with concentrations of PAN and ozone found in polluted urban atmospheres, various combinations of cutoff filters were tested. A 500-nm cutoff filter (transparent: $\lambda < 550$ nm) in conjunction with a 665-nm cutoff filter (transparent: $\lambda > 665$ nm) provided relative intensity values characteristic for both the PAN and ozone induced emissions. In the case of ozone-triethylamine reaction, a value of $I_{665}/I_{550} < 1$ was predicted from the

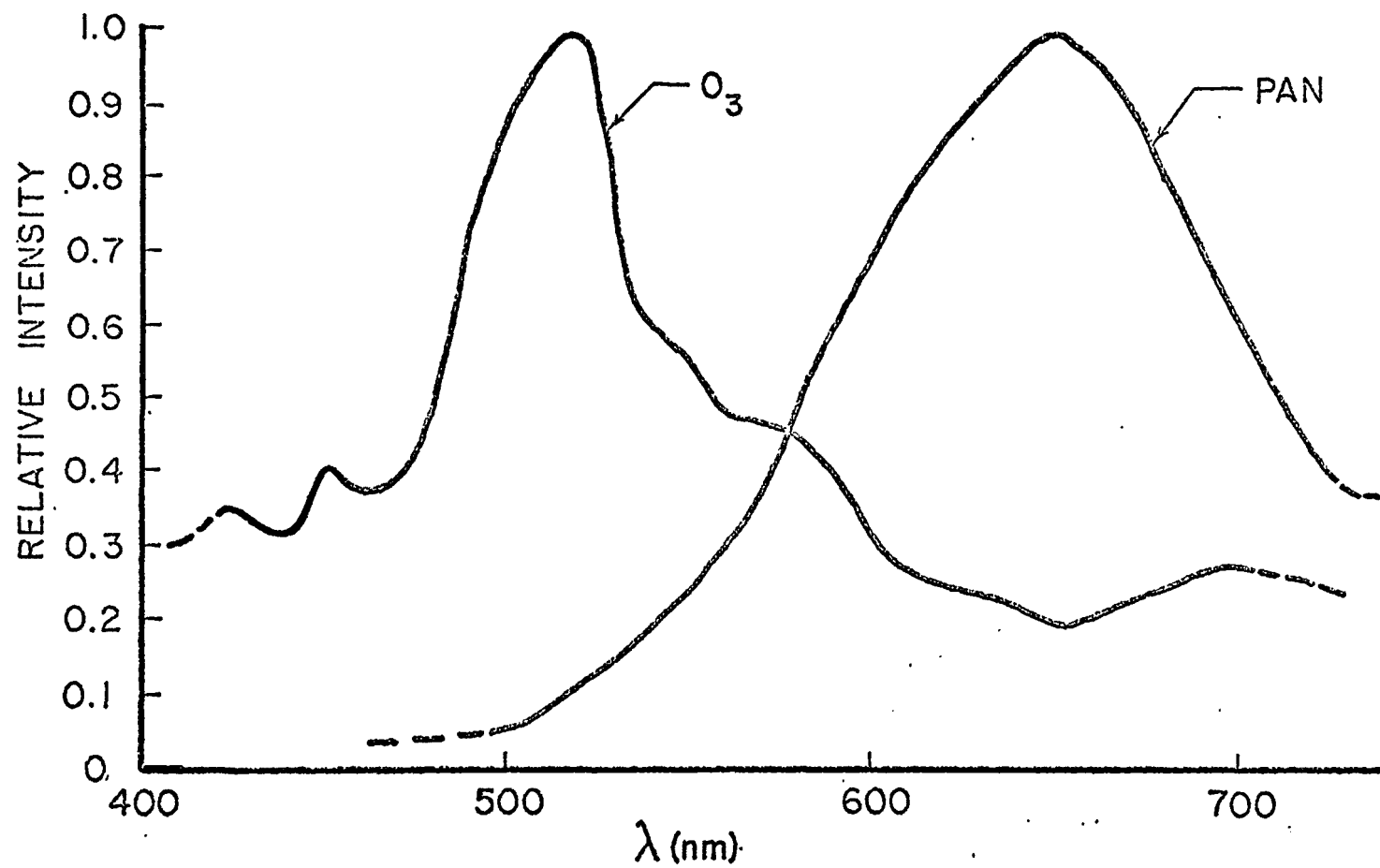


Figure 6.2 Emission spectra of chemiluminescence reactions of triethylamine with PAN and ozone. Relative intensity maximum arbitrarily set at unity.

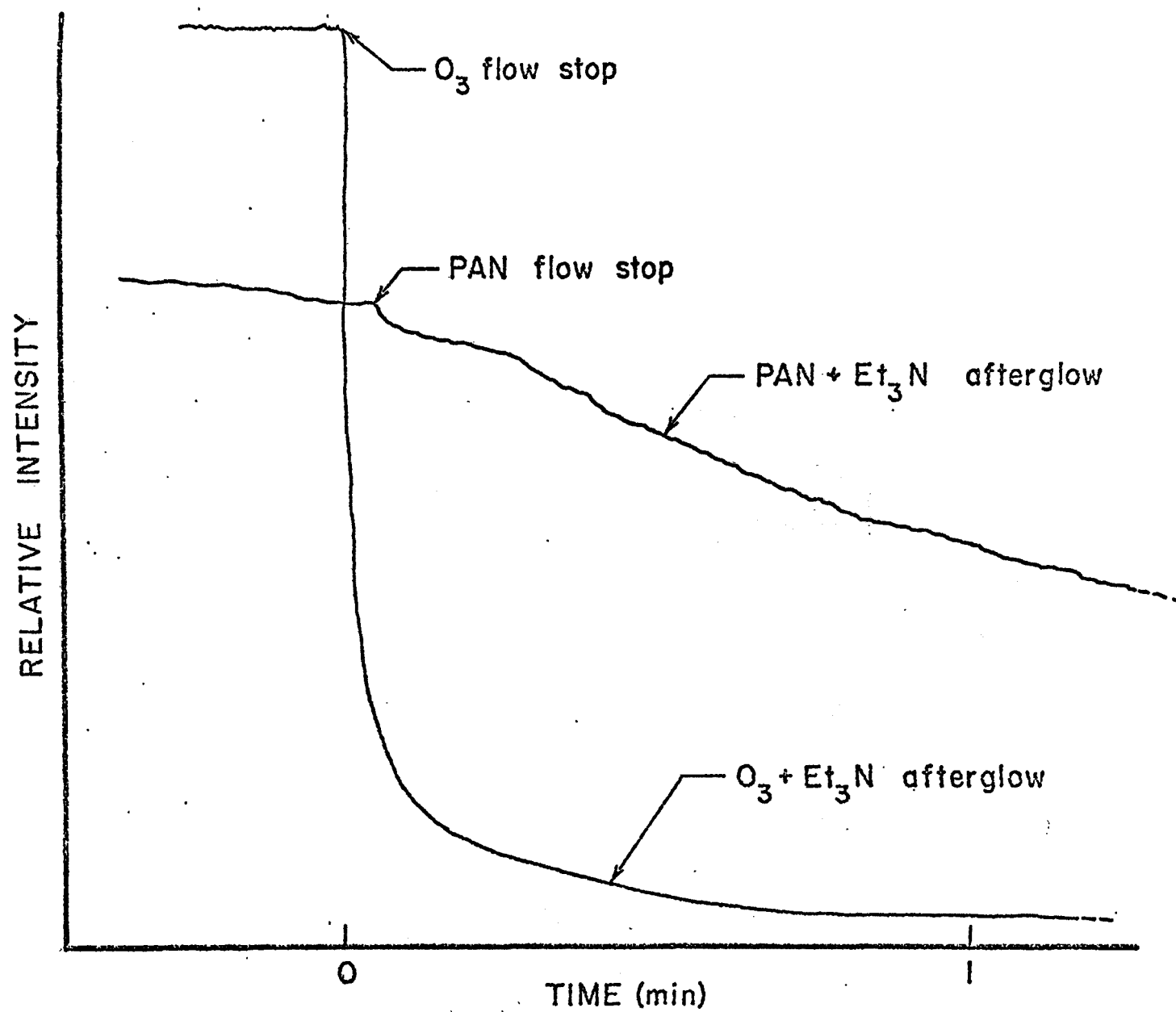


Figure 6.3 Decay curves of chemiluminescence generated in reaction of triethylamine with PAN and ozone.

monochromator spectra shown in Figure 6.2; for the PAN-triethylamine reaction, a value of $I_{665}/I_{500} > 1$ was predicted. The measured values of I_{665}/I_{500} were 0.35 and 3.44 for the ozone-amine and the PAN-amine reactions, respectively. This combination of cutoff filters affords the most appropriate means of distinguishing the two emissions at low concentrations of PAN and O_3 where the use of a monochromator is not feasible.

To test the cutoff filter technique, the chemiluminescence produced by a mixture containing a 20-fold excess of ozone to PAN, a ratio not uncommon in polluted ambient air, was investigated. In this particular case, a value of I_{665}/I_{500} of 1.35 was found, indicating a much greater chemiluminescence efficiency for the PAN-amine reaction in contrast to the ozone-amine reaction.

In an experiment designed to measure the chemiluminescence efficiency of the PAN-amine reaction relative to the corresponding O_3 -amine reaction, 1.5 ppm of O_3 produced the same uncorrected overall integrated light intensity as 0.4 ppm PAN in reaction with the amine. As an approximate correction for spectral sensitivity of the multiplier phototube over the integrated emission spectrum, the relative quantum efficiencies at the λ_{\max} values of the emissions produced by the PAN and O_3 reactions, 0.35 and 0.79, respectively, were applied. From these data, the chemiluminescence efficiency of the PAN reaction was calculated to be approximately 10 times greater than the corresponding ozone reaction.

The development of an improved chemiluminescence method of detecting PAN has been attempted. Based on a suggestion by Dr. Hanst of the EPA, a photowheel-chopper system was built to provide elimination of the ozone-amine chemiluminescence (λ_{\max} 520 nm) which tails into the PAN-amine emission (λ_{\max} 665 nm). A modulation technique (using a rotating filter wheel with quadrants alternately consisting of Corning 2-73 and 3-74/neutral density filters) was used with a lock-in amplification to provide a d.c. signal for the O_3 -amine emission and an a.c. signal for the PAN-amine emission. The resulting lock-in amplifier response (sensitive to a.c. only) thus gives a measure of the PAN concentration. With this system the ozone-amine emission is successfully eliminated but at the cost of a 10-fold reduction in detection of PAN sensitivity.

REFERENCES

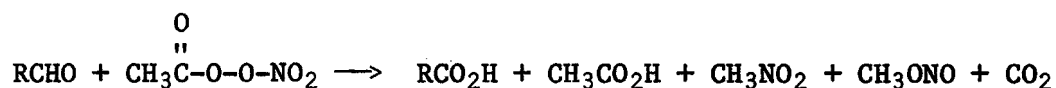
1. C. W. Nedergragt, A. Van der Horst and T. Van Duijn, *Nature*, 206, 87 (1965).
2. J. A. Hodgeson, J. P. Bell, K. A. Rehme, K. J. Krost and R. K. Stevens, Joint Conference on Sensing of Environmental Pollutants, Palo Alto, California, November 8-10, 1971, AIAA Paper No. 71-1067.
3. R. G. Smith, R. J. Bryan, M. Feldstein, B. Levadie, F. A. Miller and E. R. Stephens, *Health Lab. Sci.*, 8, 48 (1971).

7. SOLUTION PHASE REACTIONS OF PAN WITH MOLECULES OF BIOLOGICAL SIGNIFICANCE

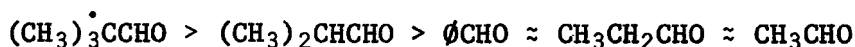
The destruction or alteration of a functional group in a molecule of biological significance is likely to alter its biochemical modes of reaction, ultimately harming the cell. PAN has already been implicated in the phytopathology of several species¹ and has been shown to be lethal to mice in sufficiently high concentrations.² The chemical reactions actually responsible for these effects are not known.

In order to understand these chemical effects, a study of the reactions of PAN with a variety of organic molecules (aldehydes, alcohols, amines, mercaptans and sulfides) containing functionality found in common biological compounds such as amino acids, proteins, fatty acids, and carbohydrates, was undertaken. The reactions of PAN in solution have been followed primarily by NMR spectroscopy, although infrared spectra of the product solution were frequently used and gas chromatography was used to follow one reaction.

Aldehydes. PAN oxidizes aldehydes to the corresponding acids according to the following general reaction:³



In either benzene or carbon tetrachloride, the relative reaction rates for several aldehydes are:



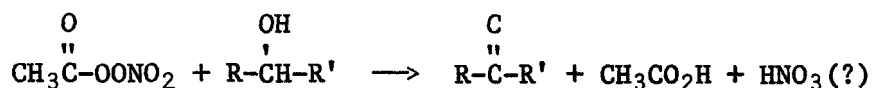
Although the final reaction products were not solvent-dependent, the reaction pathway varied with the solvent. In CCl_4 , the acid chloride corresponding to the aldehyde was observed as an intermediate which was converted to the acid. A comparison of products derived from PAN in benzene and carbon-tetrachloride is given in Table 7.1 for the reaction of PAN with isobutyraldehyde. There is some evidence that the reaction in CDCl_3 is first order in PAN.

Table 7.1

PAN products, % of total, from reaction of isobutyraldehyde

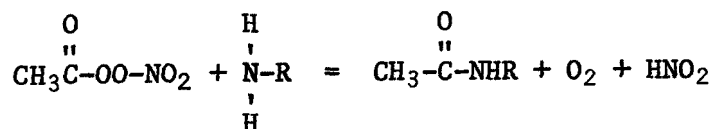
Solvent	CH ₃ CO ₂ H	CH ₃ ONO	CH ₃ NO ₂	CH ₃ Cl	Others
CCl ₄	73	7	12	8	0
Benzene	39	12	35	0	14

Alcohols. Secondary alcohols (2-propanol, α-methylbenzyl alcohol, cyclohexanol) react with PAN as follows:⁴



The reactions were run in three solvents: in acetone-d₆, the reaction is relatively clean; in CCl₄, one unidentified product occurs in low yield; in benzene, several unidentified trace products are detected.

Amines. PAN has been found to react with ammonia, primary amines (methylamine, ethylamine, n-propylamine, n-butylamine) and tertiary amines (triethylamine and N,N-dimethylaniline). In CDCl₃ solution, the reactions with ammonia and primary amines suggest the following stoichiometry and products (no by-products were detected):⁵

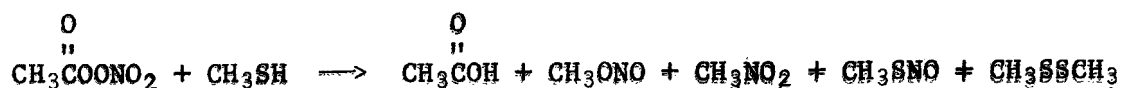


The amides were identified by comparison of their spectra with those of independently synthesized compounds. HNO₂ was identified by its characteristic, highly structured UV absorption spectrum. In the solution phase reaction of n-propyl amine, oxygen production was observed as a vigorous evolution of gas.

In solution, PAN reacts very rapidly with tertiary amines, the reaction being complete in one minute when reactant concentrations are both 0.1 M. The reaction with triethylamine yields one major amine product (80 to 90%),

as yet unidentified, along with nitrogen dioxide (detected by its chemiluminescent emission) and acetic acid. The expected amine oxide may also be present in yields of 10% or less.

Mercaptans. The reaction of PAN with a 4- to 6-fold excess of methyl mercaptan has been run in deuteriochloroform (CDCl_3) and aqueous acetone- d_6 . The number of moles of mercaptan consumed per mole of PAN was 3 to 4 in CDCl_3 and 2 to 3 in acetone- d_6 . The major products are shown in the following reaction:⁶



Small amounts of methyl methanethiosulfonate ($\text{CH}_3\text{SO}_2\text{SCH}_3$) and traces of several other compounds were also detected.

If only one equivalent or less of methyl mercaptan is reacted with PAN in CDCl_3 , the initial products are CH_3SSCH_3 and CH_3SNO . The latter rapidly disappears, accompanied by a vigorous evolution of gas and the appearance of an NMR emission peak corresponding to CH_3SSCH_3 . Ultimately, the CH_3SSCH_3 is converted to $\text{CH}_3\text{SO}_2\text{SCH}_3$ and at least one other product.

Sulfides. In CDCl_3 solutions containing a 5-fold excess of dimethylsulfide (CH_3SCH_3), PAN reacts forming approximately 2 to 3 moles of dimethylsulfoxide (CH_3SOCH_3) depending on the reaction conditions.⁶ In this system PAN is degraded to acetic acid and acetylnitrate is detected as a transient intermediate.

REFERENCES

1. O. C. Taylor, J. Air Pollut. Control Assoc., 19, 347 (1969).
2. K. I. Campbell, G. L. Clarke, L. O. Emik and R. L. Plata, Arch. Environ. Health, 15, 739 (1967).
3. P. H. Wendschuh, C. T. Pate and J. N. Pitts, Jr., Tetrahedron Letters, 31, 2931 (1973).
4. P. H. Wendschuh and J. N. Pitts, Jr., unpublished results.
5. P. H. Wendschuh, H. Fuhr, J. S. Gaffney and J. N. Pitts, Jr., J. Chem. Soc., Comm., 74, (1973).
6. K. R. Darnall, D. M. Hebert, J. M. Hughes, J. W. Wilson and J. N. Pitts, Jr., unpublished results.

8. THERMAL AND PHOTOCHEMICAL PROCESSES OF NO AND NO₂ AND THE APPLICATION OF THE RESULTS TO THE CHEMISTRY OF POLLUTED ATMOSPHERES

Introduction. The NO₂ catalyzed geometric isomerization of 2-butene and 2-pentene has been examined over the temperature range 298° to 400°K. Both kinetic and equilibrium data have been obtained. The combination of these results with results from thermodynamic calculations permits the estimation of rate constants for the addition of NO₂ to the double bond of simple olefins. Comparison of these rate constants to those for the consumption of olefins by O₃ suggests that atmospheric consumption of olefins by processes initiated by NO₂ addition to an olefin double bond cannot be significant in the atmospheric consumption of olefins.

Experimental. cis-2-Butene (Matheson research grade, 0.7% trans-2-butene impurity), trans-2-butene (Matheson research grade, 0.3% cis-2-butene impurity), cis-2-pentene (Chemical Samples, 0.8% trans-2-pentene impurity), and trans-2-pentene (Chemical Samples, ≤0.1% cis-2-pentene impurity) were thoroughly degassed by bulb-to-bulb distillation, analyzed by glc for hydrocarbon impurities, and used without further purification. NO₂ (Baker CP grade) was mixed with an equal pressure of O₂ (Matheson research grade used as received) and allowed to stand overnight to remove any NO and N₂O₃ impurity ($N_2O_3 \rightleftharpoons NO + NO_2$; $2NO + O_2 \rightleftharpoons 2NO_2$). The NO₂ was then thoroughly degassed by bulb-to-bulb distillation and used without further purification.

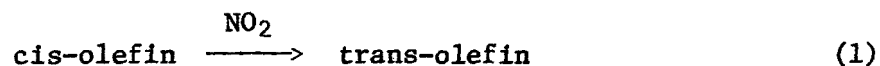
The all-glass reaction system (total volume 2.7 l) consisted of a 2.3-l bulb with two exit arms connected by a gas circulating loop. Mounted in the circulating loop was a circulating pump driven by magnetic coupling to an external motor. The reaction system was housed in a simple oven constructed of wood and insulating board. Two fans with motors mounted outside the oven provided efficient circulation of the air within the oven. Oven temperatures were measured using ice bath referenced thermocouples. The oven had a temperature range of 25-125°C and a temperature stability of ≤0.5°C. The reaction system was serviced by a conventional high vacuum line. Greaseless O-ring stopcocks were used throughout the reaction system and the high vacuum line. Reaction system pressures were measured using an MKS Baratron gauge (0.1-300 torr).

The gaseous reaction mixture was directly sampled using a Carle micro-volume gas sampling valve (sample loop volume ~200 μl) connected through a

greaseless O-ring stopcock to the circulating loop of the reaction system. Glc analyses for cis and trans olefin were performed on a 10% NaCl on alumina column (3 ft, 1/8 in.; 100-120 mesh, acid washed, activated alumina) operated at ~75°C. The Varian Aerograph gas chromatograph was equipped with a flame ionization detector. Glc peaks were displayed on a 1-mV potentiometric recorder equipped with a Disc integrator. The response and linearity of the entire analytical train (gas sample valve, gc, recorder) were calibrated, using standard gas mixtures prepared using the Baratron gauge. The combined precision of the gc analyses and calibrations was better than ±1%.

Results. The equations used to develop the experimental data were identical for all four olefins. They will be described only as they apply to cis-olefin. Exchanging the symbols C and T will yield the corresponding equations for trans-olefin.

For the reaction



the initial rate of isomerization at low conversion may be written¹

$$d[T]/dt = k_{\text{cis}}[\text{NO}_2]_0[C]_0 \quad (2)$$

where k_{cis} is the experimentally determined rate constant, T and C denote trans- and cis-olefin and the zero subscripts denote initial concentrations. This expression may also be written

$$[T]_t/[C]_0 = k_{\text{cis}}[\text{NO}_2]_0 t \quad (3)$$

Since $[T]_t/[C]_0 = (1 + [C]_t/[T]_t)^{-1}$ by measuring $[C]_t/[T]_t$ as a function of time (t), the observed rate constant, k_{cis} , can be determined easily and precisely.

All experiments were run to conversions of less than 5%. As expected for such low conversions, the observed dependence of $[C]_t/[T]_t$ on t was always linear. Figure 8.1 illustrates the precision of the linearity routinely obtained. Nevertheless, this apparent linearity must mask the perturbing effects of some reverse isomerization.

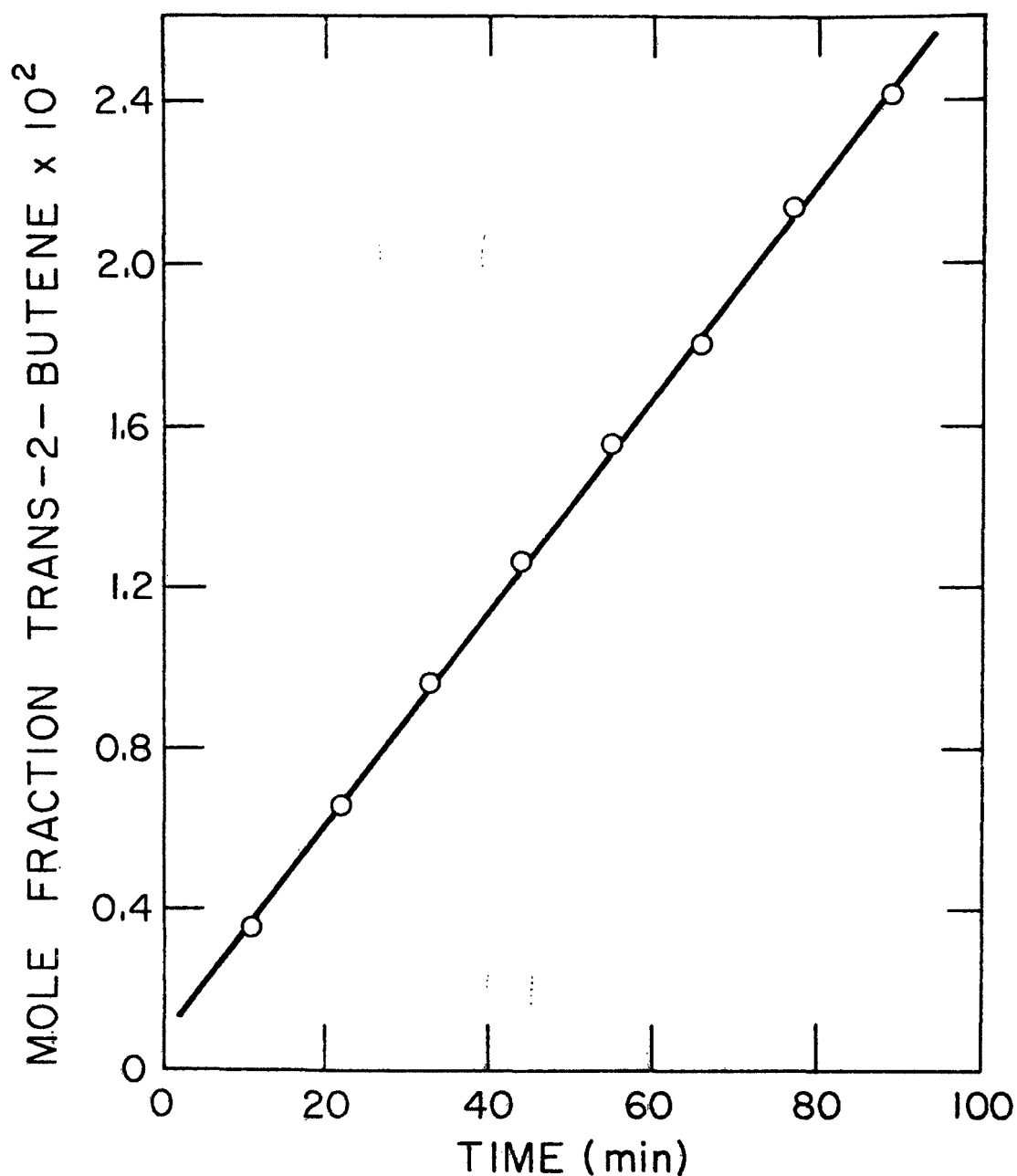
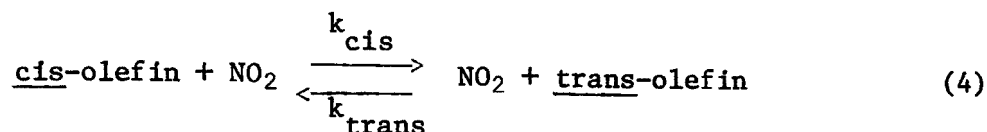


Figure 8.1 Plot of the mole fraction of trans-2-butene vs time for the cis- to trans-NO₂ catalyzed geometric isomerization of cis-2-butene. The least-squares slope of the plot is $2.64 \pm 0.03 \times 10^{-4} \text{ min}^{-1}$. Reaction conditions were 9.00 torr of cis-2-butene, 0.100 torr of NO₂, and $54.4 \pm 0.2^\circ\text{C}$. The nonzero intercept is due to the presence of a trace of trans-2-butene impurity in the starting cis-2-butene.

Normal kinetic treatment of the following reaction scheme



yields eq. 5, where $K_{\text{TC}} = k_{\text{trans}}/k_{\text{cis}}$. Iterative use of

$$k_{\text{cis}}^t = \frac{1}{[1 + K_{\text{TC}}][\text{NO}_2]_0} \times \ln \left\{ 1 - [1 + K_{\text{TC}}] \frac{[\text{T}]_t}{[\text{C}]_0 + [\text{T}]_0} \right\} \quad (5)$$

eq. 5 allowed the raw rate constants (k_{cis} or k_{trans}) calculated using eq. 3 to be corrected for the perturbing effects of reverse isomerization. To do this the raw values for k_{cis} and k_{trans} were used to calculate an initial set of Arrhenius parameters for these rate constants. An initial value of K_{TC} (or K_{CT}) was then calculated from these Arrhenius parameters. Substitution of this value into eq. 5 now allowed a new set of values for k_{cis} (or k_{trans}) to be calculated. This process was repeated until a consistent set of values was obtained for k_{cis} and k_{trans} .

Figures 8.2 and 8.3 present plots of $\log k$ vs. θ^{-1} where $\theta = 2.3RT$. The lines are the least-squares lines calculated from the data. The slope and intercept of each least-squares line give the Arrhenius parameters of that reaction. Table 8.1 summarizes the experimental results:

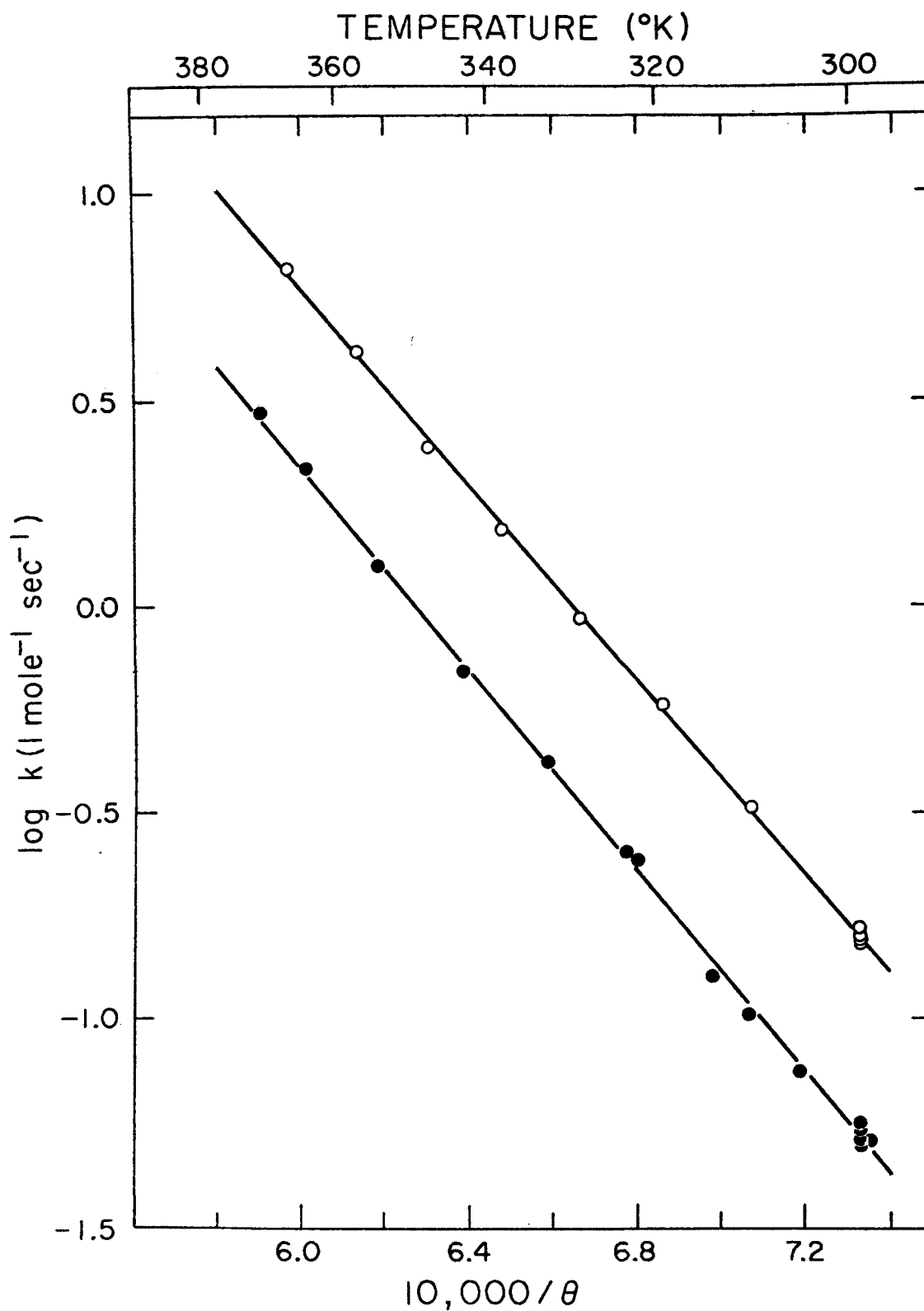


Figure 8.2 Arrhenius parameters for the NO_2 catalyzed geometric isomerization of cis- or trans-2-butene. Plot of $\log k$ vs θ^{-1} where $\theta = 2.3RT$: (O) cis-2-butene; (●) trans-2-butene.

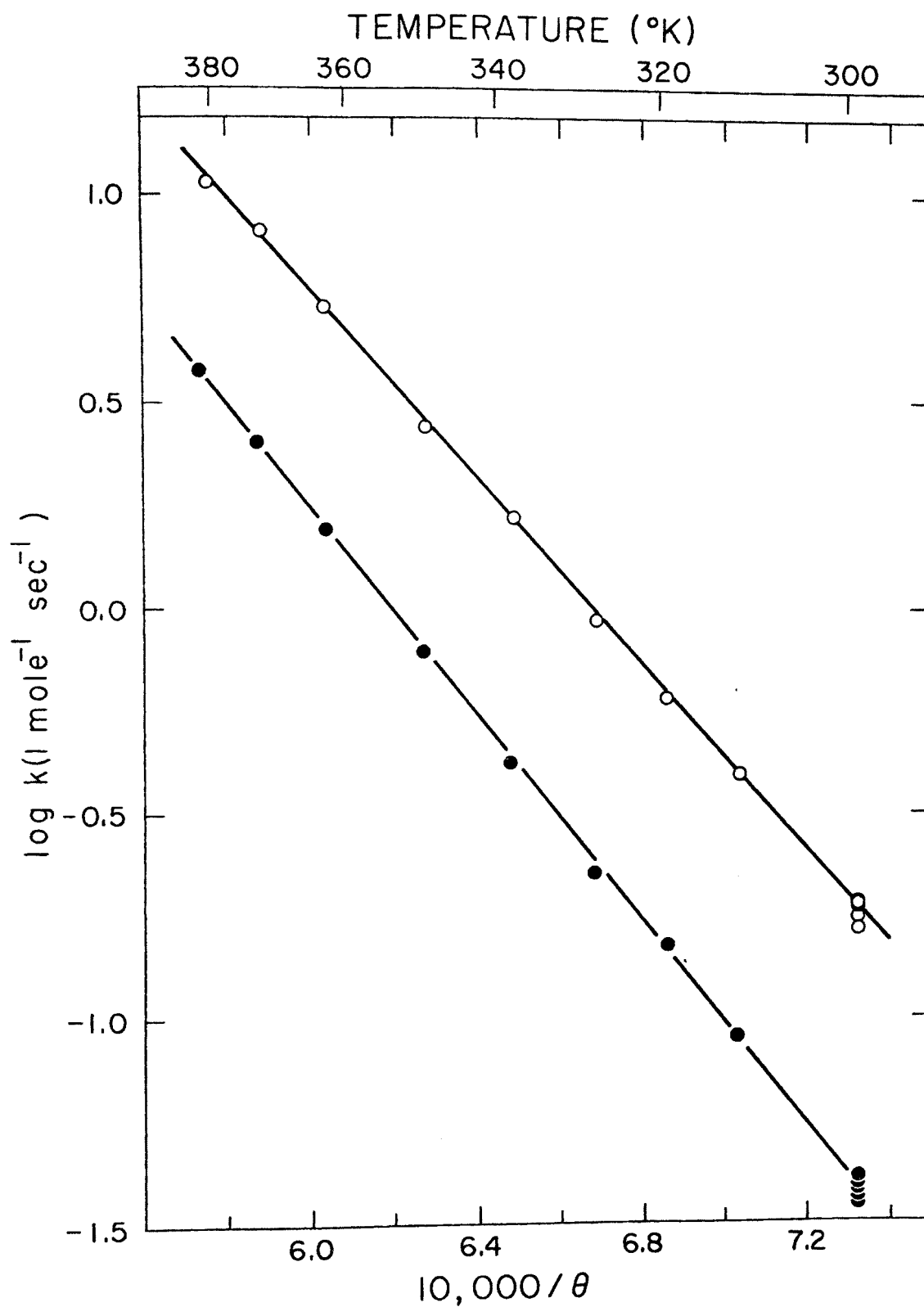


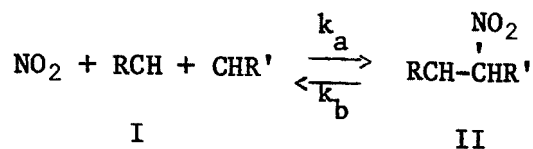
Figure 8.3 Arrhenius parameters for the NO_2 catalyzed geometric isomerization of cis- or trans-2-pentene. Plot of $\log k$ vs θ^{-1} where $\theta = 2.3RT$: (O) cis-2-pentene; (●) trans-2-pentene.

Table 8.1

Thermodynamic and Arrhenius parameters for the NO₂ catalyzed geometric isomerization of the 2-butenes
and 2-pentenenes

Olefin	cis-2-Butene	trans-2-Butene	cis-2-Pentene	trans-2-Pentene
$k(1 \text{ mole}^{-1} \text{ sec}^{-1} \text{ at } 25^\circ)$	0.159 ± 0.002	0.053 ± 0.001	0.183 ± 0.005	0.038 ± 0.001
$\text{Log } A(1 \text{ mole}^{-1} \text{ sec}^{-1})$	7.86 ± 0.06	7.65 ± 0.08	7.49 ± 0.06	7.72 ± 0.06
$E(\text{kcal mole}^{-1})$	$11.8 \pm .1$	12.2 ± 0.1	11.2 ± 0.1	12.5 ± 0.1
$\Delta H_r^0, 298(\text{kcal mole}^{-1})$	-1.00 ± 0.02		-1.16 ± 0.07	
$\Delta H_r^0, 298(\text{eu})$	-1.15 ± 0.03		-0.81 ± 0.10	

For the reaction



several thermodynamic quantities may be defined as follows:

$$K_{ab} = \frac{k_a}{k_b} \text{ where } k_a = A_a e^{-E_a/RT} \text{ and } k_b = A_b e^{-E_b/RT}$$

$$-RT \ln K_{ab} = \Delta H_{ab}^{O,c} - T \Delta S_{ab}^{O,c} \quad (3)$$

$$\Delta H_{ab}^{O,c} = E_a - E_b \quad (4)$$

$$A_b = \frac{ekt}{h} e^{\Delta S_b^*/R} \text{ and } A_a = A_b e^{\Delta S_{ab}^{O,c}/R}$$

As described elsewhere² $\Delta H_{ab}^{O,c}$ and $\Delta S_{ab}^{O,c}$ can be estimated from thermochemical data and ΔS_b^* can be estimated by incremental methods.³

The activation energy for C-C bond rotation in the radical II should be small ($\sim 5 \text{ kcal mole}^{-1}$)⁴ compared to the activation energies (E_a and E_b) for the formation and unimolecular decomposition of the radical. Therefore, values of E_a for the 2-butene and the 2-pentenenes may be calculated directly from the experimental data presented above. For simple olefins, however, E_b is unlikely to be very sensitive to whether R or R' is an alkyl group of an H atom. Therefore, equation (4) permits E_b to be estimated from the calculated 2-butene and 2-pentene values for ΔH_{ab} and E_a . Using a 3 σ error limit gives $E_b = 12.8 \pm 2 \text{ kcal mole}^{-1}$ for the unimolecular decomposition of the radical (II) derived from any simple olefin.

Once a value for E_b is available, E_a can be estimated for any olefin for which $\Delta H_{ab}^{O,c}$ can be calculated. Then, because A_a can be calculated from ΔS_b^* and $S_{ab}^{O,c}$, k_a can also be estimated. Table 8.2 summarizes the results of our thermodynamic calculations. It should be noted that unsymmetrical olefins give two values of ΔS_b .

In polluted urban atmospheres, at least during the day, the concentrations of O_3 and NO_2 are roughly comparable. Therefore, since the rate constants

Table 8.2

Calculated and experimental data for the reactions of nitrogen dioxide with selected olefins.

Olefin	$\Delta H^{O,c}_{ab}$	$\Delta S^{O,c}_{ab}$	ΔS^{\ddagger}_b	$A_a \times 10^{-7}$	E_a	calc $k_a \times 10^3$ a)	$k_{NO_2} \times 10^3$ b)
	kcal mole ⁻¹	eu	eu	1 mole ⁻¹ sec ⁻¹	kcal mole ⁻¹	1 mole ⁻¹ sec ⁻¹	
Acetylene	2.60	-25.0	4.5	58.1	14.4	0.017	
Ethylene	2.19	-24.1	4.6	93.6	14.0	0.053	1.8
Propylene	1.75	-25.4	0.8	7.40	13.6	0.009	0.031
	1.70	-27.7	4.8	17.4	13.5	0.022	
1-Butene	1.51	-25.7	0.8	6.24	13.3	0.011	0.359
	-0.14	-28.4	4.8	12.0	11.7	0.348	
iso-Butene	0.61	-25.2	3.9	37.5	12.4	0.301	0.301
	4.46	-30.0	5.1	6.15	16.3	0.0001	
cis-2-Butene	-0.37	-27.0	1.4	4.41	11.4	0.189	23.0
trans-2-Butene	-0.17	-25.9	1.4	7.44	11.6	0.023	32.0
1-Pentene	1.29	-26.1	1.2	6.21	13.1	0.016	0.337
	-0.16	-28.6	4.8	10.8	11.6	0.321	
cis-2-Pentene	-0.65	-28.5	1.4	2.05	11.2	0.140	0.189
	0.15	-28.1	1.6	2.76	12.0	0.049	
trans-2-Pentene	-0.56	-27.1	1.4	4.13	11.3	0.243	0.328
	0.24	-26.7	1.6	5.59	12.1	0.085	

a) For unsymmetrical olefins, the overall rate constant is the sum of the rate constants for the formation of each of the two possible intermediates.

b) See Ref. 5.

for atmospheric consumption of simple olefins by O_3 are all $10^3 - 10^4$ l mole⁻¹ sec⁻¹, it is obvious that consumption of olefins by reaction pathways initiated by NO_2 addition to the double bond of an olefin cannot compete kinetically with olefin consumption by O_3 .

REFERENCES

1. J. L. Sprung, H. Akimoto and J. N. Pitts, Jr., J. Amer. Chem. Soc., 93, 4358 (1971).
2. J. L. Sprung, H. Akimoto and J. N. Pitts, Jr., J. Amer. Chem. Soc., 96, 6549 (1974).
3. S. W. Benson and H. E. O'Neal, Nat. Stand. Ref. Data Ser., Nat. Bur. Stand., No. 21 (1970).
4. S. W. Benson, K. W. Egger and D. M. Golden, J. Amer. Chem. Soc., 87, 468 (1965).
5. S. Jaffe in "Chemical Reactions in Urban Atmospheres," C. S. Tuesday, ed., Elsevier, New York, N.Y. (1971).

9. 40 METER LONG-PATH INFRARED STUDIES OF THE PROPYLENE/NO_x/h ν SYSTEM

Experimental. The experimental system consisted of a long-path infrared (LPIR) spectrometer (Perkin-Elmer Model 621; dual beam, 40-m pathlength), whose sample and reference tanks (Perkin-Elmer Model 198; diam 27 cm, length 115 cm, volume ~66 liters) were connected to a conventional high vacuum system. To minimize wall reactions, the optical benches housed in the sample and reference tanks and the interior surface of each tank were coated with FEP Teflon ($\tau_{1/2}$ = 11 hr for the thermal decay of O₃). Both tanks were evacuable to better than 7×10^{-4} torr (1 ppm). A 20-liter, all-glass reaction vessel in which preliminary studies can be run was connected to the high vacuum line. Stainless steel valves and O-ring stopcocks were used throughout the system.

Irradiations of the sample tank were carried out using a medium pressure mercury arc (Hanovia, 1200 watt). Light from the arc entered the sample tank through six quartz windows ($7.5 \times 7.5 \times 0.6$ cm), mounted axially along the top of the tank. The windows transmitted light of wavelength $\lambda \geq 210$ nm. Sets of cut-off filters were used to block light of wavelengths shorter than 290, 300, or 320 nm, respectively. When the 300-nm cut-off filters were used, the photolysis rate of NO₂ was 0.042 min⁻¹.

Pressures in the 20-liter glass reaction vessel and in the greaseless, mercury-free, high-vacuum line were measured using a Wallace and Tiernan gauge (0 to 800 torr) or an MKS Baratron capacitance manometer (10^{-3} to 10 torr). Pressures in the LPIR sample or reference tank were measured using the Wallace and Tiernan gauge or an Alphatron gauge (10^{-4} to 10^{-3} torr). Expansion of known pressures of reactants, measured with the MKS Baratron capacitance manometer, from calibrated volumes on the vacuum line into the sample tank of the LPIR allowed low concentrations (1 to 500 ppm) of reactants to be accurately metered into the tank.

All reagents (hydrocarbons, aldehydes, NO, and NO₂) and diluents (N₂, O₂, and He) were obtained in the highest purity available. Organic gases and NO₂ were further purified by repeated freeze-thaw cycles using appropriate cryogenics. Traces of NO₂ and H₂O were removed from NO by passage through a molecular sieve (Linde 13X) at liquid nitrogen temperature. Ultra high purity N₂, O₂, or He were used as received. Ozone in O₂ was prepared using a Welsbach ozonizer and was used without further purification.

Adsorption of ozone on silica gel, followed by elution with N₂ or He, allowed mixtures of O₃ in N₂ or He to be prepared which contained low concentrations of O₂ ([O₃]:[O₂] ~100:1). Ozone concentrations were determined by infrared absorption at $\lambda = 9.48 \mu$, where $\epsilon = 3.74 \times 10^{-4} \text{ ppm}^{-1} \text{ m}^{-1}$.¹

Table 9.1 summarizes the analytical techniques which were used to analyze reaction mixtures produced in either the glass tank, used for preliminary studies, or the LPIR sample tank. All of the sampling methods were routine except for the use of chromosorb adsorbents to effect enhancements of product concentrations by factors of 100 to 1000. In this case, volumes up to the entire contents of the LPIR sample tank were evacuated through tubes packed with chromosorb. The tubes were transferred to an oven and the adsorbed compounds were thermally desorbed at 120°C and collected in a liquid nitrogen-cooled trap. This condensate was then analyzed by flash vaporization onto the GC column of the Finnigan 3100D GC/MS.

Results. The following characterization experiments were run in the 66 l FEP Teflon-coated sample tank of the LPIR reaction system:

- (1) Dark decay of O₃: $\tau_{\frac{1}{2}, \text{dark}}^{\text{O}_3} = 11.0 \text{ hrs.}$
- (2) Dark decay of NO₂: $\tau_{\frac{1}{2}, \text{dark}}^{\text{NO}_2} = 73.4 \text{ hrs.}$
- (3) Photolysis of NO₂ in N₂: $k_d = 0.042 \text{ min}^{-1}$ for $\lambda \geq 300 \text{ nm}$ using a medium pressure Hg arc.

The response and linearity of the entire analytical train (LPIR sample tank, gas sample valve, gas chromatograph, recorder) was calibrated by removing and analyzing known pressures (MKS Baratron capacitance manometer) of authentic samples of all reactants (C₃H₆) and most major reaction products (C₂H₅CHO, (CH₃)₂CO, CH₃CHCH₂O, C₂H₅ONO, CH₃ONO₂, CH₃CHO) which were analyzed by gas chromatography.

A complete study has been made of the reaction products formed by the NO₂ photooxidation of C₃H₆ (typical conditions: [NO₂]₀ = 25 ppm, [C₃H₆]₀ = 125 ppm, synthetic air [N₂/O₂ = 4.0], rel. hum. = 0, medium pressure Hg arc, 300 nm cut-off filters, $k_d^{\text{NO}_2} = 0.042 \text{ min}^{-1}$). Figures 9.1 and 9.2 present typical concentration/time profiles for these experimental conditions.

Table 9.1

Analytical methods

Instrument	Sampling method	Compounds detected	Sensitivity
40-m LPIR spectrometer	In situ	NO ₂ , CO, CO ₂ , carbonyl compounds, olefins, PAN, nitrites, and nitrates	5 to 100 ppm
Dual-column flame ionization	Carle valve (1.0-ml sample loops)	Hydrocarbons, aldehydes (except formaldehyde), ketones, epoxides, and other oxygenates	≥0.1 ppm
Single-column electron capture	Carle valve (0.5-ml sample loops)	PAN, nitrites, nitrates, nitro compounds, O ₂	≥0.1 ppm
Chemiluminescence detector	Calibrated leak (flow ~3 ml s ⁻¹)	O ₃ , NO	≥0.1 ppm
Gas chromatograph/mass spectrometer (GC/MS)	Syringe samples (100 ml) adsorption technique	Same as above for GC methods	≥1 ppm ≥3 ppm

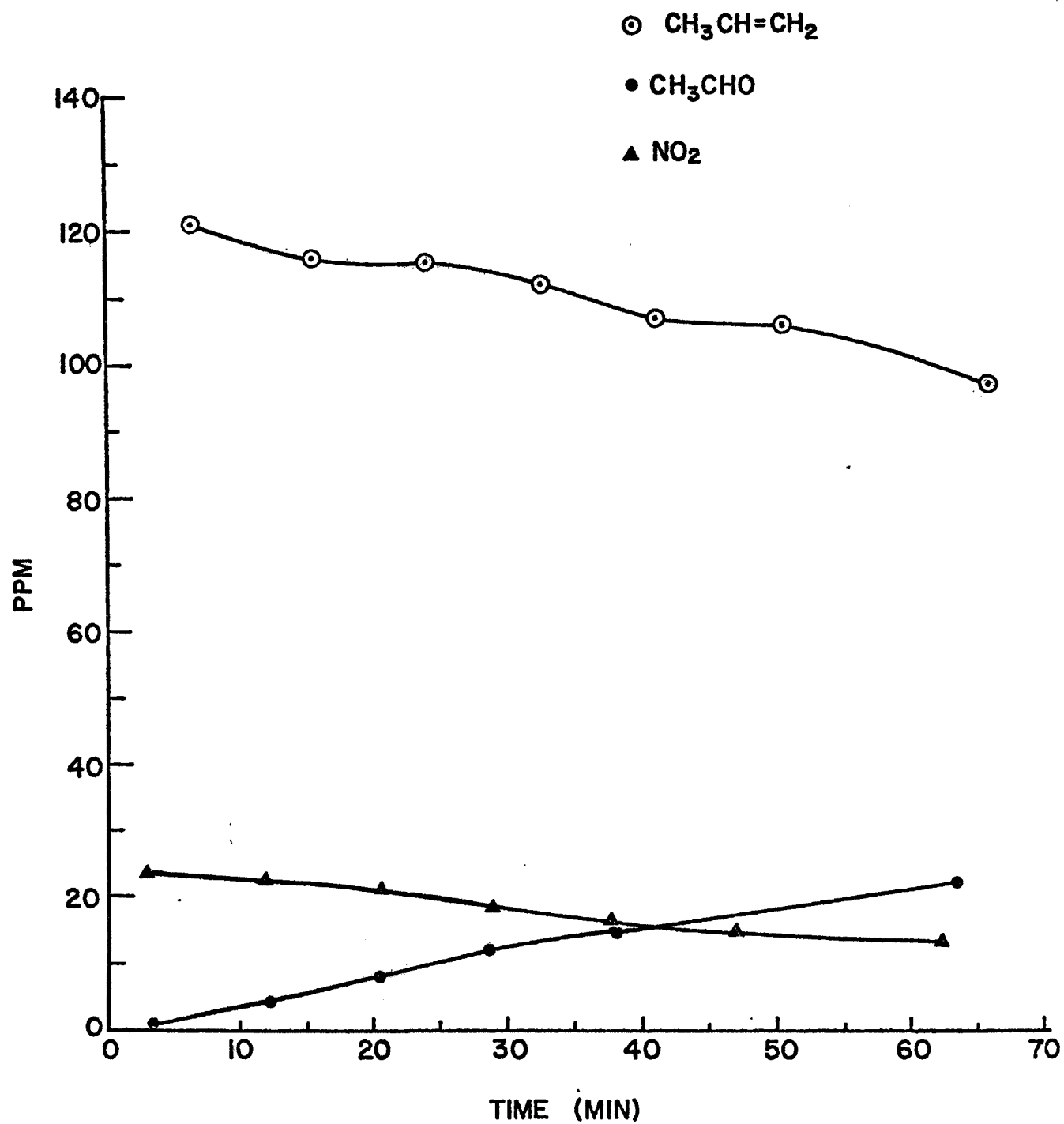


Figure 9.1 Typical concentration-time profile for the NO_2 photooxidation of C_3H_6 .

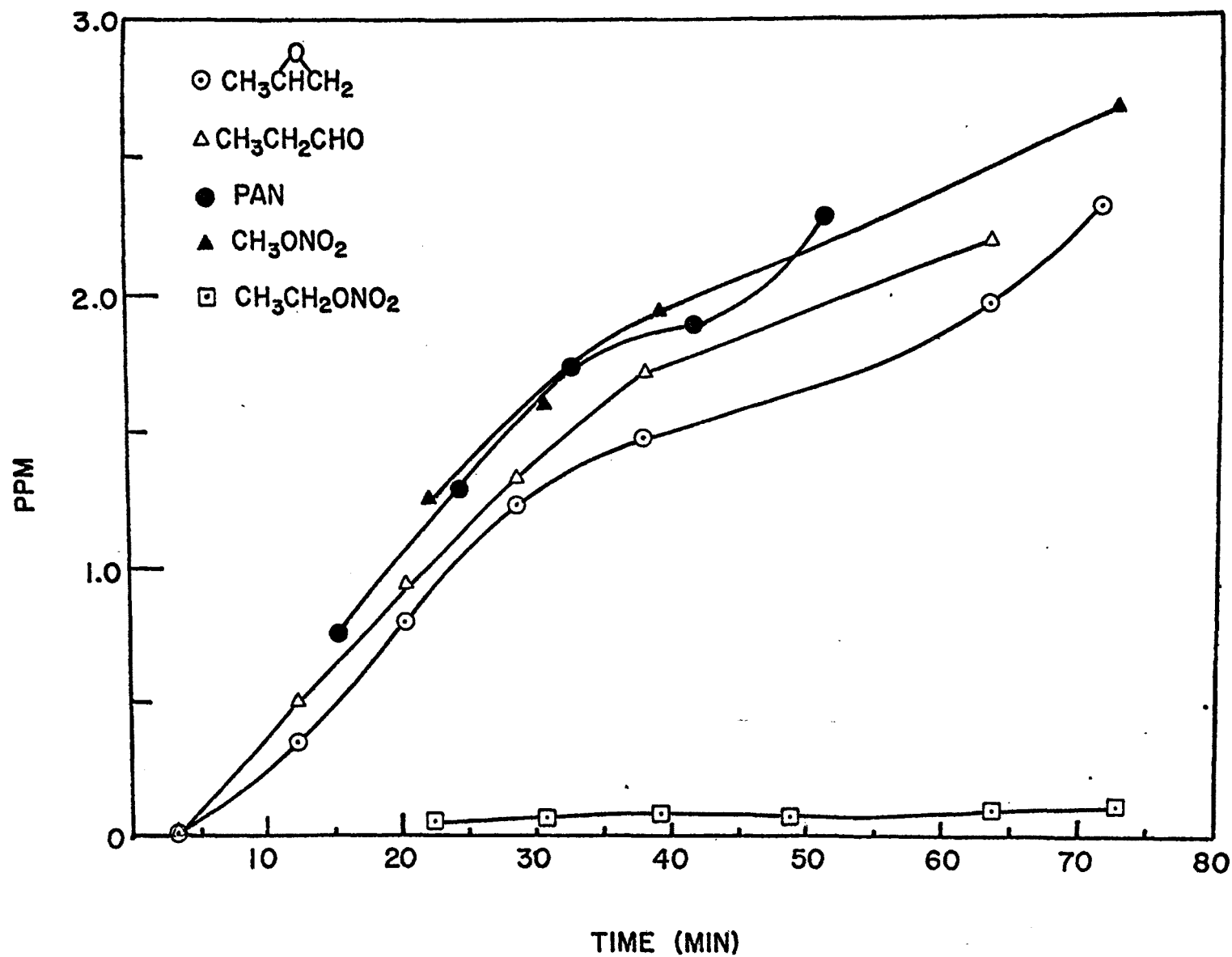


Figure 9.2 Typical concentration-time profile for the NO_2 photooxidation of C_3H_6 .

Table 9.2 presents the products identified, their methods of identification and their approximate yields. Figure 9.3 presents a typical total ion chromatogram of a product mixture analyzed by GC/MS. Product sampling for this analysis was done by Chromosorb adsorption. The presence of acetone impurity in the carrier gas of the GC/MS and its condensation in the liquid N₂-cooled sample loop of the GC accounts for the unreasonably high yield of acetone in this total ion chromatogram. Figures 9.4, 9.5 and 9.6 present representative computer reduced mass spectra of three products [CH₃CHO, (CH₃)₂CO, CH₃OH] present in this total ion chromatogram.

Samples of a C₃H₆/NO_x photooxidation product mixture were adsorbed on Chromosorb adsorbents and analyzed by GC/MS (Carbowax 600 column). This analysis detected CH₃CHCH₂O and C₂H₅CHO, the first having been previously undetected by the procedures then used to analyze for oxygenates from hydrocarbon/NO_x chamber photooxidation runs. Adoption of the Carbowax 600 column used in the GC/MS analysis for GC analysis of chamber oxygenates directly confirmed the presence of these two O(³P) atom/propylene addition products in chamber product mixtures. CH₃ONO₂ was also identified by GC/MS analysis of chamber product mixtures sampled by adsorption on Chromosorbs. Fourier interferometry had previously detected an alkyl nitrate, tentatively identified as C₂H₅ONO₂, in the C₃H₆/NO_x photooxidation product mixtures run in the evacuable chamber.

Table 9.2

Reaction products from the photooxidation of C₃H₆ by NO₂

Product	LPIR	Analytical technique			Approximate yield at 115 min (ppm)
		FID-GC ^{a)}	EC-GC ^{b)}	GC-MS ^{c,d)}	
C ₂ H ₅ CHO	✓	✓		✓	2.9
(CH ₃) ₂ CO	✓	✓		✓	0.3
CH ₃ CHCH ₂ O		✓		✓	2.7
CH ₃ CHO	✓	✓		✓	29.8
HCHO	✓				major
CH ₃ ONO			✓	✓	minor
CH ₃ ONO ₂	✓		✓	✓	2.5
C ₂ H ₅ ONO			✓	✓	trace
C ₂ H ₅ ONO ₂	✓		✓	✓	0.1
PAN	✓				2.6
HCO ₂ CH ₃ ^{e)}				✓	minor
CH ₃ CO ₂ CH ₃ ^{e)}				✓	trace
CH ₃ OH				✓	trace
C ₂ H ₅ OH				✓	trace
CO	✓				minor
CO ₂	✓				minor
O ₃	UV absorption (Dasibi)				0.2

a) 10 ft, 1/8 in, 10% Carbowax 600 on 80/100 C-22 firebrick at 50°C

b) 20 ft, 1/8 in, 10% Carbowax 600 on 80/100 C-22 firebrick at 50°C

c) 20 ft, 1/8 in, 10% Carbowax 600 on 80/100 C-22 firebrick at 50°C

d) Samples removed from LPIR by adsorption on chromosorbs.

e) Possibly formed by esterification of the related acid during adsorption on chromosorb or collection in lq. N₂ trap.

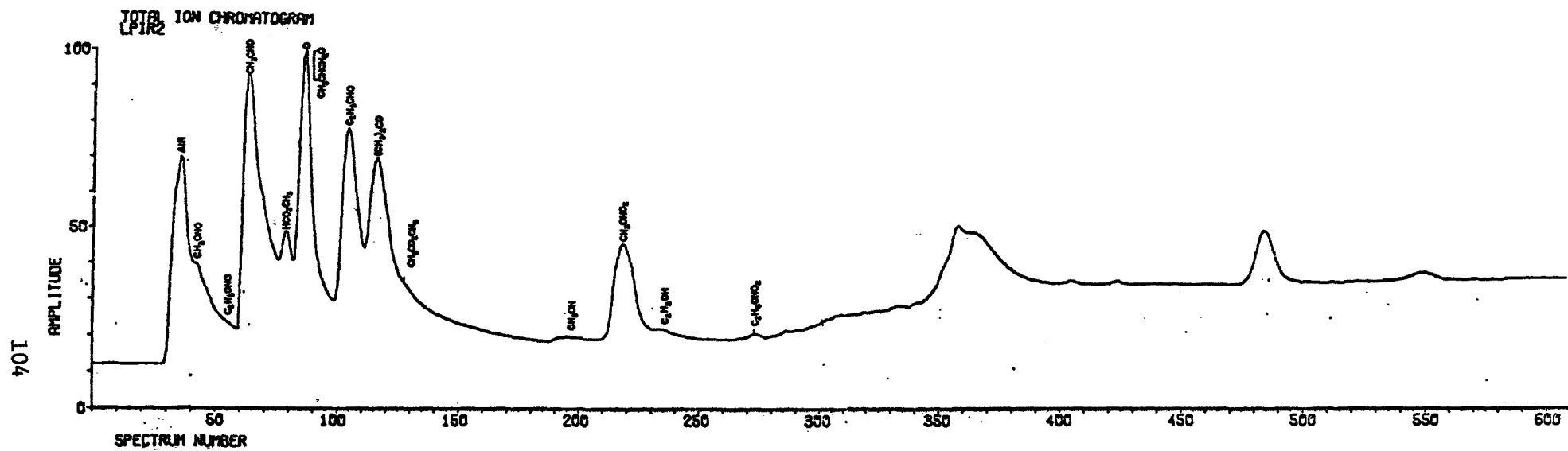


Figure 9.3 A typical GC-MS total ion chromatogram of an irradiated $\text{NO}_2\text{-C}_3\text{H}_6\text{-air}$ mixture.

ACETALDEHYDE
SPECTRUM NUMBER 60
-59
LPIR2

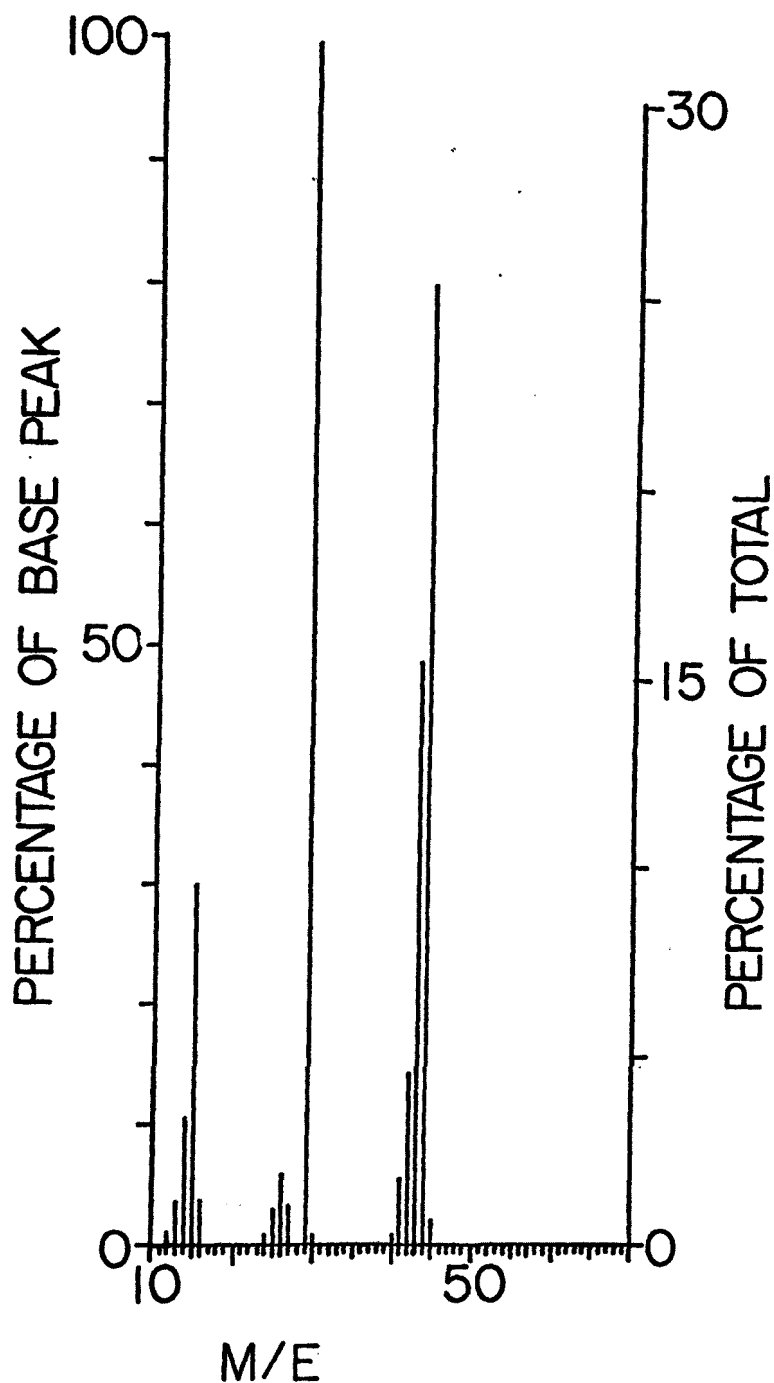


Figure 9.4 GC-MS computer spectrum of CH_3CHO as obtained from the total ion chromatogram of an irradiated $\text{NO}_2\text{-C}_3\text{H}_6\text{-air}$ mixture.

ACETONE

SPECTRUM NUMBER 115

-III

LPIR2

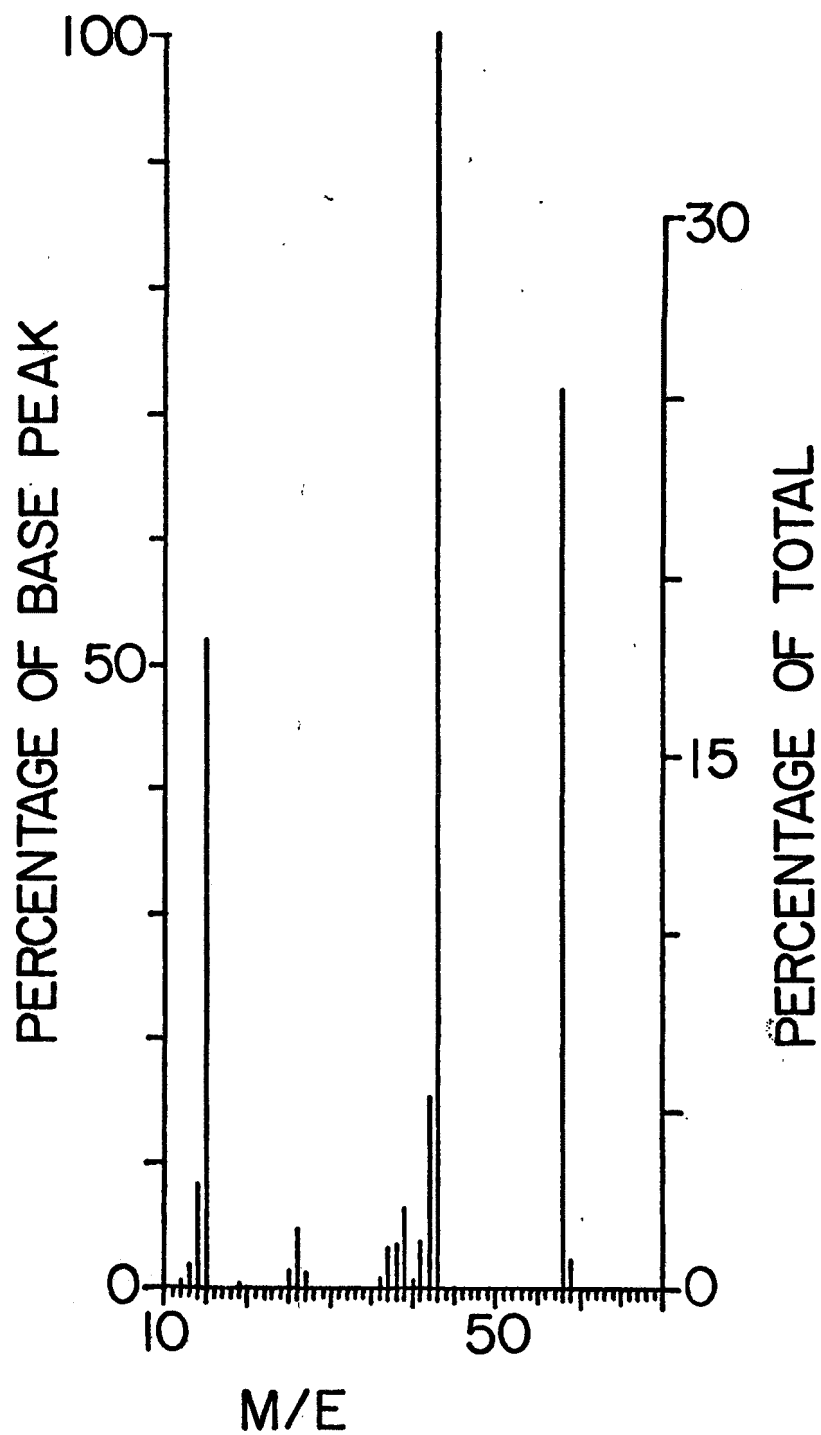


Figure 9.5 GC-MS computer spectrum of $(\text{CH}_3)_2\text{CO}$ as obtained from the total ion chromatogram of an irradiated $\text{NO}_2\text{-C}_3\text{H}_6$ -air mixture.

METHANOL
SPECTRUM NUMBER 193
-186
LPIRS

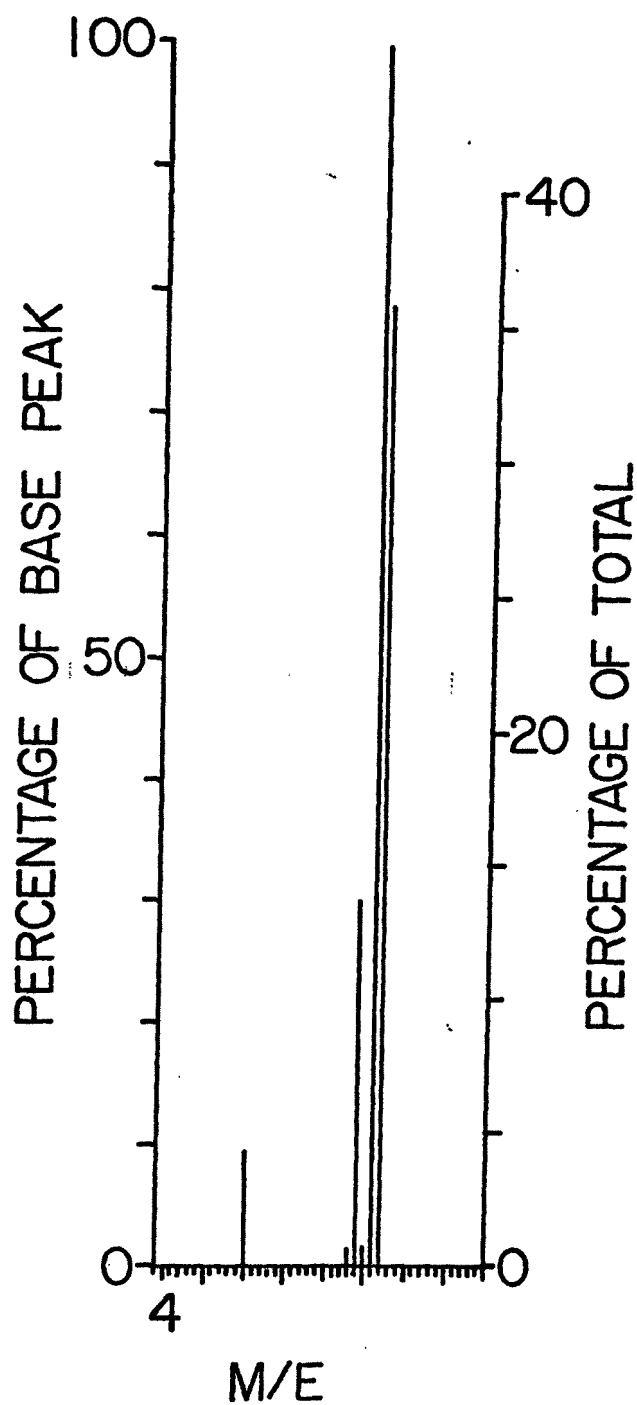


Figure 9.6 GC-MS computer spectrum of CH_3OH as obtained from the total ion chromatogram of an irradiated $\text{NO}_2\text{-C}_3\text{H}_6\text{-air}$ mixture.

REFERENCES

1. P. L. Hanst, E. R. Stephens, W. E. Scott and R. C. Doerr, *Anal. Chem.*, 33, 1113 (1961).

10. THE OZONE-INDUCED CHEMILUMINESCENT OXIDATION OF ACETALDEHYDE

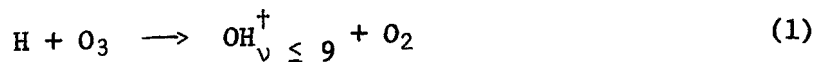
Experimental. A conventional gas handling and flow system with a 1 m flow tube was used. Emission spectra were recorded with a 0.3 m McPherson scanning monochromator (600 grooves/mm blazed at 500 nm) and a dry ice cooled EMI 9558A (500 to 800 nm) or 9684A (700 to 1100 nm) photomultiplier. A lock-in amplifier (Princeton Applied Research, Model 120) and a mechanical chopper (360 Hz) were used to enhance the emission signal to noise ratio.

Approximately 3 mole percent ozone in oxygen (determined by UV absorbance of O_3 at 250 nm) was produced by passing Matheson ultra-high purity (>99.95%) grade oxygen through a Welsbach ozonizer (Model T-408). Flow rates of the O_3/O_2 mixture were typically 300 $\mu\text{moles/sec}$.

Formaldehyde was produced by the method of Spence and Wild¹ from para-formaldehyde (Matheson, Coleman and Bell) and was used without further purification. The source and percentage of total organic impurities as measured by gc analysis (Carbowax 400/chromosorb W column, 60°C, flame ionization detector) of the remaining aldehydes were as follows: propionaldehyde (Matheson, Coleman and Bell, $\leq 0.3\%$), benzaldehyde (Matheson, Coleman and Bell, 0.2%) and acetaldehyde (Matheson, Coleman and Bell, 0.2%; Mallinckrodt, 0.1%; Chemical Samples Company, 0.02%; Aldrich, 0.08%, Eastman 0.8%). In searching for a detectable emission, reactant flow rates, total pressure and linear flow rate were varied. The acetaldehyde flow rate during spectral runs was typically 5 $\mu\text{moles/sec}$ and the total pressure was about 3 torr.

Results and Discussion. In addition to the observed OH emission, an emission in the visible about a factor of forty less intense than the OH emission with a maximum of 430 nm was also recorded. Although the signal to noise ratio was not sufficient to obtain a well-resolved spectrum, a comparison to the visible emission from the ozone-olefin reactions^{2,3} shows that this emission is probably formaldehyde fluorescence.

Figures 10.1 and 10.2 give the chemiluminescent emission spectra of the acetaldehyde oxidation from 500 to 1000 nm. For comparison, the vibration-rotation bands of $OH(^2\Pi_1)$ produced in the same apparatus by the reaction



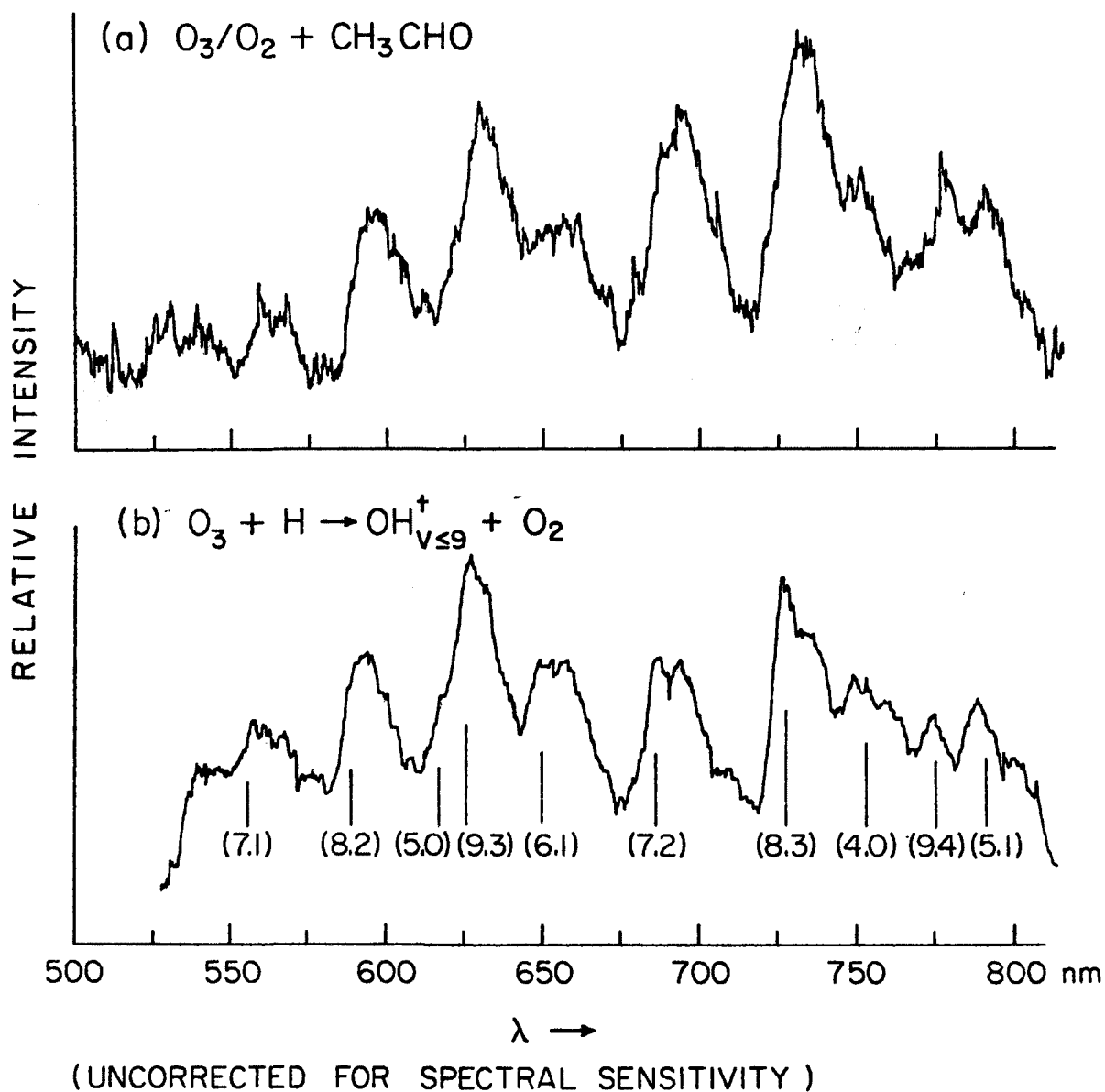


Figure 10.1 Emission spectra from 500 to 800 nm in the chemiluminescent reactions of ozone with (a) acetaldehyde. Total pressure 4.0 torr; spectral bandwidth 9 nm. (b) H atoms. Total pressure 4.0 torr; spectral bandwidth 6.9 nm.

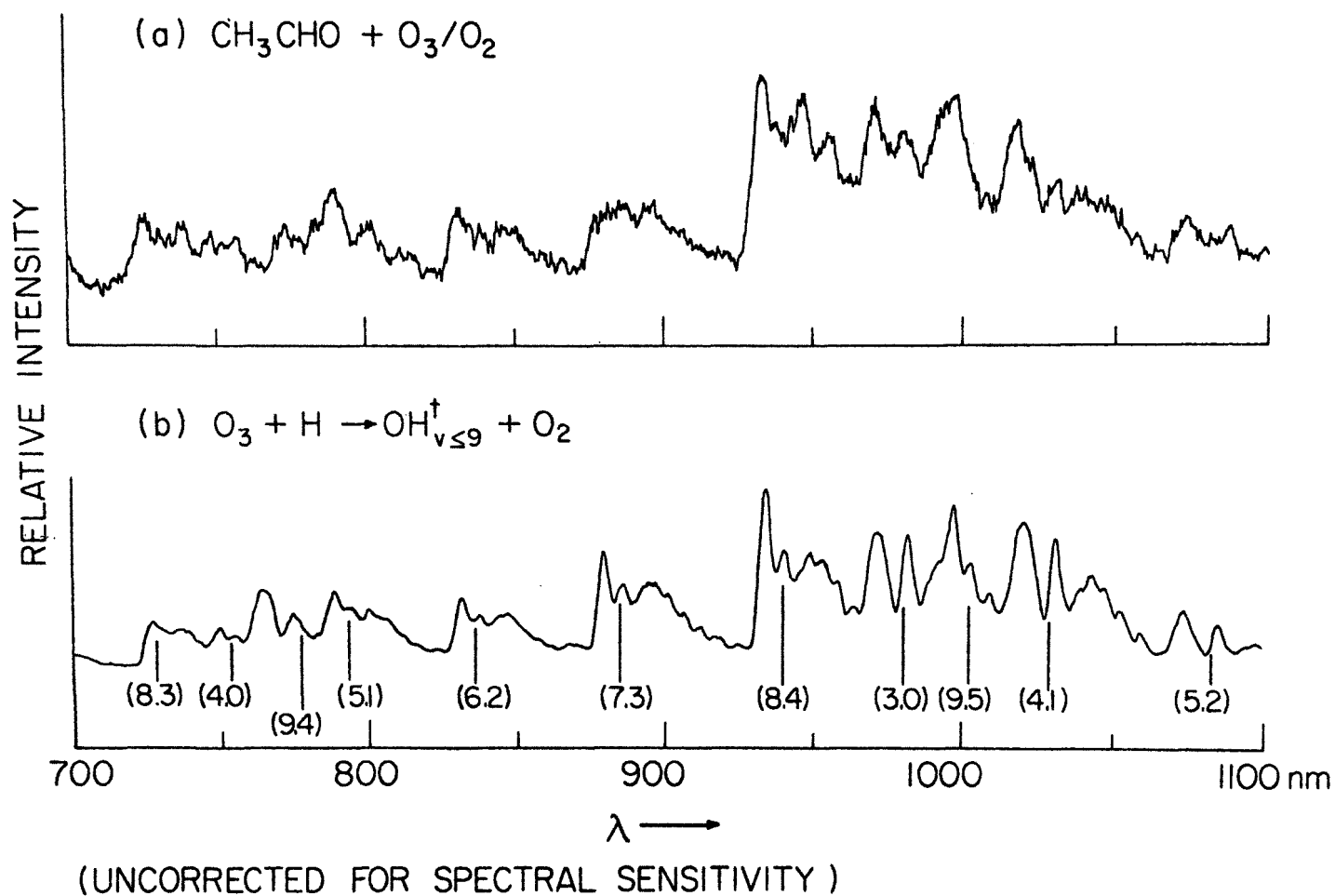


Figure 10.2 Emission spectra from 700 to 1100 nm from the chemiluminescent reactions of ozone with (a) acetaldehyde. Total pressure 3.3 torr; spectral bandwidth 5.3 nm. (b) H atoms. Total pressure 2 torr; spectral bandwidth 2 nm.

are also presented in these figures. Since the spectra are identical, the chemiluminescence produced by the acetaldehyde- O_3/O_2 reaction must also be due to the Meinel bands of the OH radical.⁴ The similarity of the vibrational distribution of the two spectra suggests that reaction (1) is the likely source of the vibrationally excited OH produced during the oxidation of acetaldehyde by O_3 .

Because only the acetaldehyde oxidation was chemiluminescent, a rather surprising result, the possibility of light emission due to impurities in the acetaldehyde, particularly unsaturated hydrocarbons, was examined. The fact that the same emission was observed when five different sources of acetaldehyde were used argues strongly against this possibility. Furthermore, even if all the organic impurities in the acetaldehyde samples were olefins, one would have expected to observe an emission at most a factor of one hundred less intense than is observed.² Since the observed emission was only a factor of two less intense than the ozone -- tetramethylethylene OH emission, we therefore conclude that the observed emission is not due to impurities.

These preliminary results do not permit the formulation of a detailed reaction mechanism; the mechanisms of ozonolysis of aldehydes are known to be very complex.⁵⁻⁸ While there is no obvious explanation of why only the acetaldehyde oxidation is chemiluminescent, studies of the thermal oxidation of aliphatic aldehydes have revealed differences in the oxidative rates and mechanisms of formaldehyde as compared to higher aldehydes.⁹ In the case of propionaldehyde, the presence of β hydrogens may alter the decomposition mode of intermediates which, in the acetaldehyde oxidation, lead to excited OH.

Further investigations of the detailed mechanisms of these reactions are currently in progress.

REFERENCES

1. R. Spence and W. Wild, J. Chem. Soc., 338 (1935).
2. B. J. Finlayson, J. N. Pitts, Jr. and H. Akimoto, Chem. Phys. Letters, 12, 495 (1972).
3. W. A. Kummer, J. N. Pitts, Jr. and R. P. Steer, Environ. Sci. Technol., 5, 1045 (1971).
4. A. B. Meinel, Astrophys. J., 111, 555 (1950).
5. P. S. Bailey, Chem. Rev., 58, 925 (1958).
6. R. E. Erickson, D. Bakalik, C. Richards, M. Scanlon and G. Huddleston, J. Org. Chem., 31, 461 (1966).
7. H. M. White and P. S. Bailey, J. Org. Chem., 30, 3037 (1965).
8. A. A. Syrov and V. K. Tsykovskii, J. Org. Chem., USSR, 6, 1406 (1970).
9. J. F. Griffiths and G. Skirrow, Oxid. Combust. Rev., 3, 47 (1968).

11. LOW-PRESSURE GAS-PHASE OZONE-OLEFIN REACTIONS.
CHEMILUMINESCENCE, KINETICS, AND MECHANISMS

Extensive mechanistic investigations of the liquid-phase reactions of ozone with olefins have identified many of the reaction intermediates and have established the Criegee zwitterion mechanism as a major reaction pathway.¹⁻⁴ Until recently, the Criegee mechanism has also been widely assumed to apply to the initial steps of the gas-phase reaction. However, in the gas phase at room temperature, unimolecular decomposition or rearrangement of the "zwitterion" (more likely a biradical in the gas phase) is expected to predominate over recombination with the carbonyl fragment.^{5,6} Although several reports⁵⁻¹⁰ of gas-phase products, including secondary ozonides,^{6,9} are consistent with this mechanism, it fails to explain the formation of free radical intermediates^{11,12} in low-pressure (~2 torr) ozone-olefin reactions and of "unusual" ozonolysis products, both at low¹² and high total pressures.^{7,8,13,14}

Recently, evidence on the nature of certain excited intermediates in gas-phase ozone-olefin reactions has appeared. Thus, chemiluminescence from the room-temperature gas-phase ozone-ethylene reaction at atmospheric pressure was first observed by Nederbragt, *et al.*,¹⁵ and further investigated by Warren and Babcock¹⁶ and Hodgeson and coworkers.¹⁷⁻¹⁹ Subsequently, studies^{11,20-22} in our laboratories showed that at low pressures (~1 torr) all simple olefins chemiluminesce on reaction with 2% O₃/O₂. Meinel band emission from vibrationally excited OH radicals was observed for the first time in these oxidations, and formaldehyde fluorescence was tentatively identified¹¹ in the reactions of ethylene, propylene, and 1-butene.

Concurrently, on the basis of thermochemical-kinetic calculations, O'Neal and Blumstein²³ proposed alternatives to the gas-phase Criegee mechanism. These involve internal hydrogen abstractions of the initial molozonide in addition to its decomposition to the Criegee fragments. Their mechanism rationalizes most of the "unusual" products observed in previous studies, as well as the production of chemiluminescence.

Reported here are the results of further detailed studies of low-pressure ozone-olefin reactions, using more sensitive and more quantitative spectroscopic techniques to provide the requisite resolution for conclusive identification of the light-emitting species and to permit estimates to be made

of their absolute rates of light emission. Additionally, the kinetics of the light intensities and of ozone decay, measurement of the self-heating of the gas mixture in these exothermic reactions, analysis of the major stable products, and the effects on these parameters of replacing the oxygen carrier gas by nitrogen are presented. This evidence, along with our recent results on intermediate species obtained using a photoionization mass spectrometer¹² (hereafter referred to as PMS), is discussed in terms of the O'Neal-Blumstein mechanism.

Experimental. The flow system used in these studies is shown schematically in Figure 11.1. Along the length of the Pyrex flow tube (5-cm i.d., 1-m length) were five substrate inlet jets (J_1 - J_5) and five Pyrex bead-type thermistors (T_1 - T_5) (Fenwal Electronics Inc.) which had been calibrated against a quartz thermometer. Pyrex or quartz windows were attached to the ends of the flow tube using Teflon-lined end couplings. Flow tube pressure was measured with a Statham 0-5 psia transducer (A) calibrated against an MKS Baratron gauge. Flow tube pressures were not corrected for pressure drop along the flow tube, as the Poiseuille equation predicts a pressure drop of $\sim 1 \mu$, $\leq 0.1\%$ of the total pressure. The flow tube was connected to a conventional high-vacuum line via Teflon stopcocks and Teflon-lined ball and socket joints. Where appropriate, a fluorinated grease (Krytox 240AC) was used to minimize O_3 decomposition. The flow tube was periodically cleaned by baking overnight at 565°C .

For studying the kinetics of the chemiluminescent emission of individual excited species, appropriate optical filters (C) were used to isolate the emission which was detected by a cooled EMI 9558A photomultiplier (B). The following optical filters were used: (1) for $\text{HCHO}(^1A'' \rightarrow ^1A_1)$, cutoff filters isolating the $373 < \lambda < 473 \text{ nm}$ region; (2) for $\text{OH}(X^2\Pi_i)_{v' \leq 9}$ Meinel band emission, a cutoff filter transmitting $\lambda > 555 \text{ nm}$; (3) for $\text{OH}(A^2\Sigma^+ \rightarrow X^2\Pi_i)$, a $317 \pm 6 \text{ nm}$ interference filter; and (4) for the emissions at $517\text{--}520 \text{ nm}$, cutoff filters isolating the $510 < \lambda < 555 \text{ nm}$ region.

The kinetics of O_3 consumption were followed by monitoring the 253.7 nm absorption of O_3 using a pen-ray lamp (D) and RCA 1P28A photomultiplier (G). The filter combination (E,F) isolated the 253.7 nm line and reduced scattered light at other wavelengths.

Chemiluminescent emission spectra were scanned using a McPherson 0.3 m scanning monochromator (H) and a cooled photomultiplier (I) (EMI 9684B,

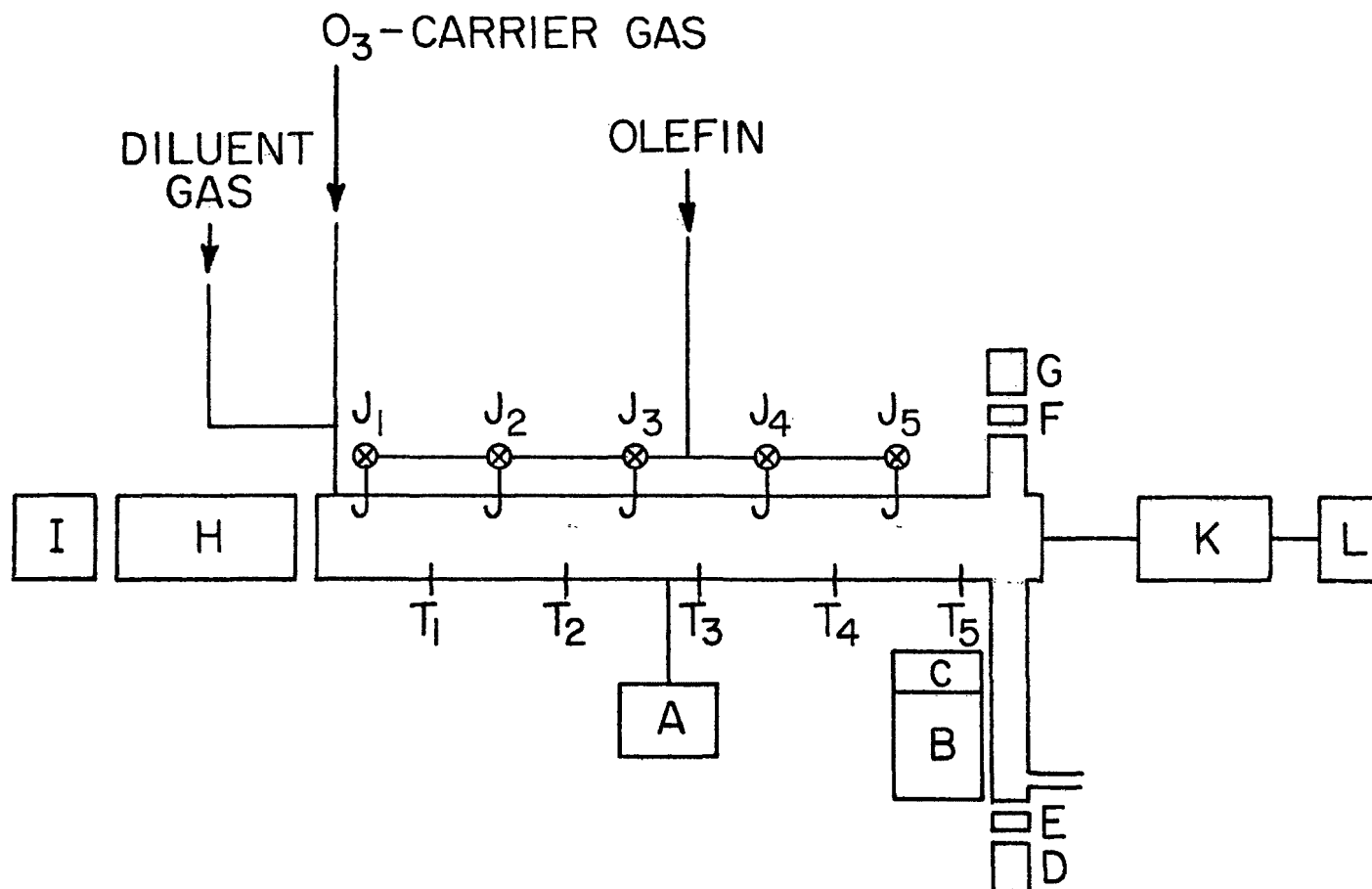


Figure 11.1 Schematic of apparatus used in chemiluminescence and kinetic studies:
 A, pressure transducer; B, EMI 9558A photomultiplier; C, optical filters;
 D, pen-ray mercury lamp; E, Corning 7-54 filter; F, 254 ± 26 nm filter;
 G, RCA IP28A photomultiplier; H, 0.3-m McPherson scanning monochromator;
 I, photomultiplier; K, Carle gas sampling valve; L, gas chromatograph;
 J₁-J₅, inlet jets; T₁-T₅, thermistors.

9558A or 9659QB) whose output was amplified by a lock-in amplifier (PAR Model 120, operated at 360 Hz) or a photon counter (SSR Instruments Model 1120 amplifier discriminator, and Model 1105 data converter console) and displayed on a potentiometric recorder. To enhance the observed emission intensities, a plane mirror was placed opposite the monochromator at the downstream end of the flow tube.

Gas chromatographic analysis of the cis-2-butene-ozone reaction was carried out using a Carle gas sampling valve (K) with 5 cm³ sample loops attached to a Varian Aerograph Model 1200 gas chromatograph (L) with a flame ionization detector. The columns used were a 10 ft by 1/8 in. 20% SE-30 column on 6/8 firebrick, operated at room temperature, and a 10 ft by 1/8 in. 10% β , β -oxydipropionitrile column, on 80/100 HMDS Chromosorb P, operated at 90°C. Products were identified by comparison of their retention times to those of authentic compounds introduced into the Carle valve as a mixture with air.

O₃/diluent and substrate flow rates were measured using calibrated flowmeters. Flow rates were typically 20-30 $\mu\text{mol sec}^{-1}$ of olefin and ~130 $\mu\text{mol sec}^{-1}$ of the O₃/diluent gas mixture at total flow tube pressures of 2-10 Torr. Linear flow velocities were ~80 cm sec⁻¹ corresponding to a mean flow tube residence time of ~1.3 sec.

The absolute rate of light emission from individual emitting species was determined by comparison²⁴ of the light intensity in the appropriate wavelength region from the O-NO reaction, $I_{\text{O-NO}}$, to that from the ozone-olefin reaction, $I_{\text{O}_3\text{-OL}}$, where

$$I_{\text{O-NO}} = k_s [\text{O}][\text{NO}] \quad (\text{I})$$

and

$$I_{\text{O}_3\text{-OL}} = k_x [\text{O}_3][\text{olefin}] \quad (\text{II})$$

k_s and k_x are the respective absolute rates of light emission in that wavelength region.

O(³P) atoms were generated by the microwave discharge of N₂ and subsequent titration of the N atoms by nitric oxide²⁵



with the $\text{O}(^3\text{P})$ atom concentration being obtained from the end point of the titration. The 10.3% NO/N_2 was passed through a trap at Dry Ice temperature containing Linde Molecular Sieve 13X to remove any NO_2 and H_2O present.

The concentrations of O_3 and olefin were calculated, assuming 1:1 stoichiometry, from their initial concentrations using the measured rate constant for O_3 decay under these experimental conditions and the reaction time to the observation port.

Then, using the experimentally determined values of $I_{\text{O-NO}}$ and $I_{\text{O}_3\text{-OL}}$ and the known value of k_s ,²⁴ k_x was calculated. The total rate of light emission from that emitting species was then determined from the fraction of the total light emission from that excited species transmitted by the filter. For $\text{HCHO}(^1\text{A}'' \rightarrow ^1\text{A}_1)$ this fraction, isolated using a 430 ± 11 nm interference filter, was measured from its photoexcitation emission spectrum by planimetry. Similarly, in the cis-2-butene reaction, the rate of light emission from glyoxal from 510 to 555 nm, isolated using cutoff filters, was measured and the fraction this comprised of the total emission was calculated from the photoexcitation emission spectrum. It was assumed that at these total pressures no glyoxal fluorescence would occur due to rapid intersystem crossing from the singlet to the triplet state.²⁶⁻²⁸

The total OH Meinel band emission which extends to 4.5μ ²⁹ could not be recorded in this study due to instrumental limitations. Therefore, the intensity of a fraction of the (9,3) band was measured, and the total rate of light emission in the (9,3) band was calculated from the known transmission characteristics of the filter.

Ethylene, cis-2-butene, and isobutene (Matheson Research Grade $\geq 99.8\%$) were used without further purification. Gas chromatographic analysis of these olefins showed no detectable impurities. 2-Butene- d_8 (mixture of cis and trans) and isobutene- d_8 (Merck Sharp and Dohme, with stated D atom purities of $\geq 98\%$ and $\geq 99\%$, respectively) were used as received.

Ozone ($\sim 2\%$ in O_2) was prepared from O_2 (Matheson ultra-high purity) using a Welsbach ozonator Model T-408. O_3/N_2 or O_3/He (both containing $\leq 0.2\%$ O_2) were prepared by selective absorption of O_3 on silica gel^{30,31} at -78°C followed by elution with the diluent gas (N_2 or He).

H_2 ($\geq 99.999\%$), He ($\geq 99.95\%$), and N_2 ($\geq 99.95\%$) were used as received. H

atoms were generated by methods described previously.¹¹

Formaldehyde was prepared from paraformaldehyde (Matheson Coleman and Bell) by the method of Spence and Wild.³² Acetaldehyde (Matheson Coleman and Bell), acetone (Mallinckrodt Spectra Grade), and biacetyl (Matheson Coleman and Bell) were thoroughly degassed at liquid nitrogen temperature and used without further purification. Glyoxal was prepared from glyoxal trimer (Matheson Coleman and Bell) by heating a mixture of trimer and P_2O_5 and collecting the glyoxal distillate in a liquid nitrogen trap. Volatile impurities in the glyoxal were removed by degassing at Dry Ice temperature.

Results

Identification of Chemiluminescing Species. Electronically excited formaldehyde, $HCHO(^1A'')$, has now been confirmed as a chemiluminescing species common to all the ozone-olefin reactions that were studied at sufficient resolution to resolve the vibrational structure. Typical chemiluminescent emission spectra ($350 < \lambda < 600$ nm) are shown in Figure 11.2; also shown for comparison is the formaldehyde fluorescence excited by tesla coil discharge³³ and recorded with the same detection system.

The reactions of cis- and trans-2-butene with ozone have identical chemiluminescent emission spectra, an example of the latter being shown in Figure 11.2ii. The 520-nm peak from these reactions is assigned to glyoxal phosphorescence ($^3A_u \rightarrow ^1A_g$) by comparison with the (0,0) band obtained by photoexcitation of glyoxal vapor at 430 ± 11 nm. The remaining vibrational bands of the triplet system^{34,35} are obscured at these pressures by the much stronger Meinel band emission of the $OH-(X^2\Pi_{1/2})_{v' \leq 9}$ radical¹¹ (referred to hereafter as OH^\dagger). However, current work³⁶ at pressures approaching atmospheric where the OH^\dagger emission is strongly quenched also shows the 551.4- and 572.9-nm bands of glyoxal phosphorescence. The observation¹² of glyoxal as a minor product in the low-pressure cis-2-butene reaction with 2% O_3/O_2 further supports this assignment.

The broad peak at approximately 517 nm from the reaction of 2% O_3/O_2 with isobutene (Figure 11.2iv) is identical with that from the 2-methyl-2-butene and 2,3-dimethyl-2-butene reactions at this spectral resolution. These spectra were compared with the phosphorescence of glyoxal, methylglyoxal,³⁷ and biacetyl. Glyoxal and biacetyl, whose emission spectra were recorded with the same detection system, were eliminated as the emitting species. However, a phosphorescence spectrum of methylglyoxal furnished by

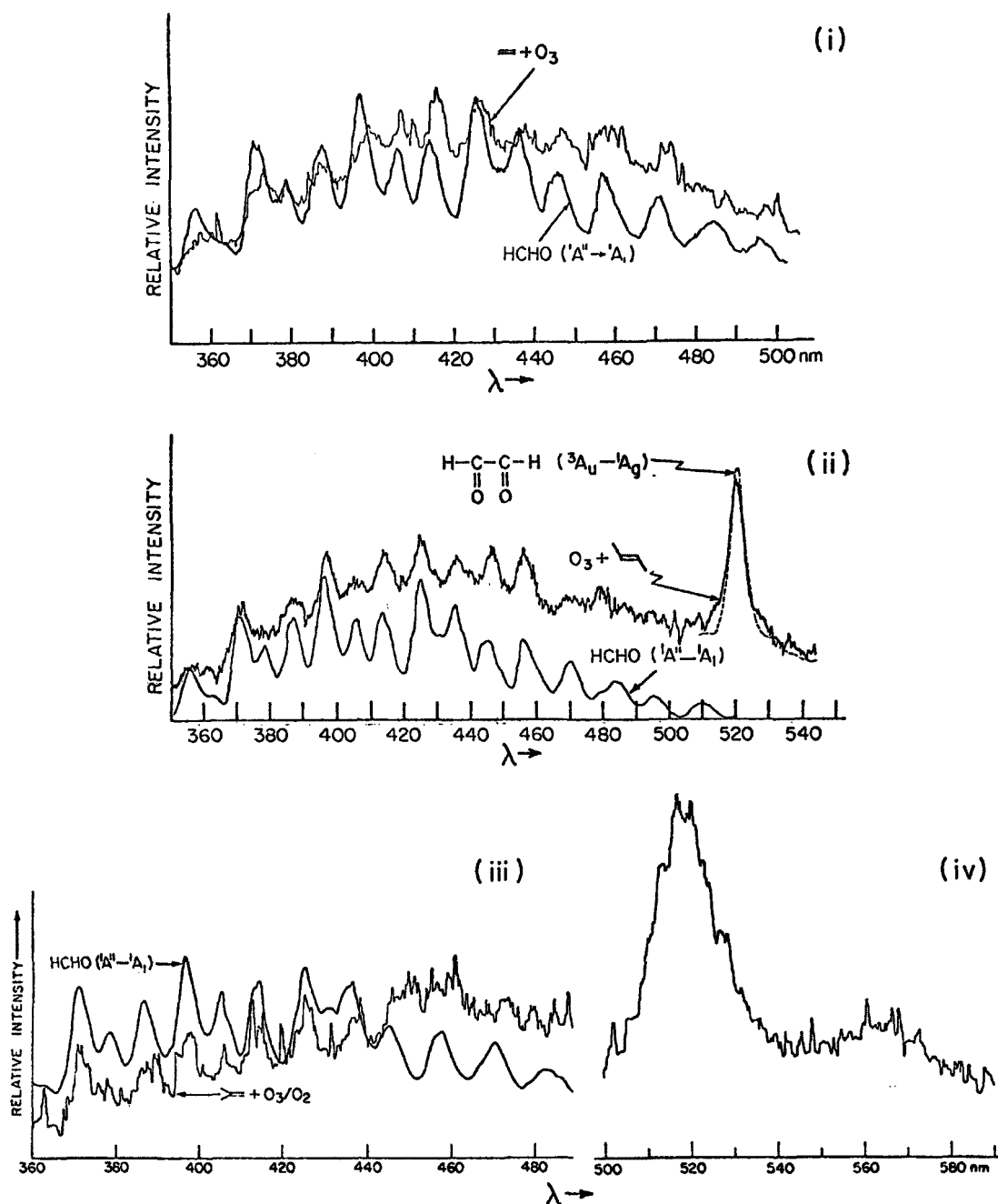
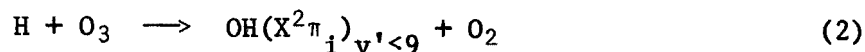


Figure 11.2 Chemiluminescent emission spectra in the visible region from the reaction of 2% O_3/O_2 with: (i) ethylene, total pressure 4.5 torr, spectral slit width 3.2 nm; (ii) *trans*-2-butene, total pressure 3.5 torr, spectral slit width 2.5 nm; (iii) isobutene, total pressure 4.4 torr, spectral slit width 3.2 nm; (iv) isobutene, total pressure 4.4 torr, spectral slit width 1.9 nm; (i-iii) $HCHO ({}^1A'' \rightarrow {}^1A_1)$, total pressure 4.9 torr, spectral slit width 2.5 nm; (ii) $(CHO)_2 ({}^3A_u \rightarrow {}^1A_g)$, total pressure 1.33 torr, spectral slit width 0.45 nm.

Yardley and coworkers³⁷ was in good agreement and hence it is believed that this is the emitting species. The chemiluminescence at $\lambda > 440$ nm (Figure 11.2iii) may be the sum of formaldehyde fluorescence and methylglyoxal fluorescence.

The chemiluminescent emission spectrum from the cis-2-butene-ozone reaction in the region $700 < \lambda < 1100$ nm is compared in Figure 11.3 to that from the $H + O_3$ reaction under similar conditions of temperature and pressure. Reaction 2 is known^{38,39} to produce the Meinel bands²⁹ of vibrationally excited $OH^{\dagger}_{v' \leq 9}$, with $v' = 9$ corresponding to the exothermicity of the reaction



$$\Delta H_0^\circ = -77 \text{ kcal/mol}$$

Both reactions have virtually identical vibrational distributions especially in that emission from levels $v' > 9$ is not observed. In addition, the rotational distributions are similar, further confirming H atoms as the precursors of the OH^{\dagger} chemiluminescence in ozone-olefin reactions.¹¹

Secondary reactions of the major products cannot be responsible for the Meinel band chemiluminescence since only acetaldehyde⁴⁰ gives this emission on reaction with O_3 and the intensity in this case is at least a factor of 10 less than that observed in the cis-2-butene-ozone reaction.

To determine whether oxygen was involved in the chemiluminescent processes, spectra from the reactions of ozone with ethylene, cis-2-butene, and isobutene were recorded first in N_2 and then in O_2 as diluent. Use of He rather than N_2 caused no detectable change in the spectra. Figure 11.4 shows that the $HCHO(^1A'' \rightarrow ^1A_1)$ fluorescence is unaffected by the removal of O_2 . However, the Meinel bands appeared to increase in intensity and the (0,0) band of electronically excited $OH(A^2\Sigma^+ \rightarrow X^2\pi_1)$ (hereafter referred to as OH^*) was observed at 306.4 nm (the (1,0) band at 281.1 nm was not detected). While the intensity of OH^* in the presence of O_2 was not sufficient to be recorded using a monochromator, a signal was observed using a 317 ± 6 nm interference filter in the cis-2-butene and isobutene reactions.

Because of the increased intensity of the OH^{\dagger} Meinel bands in N_2 , it could not be ascertained whether the 517 and 520 nm peaks observed in the isobutene and cis-2-butene reactions in O_2 were still present. Therefore, in order to eliminate the OH^{\dagger} emission, the spectra from the reactions of

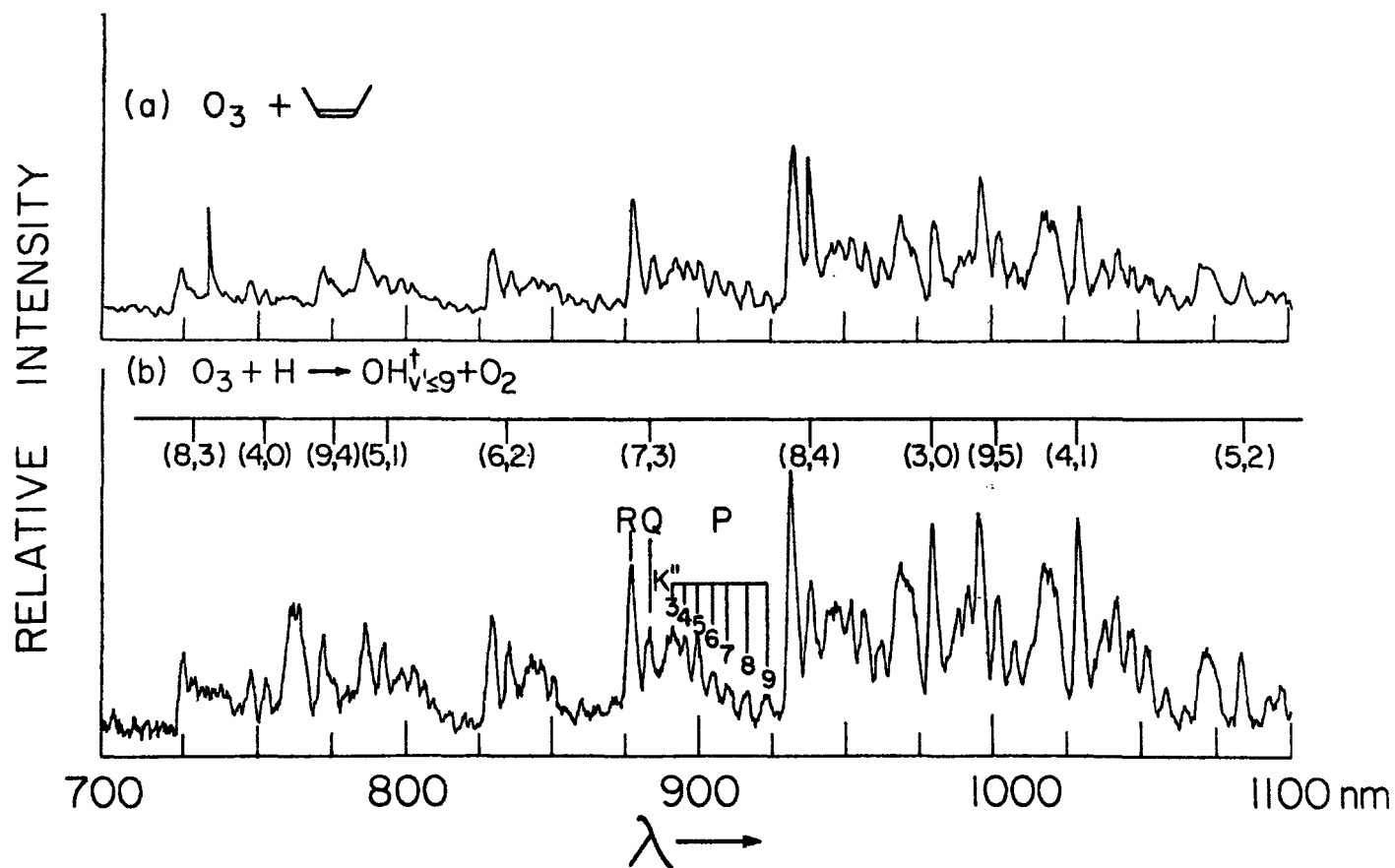


Figure 11.3 Comparison of the chemiluminescent emission (700–1100 nm) from the ozone-cis-2-butene reaction to the OH Meinel bands from the $\text{H} + \text{O}_3$ reaction: (i) total pressure 3.2 torr, spectral slit width 1.2 nm; (ii) total pressure 1.02 torr, spectral slit width 0.72 nm.

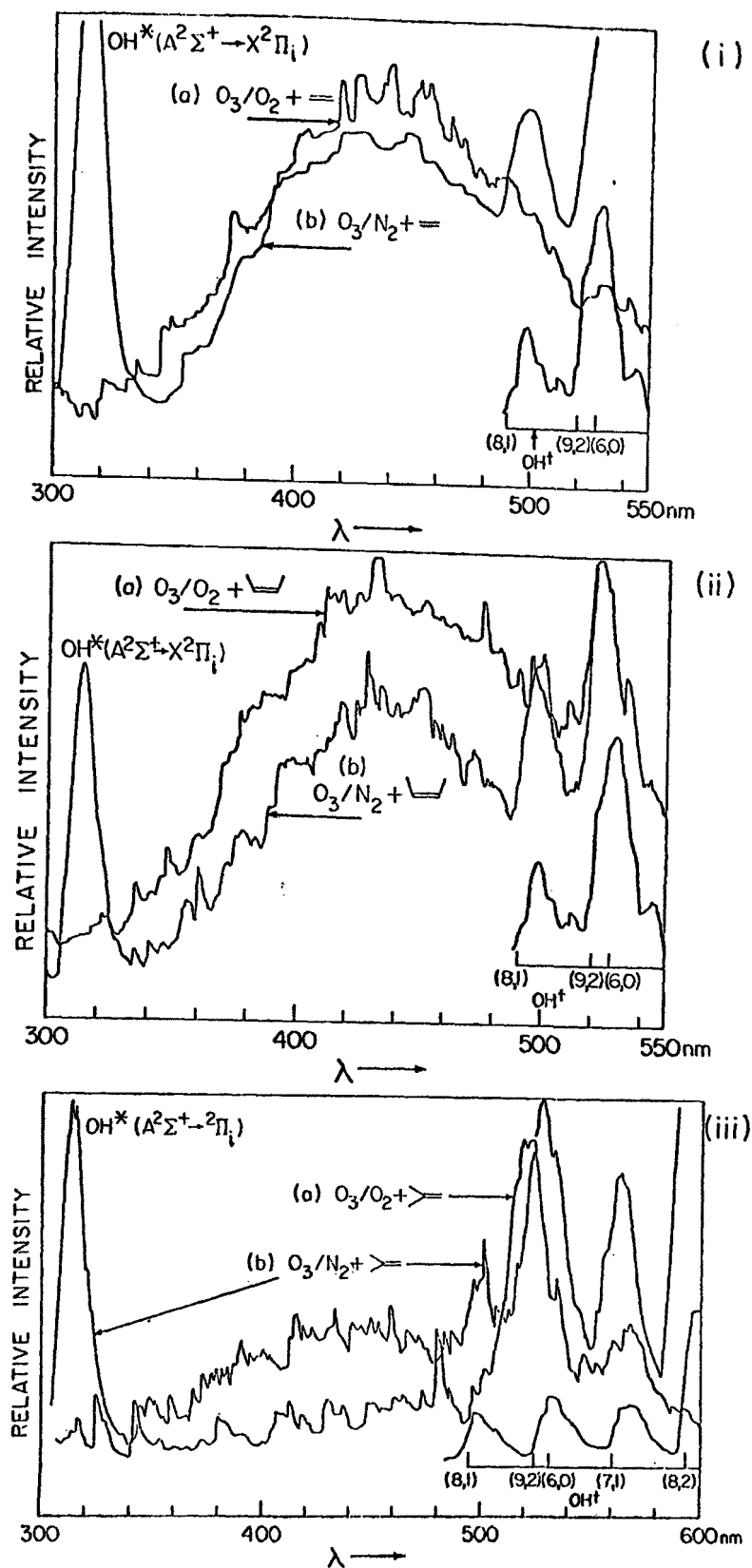


Figure 11.4 Chemiluminescent emission spectra (300–550 nm) from the reactions of 2% O_3 in (a) O_2 and (b) N_2 with: (i) ethylene, total pressure 1.79 torr, spectral slit width 9.0 nm; (ii) *cis*-2-butene, total pressure 1.58 torr, spectral slit width 7.4 nm; (iii) isobutene, total pressure 1.60 torr, spectral slit width 7.4 nm.

the corresponding perdeuterated olefins with O_3/O_2 and O_3/N_2 were recorded, as shown in Figure 11.5. As expected, no OD^+ emission was observed up to 700 nm. This was confirmed by the lack of OD^+ emission from the $D + O_3$ reaction in the same system. It appears that O_2 is necessary for production of the 517 nm peak tentatively identified as methylglyoxal phosphorescence in the isobutene-ozone reaction. However, the experiments with the 2-butene- d_8 were inconclusive since the glyoxal- d_2 phosphorescence was reduced by more than a factor of 2.5 even in O_2 , suggesting a kinetic isotope effect.⁴¹

Table 11.1 summarizes the emitting species identified from the chemiluminescent emission spectra of the ozone-olefin reactions in the wavelength region 200 to 1100 nm.

Kinetics of Light Emission

a. Intensity of Light Emission as a Function of Reactant Concentration. The dependence of each of the emission intensities on olefin and ozone concentration was investigated under pseudo-first-order conditions. Reaction orders were determined from least-squares analyses of the slopes of log-log plots of emission intensity vs. reactant concentration. Table 11.2 shows that the emission intensities were first order in each reactant, with the exception of the isobutene reaction where the order of the 517 nm peak in ozone was 0.39 ± 0.02 in O_2 as carrier gas. With N_2 as carrier gas, the light emission generally exhibited a maximum at very low olefin concentrations and then decreased with increasing olefin concentration.

b. Decay of Light Intensity and Ozone. For ethylene, cis-2-butene, and isobutene, the intensities of each of the chemiluminescent emissions and the O_3 concentration were determined as a function of time with O_2 or N_2 as the diluent gas over total pressures of 2-10 torr. In order to maintain pseudo-first-order conditions, the initial olefin concentrations were a minimum of six, and typically ten, times the initial ozone concentration. Decay rates were determined from the least-squares slopes of plots of the logarithms of either emission intensity or ozone absorbance against reaction time. Typical data for the cis-2-butene reaction with ozone are shown in Figure 11.6. Similar behavior was observed for the ethylene and isobutene reactions.

Figure 11.61 shows that in O_2 as carrier gas the emission intensities and the ozone concentration both decay exponentially at times >0.1 sec. The ratio (decay rate of emission intensity)/(rate of ozone decay) was determined for each run from plots such as those shown. The average value of this ratio

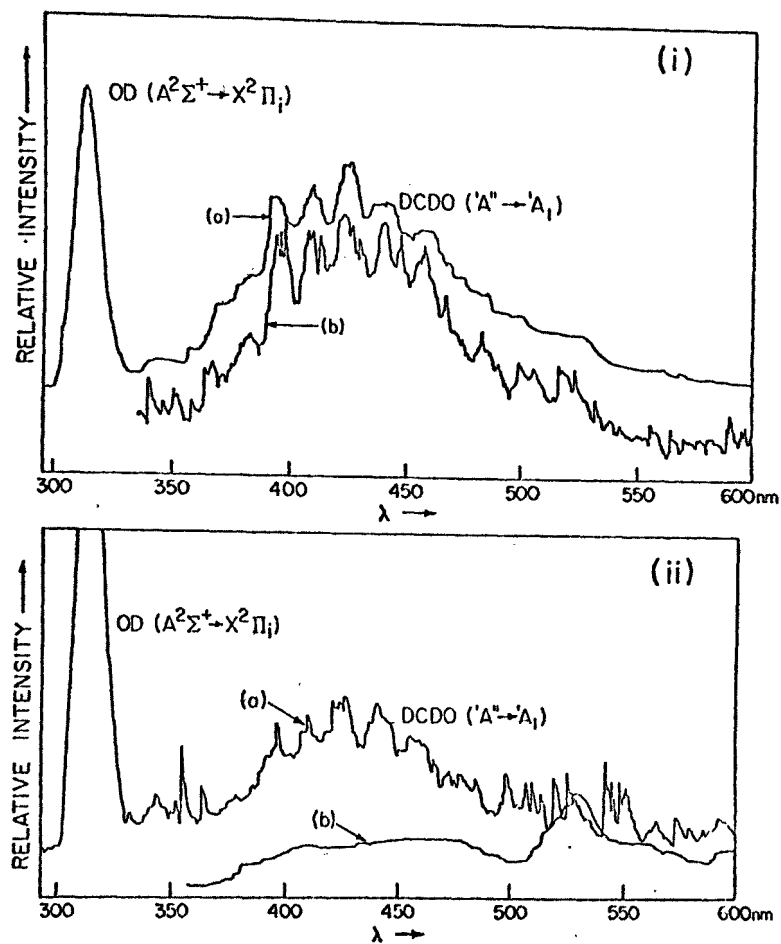


Figure 11.5 Chemiluminescent emission spectra (300–600 nm) from the reactions of 2% O₃ in (a) N₂ and (b) O₂ with: (i) 2-butene-d₈, total pressure 1.72 torr, spectral slit width 9.0 nm; (ii) isobutene-d₈, total pressure 1.93 torr, spectral slit width 9.0 nm.

Table 11.1

Summary of the chemiluminescing species ($200 < \lambda < 1100$ nm) identified in ozone-olefin reactions in the presence and absence of oxygen.^a

Olefin	Carrier gas	Chemiluminescing species				
		OH [†]	OH [*]	HCHO [*]	(CHO) ₂ [*]	CH ₂ CO- CHO ^{*b}
Ethylene	O ₂	+		+		
	N ₂	+	+	+		
<u>cis</u> -2-Butene	O ₂	+	+	+	+	
	N ₂	+	+	+	?	
<u>trans</u> -2-Butene	O ₂	+		+	+	
Propylene	O ₂	+		+	c	
1-Butene	O ₂	+		+	c	
Isobutene	O ₂	+	+	+		+
	N ₂	+	+	+		
2-Methyl-2-butene	O ₂	+		+		+
2,3-Dimethyl-2-butene	O ₂	+		+		+

^a + denotes positive identification of emitting species; a blank indicates that chemiluminescence from this species was not observed.

^b Tentative identification; see text.

^c Not studied at high resolution.

Table 11.2

Reaction orders of emitting species in ozone and olefin in the presence and absence of oxygen, respectively.^a

Olefin	Carrier gas	HCHO [*]	Emitting species	
			OH [†]	517- or 520-nm peak
Ozone				
Ethylene	O ₂	1.04 ± 0.04	1.04 ± 0.03	
	N ₂	1.09 ± 0.07	1.03 ± 0.05	
Isobutene	O ₂	1.06 ± 0.04	0.93 ± 0.05	0.39 ± 0.02 ^b
	N ₂	0.99 ± 0.04	1.00 ± 0.01	
<u>cis</u> -2-Butene	O ₂	0.95 ± 0.03	1.14 ± 0.01	0.97 ± 0.02 ^c
	N ₂	0.89 ± 0.03	1.01 ± 0.03	
Olefin				
Isobutene	O ₂	1.06 ± 0.05	0.97 ± 0.04	1.00 ± 0.05 ^b
<u>cis</u> -2-Butene	O ₂	0.96 ± 0.06	1.12 ± 0.11	1.10 ± 0.09 ^c

^a Errors given are least-squares standard deviations.

^b Tentatively identified as methylglyoxal phosphorescence.

^c Assigned as glyoxal phosphorescence, (CHO)₂(³A_u → ¹A_g).

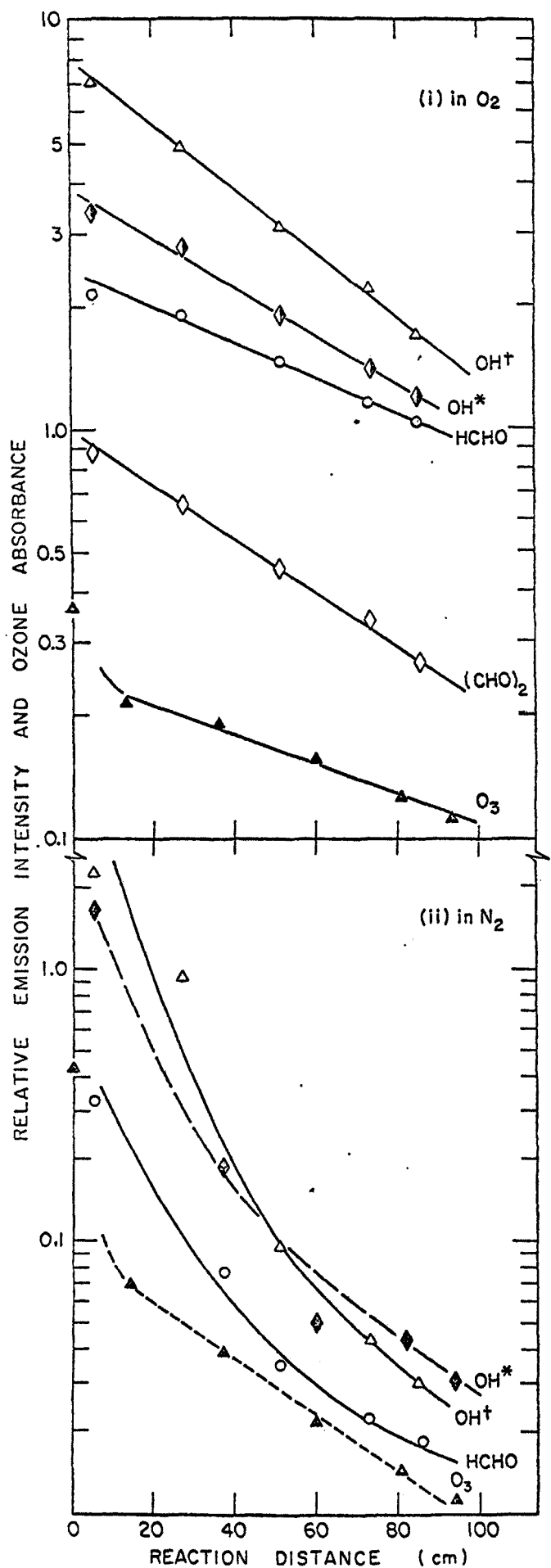


Figure 11.6 Semilogarithmic plots of relative emission intensities and ozone absorbance vs reaction distance for the reaction of cis-2-butene with (i) 2% O₃/O₂ and (ii) 2% O₃/N₂. Initial flow rate of cis-2-butene, 16-22 $\mu\text{mol}/\text{sec}$; initial ozone flow rate 2.5 $\mu\text{mol}/\text{sec}$; total pressure 5.3-9.2 torr; 100 cm corresponds to a reaction time of 1.3 sec.

in the pressure range of 2-10 torr was approximately 1.4 for all emissions. However, this ratio was observed to decrease with increasing oxygen or olefin concentration. For example, at 1.8 torr total pressure, this ratio was 1.6 for formaldehyde fluorescence; on addition of O_2 to a total pressure of 9.6 torr, this ratio fell to 1.0.

In N_2 as carrier gas, high initial light intensities occurred, followed by nonexponential decays as seen in Figure 11.6ii. The apparent increase in the intensity of the Meinel bands (Figure 11.4) on the replacement of O_2 by N_2 is thus due to the increased initial light intensity rather than to an overall increase at all reaction times. While the ozone decayed even more rapidly than in O_2 at times ≤ 0.1 sec., a slower exponential decay followed.

c. Relationship of OH^* and OH^\dagger . In the cis-2-butene reaction, the relationship of the OH^* emission intensity to that of OH^\dagger in both O_2 and N_2 as diluent gas was investigated by simultaneously following both emission intensities as a function of reaction time. The least-squares slopes of the log-log plots of OH^* emission intensity vs. OH^\dagger intensity for each run in a series of experiments at varying total pressure and reactant concentrations averaged 0.97 ± 0.04 in the presence of O_2 and 0.91 ± 0.06 in N_2 .

Similar investigations were carried out for the reactions of ethylene and isobutene with O_3 in N_2 as carrier gas. While the data were more scattered than that for the cis-2-butene reaction, the average slopes of the log-log plots were 1.09 ± 0.08 and 1.35 ± 0.11 , respectively.

Kinetics of Ozone Decay. With olefin at least a factor of 6 in excess over O_3 , the rate of decay of ozone was measured under similar conditions as those used for recording the chemiluminescent emission spectra. Varying flows of nitrogen or oxygen were then added to a maximum total pressure of 10 torr, and the rate of ozone decay was measured at each pressure. The results of these experiments for the cis-2-butene and isobutene reactions are given in Table 11.3.

Although the overall uncertainties in the rate constants measured are approximately $\pm 30\%$, Table 11.3 shows that the measured rates are larger by a factor of 2-5 in the presence of N_2 as compared to those measured in O_2 and decrease slightly with increasing O_2 concentration, as has been observed since.⁴⁷⁻⁵⁰

Under these experimental conditions, the rate constant for the ethylene-ozone reaction was estimated to be $1 \pm 1 \times 10^3 \text{ l mol}^{-1} \text{ sec}^{-1}$ in O_2 and

Table 11.3

Rate constants for the cis-2-butene and isobutene reactions with ozone under varying conditions of total pressure and oxygen concentrations.^a

Experimental conditions	<u>cis</u> -2-Butene		Isobutene	
	Total pressure, torr	$10^{-4} \times k$, $\text{l mol}^{-1} \text{sec}^{-1}$	Total pressure, torr	$10^{-4} \times k$, $\text{l mol}^{-1} \text{sec}^{-1}$
O_3/O_2 from ozonizer used; no additional diluent added	1.8-2.1	9.2 ± 2.3	1.7-1.9	1.4 ± 0.4
O_3/O_2 from ozonizer used; O_2 as diluent	3.9-4.0	7.3 ± 2.0	3.9-4.2	0.82 ± 0.28
	4.5-5.9	6.7 ± 1.8	6.4-6.6	0.63 ± 0.23
	7.3-7.4	7.1 ± 2.0	9.3-9.7	0.54 ± 0.23
	8.9-9.6	6.3 ± 1.9		
O_3/N_2 from silica gel trap used; O_2 added as diluent	5.5-5.6	6.5 ± 1.9	4.4-4.5	0.84 ± 0.29
	8.9-9.1	6.0 ± 1.9		
O_3/N_2 from silica gel trap used; no additional diluent added	1.9-2.0	17 ± 5	1.9-2.0	4.2 ± 1.2
O_3/N_2 from silica gel trap used; N_2 added as diluent	5.4-6.1	13 ± 4	4.2-4.5	3.8 ± 1.3
	9.1-10.0	16 ± 5	6.8-7.1	3.0 ± 1.0
			9.6-9.9	3.7 ± 1.1

^a Error limits shown are the estimated overall errors which include both the precision of the data as well as experimental errors

$5 \pm 2 \times 10^3 \text{ l mol}^{-1} \text{ sec}^{-1}$ in N_2 .

The rate constants from this work are compared in Table 11.4 with literature room-temperature absolute values.^{6,10,42-50} The values in O_2 are seen to be in general agreement with the literature, indicating no significant change in the kinetics with total pressure.

Stable Product Analysis. The major stable products identified by gc from the cis-2-butene-ozone reaction at 2 to 10 torr were acetaldehyde and 2-butanone in both O_2 and N_2 as diluents and methyl vinyl ketone in O_2 only. Two unidentified products were also observed in O_2 . The acetaldehyde yield increased relative to that of the 2-butanone with increasing pressures of O_2 . These product identifications are supported by the observations of mass peaks corresponding to all of these products in earlier photoionization mass spectrometer studies¹² of this reaction.

Absolute Rates of Light Emission. The total rate of light emission from each emitting species in the ethylene and cis-2-butene reactions with 2% O_3/O_2 is given in Table 11.5; that for OH^\dagger refers to light emission from the (9,3) transition only.

Table 11.5

Absolute rates of light emission^a ($\text{l mol}^{-1} \text{ sec}^{-1}$) for each emitting species in the reactions of 2% O_3/O_2 with ethylene and cis-2-butene at a total pressure of 4.6 torr.

Olefin	Emitting species		
	HCHO^*	OH^\dagger	$(\text{CHO})_2^*$
Ethylene	1×10^{-4}	1×10^{-4}	
<u>cis-2-Butene</u>	7×10^{-2}	5×10^{-3}	0.7

^a For HCHO^* AND $(\text{CHO})_2^*$, the total rate of light emission, $k_x(\text{TOT})$, calculated as described in the text, is given. For OH^\dagger , the rate of light emission is that in the (9,3) transition only, which is expected to be a function of the reactant concentrations (see Discussion).

Temperature Rise Studies. In order to investigate the self-heating of the gases^{7,8,42} during these exothermic reactions, the temperature rise was

Table 11.4

Comparison of the rate constants obtained in this work with literature room-temperature absolute values.

Olefin	Rate constant $\times 10^{-3}$ $\ell \text{ mol}^{-1} \text{ sec}^{-1}$	Ref
Ethylene	0.93 ± 0.09	46
	1.8^a	45
	0.8	6
	2.1 ± 0.8	43
	1.06	47, 49
	1.14	48
	1.68	50
	$1 \pm 1(\text{O}_2)$	This work
	$5 \pm 2(\text{N}_2)$	
<u>cis</u> -2-Butene	85	
	90(N_2)	10
	200	45
	29	6
	97	48
	75.6	49
	120	50
	60-92(O_2)	This work
	130-170(N_2)	
Isobutene	8.8 ± 2.2	44
	3.7	6
	14 ± 2	45
	8.2	48
	7.01	49
	10.8	50
	5-14(O_2)	This work
	30-42(N_2)	

^a Dynamic system, $k = 1.6 \pm 0.2 \times 10^3 \ell \text{ mol}^{-1} \text{ sec}^{-1}$. Static system, $k = 2.0 \times 10^3 \ell \text{ mol}^{-1} \text{ sec}^{-1}$.

recorded at each of the five thermistors for the reaction of a series of olefins with O_3/O_2 or O_3/N_2 . In the reaction with O_3/O_2 , the magnitude of the maximum temperature rise increased in the order ethylene < propylene ~ 1-butene ~ isobutene < cis-2-butene < 2-methyl-2-butene ~ 2,3-dimethyl-2-butene which is also the order in which the rate constants increase.^{6-10,42-50} Furthermore, the temperature rise increased with flow rate of either ozone or olefin and decreased with increasing reaction time, showing that the heat release is related to the amount of reaction occurring.

The reactions of ethylene, cis-2-butene, and isobutene with O_3/N_2 showed a greater temperature rise than the corresponding reactions in oxygen, although the increase in temperature was confined to shorter reaction times in agreement with the above observations. The maximum temperature rise observed was $\leq 7^\circ C$, which would not have a significant effect on the rate constants^{9,43,45,47,49,50} measured here.

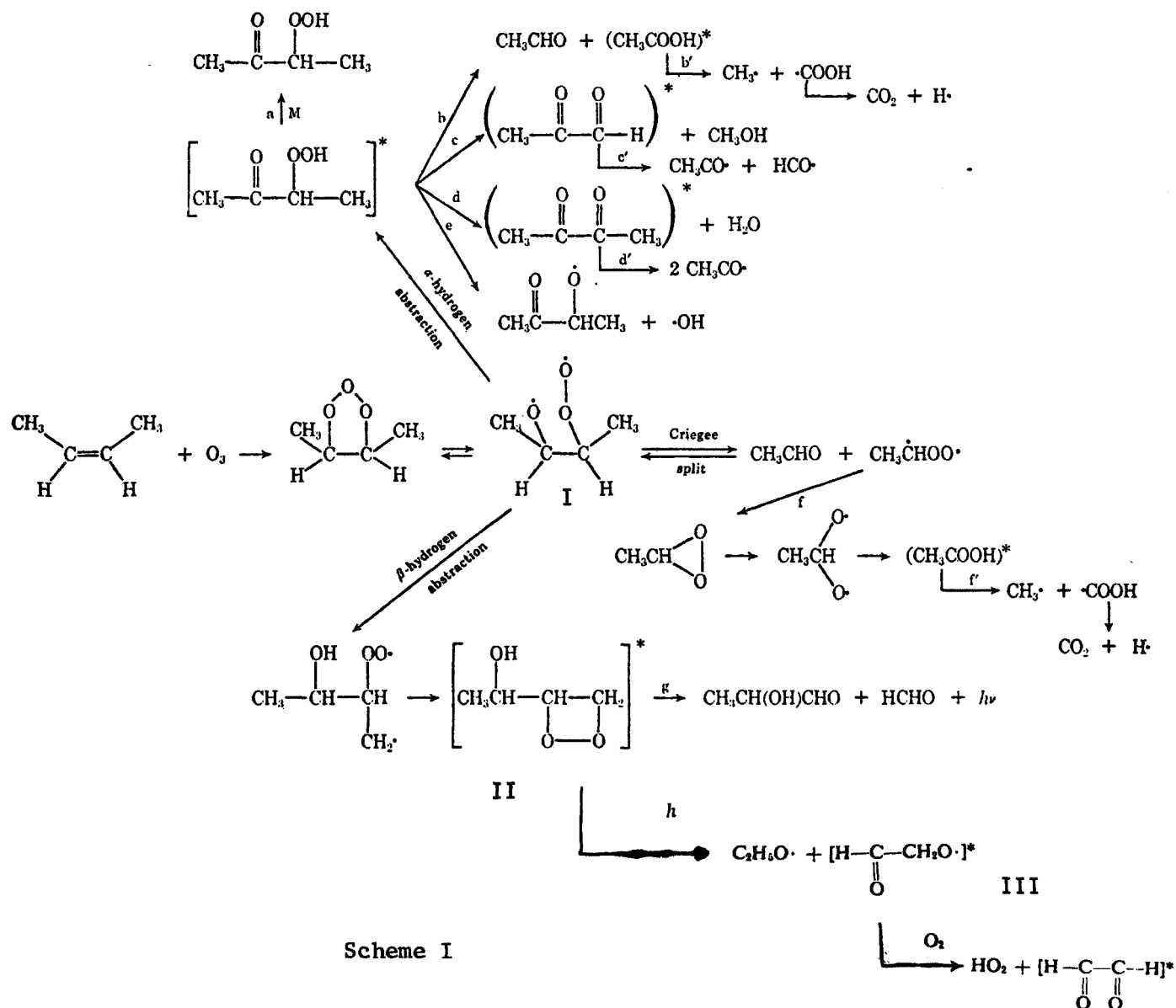
Discussion

cis-2-Butene Reaction. The mechanism of ozone-olefin reactions proposed by O'Neal and Blumstein²³ is applied to the ozone-cis-2-butene reaction in Scheme I. Included are recent modifications⁵¹ to the original scheme relevant to our studies.

At a total pressure of ~2 torr, it is anticipated that (1) α -hydrogen abstraction should occur at a rate approximately 2.5 faster than the Criegee fragmentation assuming some stabilization of the Criegee biradical by polarization of charge, (2) collisional stabilization of the excited α -keto hydroperoxide (reaction a) and decomposition (reactions b to e) should be competitive such that both the α -keto hydroperoxide and the intermediates and stable products predicted by reactions b to e should be observed, and (3) β -hydrogen abstraction of the peroxy biradical will occur at a rate slower by a factor of ~8 than the α -hydrogen abstraction path, leading to the formation of an excited 1,2-dioxetane.

One can now compare these predictions to the experimental data for the cis-2-butene-ozone reaction obtained in this and earlier studies.^{11,12}

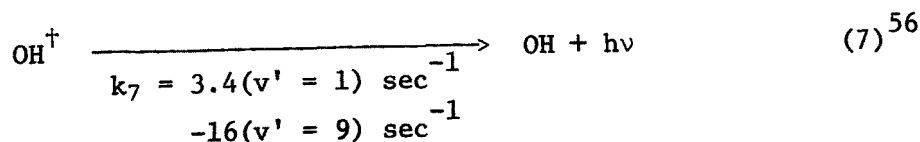
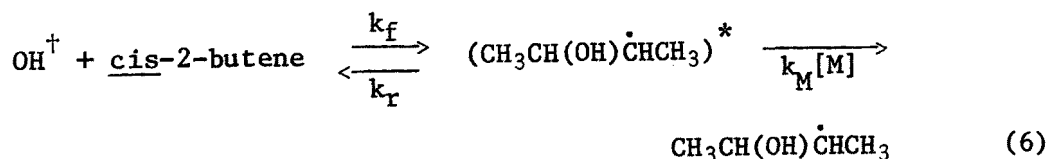
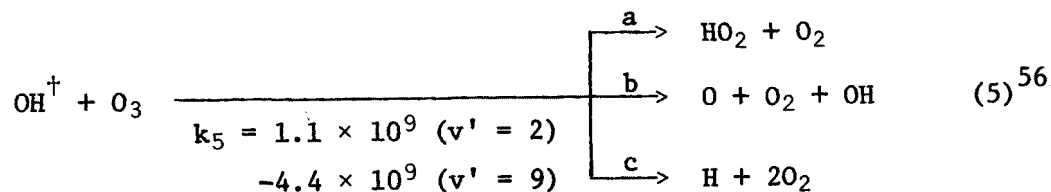
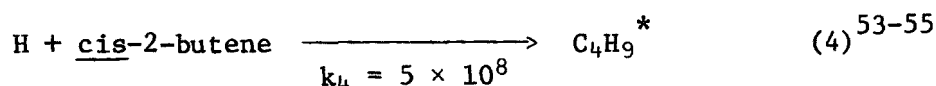
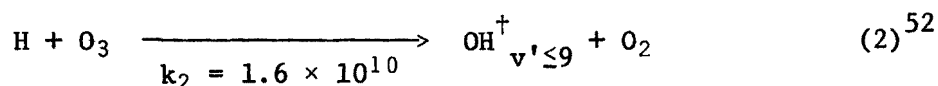
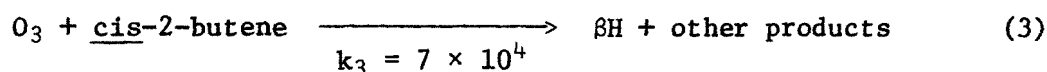
a. OH^\dagger Meinel Band Emission. Application of simple unimolecular (RRK) theory to the thermochemistry predicted by O'Neal indicates that due to the ~140 kcal/mol released in the rearrangement of the biradical to acetic acid (step f) its decomposition (step f') should occur at a rate several orders of magnitude greater than collisional quenching at 2 torr.⁵¹ It is



also possible⁵¹ that the acetic acid formed in step b may contain enough of the reaction exothermicity to decompose in an analogous manner. Since the observed yield of CH₃CHO at 2 torr is ~1,¹² but CH₃COOH was not observed, the yield of H atoms may approach unity under our experimental conditions.

The dominant loss process for H atoms formed in step f' and possibly b' under these conditions¹² must be the well-known chemiluminescent reaction^{29,38,39} with O₃.

A simplified scheme for the formation and loss of OH⁺ is then given by



where the rate constants are in liters per mole second units unless otherwise specified and β is the fraction of reaction 3 giving H atoms. Hence

$$[\text{OH}^\dagger] = \frac{\beta_3 k_2 [\text{O}_3]^2 [\text{olefin}]}{\{k_5 [\text{O}_3] + k_6 [\text{olefin}] + k_7\} \{k_2 [\text{O}_3] + k_4 [\text{olefin}]\}} \quad (\text{III})$$

where $k_6 = k_f k_M [\text{M}] / (k_r + k_M [\text{M}])$, k_f , k_r , and k_M are the rate constants for the steps outlined in reaction 6 above, and in all cases $k_7 \ll k_5 [\text{O}_3]$.

The overall rate constant for reaction 6 for ground state $\text{OH}(v' = 0)$ with cis-2-butene at a total pressure of ~1 torr is $\sim 4 \times 10^{10} \text{ l mol}^{-1} \text{ sec}^{-1}$.^{57,58,59} The observed⁵⁷ enhancement of the OH-propylene adduct mass peaks as the total pressure was increased from 1 to 4 torr suggests that at least for propylene the adduct can also decompose, one path possibly being that back to the reactants. Because of the high room-temperature rate constant, the activation energy for the reaction of $\text{OH}(v' = 0)$ with cis-2-butene is negative⁵⁹ and hence an increase in the vibrational energy of the reacting OH radical is anticipated to substantially increase the rate of decomposition of the adduct, k_r , while not significantly affecting the forward rate, k_f . Hence the overall rate constant, k_6 , is expected to decrease as the vibrational energy content of the OH radical increases.

An estimate of k_6 for vibrationally excited OH^\dagger can be obtained as follows: assuming an activation energy for the forward reaction of ~1 kcal/mol and $\Delta H_f^\circ = -28 \text{ kcal/mol}$ ⁶⁰ for the adduct, $\text{CH}_3\text{CH}(\text{OH})\dot{\text{C}}\text{HCH}_3$, then from unimolecular theory,⁶¹ $k_r \sim 2 \times 10^8 \text{ sec}^{-1} (v' = 7-8)$. Assuming $k_M [\text{M}] = 2 \times 10^7 \text{ sec}^{-1}$, then $k_6 \sim 4 \times 10^9 \text{ l mol}^{-1} \text{ sec}^{-1}$,⁶² which, though very approximate, can now be applied to the kinetics of OH^\dagger formation.

In the experiments to determine the reaction order of OH^\dagger with respect to olefin, $[\text{O}_3] \geq 2 \times [\text{olefin}]$, thus $k_2 [\text{O}_3] \gg k_4 [\text{olefin}]$ and hence equation III simplifies to

$$[\text{OH}^\dagger] = \frac{\beta k_3 [\text{O}_3] [\text{olefin}]}{k_5 [\text{O}_3] + k_6 [\text{olefin}]} \quad (\text{IV})$$

Using $k_6 \approx 4 \times 10^9 \text{ l mol}^{-1} \text{ sec}^{-1}$, $k_5 [\text{O}_3] > k_6 [\text{olefin}]$, and hence $[\text{OH}^\dagger] \propto [\text{olefin}]$, consistent with Table II.

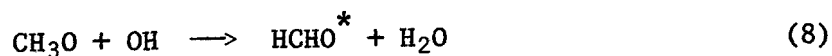
Similarly, when studying the dependence of OH^\dagger on $[\text{O}_3]$, $[\text{olefin}] \geq 10 [\text{O}_3]$. Then $k_2 [\text{O}_3] > k_4 [\text{olefin}]$ and $k_6 [\text{olefin}] > k_5 [\text{O}_3]$. Hence $[\text{OH}^\dagger] \propto [\text{O}_3]$, as observed.

In order to calculate the total rate of light emission from all vibrational levels of OH^\dagger , and hence the yield of OH^\dagger , the vibrational distribution must be known. It was not possible in these experiments to determine this distribution and hence only a crude estimate of the total rate of light emission can be obtained. Garvin, et al.,⁶³ have shown that at 4.2 torr total pressure in O_2 and H_2 the vibrational distribution of OH^\dagger from reaction 2 is Boltzmann and corresponds to a vibrational temperature of 9250°K. However, in the presence of olefin with which OH^\dagger reacts, the lower vibrational levels may be preferentially removed leading to a higher effective vibrational temperature. Calculating k_6 as a function of OH^\dagger vibrational energy content as described above, and modifying the Boltzmann distribution found by Garvin, et al.,⁶³ for the increased removal of OH^\dagger in lower vibrational energy levels, the H atom yield per molecule of reactant consumed is estimated to be approximately 1 within order of magnitude error limits, under these experimental conditions.

b. $\text{HCHO}(^1\text{A}'') \rightarrow ^1\text{A}_1$). The experimentally observed first-order kinetics of formaldehyde fluorescence are consistent with the production of electronically excited HCHO from the decomposition of an excited 1,2-dioxetane, step g of Scheme I.

Using $k_3 = 7 \times 10^4 \text{ l mol}^{-1} \text{ sec}^{-1}$ for the cis-2-butene- O_3 reaction at 4.6 torr (Table 11.3) and $k_x(\text{TOT}) = 7 \times 10^{-3} \text{ l mol}^{-1} \text{ sec}^{-1}$ for formaldehyde fluorescence (Table 11.5), the number of light quanta emitted from electronically excited formaldehyde per molecule of reactant consumed is $\sim 1 \times 10^{-7}$. These low values are consistent with the concerted process (step g) since both the decomposition of 1,2-dioxetanes to produce the first excited singlet state⁶⁴ and HCHO fluorescent emission are inefficient processes.

Other sources of $\text{HCHO}(^1\text{A}'')$ such as

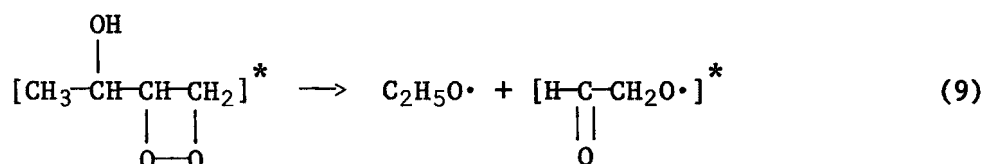


cannot be definitely excluded, particularly at the low pressures and relatively high OH concentrations present under these conditions. Reaction 8 is thought to be responsible for the weak formaldehyde fluorescence observed as a general phenomenon in the low-temperature gas-phase oxidation of organic compounds.⁶⁵ Although OH radicals are known to be present in the cis-2-butene-ozone reaction, no CH_3O radicals were detected in the PMS studies.¹² This does not preclude

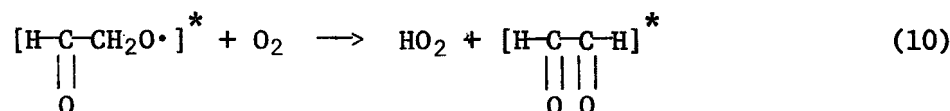
the production of CH_3O since if its loss is by reaction with olefin with a rate constant of $10^7\text{--}10^8 \text{ l mol}^{-1} \text{ sec}^{-1}$,⁶⁶ then its steady state concentration would have been below the detection limits.

c. Glyoxal Phosphorescence. Although glyoxal phosphorescence has been observed from the recombination of HCO radicals,⁶⁷ this seems highly unlikely in the presence of excess O_2 which reacts rapidly with HCO .⁶⁸ In addition, this recombination, which is second order in HCO , would not be kinetically consistent with both the first-order dependence of light intensity on reactants and with the direct production of HCO from the ozone-olefin adduct via steps c and c'.

The observation of glyoxal phosphorescence in the presence of 2 Torr of O_2 , and indeed at higher pressures,³⁶ is rather surprising. One energetically possible route involves an alternate mode of decomposition of the 1,2-dioxetane formed by β -H abstraction

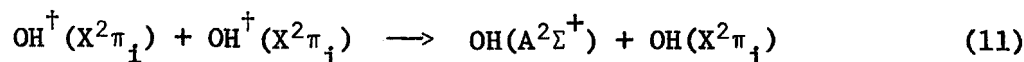


followed by reaction of the excited alkoxy radical with O_2 .



While (9) and (10) are speculative, it appears that the partitioning of energy in these reactions may result in sufficient energy input to the glyoxal to cause electronic excitation. Furthermore, this mechanism is consistent with the observed kinetic isotope effect (Figure 11.5), the first-order kinetics of the light emission, and the observation of glyoxal phosphorescence at pressures approaching atmospheric.³⁶

d. Electronically Excited OH. OH^* has been observed⁶⁹ in the $\text{H} + \text{O}_3$ reaction as a product of energy pooling.



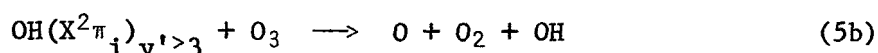
However, the width of the (0,0) band envelope of $\text{OH}(\text{A}^2\Sigma^+ \rightarrow \text{X}^2\pi_1)$ from

reaction 11 was greater than that from the ozone-olefin reactions. In addition, the observed first-order dependence of electronically excited OH^* on the vibrationally excited OH^\dagger radical rules out reaction 11 as the source of OH^* .

One possible source of electronically excited OH^* radicals in this system involves O atom reactions. Thus, Becker, Kley, and Norstrom⁷⁰ in their studies of OH^* chemiluminescence in the $\text{O}-\text{C}_2\text{H}_4$ flame observed rotationally cool emission from OH^* . The reactions of an O atom with either an H atom or an excited HCO radical to produce OH^* were suggested.

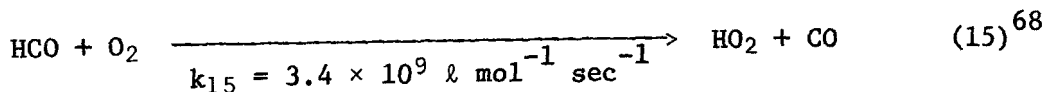
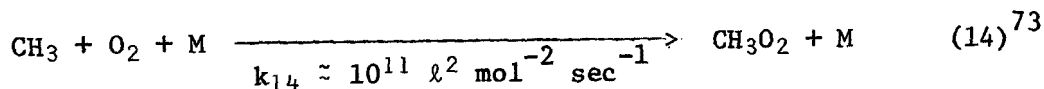


A mode of production of O atoms in the ozone-olefin system is the decomposition of O_3 by OH^\dagger radicals with $v' \geq 3$.⁷¹

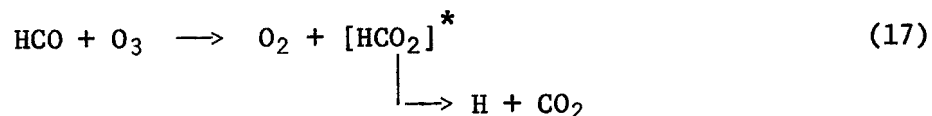
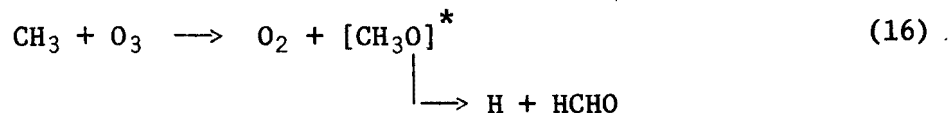


The OH^* emission intensity is strongest for the ethylene reaction, relative to the HCHO^* and OH^\dagger emissions, supporting an O atom precursor as the relative rates of reaction of $\text{O}(^3\text{P})$ with ethylene, isobutene, and cis-2-butene are 1:25:24.⁷²

e. Effects of Oxygen. In nitrogen as diluent, the initial steps of the ozone-cis-2-butene reaction as outlined above must remain the same. However, the secondary reactions of radicals which react rapidly with O_2 will be strongly dependent on its presence. For example, CH_3 and HCO which react with O_2 under these conditions, will, in N_2 as diluent, react with O_3 .



The products of their reactions with O_3 are likely more reactive than the CH_3O_2 and HO_2 produced in reactions 14 and 15, respectively. For example, if excited CH_3O and HCO are formed, H atoms could be produced.^{66,72}



Therefore in the absence of O_2 one anticipates increased rates of O_3 decay due to secondary radical attack and possibly increased Meinel band emission intensity if H atoms are indeed produced in reactions 16 and 17.

This is in qualitative agreement with our experimental observations that: (1) the measured rate constant for O_3 decay in N_2 as diluent is larger than in O_2 , (2) a rapid loss of O_3 occurs in the first ≤ 0.1 sec which is accompanied by intense light emission, particularly of OH^+ and OH^* , and (3) a measurable temperature rise occurs, particularly in the vicinity of the mixing jet.

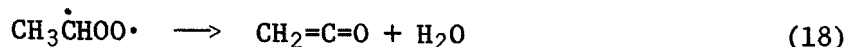
The nonexponential decay of each of the light emissions in N_2 as diluent may then be due to a change in the relative rates of competing reactions such as (5) and (6) over the time period studied, since reaction 6 is a termination step in the chain formed by reactions 2 and 5c. Similar processes must also occur to some extent in 2 torr of O_2 since the emitting species generally show first-order behavior on O_3 (Table 11.2) and yet the rate of decay of light intensity is generally greater than the rate of O_3 decay. Increasing the pressures of O_2 up to 10 torr appears to further quench one or more radical precursors to the chemiluminescence since the ratio (rate of decay of light intensity)/(rate of O_3 decay) approaches unity at ~10 torr of O_2 .

f. Intermediates and Products. Many of the intermediates and stable products predicted by Scheme I were observed either by photoionization mass spectrometry,¹² gc, or both. Thus, HCO and HO₂, possibly from reactions c, c', and 15,⁶⁸ were observed.¹² In addition, HCHO, CH₃OH, CH₃CHO, CH₂CO, and an ozone-olefin adduct believed to be the α-keto hydroperoxide, CH₃CH(OOH)COCH₃, were detected.¹²

On the other hand, 2-hydropropanal which should have been formed in equal quantities to HCHO (step g) was not seen. In addition, while CH_3O_2 and $\text{C}_2\text{H}_5\text{O}$ radicals were observed,¹² their nonsteady state behavior suggested

that they were not primary reaction products but were formed in the mass spectrometer. Hence, their production is uncertain, although reactions 14 and 9 may be possible contributors.

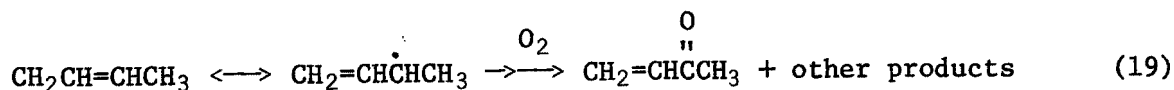
In the PMS studies, ketene was also observed as a major product.¹² Its formation can be rationalized in terms of a "classical" rearrangement of the Criegee zwitterion as suggested by Scott, Hanst, and co-workers.^{5,6,75}



Significant quantities of methyl vinyl ketone and 2-butanone were observed by gc and peaks corresponding to these products were observed by photoionization mass spectrometry.¹² The identification of 2-butanone by gc provides the best explanation of the m/e 72 peak although it might contain some contribution due to methylglyoxal (reaction c).

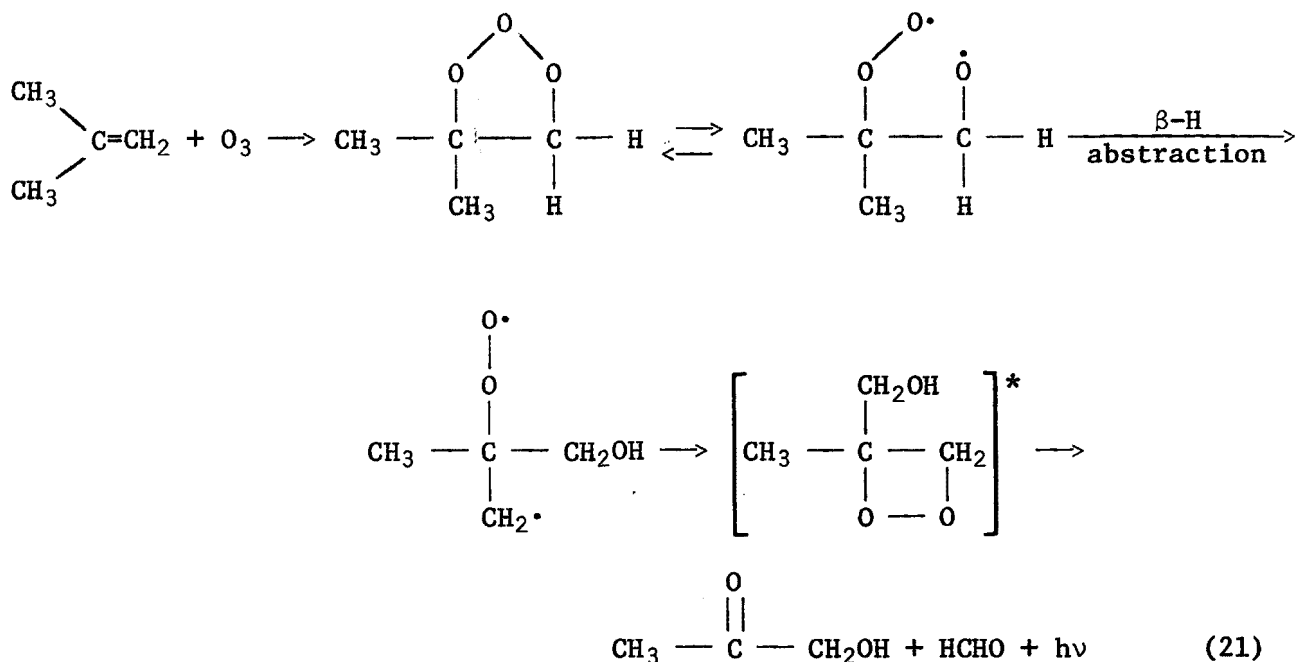
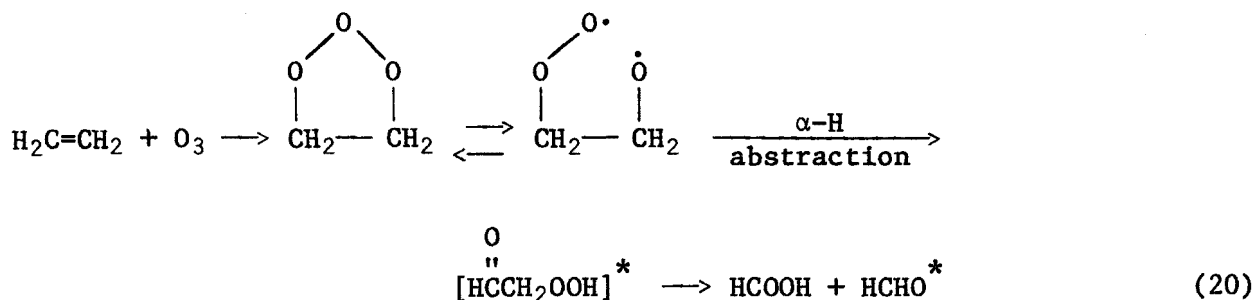
The 2-butanone may be due to the reaction of OH with cis-2-butene. The mechanism of this reaction is not clear, although an OH-olefin adduct has been observed mass spectrometrically.⁵⁷ Preliminary studies⁷⁶ of the OH-cis-2-butene reaction in the presence and absence of oxygen indicate that both 2-butanone and acetaldehyde are formed in significant yields, with the ratio of acetaldehyde to 2-butanone increasing on the addition of oxygen, consistent with our observations.

Radical abstraction from cis-2-butene will form the radical $\text{CH}_2\text{CH}=\text{CHCH}_3$. It was suggested in earlier studies¹² that in the presence of O_2 this radical might subsequently react with O_2 to form methyl vinyl ketone and hence a peak at m/e 70.

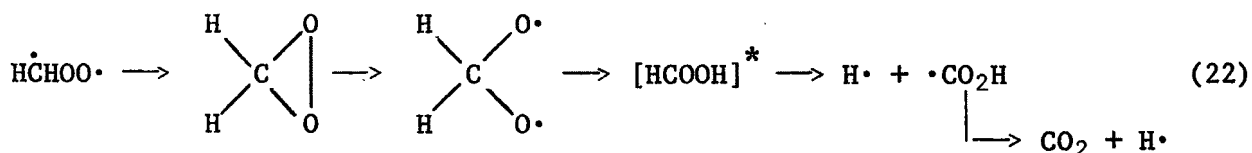


Formation of methyl vinyl ketone by reaction 19 is supported by the fact that it was below the gc detection limit in the cis-2-butene- O_3/N_2 system but was observed on O_2 as diluent.

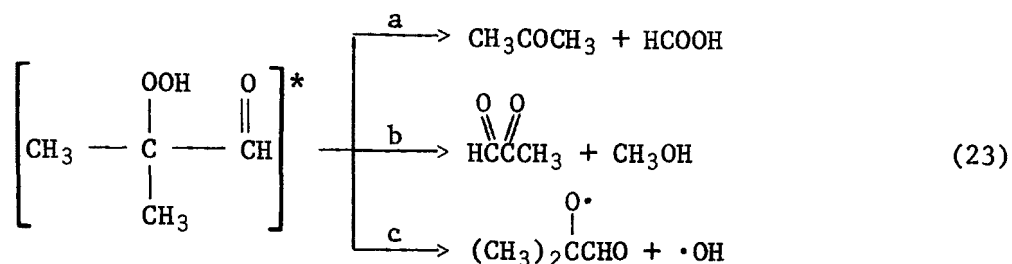
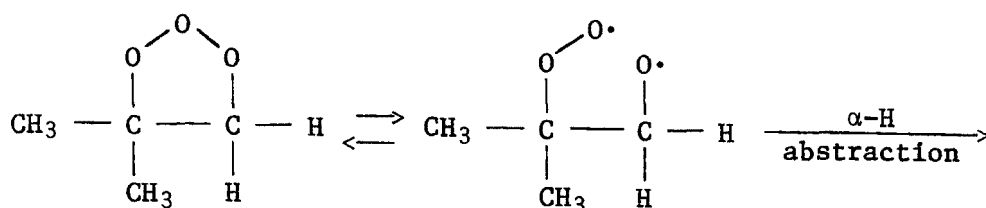
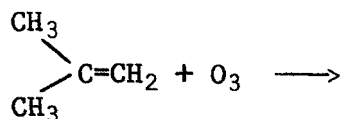
Ethylene and Isobutene Reactions. Formaldehyde fluorescence and OH^\dagger Meinel band emissions are common to all three olefin reactions studied. Possible routes to the formation of electronically excited formaldehyde which are consistent with the observed first-order kinetics involve α -H abstraction and β -H abstraction, respectively.^{23,51}



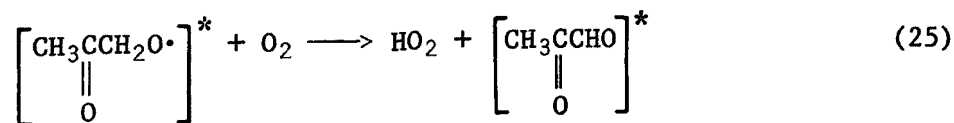
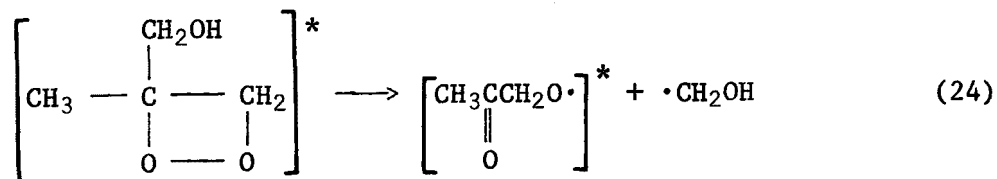
As in the cis-2-butene-ozone reaction, efficient H-atom production and hence relatively strong OH⁺ Meinel band emission are anticipated in both of these reactions at 2 torr from the decomposition of excited HCOOH formed by the Criegee path.



While in the isobutene reaction, a proposed^{23,51} route to the formation of methylglyoxal is the α -H



abstraction, reaction 23b; the kinetics of the emission (Table 11.2) suggest a more complex mechanism than reaction 23b. The apparent involvement of O_2 is also difficult to rationalize by this scheme, as is the observation of excited methylglyoxal from the 2-methyl-2-butene and 2,3-dimethyl-2-butene reactions. However, in the alternate mode of decomposition of the 1,2-dioxetane formed by β -hydrogen abstraction, analogous to that proposed above for the cis-2-butene, reactions 9 and 10 may give electronically excited methylglyoxal.



Reactions 24 and 25 would explain why O_2 is necessary to produce excited methylglyoxal. In addition, one anticipates a decreased ratio of the intensities

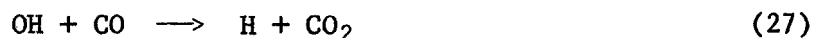
of methylglyoxal phosphorescence to formaldehyde fluorescence in the iso-butene-d₈ reaction, due to kinetic isotope effects,⁴¹ as is observed (Figure 11.5ii).

The effects of replacing the O₂ diluent by N₂ are expected to be similar to those in the cis-2-butene reaction, consistent with experiment.

Atmospheric Implications. In the formation of photochemical smog, the rate of oxidation of NO to NO₂ in excess of that due to O atom and O₃ reactions is currently thought⁷⁷⁻⁷⁹ to be due at least in part to the HO₂ reaction



HO₂ may then be regenerated in a chain process involving the OH radical



Hence any reaction producing H atoms or OH in the atmosphere may contribute to the NO to NO₂ oxidation. OH has recently been detected⁸⁰ in ambient air, lending support to this postulate.

REFERENCES

1. L. Long, *Chem. Rev.*, 27, 437 (1943).
2. P. S. Bailey, *Chem. Rev.* 58, 925 (1958), and references therein.
3. P. S. Bailey, 161st National Meeting of the American Chemical Society, Los Angeles, Calif., March 29-30, 1971, PETR No. 11; *Advan. Chem. Ser.*, No. 112 (1972).
4. R. W. Murray, *Accounts Chem. Res.*, 1, 313 (1968), and references therein.
5. W. E. Scott, E. R. Stephens, P. L. Hanst, and R. C. Doerr, *Proc. Amer. Petrol. Inst.*, Sect. 3, 171 (1957).
6. P. L. Hanst, E. R. Stephens, W. E. Scott, and R. C. Doerr, "Atmospheric Ozone-Olefin Reactions," The Franklin Institute, Philadelphia, Pa., 1958.
7. T. Vrbaski and R. J. Cvetanovic, *Can. J. Chem.*, 38, 1053, 1063 (1960).
8. Y. K. Wei and R. J. Cvetanovic, *Can. J. Chem.*, 41, 913 (1963).
9. W. B. DeMore, *Int. J. Chem. Kinet.*, 1, 209 (1969).
10. R. A. Cox and S. A. Penkett, *J. Chem. Soc., Faraday Trans. 1*, 69, 1735 (1972).
11. B. J. Finlayson, J. N. Pitts, Jr., and H. Akimoto, *Chem. Phys. Lett.*, 12, 495 (1972).
12. R. Atkinson, B. J. Finlayson, and J. N. Pitts, Jr., *J. Amer. Chem. Soc.*, 95, 7592 (1973).
13. E. Briner and P. Schnorf, *Helv. Chem. Acta*, 12, 154, 151 (1929).
14. E. Briner and R. Meier, *Helv. Chem. Acta*, 12, 529 (1929).
15. G. W. Nederbragt, A. Van der Horst, and J. Van Duijn, *Nature (London)*, 206, 87 (1965).
16. G. J. Warren and G. Babcock, *Rev. Sci. Instrum.*, 41, 280 (1970).
17. J. A. Hodgeson, B. E. Martin, and R. E. Baumgardner, 160th National Meeting of the American Chemical Society, Chicago, Ill., Sept. 13-18, 1970, WATR No. 011.
18. J. A. Hodgeson and R. K. Stevens, Abstracts, 161st National Meeting of the American Chemical Society, Los Angeles, Calif., March 28-April 2, 1971, Anal. No. 069.
19. J. A. Hodgeson, B. E. Martin, and R. E. Baumgardner, paper 77 presented at the Eastern Analytical Symposium, New York, N. Y., 1970.

REFERENCES (cont.)

20. W. A. Kummer, J. N. Pitts, Jr., and R. P. Steer, *Environ. Sci. Technol.*, 5, 1045 (1971).
21. J. N. Pitts, Jr., B. J. Finlayson, H. Akimoto, W. A. Kummer, and R. P. Steer, *Int. Symp. Identification Meas. Environ. Pollut.*, [Proc.], 32 (1971).
22. J. N. Pitts, Jr., W. A. Kummer, R. P. Steer, and B. J. Finlayson, *Advan. Chem. Ser.*, No. 113, 246 (1972).
23. H. E. O'Neal and C. Blumstein, *Int. J. Chem. Kinet.*, 5, 397 (1973).
24. A. Fontijn, C. B. Meyer, and H. I. Schiff, *J. Chem. Phys.*, 40, 64 (1964).
25. A. N. Wright and C. A. Winkler, "Active Nitrogen," Academic Press, New York, N.Y., 1968, pp 74-75, and references therein.
26. L. G. Anderson, C. S. Parmenter, H. M. Poland, and J. D. Rau, *Chem. Phys. Lett.*, 8, 232 (1971).
27. J. T. Yardley, G. W. Holleman, and J. I. Steinfeld, *Chem. Phys. Lett.*, 10, 266 (1971).
28. J. T. Yardley, *J. Chem. Phys.*, 56, 6192 (1972).
29. A. B. Meinel, *Astrophys. J.*, 111, 555 (1950).
30. G. A. Cook, A. D. Kiffer, C. V. Kumpp, A. H. Malik, and L. A. Spence, *Advan. Chem. Ser.*, No. 21, 44 (1959).
31. P. N. Clough and B. A. Thrush, *Chem. Ind. (London)*, 1971 (1966).
32. R. Spence and W. Wild, *J. Chem. Soc., London*, 338 (1935).
33. G. W. Robinson, *J. Chem. Phys.*, 22, 1147, 1384 (1954).
34. W. Holzer and D. A. Ramsay, *Can. J. Phys.*, 48, 1759 (1970).
35. R. Y. Dong and D. A. Ramsay, *Can. J. Phys.*, 51, 1491 (1973).
36. J. N. Pitts, Jr., and D. A. Hansen, unpublished data.
37. J. T. Yardley, A. V. Pocius, and C. Dykstra, personal communication, 1973.
38. J. D. McKinley, Jr., D. Garvin, and M. J. Boudart, *J. Chem. Phys.*, 23, 784 (1955).
39. P. E. Charters, R. G. MacDonald, and J. C. Polanyi, *Appl. Opt.*, 10, 1747 (1971), and references therein.
40. B. J. Finlayson, J. S. Gaffney, and J. N. Pitts, Jr., *Chem. Phys. Lett.*, 17, 22 (1972).

REFERENCES (cont.)

41. R. Livingston in "Techniques of Organic Chemistry," 2nd ed., S. L. Friess, E. S. Lewis, and A. Weissberger, Ed., Interscience, New York, N.Y., 1961, Chapter II.
42. H. E. Smith and R. H. Eastman, J. Amer. Chem. Soc., 83, 4274 (1961).
43. R. D. Cadle and C. Schadt, J. Amer. Chem. Soc., 74, 6002 (1952).
44. E. A. Schuck, G. J. Doyle, and N. Endow, Air Pollution Foundation, Report No. 31, San Marino, Calif., 1960.
45. J. J. Bufalini and A. P. Altshuller, Can. J. Chem., 43, 2243 (1965).
46. D. H. Stedman, C. H. Wu, and H. Niki, J. Phys. Chem., 77, 2511 (1973).
47. J. T. Herron and R. E. Huie, J. Phys. Chem., 78, 2085 (1974).
48. S. M. Japar, C. H. Wu, and H. Niki, J. Phys. Chem., 78, 2318 (1974).
49. R. E. Huie and J. T. Herron, Symposium on "Chemical Kinetics Data for the Lower and Upper Atmosphere," Warrenton, Virginia, Sept. 16-18, 1974. Int. J. Chem. Kinet., Symposium No. 1, 165 (1975).
50. K. H. Becker, U. Schurath and H. Seitz, Int. J. Chem. Kinet., 6, 725 (1974).
51. H. E. O'Neal, personal communication, 1973.
52. L. F. Phillips and H. I. Schiff, J. Chem. Phys., 37, 1233 (1962).
53. E. E. Daby and H. Niki, J. Chem. Phys., 51, 1225 (1969).
54. J. A. Cowfer, D. G. Keil, J. V. Michael, and C. Yeh, J. Phys. Chem., 75, 1584 (1971).
55. E. E. Daby, H. Niki, and B. Weinstock, J. Phys. Chem., 75, 1601 (1971).
56. R. N. Coltharp, S. D. Worley, and A. E. Potter, Appl. Opt., 10, 1786 (1971).
57. E. D. Morris, Jr., D. H. Stedman, and H. Niki, J. Amer. Chem. Soc., 93, 3570 (1971).
58. E. D. Morris, Jr., and H. Niki, J. Phys. Chem., 75, 3640 (1971).
59. R. Atkinson and J. N. Pitts, Jr., J. Chem. Phys., 63, 3591 (1975).
60. ΔH_f° was calculated using Benson's group additivity method.⁶¹

REFERENCES (cont.)

61. S. W. Benson, "Thermochemical Kinetics," Wiley, New York, N.Y., 1968.
 $k_r = A((E - E_0)/E)^{s-1}$ where $A \approx 10^{13} \text{ sec}^{-1}$, $(s - 1)_{\text{eff}} \approx 24$, $E_0 = 37 \text{ kcal/mol}$, and $E = E_{\text{OH}^\dagger} + 36 \text{ kcal/mol}$, where E_{OH^\dagger} is the vibrational energy content of the OH^\dagger radical.
62. It is likely that diatomics (O_2 or N_2) will not stabilize the excited adduct molecule with unit efficiency, hence decreasing the calculated value of k_6 . The existence of alternate decomposition paths for the excited adduct will increase k_6 . Unfortunately, at the present time, no information is available on the fate of the excited adduct.
63. D. Garvin, H. P. Broida, and H. J. Kostkowski, J. Chem. Phys., 32, 880 (1960).
64. N. Turro and P. Lechtken, J. Amer. Chem. Soc., 94, 2887 (1972).
65. J. H. Knox in "Photochemistry and Reaction Kinetics," P. G. Ashmore, F. S. Dainton, and T. M. Sugden, Ed., Cambridge University Press, London, 1967, pp 250-286.
66. K. L. Demerjian, J. A. Kerr, and J. G. Calvert, Advan. Environ. Sci. Technol., 4, 1 (1974).
67. D. B. Hartley, Chem. Commun., 1281 (1967).
68. N. Washida, R. I. Martinez, and K. D. Bayes, Z. Naturforsch. A, 29, 251 (1974).
69. H. P. Broida, J. Chem. Phys., 36, 444 (1962).
70. K. H. Becker, D. Kley, and R. J. Norstrom, 12th International Symposium on Combustion, The Combustion Institute, Pittsburgh, Pa., 1969, p 405, and references therein.
71. W. B. DeMore, J. Chem. Phys., 46, 1813 (1967).
72. R. J. Cvetanovic, Advan. Photochem., 1, 115 (1963).
73. N. Basco, D. G. L. James, and F. C. James, Int. J. Chem. Kinet., 4, 129 (1972).
74. P. Gray, R. Shaw, and J. C. J. Thynne, Progr. React. Kinet., 4, 63 (1967).
75. Reaction 18 may proceed via the excited CH_3COOH formed from the rearrangement of the Criegee biradical $\text{CH}_3\dot{\text{C}}\text{HO}\cdot$ since the pyrolysis of CH_3COOH leads to the formation of CH_2CO and H_2O : P. G. Blake and G. E. Jackson, J. Chem. Soc. B, 94 (1964), and references therein.
76. R. J. Cvetanovic, personal communication, 1973.
77. J. Heicklen, K. Westberg, and N. Cohen, publication No. 115-69, Center for Air Environmental Studies, University Park, Pa., 1969.

REFERENCES (cont.)

78. K. Westberg, N. Cohen, and K. W. Wilson, *Science*, 171, 1013 (1971).
79. D. H. Stedman, E. D. Morris, Jr., E. E. Daby, H. Niki, and B. Weinstock, 160th National Meeting of the American Chemical Society, Chicago, Ill., Sept., 1970, WATR No. 26.
80. C. C. Wang and L. I. Davis, Jr., *Phys. Rev. Lett.*, 32, 349 (1974).

12. PHOTOIONIZATION MASS SPECTROMETER STUDIES OF GAS PHASE OZONE-OLEFIN REACTIONS

Ozone-olefin reactions are known to be involved in the formation of photochemical smog. However, because of the paucity of data on the intermediates and mechanisms of these reactions, little is known about the detailed interaction of these intermediates and products with other atmospheric constituents. While these reactions have been postulated to act as a source of chain carrying OH radicals, it is only recently that any evidence for their production from low pressure ozone-olefin reactions has been obtained.

Clearly, identification of the intermediates and labile as well as stable products is necessary in order to permit the formulation of a detailed reaction mechanism. Photoionization mass spectrometry offers several advantages in this regard.¹⁻³ First, the use of a low energy ionization source makes it feasible to detect radical species produced in the reaction, free of the fragmentation problems encountered with electron beam ionization. In addition, variation of the photoionizing resonance lamps allows selective photoionization of the species.

In this work it was therefore our purpose to detect and study the kinetics of the intermediates and products of the reaction of ozone with ethylene, cis-2-butene, and isobutene in order to clarify the chemiluminescent reaction steps and their relationship to the overall mechanism.

Experimental. The experimental system has been described in detail previously.¹ The fast flow system (i.d. = 11 mm) had a moveable inlet jet (o.d. = 4 mm) through which the olefin was added axially. By throttling the pumping system, the reaction time could be varied over the range ~1-130 msec. The pressure at the midpoint of the moveable inlet region was monitored by an MKS Baratron pressure gauge.

The gas in the flow system was sampled via a pinhole into the photoionization chamber of a quadrupole mass spectrometer. The ions were detected by a Cu-Be electron multiplier and ion counts were displayed digitally with provision for varying counting intervals. Xe, Kr, or Ar microwave powered resonance lamps⁴ were used as photoionization sources. The ionizing energies of these lamps are shown in Figure 12.1 together with the ionization potentials⁵ of some stable molecules and free radicals of interest in this study; selective photoionization can therefore be achieved by the appropriate use of these lamps.

All experiments were carried out at total pressures of approximately 2 torr. Typical partial pressures of reactants were 0.04 torr of O_3 and 0.3 torr of the olefin. Approximately 2% O_3 in O_2 flows were obtained by the passage of Matheson ultrahigh purity grade O_2 (>99.99%) through a Welsbach Model T-408 ozonator. The olefins were all of research grade purity (>99.8%) and were used without further purification. Fully deuterated 2-butene (mixture of cis and trans) was obtained from Merck, Sharp and Dohme with stated D atom purity levels >99%. A bypass system enabled the O_3 - O_2 gas flow to be replaced by a pure O_2 stream.

Results. In all experiments, background counts were taken (typically an average of several 10-sec counts) with O_2 -olefin mixtures, and these were subtracted from the ion counts obtained in the presence of O_3 . All counts were corrected for decay of the lamp intensity and small fluctuations in olefin concentration by monitoring a suitable impurity peak or the parent peak (generally C_2H_4 which occurred as an impurity in the cis-2-butene and isobutene).

The m/e scale was corrected for any nonlinearity using parent peaks of authentic compounds. The Kr lamp was used in the majority of experiments, while the Xe resonance lamp was used to selectively photoionize and hence identify the radicals C_2H_5 (m/e 29), CH_3CO , and/or C_3H_7 (m/e 43). The Ar lamp was used for the species HO_2 , H_2O_2 , $HCHO$, CH_3OH , and $HCOOH$ which are not photoionized by either the Xe or Kr lamps (Figure 12.1).

A. cis-2-Butene. Table 12.1 shows the observed product mass numbers together with the lamps with which they were observed at reaction times of ~130 msec. Column 3 of Table 12.1 gives the possible species for each mass observed. Positive identification was obtained in some cases by a combination of deuteration, kinetic behavior, and the use of various photoionization lamps. For example, with the Kr lamp, a peak was observed at m/e 29. In the present system this could be due to HCO or C_2H_5 . On deuteration, the m/e 29 peak shifted to m/e values of 30 and 34, indicating both HCO and C_2H_5 . Replacement of the Kr lamp by an Xe lamp showed a mass peak at m/e 29 confirming the presence of C_2H_5 (see Figure 12.1); furthermore, the kinetic time dependence was that expected for a radical intermediate as shown in Figure 12.3b. Column 4 of Table 12.1 thus shows the species identified by procedures similar to that described above.

For the peaks of m/e 29-47 inclusive, and for 104, their time dependent

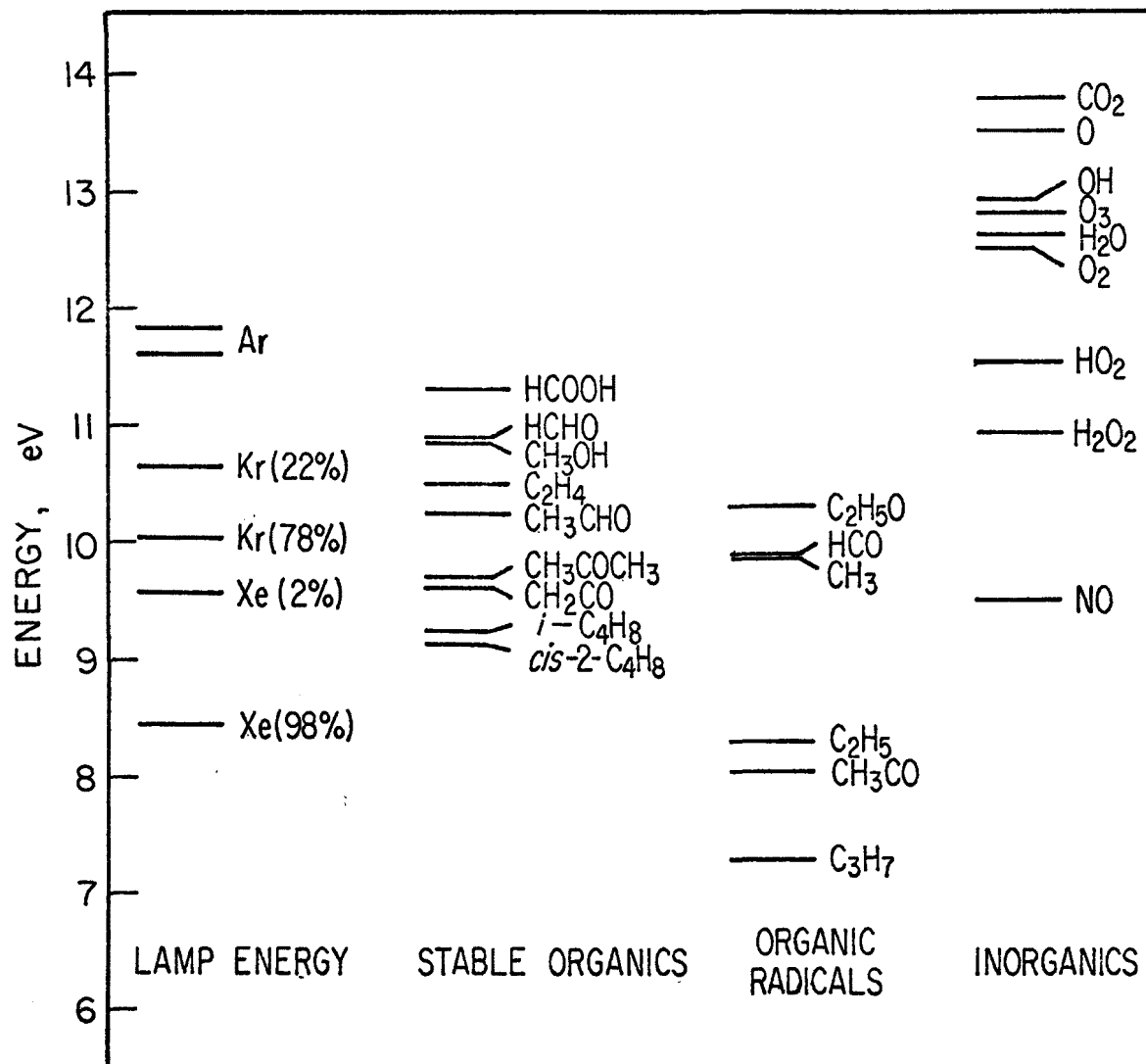


Figure 12.1 Resonance lamp energies and ionization potentials of relevant species.

Table 12.1

Observed peak mass numbers and their assignments

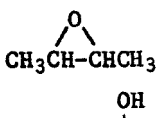
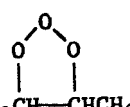
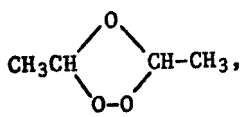
Obsd mass no. m/e	Lamp	Possible species ^a	Definite identification	Means of identification ^b
<u>cis-2-Butene</u>				
29	Kr, Xe	HCO, C ₂ H ₅	HCO and C ₂ H ₅	D, L, K
30	Ar	HCHO	HCHO	L
32	Ar	CH ₃ OH, O ₂ (¹ Δ)	CH ₃ OH ^c	K
33	Ar	HO ₂	HO ₂	L, K
34	Ar	H ₂ O ₂	H ₂ O ₂	L
42	Kr	CH ₂ CO, C ₃ H ₆	CH ₂ CO	D, K
43	Ar, Xe	CH ₃ CO, C ₃ H ₇	CH ₃ CHO ^d	D, K
44	Kr	CH ₃ CHO		
45	Kr	C ₂ H ₅ O, HCO ₂	C ₂ H ₅ O	D
46	Ar	HCOOH	HCOOH	L
47	Kr	CH ₃ O ₂	CH ₃ O ₂	D
58	Kr	(CHO) ₂ , CH ₃ COCH ₃ C ₂ H ₅ CHO	(CHO) ₂	D
70	Kr	CH ₃ COCH=CH ₂	a	
72	Kr	CH ₃ COC ₂ H ₅ or 	a	
73	Kr	C ₄ H ₉ O, CH ₃ CH-CHCH ₃ OH	a	
75	Kr	C ₃ H ₇ O ₂ , CH ₃ C(O)OO	a	
88	Kr	CH ₃ COCHOHCH ₃ , CH ₃ CH(OCH ₃)CH ₂ CH ₃ OOH	a	
89	Kr	C ₄ H ₉ O ₂ , CH ₃ CH-CHCH ₃ OOH	a	
90	Kr	CH ₃ CHCH ₂ CH ₃ OOH	a	
91	Kr		a	
104	Kr	CH ₃ CH-CHCH ₃ , 	a	
107	Kr	CH ₃ C-CHCH ₃ O OOH		
30	Ar	C ₃ H ₇ O ₄ , C ₂ H ₃ O ₅ Ethylene	HCHO	L, K
43	Kr, Xe	HCHO	CH ₃ CO ^e	L, K
30	Ar	CH ₃ CO, C ₃ H ₇ Isobutene	HCHO	L, K
42	Kr	HCHO		
		CH ₂ CO, C ₃ H ₆		

Table 12.1 (cont.)

Obsd mass no. m/e	Lamp	Possible species ^a	Definite identification	Means of identification ^b
<u>cis-2-Butene</u>				
43	Kr, Xe	CH ₃ CO, C ₃ H ₇		
44	Kr	CH ₃ CHO	CH ₃ CHO ^d	
58	Kr	CH ₃ COCH ₃ , (CHO) ₂		f
59	Kr	C ₂ H ₅ CHO		

^a For high mass numbers (m/e ≥ 70) there are several possible structures which cannot be differentiated; typical structures are given which include those products expected from the reaction scheme given in the text (see Discussion).

^b D = deuteration, L = selective use of lamps, K = kinetic behavior (see text).

^c On the basis of published rate constants for O₂(¹Δ) + O₃ → O + 2O₂ [F. D. Findlay and D. R. Snelling, J. Chem. Phys., 54, 2750 (1971)] the kinetic behavior observed is that expected of CH₃OH rather than of O₂(¹Δ).

^d On use of Xe lamp with sapphire window (see text), this mass number was not observed.

^e C₃H₇ would have to be formed by radical attack on C₂H₄, and these reactions are expected to be slow compared with radical reactions with O₃ and O₂.

^f On the basis of the known chemistry of isobutene-O₃ reactions,⁶⁻⁸ acetone is by far the most likely product.

behavior and their dependence on olefin concentration were determined. Figures 12.2 and 12.3 show the observed time dependence on these product peaks. For the peak at m/e 104, deuteration showed the presence of eight H atoms, hence the formula $C_4H_8O_3$ (Table 12.1). The observed linear dependence on both time and olefin concentration shown in Figure 12.4 indicated that this was a stable molecule over this time range. In general, the kinetic behavior confirms the identifications of Table 12.1; i.e., stable products increase linearly with time, while radical intermediates show an approach to a steady state. However, in certain cases, i.e., m/e ratios of 43, 45, and 47, anomalous behavior is observed as shown in Figure 12.2b. Experiments using a Xe lamp with a sapphire window (transmitting only the 8.44-eV line) gave no evidence for an m/e 43 peak. This observation, in conjunction with the observed kinetics, strongly suggests that this peak, and by analogy possibly those at m/e 45 and 47, arises from fragmentation in the mass spectrometer of more complex molecules whose ionization potentials are in the range $9.57 \geq IP \geq 8.44\text{eV}$.

It is seen from Figure 12.3a that the $HCOOH$ and H_2O_2 signals tend to level off at the longer time regions. This may be due to diffusion to and subsequent absorption on the wall. Average diffusion times to the walls were calculated to be ~6 msec.

The signals obtained here, although corrected for decay of lamp intensity and fluctuations in the olefin pressure within a given series of runs, are uncorrected for relative photoionization efficiencies of the species and differences in photon intensities of the resonance lines used. Thus, for example, although the signals from CH_2CO and CH_3CHO are similar (Figure 12.3a), CH_3CHO is photoionized only by the higher energy Kr line (Figure 12.1), which is typically present⁴ to the extent of 22% of the combined 10.64- and 10.03-eV Kr lines. Therefore, assuming equal photoionization efficiencies, the yield of CH_3CHO becomes approximately five times that of CH_2CO . Using a rate constant of $9 \times 10^4 \text{ l mol}^{-1} \text{ sec}^{-1}$ for the reaction of ozone with cis-2-butene as measured under similar experimental conditions,⁹ the amount of ozone reacted over the time interval of 130 msec will be ~15% or $3 \times 10^{-7} \text{ mol l}^{-1}$. With unit stoichiometry^{10,11} this corresponds to $3 \times 10^{-7} \text{ mol l}^{-1}$ cis-2-butene reacted or ~2% of the initial cis-2-butene concentration. From the photoionization mass spectrometer sensitivity, it can be calculated that the observed CH_3CHO ion counts correspond (within a factor of 2) to $3 \times 10^{-7} \text{ mol l}^{-1}$

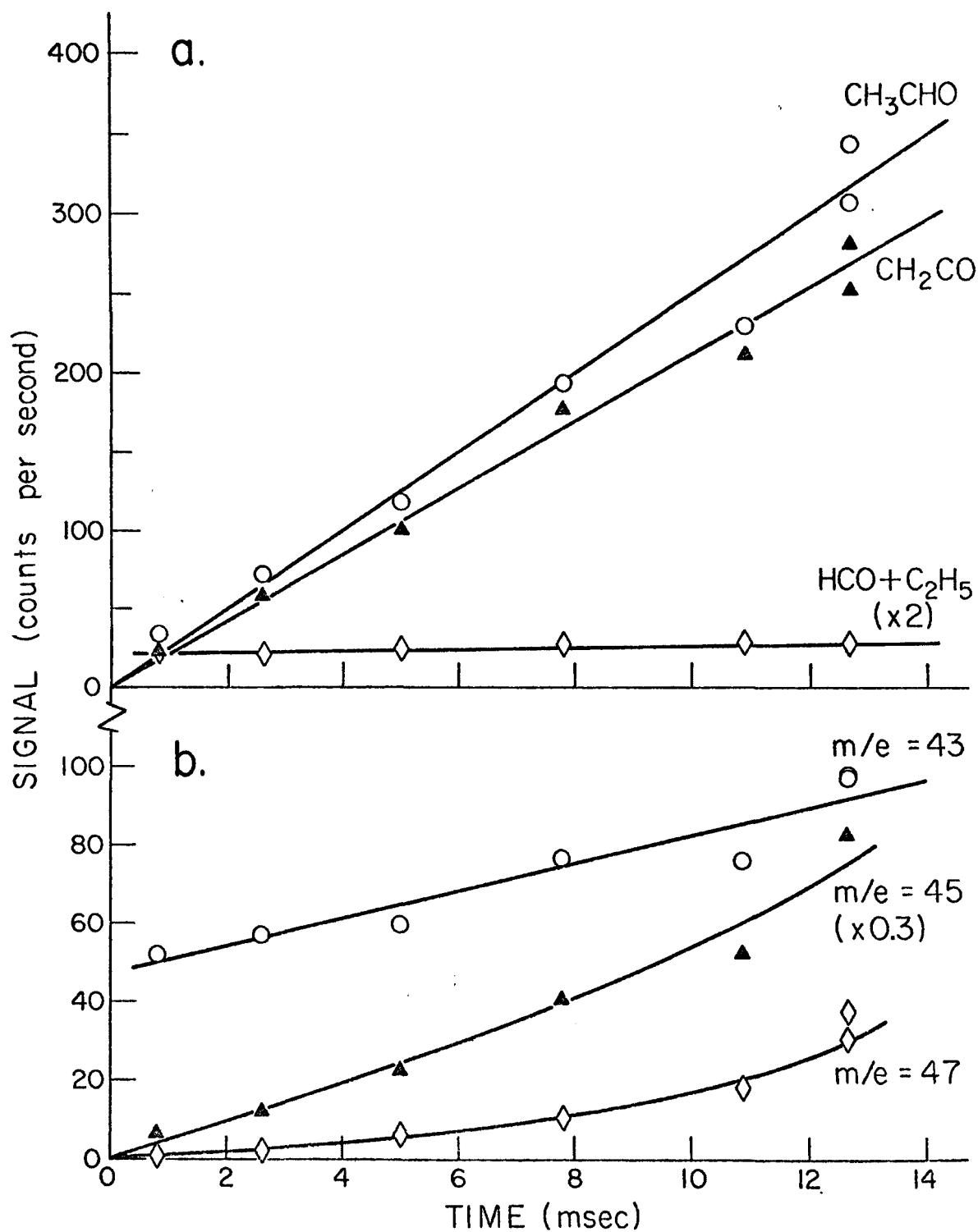


Figure 12.2 Kinetic behavior of some species observed in the cis-2-butene-ozone reaction using a krypton lamp: (a) $\text{HCO} + \text{C}_2\text{H}_5$ (m/e 29), CH_2CO (m/e 42), and CH_3CHO (m/e 44); (b) mass peaks m/e 43, 45, and 47.

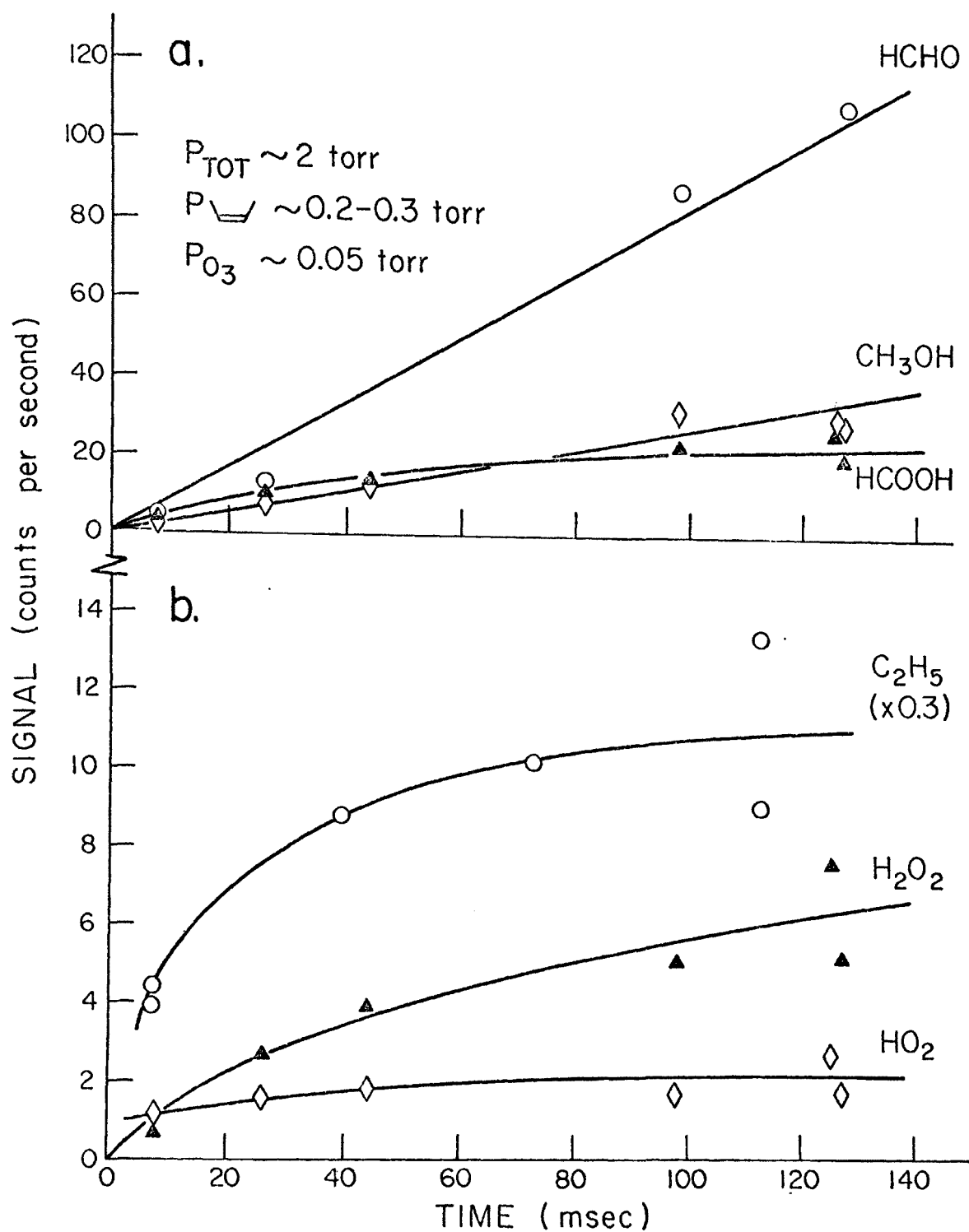


Figure 12.3 Kinetic behavior of some species observed in the cis-2-butene-ozone reaction: (a) HCHO (m/e 30), CH₃OH (m/e 32), and HCOOH (m/e 46) using an argon lamp; (b) C₂H₅ (m/e 29) using a xenon lamp, HO₂ (m/e 33) and H₂O₂ (m/e 34) using an argon lamp.

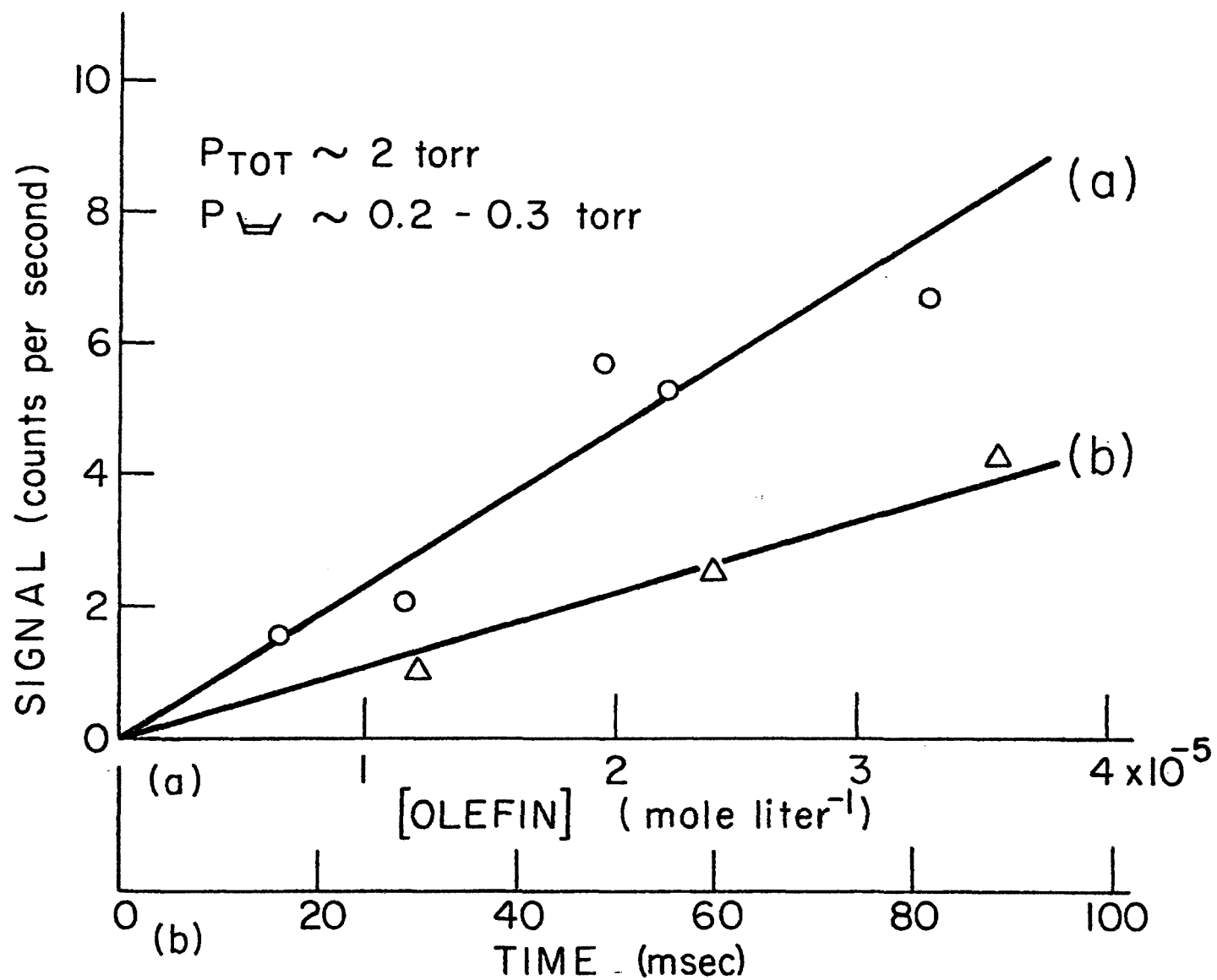


Figure 12.4 Dependence of signal at m/e 104 on (a) olefin concentration and (b) time, using a krypton lamp in the cis-2-butene-ozone reaction.

of CH_3CHO after a 130-msec reaction. Hence, within these error limits, ~1 mol of CH_3CHO is produced per mole of cis-2-butene reacting, which is in agreement with previous workers.^{6,7}

B. Ethylene. The product mass peaks observed at reaction times of ~130 msec are shown in Table 12.1. Again, use of the various resonance lamps provided confirmatory indentifications. Figure 12.5 shows the time-dependent behavior of the m/e 43 peak (presumed to be CH_3CO) using a Xe lamp and of HCHO. The CH_3CO shows the kinetic behavior expected for a radical intermediate, attaining a steady state. Furthermore, the m/e 43 peak remained, within experimental error (13 ± 11 counts above a background of ~10 counts per 10 sec), on use of a Xe lamp with a sapphire window. Deuteration was not feasible because of the generally very weak signals.

C. Isobutene. Table 12.1 shows the mass peaks observed at reaction times of ~130 msec, together with the lamps with which they were observed. The kinetic time dependence of the mass peaks is shown in Figure 12.6. As in the case of $\text{O}_3 + \text{cis-2-butene}$ the m/e 43 peak showed anomalous behavior, increasing with time (Figure 12.6b). Use of a Xe lamp with a sapphire window showed no evidence for m/e 43, again suggesting that it arises from fragmentation of a more complex molecule in the mass spectrometer. Similarly, as seen in Figure 12.6b, the time dependence of m/e 42 (CH_2CO or C_3H_6) suggests that it also arises by fragmentation; stable products are expected to increase linearly from a zero ordinate.

No identification could be made for m/e 59, and deuteration was not attempted because of the low counts obtained and because of interference that would have occurred from $i\text{-C}_4\text{D}_8$ at m/e 64.

Subsidiary experiments were carried out with acetone and acetaldehyde to determine if CH_3CO arose from fragmentation of these molecules in the mass spectrometer. A small amount of fragmentation was observed. The ratio of the signals at m/e 58:43 was approximately 30:1. Thus this cannot account for the m/e 43 signals observed in this work.

Discussion. The majority of the data was obtained for the cis-2-butene-ozone reaction because of its higher constant^{6-9,11} and therefore larger observable percentage reaction as compared to the ethylene and isobutene reactions.

The stable products observed at these short reaction times are compared in Table 12.2 with selected previous product studies reported in the literature.

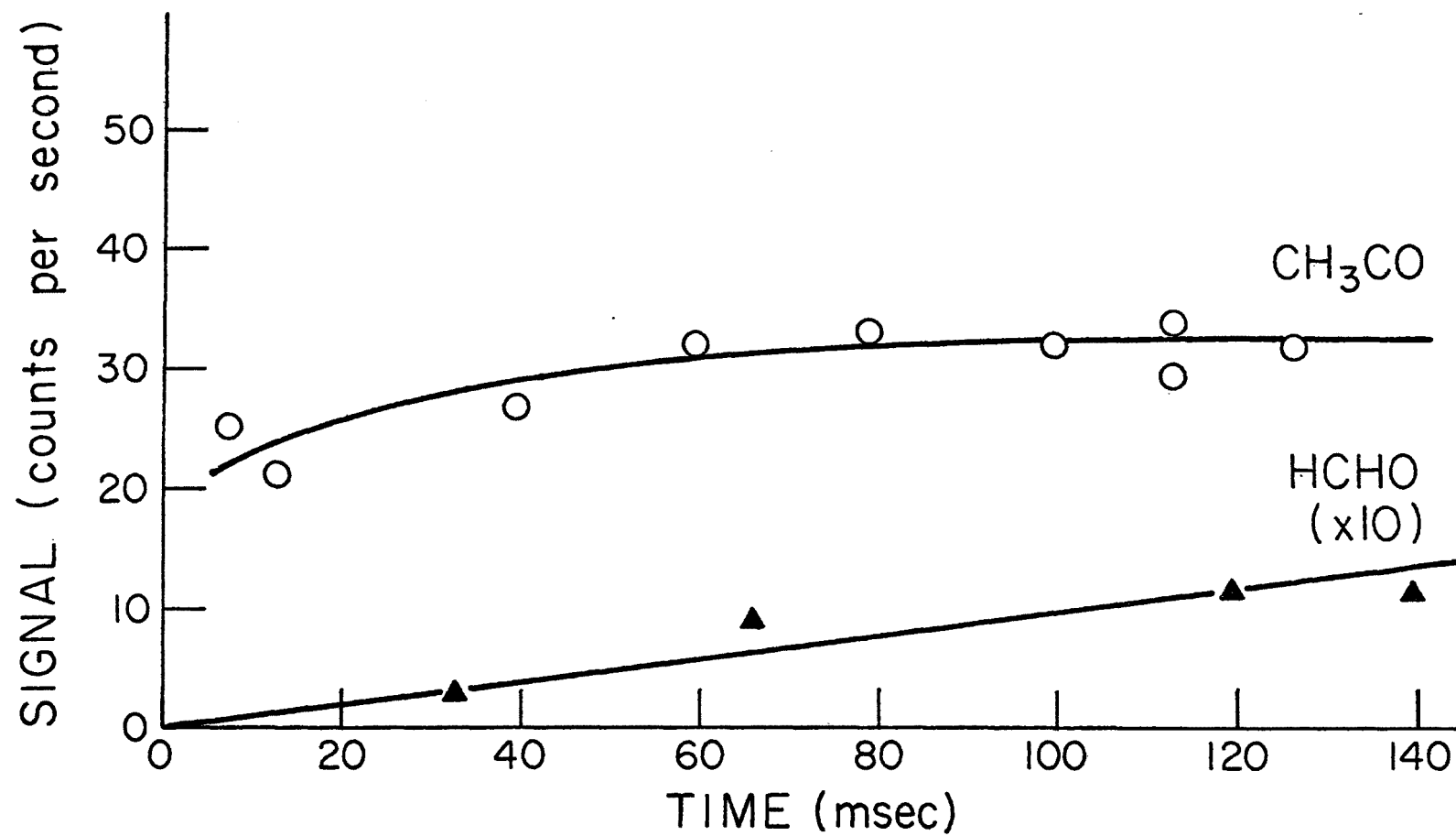


Figure 12.5 Kinetic behavior of HCHO (m/e 30) (argon lamp) and CH_3CO (m/e 43) (xenon lamp) in the ethylene-ozone reaction.

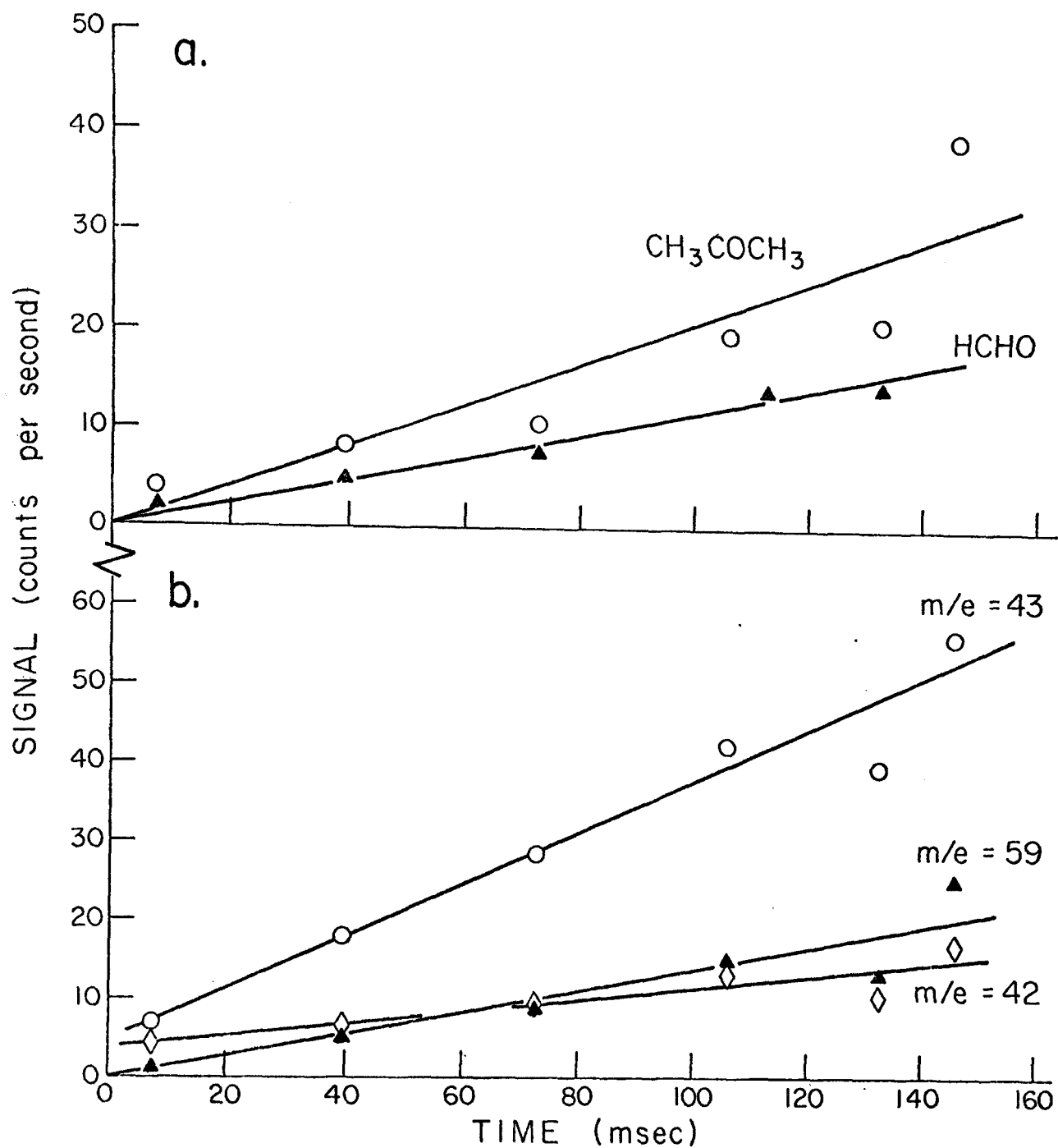


Figure 12.6 Kinetic behavior of some species in the isobutene-ozone reaction: (a) HCHO (m/e 30) (argon lamp) and CH_3COCH_3 (m/e 58) (krypton lamp); (b) mass peaks m/e 42, 43, and 59 using a krypton lamp.

Table 12.2

Stable products observed in the reaction of ozone with ethylene, isobutene, and cis-2-butene^a

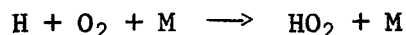
Olefin	HCHO	CH ₃ CHO	CH ₃ COCH ₃	CH ₂ CO	i-C ₃ H ₇ CHO	MF ^b	(CHO) ₂	C ₃ H ₆	C ₃ H ₈	HCOOH	CH ₃ OH	H ₂ O ₂	CO ₂	CO	H ₂ O	Ref
C ₂ H ₄		0.019								0.25						6
	0.53									<0.03			0.13	0.88	0.88	12
	Major															This work
i-C ₄ H ₈			0.53		0.005	0.005		0.005	0.009	0.66	0.013		0.37			6
		0.008	0.52										0.35			7
	Major		Major													This work
cis-C ₄ H ₈ -2		1.02						0.023		0.20	0.152		0.42			6
		0.98											0.35			7
	Major	Major		Major			Minor			Minor	Minor	Minor				This work

^a Product yields are given as the number of moles of product per mole of ozone consumed.

^b MF = methyl formate.

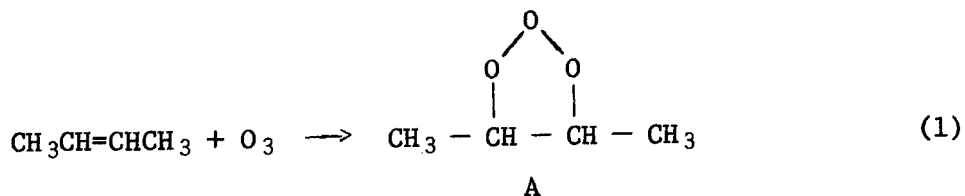
It is seen that there is good agreement with the major products observed: formaldehyde from ethylene, acetone from isobutene, and acetaldehyde from cis-2-butene. Also included in Table 12.2 are qualitative estimates from this work of the product yields using the observed ion counts as a measure of concentration. In certain cases minor amounts of products not listed in Table 12.1 may have been present. For example, in the cis-2-butene-ozone reaction, propylene could have been present in small amounts along with much larger quantities of ketene. In this work, several of the anticipated products such as CO, CO₂, H₂, and H₂O cannot be detected with photoionization mass spectrometry (Figure 12.1). In addition, it was not possible to detect the OH radical which is known¹³ to be present in the low pressure O₃-olefin reactions.

On the basis of the observed products and their kinetics in the cis-2-butene oxidation, some of the reaction steps can be tentatively identified as shown below. Reactions which are slow under these experimental conditions compared to other available reaction paths have been omitted; for example, the three-body reaction.^{14,15}



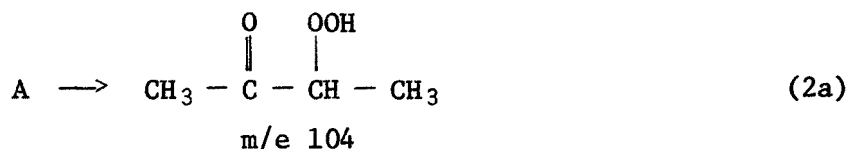
has been omitted as it is slow compared to H atom removal by ozone and cis-2-butene. The rate constants used to evaluate the relative importance of various reaction paths were the estimated or experimentally determined ones listed in the references given after each reaction. All the reactions postulated are exothermic and the observed mass numbers are consistent with the products expected from kinetic considerations.

The primary reaction step is assumed to involve the initial attack of ozone on the olefin.



The m/e 104 peak may correspond to any of the structures shown in Table 12.1. However, the hydroperoxide shown in reaction 12.2a is considered to

be the



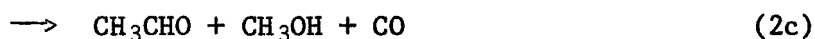
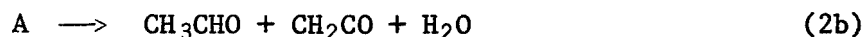
most likely product for the following reasons.

(1) The concentration of the species increases linearly with time as shown in Figure 12.4, while the primary "molozone" A is expected to show steady state kinetics. Application of simple RRK¹⁶ theory to the initially formed 1,2,3-trioxolane (A) which is assumed to contain the 45 kcal/mol exothermicity¹⁷ from reaction 1 predicts a lifetime of $\sim 10^{-11}$ sec under these experimental conditions.

(2) There is some infrared absorption evidence for production of the secondary ozonide in gas phase ozone-olefin reactions.^{11,18,19} Recent infrared studies in the condensed phase at low temperatures have shown that the secondary ozonides are major reaction products.²⁰ However, formation of the secondary ozonide must occur either by rearrangement of the initial ozone-olefin adduct or by recombination of the Criegee "zwitterion" ($\text{CH}_3\dot{\text{C}}\text{HOO}\cdot$) with aldehyde,²¹ both of which seem unlikely under our room temperature, low pressure conditions.

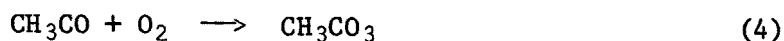
This direct observation of an adduct or rearranged product from an ozone-olefin reaction with a half-life ≥ 0.2 sec may be related to previous experimental observations. For example, while highly speculative, such a species could be the phytotoxicant in ozone-olefin reactions which causes plant damage²² and may be involved in the rapid oxidation of SO_2 reported by Cox and Penkett¹¹ in O_3 -olefin- SO_2 systems.

Reaction steps 2b-e involve the decomposition of the intermediate A, formed in the primary step 1.



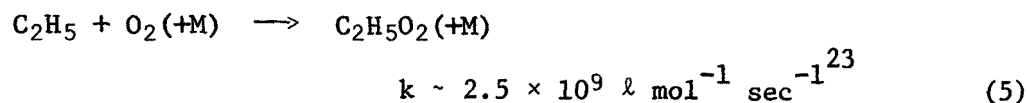
Although the products other than acetaldehyde in eq 2b and 2c can be rationalized on the basis of the decomposition of the Criegee "zwitterion" (or biradical in the gas phase), no direct evidence for its existence was found.

CH₃CO and C₃H₇ may be produced in reactions 2d and 2e. Both of these species are expected to react rapidly with O₂ (reactions 3 and 4)²³ giving rise to a



$$k \sim 4 \times 10^9 \text{ l mol}^{-1} \text{ sec}^{-1}$$

mass peak at m/e 75, consistent with the observations in Table 12.1. Similarly, C₂H₅ radicals, formed via reaction 2e would be expected to react with either O₂ or O₃.

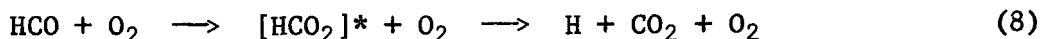
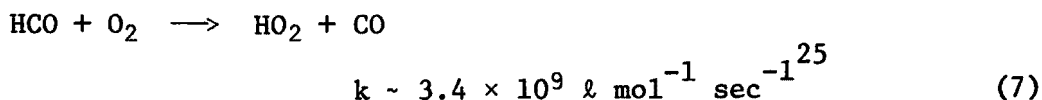


C₂H₅ appears to attain a steady state slowly (Figure 12.3b) from which estimates of k₅ and k₆ can be obtained using the simplified kinetic expression, which assumes a constant rate of formation of the intermediates where C

$$C = B(1 - e^{-Rt})$$

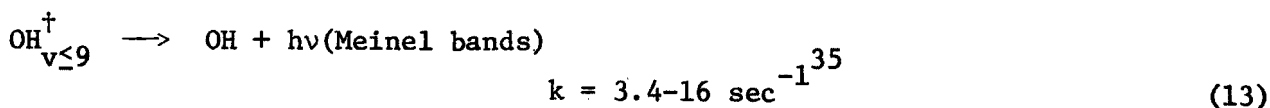
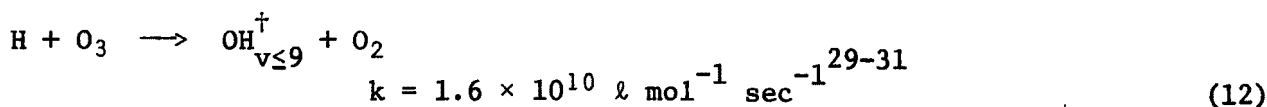
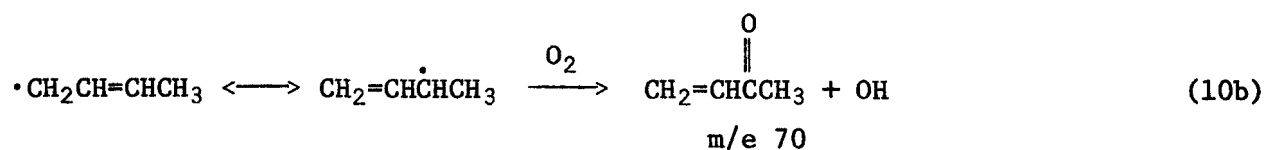
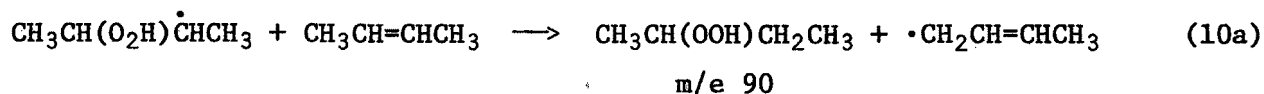
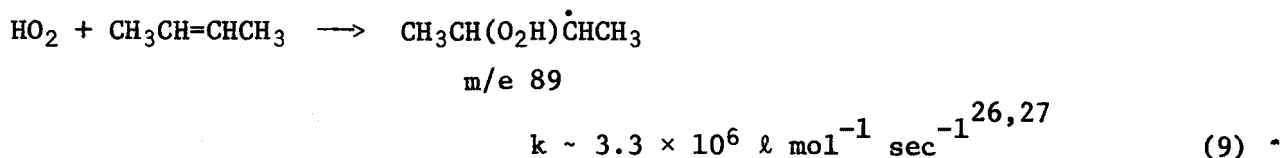
= concentration of the intermediate, B = constant, and R = the rate loss of the intermediate which, in general, will be governed by reaction with O₂, O₃, or cis-2-butene. If C₂H₅ reacts only with O₂, k₅ ~ 5 × 10⁵ l mol⁻¹ sec⁻¹, or, if in the third order pressure region,²⁴ k₅ ~ 5 × 10⁹ l² mol⁻² sec⁻¹. If C₂H₅ reacts only with O₃, then k₆ ~ 2 × 10⁷ l mol⁻¹ sec⁻¹. A possible explanation for the lack of agreement of k₅ with literature values is that C₂H₅ is not produced exclusively in reaction 2e but could also arise through a much more complex reaction sequence.

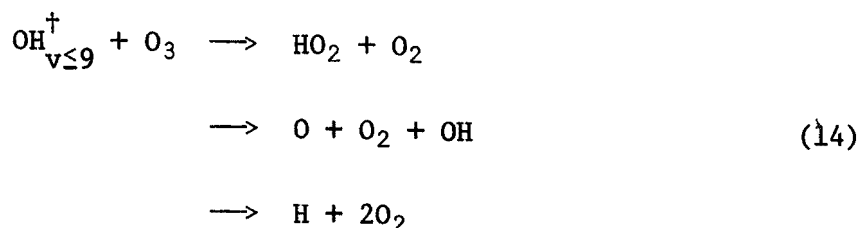
The reactions



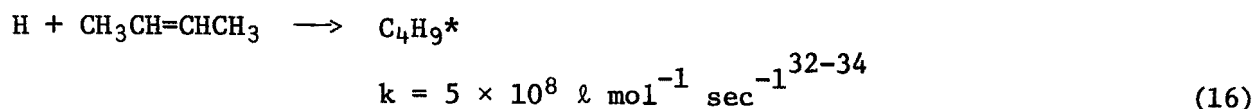
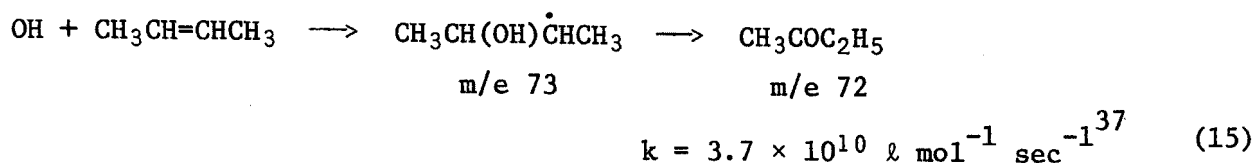
are expected to be the main removal processes for the HCO radical. While reaction 8 has not been experimentally verified, it may be one of the H atom sources responsible for the production of the Meinel band emission of the OH radical.¹³ In this work, the very rapid rise of HCO to a steady state concentration means that only lower limits of the rate constants for reactions 7 and 8 can be obtained. If HCO reacts only with O₂, then $k_7 \geq 1 \times 10^7 \text{ l mol}^{-1} \text{ sec}^{-1}$, or, if it reacts only with O₃, then $k_8 \geq 5 \times 10^8 \text{ l mol}^{-1} \text{ sec}^{-1}$.

From previous investigations, the reactions of HO₂,²⁶⁻²⁸ H,²⁹⁻³⁴ and OH³⁵⁻³⁹ expected in the present experimental system are given by reactions 9-16.





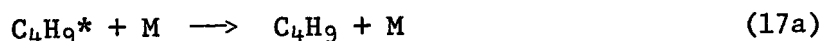
$$k = 1.2 \times 10^8 (v = 0) \text{ to } 5 \times 10^9 (v = 9) \text{ l mol}^{-1} \text{ sec}^{-1} \text{ }^{28,35}$$



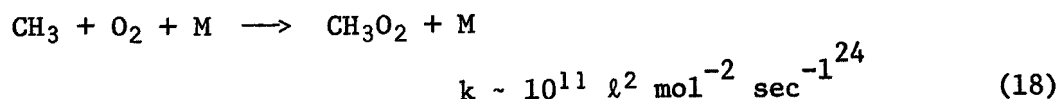
For HO_2 , reaction with O_3 is unimportant ($k = 1.8 \times 10^6 \text{ l mol}^{-1} \text{ sec}^{-1}$),²⁸ and thus assuming HO_2 reacts with cis-2-butene, k_9 can be estimated from the rise of HO_2 to its steady state to be approximately $1 \times 10^7 \text{ l mol}^{-1} \text{ sec}^{-1}$, which is consistent with literature estimates.^{26,27}

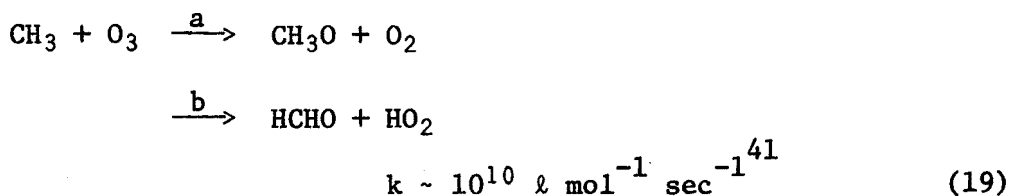
Morris and Niki³⁷ have determined by time of flight mass spectrometry that at least part of the reaction of OH radicals with cis-2-butene proceeds by addition; transient mass peaks were observed corresponding to the OH-olefin adduct. Also, by analogy with the products observed by Morris, et al.,³⁶ for $\text{OH} + \text{C}_2\text{H}_4$, C_3H_6 , it is expected that methyl ethyl ketone will be the major stable product in the case of $\text{OH} + \text{cis-2-butene}$.

The vibrationally excited C_4H_9 radical can undergo reactions 17a and 17b in the present system.⁴⁰ The



CH_3 produced in reaction 17b can react with either oxygen or ozone.

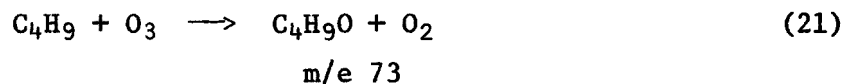
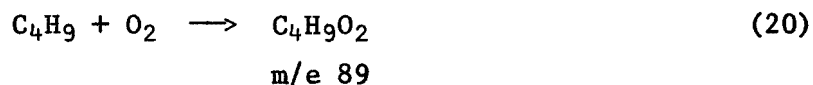




If reactions 16-19 become important at longer reaction times, the anomalous rise in CH_3O_2 (m/e 47) at longer reaction times may be explained; however, fragmentation in the mass spectrometer to produce CH_3O_2 cannot be excluded at this time.

This latter possibility is supported by the fact that, although reaction 17b is postulated as the source of CH_3 in this system, substantial quantities of C_3H_6 were not observed.

In similar manner, stabilized C_4H_9 radicals are expected to react with O_2 and O_3 .



The results of this study do not permit detailed formulation of a reaction scheme for the ethylene and isobutene oxidations. The observed major stable products are expected to arise from the decomposition of the initial ozone-olefin adduct.

While the mechanism presented for the cis-2-butene-ozone reaction is obviously tentative and incomplete, the observation of radical species, such as HCO and HO_2 , provides evidence for alternative reaction pathways to the Criegee mechanism which has previously been applied.

REFERENCES

1. I. T. N. Jones and K. D. Bayes, Symp. (Int.) Combust., [Proc], 14th (1972).
2. I. T. N. Jones and K. D. Bayes, J. Amer. Chem. Soc., 94, 6869 (1972).
3. J. R. Kanofsky and D. Gutman, Chem. Phys. Lett., 15, 236 (1972).
4. H. Okabe, J. Opt. Soc. Amer., 54, 478 (1964).
5. R. W. Kiser, "Introduction to Mass Spectrometry and Its Applications," Prentice-Hall, Englewood Cliffs, N. J., 1965.
6. T. Vrbaski and R. J. Cvetanovic, Can. J. Chem., 38, 1053, 1063 (1960).
7. Y. K. Wei and R. J. Cvetanovic, Can. J. Chem., 41, 913 (1963).
8. J. J. Bufalini and A. P. Altshuller, Can. J. Chem., 43, 2243 (1965).
9. B. J. Finlayson, J. N. Pitts, Jr. and R. Atkinson, J. Amer. Chem. Soc., 96, 5356 (1974).
10. D. H. Stedman, C. H. Wu, and H. Niki, J. Phys. Chem., 77, 2511 (1973).
11. R. A. Cox and S. A. Penkett, J. Chem. Soc., Faraday Trans. 1, 68, 1735 (1972).
12. W. E. Scott, E. R. Stephens, P. H. Hanst, and R. C. Doerr, Proc. Amer. Petrol. Inst., 3 (37), 171 (1957).
13. B. J. Finlayson, J. N. Pitts, Jr., and H. Akimoto, Chem. Phys. Lett., 12, 495 (1972).
14. M. J. Kurylo, J. Phys. Chem., 76, 3518 (1972), and references therein.
15. D. L. Baulch, D. D. Drysdale, D. G. Horne, and A. C. Lloyd, "Evaluated Kinetic Data for High Temperature Reactions. Vol. 1: Homogeneous Gas Phase Reactions of the H_2-O_2 System," Butterworths, London, 1972.
16. L. S. Kassel, "The Kinetics of Homogeneous Gas Reactions," Chemical Catalogue, New York, N. Y., 1932.
17. S. W. Benson, "Thermochemical Kinetics," Wiley, New York, N. Y., 1968, p. 173.
18. W. B. DeMore, Int. J. Chem. Kinet., 1, 209 (1969).
19. P. L. Hanst, E. R. Stephens, W. E. Scott, and R. C. Doerr, Symposium on Air Pollution Research, Division of Petroleum Chemistry, Vol. 4, Sept. 1959.

REFERENCES (cont.)

20. L. A. Hull, I. C. Hisatsune, and J. Heicklen, J. Amer. Chem. Soc., 94, 4856 (1972).
21. H. Niki, E. E. Daby, and B. Weinstock, Advan. Chem. Ser., No. 113, 16 (1972).
22. W. N. Arnold, Int. J. Air Pollut., 2, 167 (1959), and references therein.
23. G. R. McMillan and J. G. Calvert, Oxid. Combust. Rev., 1, 83 (1965).
24. N. Basco, D. G. L. James, and F. C. James, Int. J. Chem. Kinet., 4, 129 (1972).
25. N. Washida, R. I. Martinez, and K. D. Bayes, Z. Naturforsch., 29A, 251 (1974).
26. K. L. Demerjian, J. A. Kerr, and J. G. Calvert, Advan. Environ. Sci. Technol., 4 (1973).
27. A. C. Lloyd, "Estimated and Evaluated Kinetic Data for Gas Phase Reactions of the Hydroperoxyl Radical," National Bureau of Standards Report 10447, July 1971; Int. J. Chem. Kinet., 6, 169 (1974).
28. W. B. DeMore, Science, 180, 735 (1973).
29. J. D. McKinley, Jr., D. Garvin, and M. J. Boudart, J. Chem. Phys., 23, 784 (1955).
30. L. F. Phillips and H. I. Schiff, J. Chem. Phys., 37, 1233 (1962).
31. P. E. Charters, R. G. MacDonald, and J. C. Polanyi, Appl. Opt., 10, 1747 (1971).
32. E. E. Daby and H. Niki, J. Chem. Phys., 51, 1255 (1969).
33. J. A. Cowfer, D. G. Keil, J. V. Michael, and C. Yeh, J. Phys. Chem., 75, 1584 (1971).
34. E. E. Daby, H. Niki, and B. Weinstock, J. Phys. Chem., 75, 1601 (1971).
35. R. N. Coltharp, S. D. Worley, and A. E. Potter, Appl. Opt., 10, 1786 (1971).
36. E. D. Morris, Jr., D. H. Stedman, and H. Niki, J. Amer. Chem. Soc., 93, 3570 (1971).
37. E. D. Morris, Jr. and H. Niki, J. Phys. Chem., 75, 3640 (1971).
38. D. D. Drysdale and A. C. Lloyd, Oxid. Combust. Rev., 4, 157 (1970).
39. W. E. Wilson, Jr., J. Phys. Chem. Ref. Data, 1, 535 (1972).

REFERENCES (cont.)

40. B. S. Rabinovich and D. W. Setser, *Advan. Photochem.*, 3, 1 (1964).
41. J. G. Calvert and P. L. Hanst, *Can. J. Chem.*, 37, 1671 (1959).

TECHNICAL REPORT DATA
(Please read Instructions on the reverse before completing)

1. REPORT NO. EPA-600/3-77-014a		2.		3. RECIPIENT'S ACCESSION NO.	
4. TITLE AND SUBTITLE MECHANISMS OF PHOTOCHEMICAL REACTIONS IN URBAN AIR Volume I. Chemistry Studies				5. REPORT DATE February 1977	
				6. PERFORMING ORGANIZATION CODE	
7. AUTHOR(S) James N. Pitts, Jr.				8. PERFORMING ORGANIZATION REPORT NO.	
9. PERFORMING ORGANIZATION NAME AND ADDRESS University of California Statewide Air Pollution Research Center Riverside, California 92502				10. PROGRAM ELEMENT NO. 1AA603	
				11. CONTRACT/GRANT NO. Grant No 800649-13,14,15	
12. SPONSORING AGENCY NAME AND ADDRESS Environmental Sciences Research Laboratory Office of Research and Development U.S. Environmental Protection Agency Research Triangle Park, NC 27711				13. TYPE OF REPORT AND PERIOD COVERED Final Report 12/1/71-12/1/74	
				14. SPONSORING AGENCY CODE EPA-ORD	
15. SUPPLEMENTARY NOTES					
16. ABSTRACT Results are presented of a research program concerned with selected aspects of the kinetics, mechanisms and products of reactions involved in photochemical air pollution. Rate constants were determined, using competitive and modulation-phase shift techniques, for the gas phase reaction of $O(^3P)$ atoms with a variety of organic and inorganic species over the temperature range 296-423°K. Products for the gas phase reaction of $O(^3P)$ atoms with toluene and 1-methylcyclohexene were also studied. The products and mechanisms of the reaction of nitric oxide with methyl peroxy radicals were investigated at 296°K using long path infrared spectroscopic and gas chromatographic techniques. The reactions of peroxyacetyl nitrate were investigated in the gas phase with selected constituents of polluted atmospheres, and in the liquid phase with a variety of organics. Chemiluminescence from the reaction of peroxyacetyl nitrate with a series of amines was studied in the liquid phase. The mechanism and products of the gas phase reactions of ozone with a variety of organics was investigated in low pressure flow systems using chemiluminescent and photoionization mass spectrometric techniques. The NO_2 -catalyzed geometric isomerization of 2-butenes and 2-pentenenes was studied over the temperature range 298-400°K while an investigation of the NO_x -propylene photooxidation system was carried out at room temperature.					
17. KEY WORDS AND DOCUMENT ANALYSIS					
a. DESCRIPTORS		b. IDENTIFIERS/OPEN ENDED TERMS		c. COSATI Field/Group	
* Air pollution * Photochemical reactions * Reaction kinetics * Hydrocarbons * Ozone * Nitrogen oxides				13B 07E 07D 07C 07B	
18. DISTRIBUTION STATEMENT RELEASE TO PUBLIC		19. SECURITY CLASS (This Report) UNCLASSIFIED		21. NO. OF PAGES 184	
		20. SECURITY CLASS (This page) UNCLASSIFIED		22. PRICE	